Report No. UT-05.03

SHAPE MODIFICATION OF RECTANGULAR COLUMNS CONFINED WITH FRP COMPOSITES

Prepared For:

Utah Department of Transportation Research and Development Division

Submitted By:

University of Utah
Department of Civil & Environmental Engineering
Engineering

Authored By:

Chris P. Pantelides
Zihan Yan
Lawrence D. Reaveley

Date: December 2004

UDOT RESEARCH & DEVELOPMENT REPORT ABSTRACT

1. Report No. UT-05.03	**2. Government Accession No.** N/A	**3. Recipient's Catalog No.** N/A
4. Title and Subtitle: SHAPE MODIFICATION OF RECTANGULAR COLUMNS CONFINED WITH FRP COMPOSITES	**5. Report Date:** **6. Performing Organization Code:** N/A	
7. Author(s): CHRIS P. PANTELIDES ZIHAN YAN LAWRENCE D. REAVELEY	**8. Performing Organization Report No.** CVEEN-04/4	
9. Performing Organization Name and address: Civil & Environmental Engineering College of Engineering University of Utah 122 South Central Campus Drive Rm 104 Salt Lake City UT 84112-0561	**10. Work Unit No.** N/A **11. Contract No.** 03-9056	
12. Sponsoring Agency Name and Address: Utah Department of Transportation Research Division 4501 South 2700 West Taylorsville, Utah 84119	**13. Type of Report and Period Covered** **14. Sponsoring Agency Code** 81F15406	
15. Supplementary Notes:		

16. Abstract: The study investigates FRP strengthening for axial capacity improvement of concrete columns in confinement. Thirty full-scale concrete columns were tested in uniaxial compression until failure. A wet-layup procedure for columns in the as-is condition is adequate for strengthening square or rectangular columns to improve axial capacity. For strengthening existing square or rectangular columns to resist seismic forces, it is preferable to transform the square and rectangular cross-sections to circular, and elliptical or oval, respectively. This study has found that the use of FRP composite straps or hoops is beneficial for columns with a circular cross-section but not for columns with a square or rectangular cross-section. In the case of using FRP composite prefabricated shells, it is advantageous to use expansive cement concrete rather than non-shrink grout to achieve the shape modification. Square columns, which were modified to circular using FRP composite prefabricated shells and expansive cement concrete, showed a higher increase in axial strength capacity and ductility, compared to square columns, which were modified to circular using FRP composite prefabricated shells and non-shrink grout. Design guidelines for the FRP composite retrofit of circular columns, square columns, rectangular columns, and elliptical columns are provided in this report. Guidelines for the retrofit of columns with FRP composite prefabricated shells and either non-shrink grout or expansive cement concrete are also provided.

17. Key Words : Columns FRP composites Confinement Expansive cement concrete		**18. Distribution Statement** Available: UDOT Research Division Box 148410 Salt Lake City, Utah 84114-8410 www.udot.utah.gov/res	
19. Security Classification (Of this report)	**20. Security Classification (Of this report)**	**21. No. of Pages** 166	**22. Price:** N/A

DISCLAIMER

The Contents of this report reflect the view of the authors, who are responsible for the facts and accuracy of the data presented herein. The contents do not necessarily reflect the official views or policies of the Utah Department of Transportation (UDOT).

ACKNOWLEDGEMENTS

The authors would like to thank the following individuals for their support and encouragement throughout the project: Mr. Doug Anderson, Mr. Dan Avila, and Mr. Daniel Hsiao of UDOT Research.

The authors would like to acknowledge the contribution of Sika and Air Logistics Corporation for their contribution of the FRP composite materials. The authors also acknowledge the contribution of Altaview Concrete especially the assistance of Lou Nicoletti. The authors acknowledge the contribution of CTS company for the Type-K cement.

In addition they would like to thank the following individuals from the University of Utah: Mr. Mark Bryant, Mr. Oliver Burt, Mr. Joseph Emerson, Mr. Nicolas Saenz, Mr. Rajeev Surapaneni, Mr. Kyle Cook, Mr. Scott McAllister, Mr. Yasuteru Okahashi, Mr. Jeffrey Duffin, and Mr. Luis Castaneda.

TABLE OF CONTENTS

ABSTRACT i

DISCLAIMER ii

ACKNOWLEDGEMENTS iii

TABLE OF CONTENTS iv

LIST OF TABLES vii

LIST OF FIGURES viii

1. INTRODUCTION 1

2. OBJECTIVES OF THE RESEARCH 4

3. TEST SPECIMENS 5

- 3.1 Overview of Test Specimens 5
- 3.2 Material Properties 5
  - 3.2.1 Concrete 5
  - 3.2.2 Fiber Reinforced Polymer (FRP) composites 10
- 3.3 Construction of Specimens and Sample Preparation 11

4. TEST SETUP 22

- 4.1 Instrumentation 22
  - 4.1.1 Strain gauges 22
  - 4.1.2 LVDT instrumentation 23
- 4.2 Loading Apparatus 23
- 4.3 Data Acquisition System 24

5. EXPERIMENTAL RESULTS AND DISCUSSION 26

- 5.1 General 26
- 5.2 Circular Specimens 27
  - 5.2.1 Specimens with regular concrete 27
  - 5.2.2 Specimens with expansive cement concrete 36
- 5.3 Square Specimens 41
  - 5.3.1 Specimens without shape modification 41
  - 5.3.2 Specimens with shape modification 50
- 5.4 Rectangular Specimens 58
  - 5.4.1 Specimens without shape modification 58
  - 5.4.2 Specimens with shape modification 68

6. EVALUATION OF EXPERIMENTAL RESULTS AND DATA ANALYSIS 85

6.1 Description of Parameters 85
6.1.1 Volumetric ratio of the FRP jacket, ρ_{FRP} 85
6.1.2 Shape factor, k_s 86
6.1.3 Longitudinal confinement effectiveness factor, k_l 87
6.1.4 Jacket efficiency factor, k_ε 89
6.1.5 Jacket confining pressure, f_l 91
6.1.6 Effective conining stiffness for circular columns with bonded FRP jackets, C_j 93
6.2 Evaluation of Experimental Results 93
6.2.1 Evaluation of circular columns with bonded FRP jackets 93
6.2.2 Evaluation of square and rectangular columns with bonded FRP jackets 100
6.2.3 Evaluation of shape-modified columns confined by non-bonded FRP jackets with expansive cement concrete 104

7. DESIGN RECOMMENDATIONS AND DESIGN-ORIENTED FRP-CONFINED CONCRETE MODELS 108

7.1 Design Recommendations for FRP-Confined Concrete Columns 108
7.1.1 Circular concrete columns confined with bonded FRP jackets 108
7.1.2 Square and rectangular concrete columns confined with bonded FRP jackets 112
7.1.3 Elliptical concrete columns confined with bonded FRP jackets 117
7.1.4 Circular and elliptical columns with non-bonded FRP jackets and expansive cement concrete 119
7.2 Design-Oriented Model for FRP-Confined Columns 124

8. FINITE ELEMENT ANALYSIS 130

8.1 Plasticity Approach 130
8.2 FE Modeling 131
8.3 Results and Discussion of FE Analysis 137

9. PARAMETRIC STUDY 144

10. CONCLUSIONS AND RECOMMENDATIONS 148

10.1 Conclusions 148
10.2 Recommendations for Future Research 151
10.3 Recommendations for Implementation 152

11. REFERENCES 154

APPENDIX..... 157

(1). ANSYS Input File for C-C1-0 157
(2). ANSYS Input File for S-CT-E.....161

LIST OF TABLES

Table 3.1 Mix design for expansive concrete grout 7
Table 3.2 Experimental results for $\varepsilon_{j,ini}$ 9
Table 3.3 Material properties of CFRP and GFRP composites 11
Table 3.4 Matrix of test specimens: circular columns 13
Table 3.5 Matrix of test specimens: square columns 13
Table 3.6 Matrix of test specimens: rectangular columns (1) 14
Table 3.7 Matrix of test specimens: rectangular columns (2) 14
Table 5.1 Main results of circular specimen tests with regular concrete 28
Table 5.2 Main results of circular specimen tests with expansive concrete 36
Table 5.3 Main results of square specimens without shape modification 43
Table 5.4 Main results for shape-modified square specimens 51
Table 5.5 Main results for rectangular specimens without shape modification 59
Table 5.6 Details of shape-modified rectangular specimens 70
Table 5.7 Main results for shape-modified rectangular specimens 70
Table 6.1 FRP-jacket efficiency factor, k_{ε} ($k_{\varepsilon,\max}$) for different types of FRP jackets and sections 91
Table 7.1 Calculated results of circular columns with bonded FRP jackets (1) 111
Table 7.2 Calculated results of circular columns with bonded FRP jackets (2) 111
Table 7.3 Calculated results of square columns with bonded FRP jackets (1) 115
Table 7.4 Calculated results of square columns with bonded FRP jackets (2) 115
Table 7.5 Calculated results of rectangular columns with bonded FRP jackets (1) 116
Table 7.6 Calculated results of rectangular columns with bonded FRP jackets (2) 116
Table 7.7 Calculated results of elliptical columns with bonded FRP jackets (1) 118
Table 7.8 Calculated results of elliptical columns with bonded FRP jackets (2) 118
Table 7.9 Calculated results of circular columns with non-bonded FRP jackets and expansive cement concrete (1) 122
Table 7.10 Calculated results of circular columns with non-bonded FRP jackets and expansive cement concrete (2) 122
Table 7.11 Calculated results of elliptical columns with non-bonded FRP jackets and expansive cement concrete (1) 123
Table 7.12 Calculated results of elliptical columns with non-bonded FRP jackets and expansive cement concrete (2) 123
Table 9.1 Dimensions and calculated parameters for options 1-6 146
Table 9.2 Result summary for options 1-6 147
Table 9.3 Comparisons of options 2-6 with option 1 147

LIST OF FIGURES

Figure 3.1 Concrete strength vs. aging time 6
Figure 3.2 Results of preliminary test for expansive cement..... 7
Figure 3.3 Expansion history for FRP jackets with expansive cement concrete 8
Figure 3.4 Effect of aspect ratio on initial hoop strain, $\varepsilon_{j,ini}$ 10
Figure 3.5 Molds used for preparation of concrete column specimens 12
Figure 3.6(a) Wrapping methods for circular columns..... 15
Figure 3.6(b) Wrapping methods for square columns 16
Figure 3.6(c) Wrapping methods for rectangular columns (1) 17
Figure 3.6(d) Wrapping methods for rectangular columns (2) 18
Figure 3.7(a) Preparation of circular/elliptical forms (1st step) 19
Figure 3.7(b) One-layer FRP shell cut in two halves (2nd step)..... 20
Figure 3.7(c) Stay-in-place FRP forms (3rd step)..... 20
Figure 3.7(d) Casting of expansive cement concrete (4th step)..... 21
Figure 4.1 Layout of strain gauges for regular sections..... 22
Figure 4.2 Layout of strain gauges for shape-modified sections 22
Figure 4.3 Column specimen setup..... 23
Figure 4.4 Additional LVDTs for square and rectangular columns 24
Figure 4.5 Setup of the column compression tests 24
Figure 4.6 Data acquisition and MTS system during testing..... 25
Figure 5.1 Definition of stress and strain parameters 26
Figure 5.2 Specimen C-0-0 with plain concrete before and after testing 27
Figure 5.3 Specimen C-CS-0 with 2 layers of CFRP strips before and after testing... 28
Figure 5.4 Specimen C-GS-0 with 5 layers of GFRP strips before and after testing .. 29
Figure 5.5 Specimen C-C1-0 with 1 continuous CFRP layer before and after testing..... 29
Figure 5.6 Specimen C-G3-0 with 3 continuous GFRP layers before and after testing..... 30
Figure 5.7 Typical failure modes of FRP-confined circular specimens 31
Figure 5.8 Stress-strain curves for specimens with regular concrete..... 32
Figure 5.9 Definition of ductility ratio for FRP-confined concrete 32
Figure 5.10 Volumetric versus axial strain for specimen C-0-0 with plain concrete 34
Figure 5.11 Volumetric versus axial strain for specimen C-CS-0 with 2 layers of CFRP strips 34
Figure 5.12 Volumetric versus axial strain for specimen C-GS-0 with 5 layers of GFRP strips..... 35
Figure 5.13 Volumetric versus axial strain for specimen C-C1-0 with 1 continuous CFRP layer..... 35
Figure 5.14 Volumetric versus axial strain for specimen C-G3-0 with 3 continuous GFRP layers..... 35
Figure 5.15 Comparisons between different types of circular specimens 37
Figure 5.16 Specimen C-CT-E with expansive concrete and 1 CFRP layer before and after testing..... 37

Figure 5.17 Specimen C-GT-E with expansive concrete and 3 GFRP layers before and after testing 38
Figure 5.18 Stress-strain curves for specimens with expansive cement concrete 39
Figure 5.19 Normalized stress-strain curves for FRP-confined circular specimens..... 39
Figure 5.20 Volumetric versus axial strain curve for specimen C-CT-E 40
Figure 5.21 Volumetric versus axial strain curve for specimen C-GT-E 40
Figure 5.22 Specimen S-0-0 with plain concrete before and after testing..... 42
Figure 5.23 Specimen S-C2-0 with 2 CFRP layers before and after testing 44
Figure 5.24 Specimen S-CS-0 with 3 layers of CFRP strips during and after testing... 44
Figure 5.25 Specimen S-G6-0 with 6 GFRP layers during and after testing..... 45
Figure 5.26 Specimen S-GS-0 with 9 layers of GFRP strips before and after testing... 45
Figure 5.27 Stress-strain curves for S-C2-0 with 2 CFRP layers 46
Figure 5.28 Stress-strain curves for S-CS-0 with 3 layers of CFRP strips 46
Figure 5.29 Stress-strain curves for S-G6-0 with 6 GFRP layers..... 46
Figure 5.30 Stress-strain curves for S-GS-0 with 9 layers of GFRP strips..... 47
Figure 5.31 Fiber versus axial strain curves for square specimens..... 48
Figure 5.32 Volumetric versus axial strain curves for square specimens..... 49
Figure 5.33 Comparisons between square and shape-modified specimens..... 51
Figure 5.34 Specimen S-CT-E with expansive cement concrete and 2 CFRP layers before and after testing 52
Figure 5.35 Specimen S-CT-F with non-shrink cement concrete and 2 CFRP layers before and after testing 52
Figure 5.36 Specimen S-GT-E with expansive cement concrete and 6 GFRP layers before and after testing 53
Figure 5.37 Specimen S-GT-F with non-shrink cement concrete and 6 GFRP layers after testing..... 53
Figure 5.38 Stress-strain curves for S-CT-E & S-CT-F 54
Figure 5.39 Stress-strain curves for S-GT-E & S-GT-F 54
Figure 5.40 Normalized stress-strain relationships for CFRP-jacketed square specimens 55
Figure 5.41 Normalized stress-strain relationships for GFRP-jacketed square specimens 55
Figure 5.42 Volumetric versus axial strain curves for specimen S-CT-E 56
Figure 5.43 Volumetric versus axial strain curves for specimen S-CT-F..... 56
Figure 5.44 Volumetric versus axial strain curves for specimen S-GT-E 56
Figure 5.45 Volumetric versus axial strain curves for specimen S-GT-F 57
Figure 5.46 Specimen R2-0-0 with plain concrete before and after testing 60
Figure 5.47 Specimen R2-C2-0 with 2 CFRP layers before and after testing..... 60
Figure 5.48 Specimen R2-G6-0 with 6 GFRP layers before and after testing 61
Figure 5.49 Specimen R3-0-0 with plain concrete before and after testing 61
Figure 5.50 Specimen R3-C2-0 with 2 CFRP layers before and after testing..... 62
Figure 5.51 Specimen R3-G6-0 with 6 GFRP layers before and after testing 62
Figure 5.52 Stress-strain curves for R2-C2-0 63
Figure 5.53 Stress-strain curves for R2-G6-0 63
Figure 5.54 Stress-strain curves for R3-C2-0 64
Figure 5.55 Stress-strain curves for R3-G6-0 65

Figure 5.56 Stress-strain curves for R2-C2-0 comparing transverse and fiber strains .. 65
Figure 5.57 Stress-strain curves for R3-C2-0 comparing transverse and fiber strains .. 65
Figure 5.58 Stress-strain curves for R3-G6-0 comparing transverse and fiber strains .. 66
Figure 5.59 Fiber strain versus axial strain curves for R2-C2-0 66
Figure 5.60 Fiber strain versus axial strain curves for R3-C2-0 66
Figure 5.61 Fiber strain versus axial strain curves for R3-G6-0 67
Figure 5.62 Volumetric versus axial strain curve for specimen R2-C2-0 67
Figure 5.63 Volumetric versus axial strain curve for specimen R3-C2-0 68
Figure 5.64 Volumetric versus axial strain curve for specimen R3-G6-0 68
Figure 5.65 Comparisons between rectangular R2 and shape-modified specimens 71
Figure 5.66 Comparisons between rectangular R3 and shape-modified specimens 71
Figure 5.67 Specimen R2-CT-E with expansive cement concrete and 2 CFRP layers before and after testing 72
Figure 5.68 Specimen R2-CT-F with non-shrink cement concrete and 2 CFRP layers before and after testing 73
Figure 5.69 Specimen R2-GT-E with expansive cement concrete and 6 GFRP layers before and after testing 73
Figure 5.70 Specimen R2-GT-F with non-shrink cement concrete and 6 GFRP layers after testing 74
Figure 5.71 Specimen R3-CT-E with expansive cement concrete and 2 CFRP layers before and after testing 74
Figure 5.72 Specimen R3-CT-F with non-shrink cement concrete and 2 CFRP layers before and after testing 75
Figure 5.73 Specimen R3-GT-E with expansive cement concrete and 6 GFRP layers before and after testing 75
Figure 5.74 Specimen R3-GT-F with non-shrink cement concrete and 6 GFRP layers before and after testing 76
Figure 5.75 Stress-strain curves for R2-CT-E 77
Figure 5.76 Stress-strain curves for R2-CT-F 77
Figure 5.77 Stress-strain curves for R2-GT-E 77
Figure 5.78 Stress-strain curves for R2-GT-F 78
Figure 5.79 Stress-strain curves for R3-CT-E 78
Figure 5.80 Stress-strain curves for R3-CT-F 78
Figure 5.81 Stress-strain curves for R3-GT-E 79
Figure 5.82 Stress-strain curves for R3-GT-F 79
Figure 5.83 Volumetric versus axial strain curves for specimen R2-CT-E 80
Figure 5.84 Volumetric versus axial strain curves for specimen R2-CT-F 80
Figure 5.85 Volumetric versus axial strain curves for specimen R2-GT-E 80
Figure 5.86 Volumetric versus axial strain curves for specimen R2-GT-F 81
Figure 5.87 Volumetric versus axial strain curves for specimen R3-CT-E 81
Figure 5.88 Volumetric versus axial strain curves for specimen R3-CT-F 81
Figure 5.89 Volumetric versus axial strain curves for specimen R3-GT-E 82
Figure 5.90 Volumetric versus axial strain curves for specimen R3-GT-F 82
Figure 5.91 Locations of ε_{jx} and ε_{jy} for elliptical and rectangular columns 84
Figure 6.1 Comparison of shape factor for different geometries 87
Figure 6.2 Effectively confined area by FRP strips 87

Figure 6.3 Experimental verification of effectively-confined area by FRP strips 88
Figure 6.4 Relation between k_ε and $\frac{r}{L}$ 90
Figure 6.5 Relation between k_ε and the aspect ratio for elliptical bonded FRP jackets 91
Figure 6.6 Typical compressive behavior for circular columns with bonded FRP jackets 94
Figure 6.7 Hoop strain vs. axial strain at plastic zone (3rd phase) for circular columns with bonded FRP jackets 96
Figure 6.8 The relationship between ν_c' and C_e 97
Figure 6.9 Values of β for circular columns with bonded FRP jackets 99
Figure 6.10 Relation between $\frac{f_{cu}'}{f_{cc}'}$ and $\frac{f_{lu}}{f_{co}'}$ for specimens with softening behavior…..... .101
Figure 6.11 Strength enhancement ratio $\frac{f_{cc}'}{f_{co}'}$ vs. effective confinement ratio $\frac{f_{lu}}{f_{co}'}$ ... .102
Figure 6.12 Verification of hardening and softening behavior ..... .102
Figure 6.13 Values of β for square/rectangular columns with bonded FRP jackets. .103
Figure 6.14 Relationship between β and f_{lu} / f_{co}' using circular, square and rectangular columns ..... .104
Figure 6.15 Values of α for columns with expansive concrete and non-bonded FRP jackets ..... .105
Figure 6.16 Relationship between f_{lu} / f_{co}' and α ..... .107
Figure 6.17 Relationship between $\frac{\varepsilon_{jx}}{\varepsilon_{jy}}$ and $\frac{B_j}{D_j}$ for elliptical columns ..... .107
Figure 7.1 Design procedure for circular columns confined by bonded FRP jackets.110
Figure 7.2 Design procedure for square and rectangular columns confined by bonded FRP jackets..... .114
Figure 7.3 Design procedure for elliptical columns confined by bonded FRP jackets ..... .117
Figure 7.4 Calculation of ε_0 for columns with non-bonded jackets and expansive cement concrete ..... .120
Figure 7.5 Design procedure for columns with non- bonded FRP jackets and expansive cement concrete ..... .121
Figure 7.6 Parameters of four-parameter confinement model ..... .124
Figure 7.7 Calculation of f_i and E_p ..... .125
Figure 7.8 Normalized Stress-strain relationships with different values of n ..... .126
Figure 7.9 Comparison between the design-oriented model and experimental results for C-C1-0 ..... .128
Figure 7.10 Comparison between the design-oriented model and experimental results for S-C2-0..... .128

Figure 7.11 Comparison between the design-oriented model and experimental results for R2-C2-0 ..... .128
Figure 8.1 Yield surface of Drucker-Prager model and its cross-section ..... .131
Figure 8.2 Typical elevation of circular model with the FRP jacket ..... .132
Figure 8.3 Typical elevation of the circular FRP jacket ..... .132
Figure 8.4 Typical cross-section of circular model ..... .133
Figure 8.5 Typical elevation of square model with the FRP jacket ..... .133
Figure 8.6 Typical elevation of the square FRP jacket ..... .133
Figure 8.7 Typical cross-section of square model ..... .134
Figure 8.8 Typical elevation of rectangular model with the FRP jacket ..... .134
Figure 8.9 Typical elevation view of the rectangular FRP jacket ..... .134
Figure 8.10 Typical cross-section of rectangular model ..... .135
Figure 8.11 Typical elevation of elliptical model with the FRP jacket ..... .135
Figure 8.12 Typical elevation of the elliptical FRP jacket ..... .135
Figure 8.13 Typical cross-section of elliptical model ..... .136
Figure 8.14 Typical elevation of elliptical model with the FRP jacket and expansive cement concrete ..... .136
Figure 8.15 Typical cross-section of elliptical model with the FRP jacket and expansive cement concrete ..... .137
Figure 8.16 Deformed shape of circular model after axial loading ..... .138
Figure 8.17 Deformed shape of cross section of circular model ..... .138
Figure 8.18 Deformed shape of square model after axial loading ..... .139
Figure 8.19 Deformed shape of cross section of square model ..... .139
Figure 8.20 Deformed shape of rectangular model after axial loading ..... .139
Figure 8.21 Deformed shape of cross section of rectangular model ..... .140
Figure 8.22 Deformed shape of elliptical model after axial loading ..... .140
Figure 8.23 Deformed shape of cross section of elliptical model ..... .140
Figure 8.24 Comparison of FE model with experimental results for C-C1-0 ..... .141
Figure 8.25 Comparison of FE model with experimental results for S-C2-0 ..... .142
Figure 8.26 Comparison of FE model with experimental results for R3-C2-0 ..... .142
Figure 8.27 Comparison of FE model with experimental results for S-CT-E ..... .143
Figure 8.28 Comparison of FE model with experimental results for R3-CT-E ..... .143
Figure 9.1 Strengthening options 1-6 ..... .145
Figure 9.2 Axial stress- axial strain relationships for options 1-6 ..... .146

1. INTRODUCTION

In recent years, Fiber Reinforced Polymer (FRP) composites have emerged as an alternative to traditional materials for strengthening/rehabilitation of existing structures. The light weight of the material, high-strength to weight ratio, corrosion resistance, and high efficiency of construction are among many of the advantages which encourage civil engineers to use this material. FRP composites have been used in the retrofit of bridge columns due to insufficient capacity or displacement ductility. It is a well-established fact that FRP jackets can provide effective lateral confinement to the concrete columns that can substantially enhance their compressive strength and ultimate axial strain. One of the most important problems civil engineers are concerned with is the stress-strain curve for FRP-confined concrete.

Due to the increasing need for repair of structures, research has been carried out to investigate the capacity of FRP-confined concrete columns. Several investigators including Fardis and Khalili (1981), Karbhari and Gao (1997), Mirmiran and Shahawy (1997), Miyauchi et al. (1997), Gergely et al. (1998), Stanton et al. (1998), Spoelstra and Monti (1999), Xiao and Wu (2000), and Moran and Pantelides (2002b) have introduced a series of stress-strain models for concrete confined by FRP jackets. Most of these studies show that the compressive stress-strain behavior of FRP confined concrete cylinders is nonlinear and the initial portion of the stress-strain response typically follows that of the unconfined concrete. Moreover, after reaching the peak unconfined concrete stress level, the response of the FRP-confined concrete is modified. Softening can occur with a localized descending branch that may stabilize as the dilation of the concrete core progresses, or hardening behavior may occur until the FRP composite jacket fails.

Xiao and Wu (2000) introduced a bilinear stress-strain model in which the compressive behavior of the FRP-confined concrete is described in terms of the properties of the concrete core and the confining FRP jacket. Spoelstra and Monti (1999) developed an iterative equilibrium-based stress-strain model in which the behavior of the FRP confined concrete is governed by both the Mander et al. (1988) model for steel confined concrete, and the Pantazopoulou and Mills (1995) constitutive model for concrete. In the Spoelstra and Monti (1999) model, the stress-strain curve of FRP confined concrete is considered to be a curve that crosses a series of Mander's curves, each one pertaining to a certain level of confinement. The same concept was introduced earlier based on energy principles by Gergely et al. (1998).

Small-scale tests performed by Rochette and Labossière (2000) illustrate the effect of rounding the column corners on confinement efficiency. The rounding of corners increased the ultimate strength by 80% compared to square columns without rounding. In addition to higher strengths, higher ultimate compressive strains can be achieved for columns with rounded corners, which is more important for seismic applications. Typical ultimate strain increases range from 200% to 300%. Mirmiran et al. (1998) proposed a modified confinement ratio (MCR) as a function of corner rounding for rectangular columns, and for MCR>0.15 they suggested that the stress-strain model could be predicted by the Samaan et al. model (1999).

Through an extensive experimental investigation on FRP-confined square and circular columns, Pessiki et al. (2001) noted that the cross-section geometry significantly influences the axial behaviour of FRP jacketed columns, and that in-situ jacket strains at rupture are less than

the strain capacity obtained from tests of tensile coupons; therefore, they suggested a jacket efficiency factor to account for both reduced in-situ jacket properties and the effect of strain localization.

In a recent study, Moran and Pantelides (2002a, 2002b) proposed a confinement model, which is based on the concept of a variable strain ductility ratio. They suggested that the compressive behavior of FRP-confined concrete can be separated into a strain-softening and a bilinear strain-hardening component. This model shows good agreement with experimental results for circular columns.

Lam and Teng (2003) presented a simple design-oriented stress-strain model for FRP-confined rectangular columns based on a large database of existing test results and their own tests. In their model they introduced the concept of the equivalent circular column.

Carey and Harries (2003) performed a series FRP-confined concrete test on columns with small, medium and large sizes. They studied the effect of shape, concrete strength, slenderness and "gap" on confinement of the FRP jacket. The confinement model they developed was based on existing strength models and comparisons were made between the different models.

Most of the FRP confinement models mentioned above concern circular sections; moreover, test results are largely based on the standard 6 in.×12 in. concrete cylinder tests. However, for FRP-confined rectangular columns, FRP jackets provide a non-uniform confinement over the cross-section and only a portion of the concrete section is effectively confined. Because of this reason, much less is known about the behavior of FRP-confined rectangular sections. In the most recently published American Concrete Institute 440 Committee (ACI 2002) document there is no model regarding FRP-confined rectangular sections.

Fundamental to the study of FRP-confined rectangular columns is the issue of effectiveness of FRP confinement, which may significantly decrease due to the presence of 90° corners or abrupt change of direction around the perimeter. In general, the effectiveness of confinement increases with the corner radius; however, the rounding of the corners cannot be made in practice as large as ideally desired because of the presence of the hoop steel reinforcement, typically 1.5 -2.5 in. from the exterior concrete surface.

It is obvious that FRP composite jackets subjected to membrane loading are more effective than rectangular column sections having long flat sides. This is because of the predominant bending action. Therefore, one possible way for increasing the effectiveness of FRP-confined rectangular columns is to perform shape-modifications, that is to modify the column section into an elliptical, an oval, or a circular section from a rectangular or square, respectively. Shape modification can be achieved in two ways. One method is to change the rectangular/square section directly to an elliptical/oval/circular one and then wrap the section with FRP composites, although this is hard to realize in practice. Alternatively, a prefabricated elliptical/oval/circular FRP shell may be used as the formwork for casting additional grout around the section to achieve the shape modification; by using expansive cement concrete as the grout, a post-tensioning effect to the FRP-jackets is achieved.

Expansive cement consists of a Portland cement component and a calcium-sulfoaluminate anhydrite component; the hydration of the latter causes expansion. This material has been put into use since 1960 for the purpose of making chemical prestressed concrete. Klein et al. (1961) investigated the properties of expansive cement for chemical prestressing and they found that the factors influencing the magnitude and rate of the expansive reaction include: chemical composition of the components, proportions of the two components in the total cementing material, richness of mix, conditions of curing, and degree of restraint.

Benuska et al. (1971) further studied the curing effects on expansion and mechanical behavior of expansive cement concrete; their experimental tests showed that the expansive cement concrete was very good for prefabricated elements or structural elements and systems in which the optimum amount of prestress required was relatively low.

In the present case, when expansive cement concrete is applied to prefabricated FRP shells, the expansion of the cement grout is restrained by the FRP jacket; the FRP is stressed in tension, thus creating a post-tensioning effect. It is obvious that this post-tensioning effect would increase the confinement behavior of FRP jackets and it changes the confinement action from "passive" to "active".

The technique of shape modification combined with FRP-wrapping and expansive cement concrete is attractive for providing an effective method in the retrofit of rectangular columns. The main purpose of this research is to develop a comprehensive model that will better explain the stress-strain behavior of rectangular/square columns modified with elliptical/circular FRP jackets. In order to achieve this, the following tasks have been performed: (1) Tests of a series of full-size column sections including circular, square, rectangular and elliptical columns with FRP composite jackets, some of which were "chemically" post-tensioned using expansive cement concrete, (2) Development of a finite element model, corresponding to each experimental specimen, and (3) Design and implementation recommendations based on the tests and analyses of the various specimens.

2. OBJECTIVES OF THE RESEARCH

The overall objective of this research is to develop a model for columns confined with FRP composite jackets after shape modification. Specifically the following objectives were set:

1. Perform full-scale laboratory experiments in uniaxial compression of circular, square, rectangular, and elliptical columns wrapped with FRP composites. Compare the performance as a function of column aspect ratio, and the effectiveness of shape modification.

2. Develop a general analytical model to describe the compressive behavior of concrete columns with different types of FRP confinement, in which the application of stay-in-place FRP forms is combined with expansive cement concrete.

3. Develop a finite element model to investigate possible new efficient cross sections with modified geometry.

4. Further develop the new technique of shape modification combined with FRP jackets and establish guidelines for design of FRP jackets for strengthening/retrofit of columns based on an overall comparison of effects such as ease of construction, cost, and other issues.

3. TEST SPECIMENS

3.1 Overview of Test Specimens

The experimental program involved the testing of 30 specimens. All specimens were designed as full-scale models due to the need for testing larger and more realistic column sections. There was no steel reinforcement inside any of the specimens. A number of columns were wrapped with Carbon Fiber Reinforced Polymer (CFRP) composites or Glass Fiber Reinforced Polymer (GFRP) composites to investigate the effect of confinement for different types of FRP composites. The number of plies of FRP material used was chosen so that an approximately equal level of confinement was provided for the CFRP-jacketed and GFRP-jacketed specimens with the same geometry. Three basic geometric types including circular, square and rectangular columns with approximately the same cross-sectional area were studied in this research program. The radius of the 90 degree corners for the square and rectangular columns was designed to be 3/4 in., taking into account the steel tie reinforcement that would have been present at the 90 degree corners. Two methods were considered for achieving the desired geometry for the square/rectangular sections with shape modification: The first was to change the rectangular/square section directly to an elliptical/circular one by using non-shrink cement grout; the form was then removed, and the modified section was wrapped with FRP composite fabrics using a wet lay-up. Alternatively, a prefabricated elliptical/circular FRP shell was used as the stay-in-place formwork for casting additional grout around the section to achieve the shape modification; expansive cement concrete was used as the grout to fill the gap and to provide post-tensioning. The principle of the geometric consideration was to minimize the area inscribing the square/rectangular section. For both cases, a minimum gap size of ¼ in. was adopted to allow unobstructed flow of concrete.

3.2 Material Properties

3.2.1 Concrete

3.2.1.1 Regular concrete

All columns were cast in one batch to eliminate variations between them; 6"x12" and 4"x8" standard cylinders were made along with the column specimens. The compressive strength was obtained from compressive tests of cylinders at 28 days after casting the concrete and at subsequent intervals. The concrete strength versus time relationship is shown in Figure 3.1.

It is seen from Figure 3.1 that the concrete strength increased in the first 6 months; after six months, the strength approached a constant value of 2600 psi.

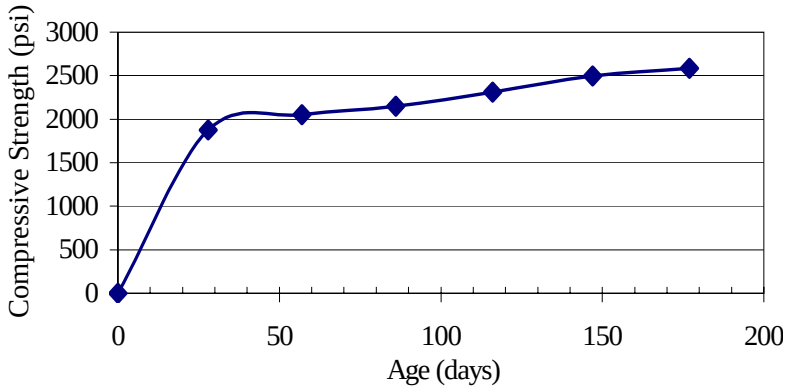

Figure 3.1 Concrete strength vs. aging time

3.2.1.2 Expansive concrete

It is a well-known fact that FRP composite jackets will not participate in the confinement of regular concrete until the concrete starts expanding. One of the advantages of expansive concrete is that it can prestress the FRP composite jacket in the hoop direction even before any vertical compression is applied to the column. In addition, the expansive concrete can participate in the active confinement of the regular concrete column when vertical load is applied.

The expansive cement used for this program was Type-K and Komponent, manufactured by CTS Company. The two principal constituents of Komponent are calcium sulfoaluminate and gypsum (calcium sulfate). The formation of ettringite crystals, which result from hydration of the two ingredients, is what creates the expansion. When expansion is restrained, for example by an FRP composite jacket, expansive cement concrete would induce tensile stress in the FRP composite jackets, that cause chemical “post-tensioning”.

To determine the optimal mixing ratio of Type-K cement and Komponent, a preliminary test was conducted. In this test, four types of expansive cement mixes were investigated:

(1) MIX 1: 100% Expansive Komponent
(2) MIX 2: 75% Expansive Komponent + 25% Portland Cement
(3) MIX 3: 50% Expansive Komponent + 50% Portland Cement
(4) MIX 4: 15% Expansive Komponent + 85% Portland Cement

Different types of concrete were made based on the above mixes and four prefabricated CFRP cylinder shells (6"x12") were filled with the expansive cement grout. Strain gauges were placed at midheight of the cylinders on the FRP in the fiber direction to monitor the hoop expansion history over time. The resulting strain curves are shown in Figure 3.2.

It was found that both mix (2) and mix (3) gave the largest hoop strain for the CFRP jacket compared to the other mixes. Data from compression cylinder tests showed that the 7-day compressive strength of mix (3) was 920 psi compared to 850 psi for mix (2). Mix (3) was selected since it contained less expansive cement. The final mix design, based on mix 3, for the expansive cement grout is shown in Table 3.1. The compressive strength of the expansive cement concrete after 28 days was approximately 1500 psi obtained from compression cylinder

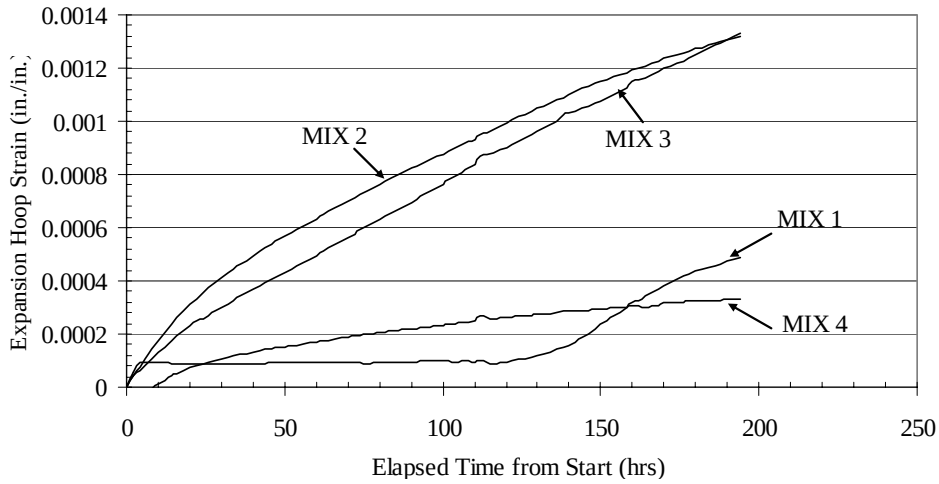

Figure 3.2 Results of preliminary test for expansive cement

Table 3.1 Mix design for expansive concrete grout

Weight & Design Information		Weight (lbs)	Volume (ft^3)
CEMENT	TYPE K EXPANSIVE CEMENT	351	1.79
	KOMPONENT	166	0.84
WATER	VOLUME/WEIGHT	375	6.00
ROCK	ASTM C-33 (SSD) 3/8" PEA GRAVEL	520	3.22
SAND	ASTM C-33 (SSD)	2143	13.26
TOTAL	_	3555	27.00

tests. The restraining effect of the FRP jacket on the expansive concrete compressive strength was considered; cylinders were made by using 1-layer prefabricated CFRP forms and these forms were removed at the time of testing.

Several concrete columns with different cross-sections were cast; these included 12 in. diameter circular columns, 16 in. diameter circular and elliptical (aspect ratio 2:1 and 3:1) columns with CFRP and GFRP jackets. It is noted that for the elliptical columns, the aspect ratio, $\frac{B_j}{D_j}$ is defined as the ratio of the length of the major axis, B_j, to the length of the minor axis, D_j. The columns were cast in the Structures Laboratory at the University of Utah and cured inside the lab at an indoor temperature of 70ºF. The details of construction are given in Chapter 3.3. A data acquisition system was used to monitor the hoop expansion of the FRP composite jacket for each specimen. Figures 3.3(a)-3.3(d) show the hoop expansion strain of the circular and elliptical columns from the day of casting for a period of approximately two months.

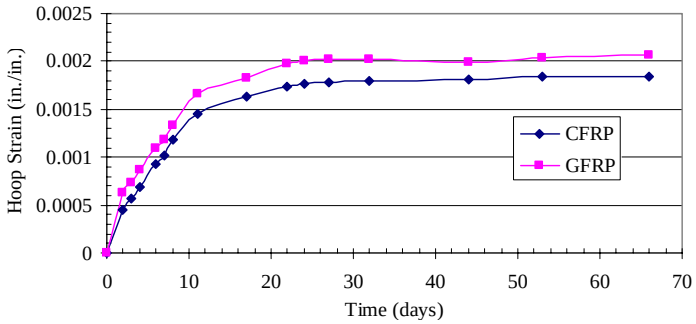

(a)

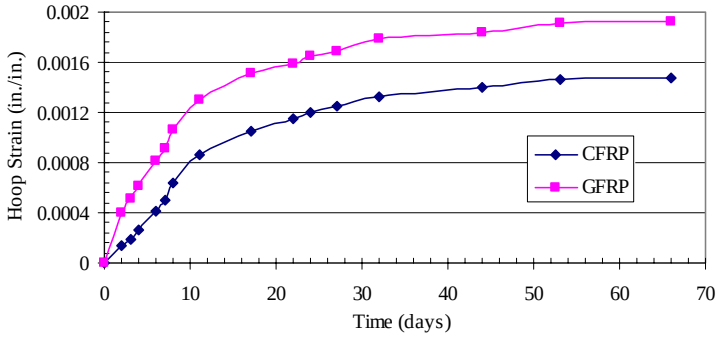

(b)

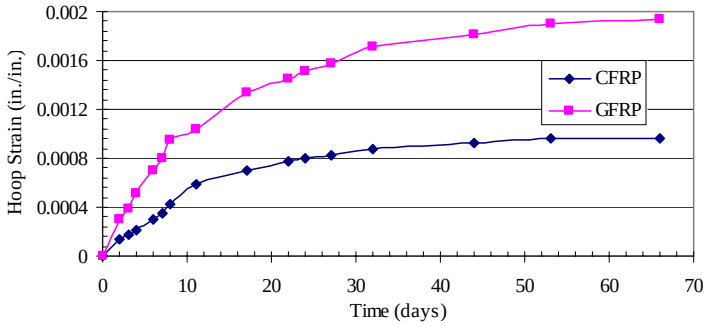

(c)

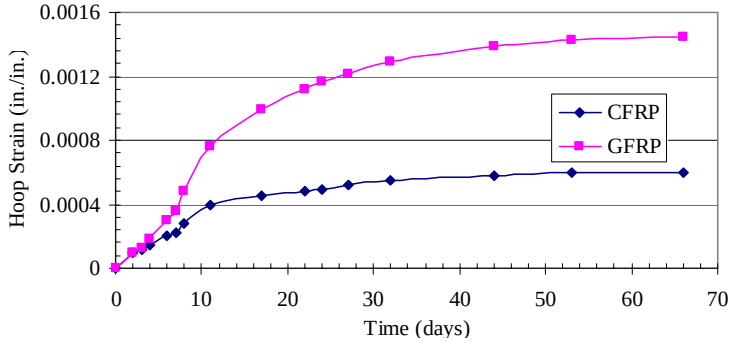

(d)

Figure 3.3 Expansion history for FRP jackets with expansive cement concrete: (a) 12” circular columns; (b) 16” circular columns; (c) 2:1 elliptical columns; (d) 3:1 elliptical columns

It is seen from Figure 3.3 that the hoop strains on the FRP jackets due to the expansion of the expansive grout reached an asymptotic value after 60 days; this strain is defined as the initial hoop strain, $\varepsilon_{j,ini}$ which refers to the state before the axial load is applied. Table 3.2 lists the values of $\varepsilon_{j,ini}$ for different types of columns.

Table 3.2 Experimental results for $\varepsilon_{j,ini}$

Column type*	B_j / D_j	FRP type	$\varepsilon_{j,ini}$ (in./in.)
12” circular	1:1	CFRP (1 Layer)	0.0018
12” circular	1:1	GFRP (3 Layers)	0.0022
16” circular	1:1	CFRP (2 Layers)	0.0015
16” circular	1:1	GFRP (6 Layers)	0.0020
elliptical	2:1	CFRP (2 Layers)	0.0010
elliptical	2:1	GFRP (6 Layers)	0.0018
elliptical	3:1	CFRP (2 Layers)	0.0006
elliptical	3:1	GFRP (6 Layers)	0.0015

* Details of column geometries are presented in Figures 3.4-3.7.

The initial hoop strain $\varepsilon_{j,ini}$ is dependent on the shape and stiffness of the prefabricated FRP jackets. In general, the circular jackets would achieve the highest expansion while the elliptical jacket with the highest aspect ratio had the smallest expansion. Also, the GFRP jackets would obtain a higher expansion compared to the CFRP jackets. These observations can be visualized from Figure 3.4 for the relationship between $\varepsilon_{j,ini}$ and the aspect ratio $\frac{B_j}{D_j}$.

From Figure 3.4, the proposed relationship between $\varepsilon_{j,ini}$ and $\frac{B_j}{D_j}$ for the CFRP jackets is:

$$\varepsilon_{j,ini} = 0.0020 - 0.00041\left(\frac{B_j}{D_j}\right) \tag{3.1}$$

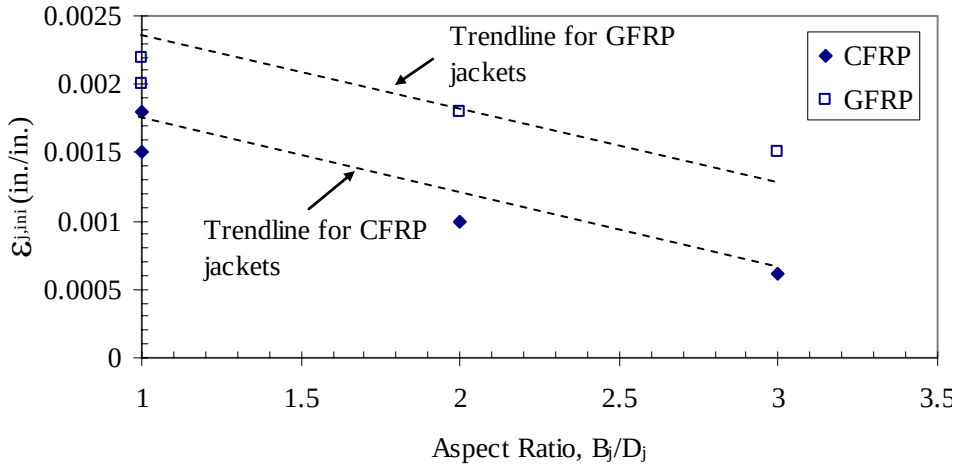

Figure 3.4 Effect of aspect ratio on initial hoop strain, $\varepsilon_{j,ini}$

and for GFRP jackets, it is:

$$\varepsilon_{j,ini} = 0.0025 - 0.00041\left(\frac{B_j}{D_j}\right) \tag{3.2}$$

3.2.1.3 Non-shrinkage concrete

As an alternative to expansive cement, a shrinkage compensated cement was also used to compare the differences between the expansive cement FRP jackets and the non-shrinkage FRP jackets. In this case, the non-shrinkage grout was used to modify the rectangular/square sections to elliptical/circular sections. Once aging of concrete was sufficient, FRP jackets were wrapped around the modified cross-section using a wet layup. A structural grout, *SikaGrout 212* was selected as the grout to make non-shrink concrete. The mix ratio was designed to be: *SikaGrout* 212 : Water : Fine aggregate = 2 : 0.5 :1. The compressive strength of non-shrink concrete after 28 days was obtained from cylinder compression tests as 2200 psi.

3.2.2 Fiber Reinforced Polymer (FRP) Composites

Two FRP composite materials were used to confine the concrete columns. One was *SikaWrap Hex 103C* by Sika Company, which is a high strength, unidirectional carbon fiber fabric with epoxy resin. The other was Aquawrap G-06 by Airlogistics Company, which is a unidirectional pre-impregnated glass fiber fabric. The main material properties determined at the University of Utah are shown in Table 3.3:

Table 3.3 Material properties of CFRP and GFRP composites*

FRP Composite	Tensile Strength (ksi)	Tensile Modulus (Msi)	Tensile Strain (%)	Ply Thickness (in.)
CFRP	177	12.6	1.4	0.038
GFRP	33	2.45	1.4	0.064

*Determined at University of Utah, following ASTM D3039 after curing at room temperature.

3.3 Construction of Specimens and Sample Preparation

In all, the program involved the testing of 30 specimens. All specimens had almost the same area prior to shape modification and the same height of 3 ft. Thus, comparisons could be made for different cross-sections and aspect ratios. Molds for specimens were made out of plywood and sonatubes as shown in Figure 3.5.

In addition, both CFRP and GFRP confined specimens were tested and compared with concrete baseline specimens without FRP composites. A breakdown of the test matrix is presented in Tables 3.4-3.7. Figures 3.6 (a)-3.6 (d) show the details of the wrapping methods for all specimens.

Specimens were labeled with the following notation:

W-XY-Z

W: a letter "C", "S", "R1" or "R2" representing the geometry of cross-section: "C" means circular cross-section; "S" means square cross-section; "R2" and "R3" correspond to the rectangular cross-section with an aspect ratio of 2:1 and 3:1, respectively. As for shape-modified specimens, this letter is referred to as the geometry of the cross-section before shape modification;
X: "C" denotes a CFRP jacket, "G" denotes a GFRP jacket and "0" denotes no FRP jacket or plain concrete;
Y: "T" denotes a shape-modified specimen, an Arabic number indicates the layers of FRP for specimen without shape modification and "S" denotes FRP strips;
Z: "0" means no shape modification; As for shape-modified specimens, "E" indicates the use of expansive cement grout while "F" indicates non-shrink grout.

For wrapping with wet-layup, regardless of the number of layers, the entire bonded jackets were made of one continuous sheet of FRP fabric that was cut to the proper length and width. An additional 6" of overlap splice was provided horizontally.

To make expansive cement concrete specimens, the following steps were followed:

(a) Prepare circular/elliptical forms (Figure 3.7(a)).
(b) Build 1st layer of FRP shell and cut the shell into two halves (Figure 3.7(b)).
(c) Make stay-in-place FRP forms by lap splicing with one FRP layer and apply the other remaining layers (Figure 3.7(c)).

(d) Cast expansive cement concrete in the gap between the original concrete column and FRP shell (Figure 3.7(d)).

Figure 3.5 Molds used for preparation of concrete column specimens

Table 3.4 Matrix of test specimens: circular columns

NO.	COLUMN DESIGNATION	INITIAL TYPE	LENGTH	INITIAL SIZE	FRP TYPE	Note
1	C-0-0	Circular	36"	12" Dia.	None	
2	C-C1-0	Circular	36"	12" Dia.	Carbon 1 Layer	
3	C-G3-0	Circular	36"	12" Dia.	Glass 3 Layers	
4	C-CT-E	Circular	36"	12" Dia.	Carbon Fiber Tube (1 Layer)	Use expansive concrete
5	C-GT-E	Circular	36"	12" Dia.	Glass Fiber Tube (3 Layers)	Use expansive concrete
6	C-CS-0	Circular	36"	12" Dia.	Carbon Fiber Strips	2 Layers of CFRP
7	C-GS-0	Circular	36"	12" Dia.	Glass Fiber Strips	6 Layers of GFRP

Table 3.5 Matrix of test specimens: square columns

NO.	COLUMN DESIGNATION	INITIAL TYPE	LENGTH	INITIAL SIZE	FRP TYPE	Note
8	S-0-0	Square	36"	11" x 11"	None	
9	S-C2-0	Square	36"	11" x 11"	Carbon 2 Layers	3/4" rounding at 90 degree corners
10	S-CT-F	Square	36"	11" x 11"	Carbon 2 Layers	To be modified to 16in. dia. circular using non-shrink concrete
11	S-G6-0	Square	36"	11" x 11"	Glass 6 Layers	3/4" rounding at 90 degree corners
12	S-GT-F	Square	36"	11" x 11"	Glass 6 Layers	To be modified to 16in. dia. circular using non-shrink concrete
13	S-CT-E	Square	36"	11" x 11"	Carbon Fiber Tube (2 Layers)	To be modified to 16in. dia. circular using expansive concrete
14	S-GT-E	Square	36"	11" x 11"	Glass Fiber Tube (6 Layers)	To be modified to 16in. dia. circular using expansive concrete
15	S-CS-0	Square	36"	11" x 11"	Carbon Fiber Strips	3/4" rounding; 3 Layers of CFRP
16	S-GS-0	Square	36"	11" x 11"	Glass Fiber Strips	3/4" rounding; 9 Layers of GFRP

Table 3.6 Matrix of test specimens: rectangular columns (1)

NO.	COLUMN DESIGNATION	INITIAL TYPE	LENGTH	INITIAL SIZE	FRP TYPE	Note
17	R2-0-0	Rectangular	36"	8 " x 15"	None	
18	R2-C2-0	Rectangular	36"	8 " x 15"	Carbon 2 Layers	3/4" rounding at 90 degree corners
19	R2-CT-F	Rectangular	36"	8 " x 15"	Carbon 2 Layers	To be modified to elliptical using non-shrink concrete
20	R2-G6-0	Rectangular	36"	8 " x 15"	Glass 6 Layers	3/4" rounding at 90 degree corners
21	R2-GT-F	Rectangular	36"	8 " x 15"	Glass 6 Layers	To be modified to elliptical using non-shrink concrete
22	R2-CT-E	Rectangular	36"	8 " x 15"	Carbon Fiber Tube (2 Layers)	To be modified to elliptical using expansive concrete
23	R2-GT-E	Rectangular	36"	8 " x 15"	Glass Fiber Tube (6 Layers)	To be modified to elliptical using expansive concrete

Note: The geometries of shape modified section are shown in Figure 3.6 (c).

Table 3.7 Matrix of test specimens: rectangular columns (2)

NO.	COLUMN DESIGNATION	INITIAL TYPE	LENGTH	INITIAL SIZE	FRP TYPE	Note
24	R3-0-0	Rectangular	36"	6"x18"	None	
25	R3-C2-0	Rectangular	36"	6"x18"	Carbon 2 Layers	3/4" rounding at 90 degree corners
26	R3-CT-F	Rectangular	36"	6"x18"	Carbon 2 Layers	To be modified to elliptical using non-shrink concrete
27	R3-G6-0	Rectangular	36"	6"x18"	Glass 6 Layers	3/4" rounding at 90 degree corners
28	R3-GT-F	Rectangular	36"	6"x18"	Glass 6 Layers	To be modified to elliptical using non-shrink concrete
29	R3-CT-E	Rectangular	36"	6"x18"	Carbon Fiber Tube (2 Layers)	To be modified to elliptical using expansive concrete
30	R3-GT-E	Rectangular	36"	6"x18"	Glass Fiber Tube (6 Layers)	To be modified to elliptical using expansive concrete

Note: The geometries of shape modified section are shown in Figure 3.6 (d).

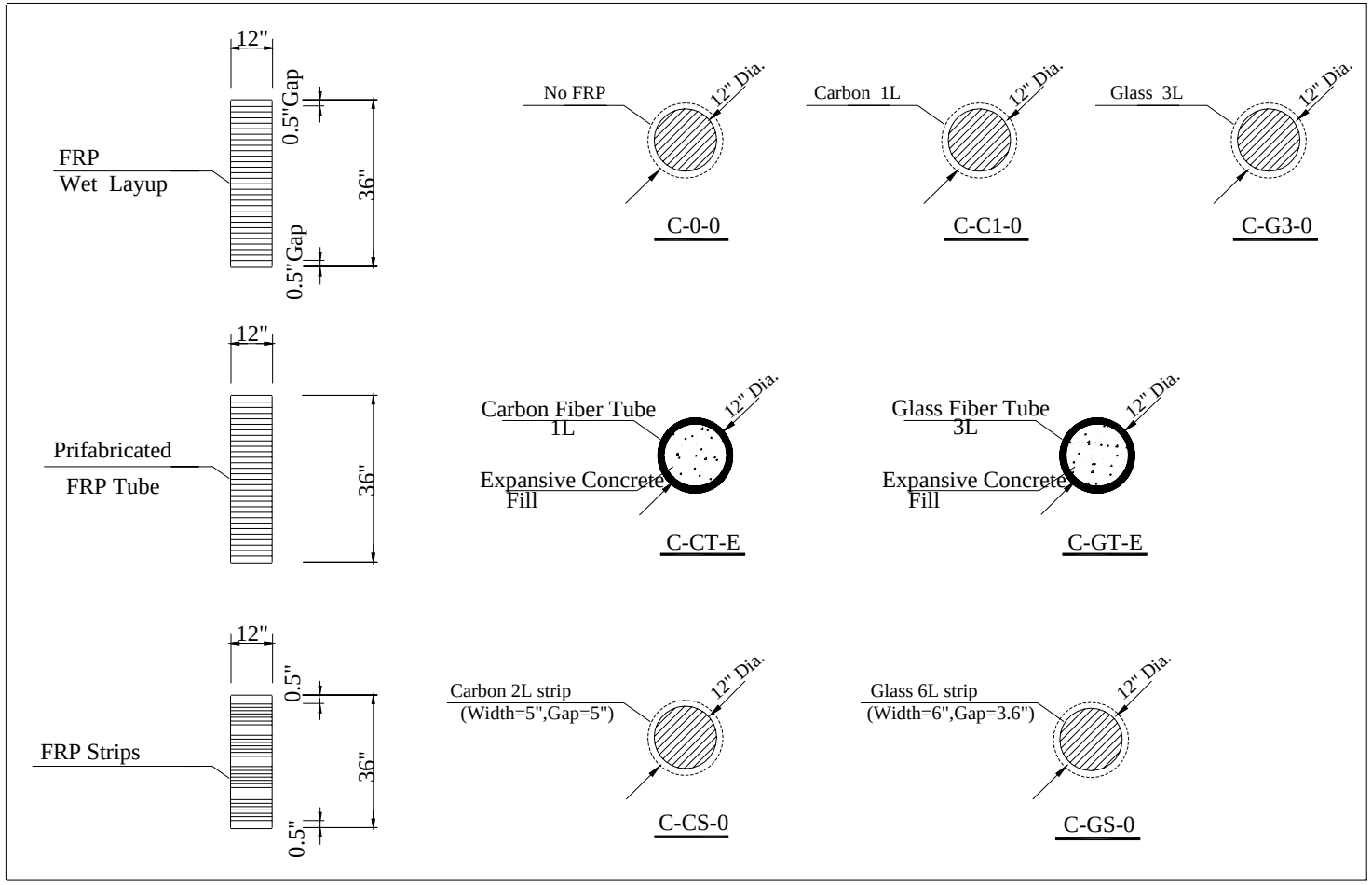

Figure 3.6(a) Wrapping methods for circular columns

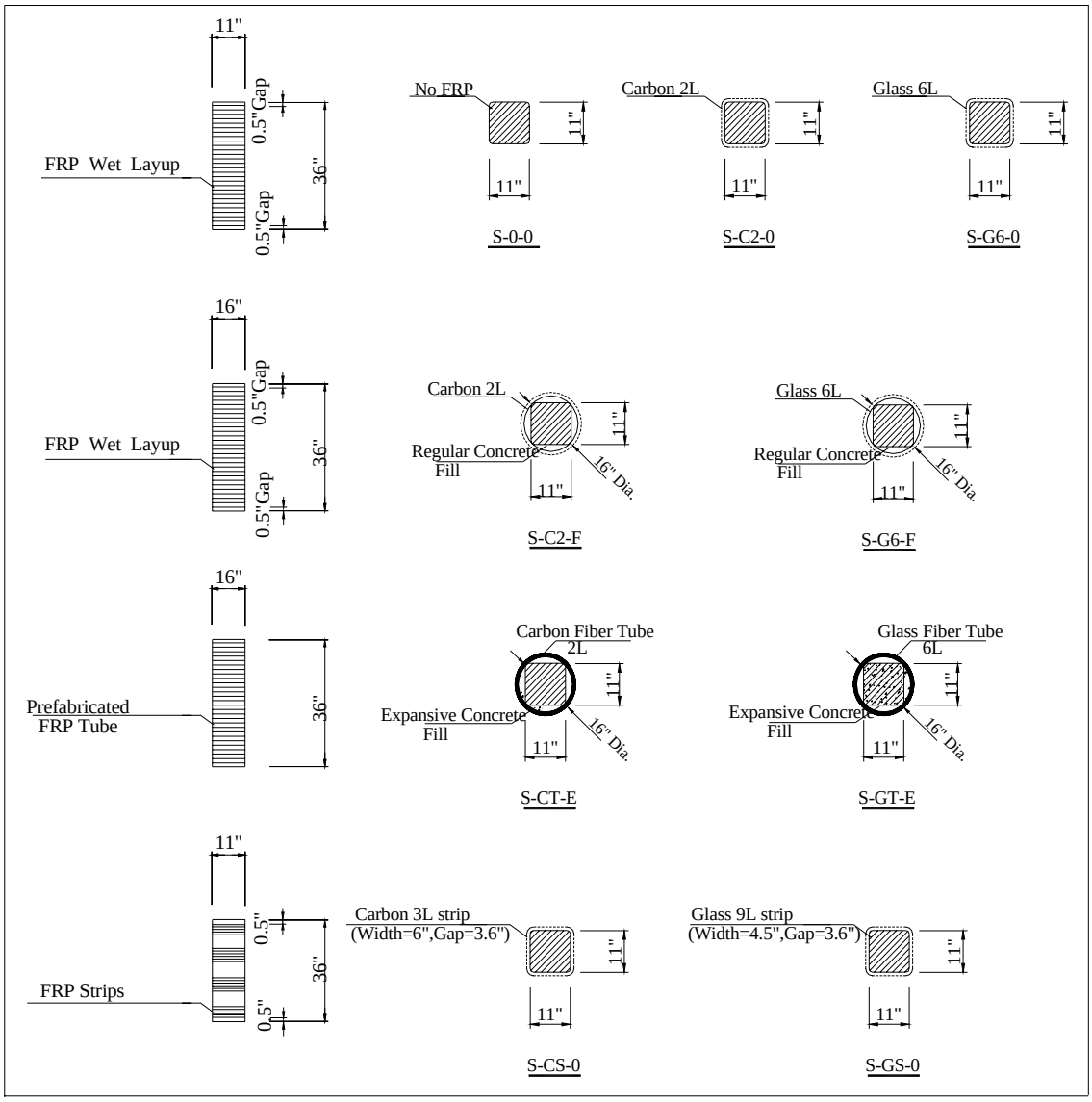

Figure 3.6(b) Wrapping methods for square columns

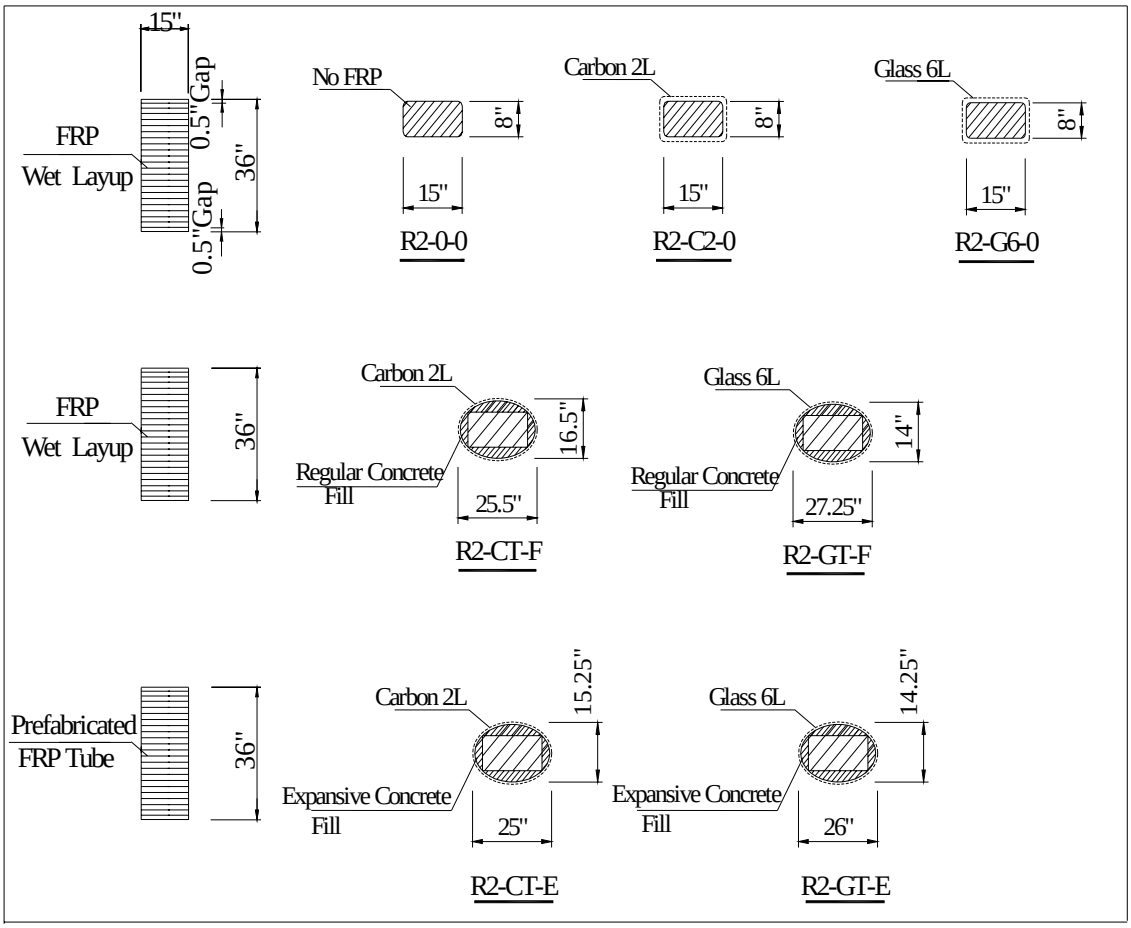

Figure 3.6(c) Wrapping methods for rectangular columns (1)

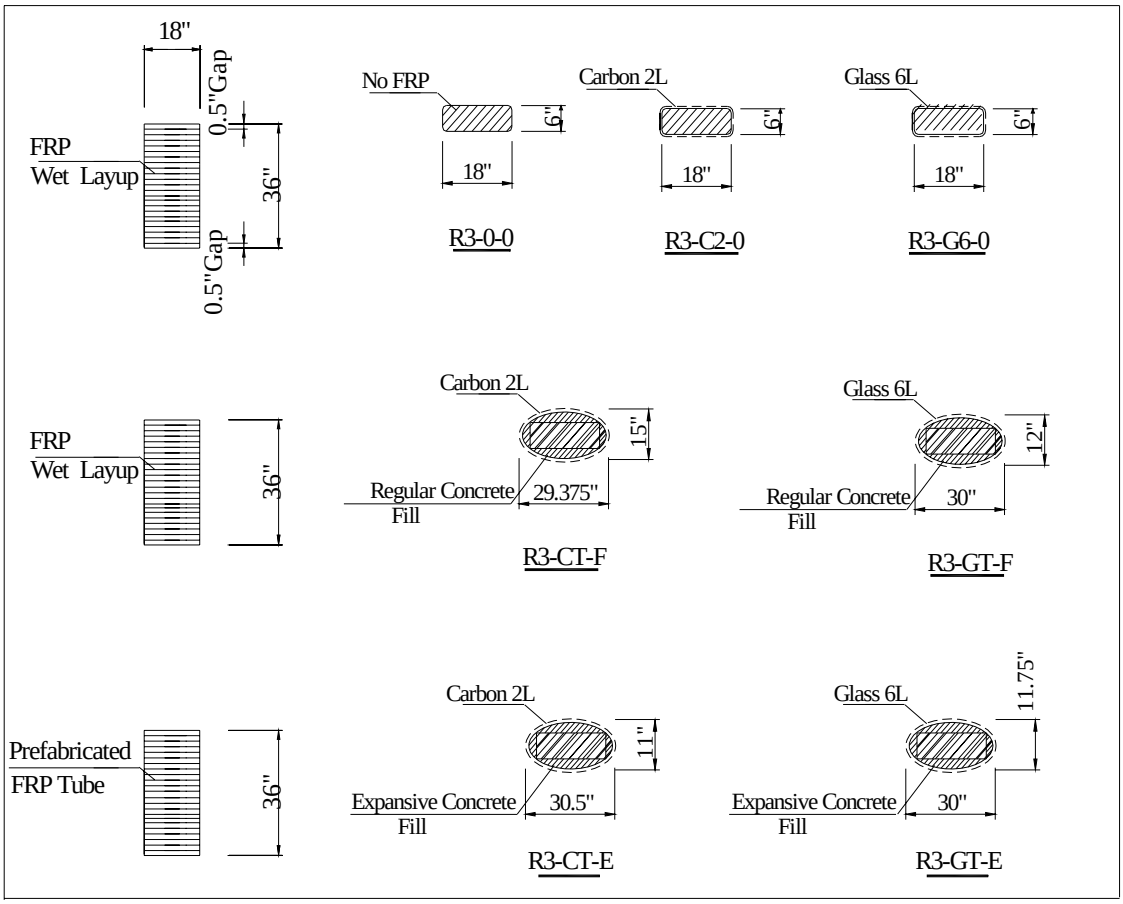

Figure 3.6(d) Wrapping methods for rectangular columns (2)

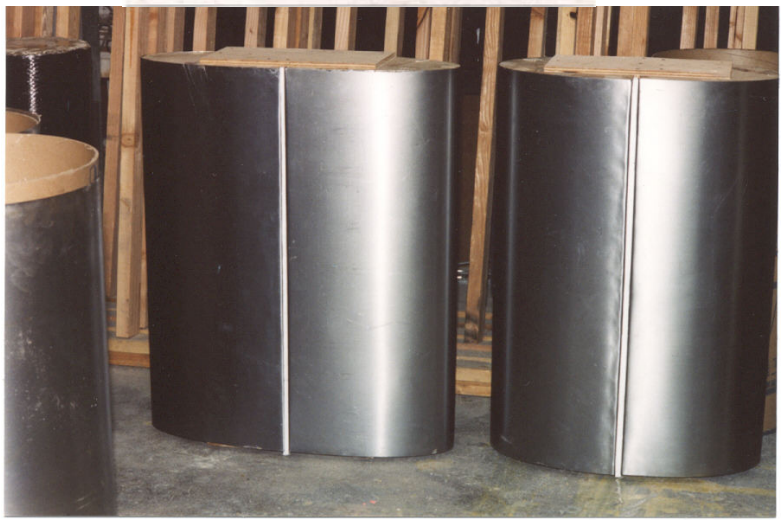

Figure 3.7(a) Preparation of circular/elliptical forms (1st step)

Figure 3.7(b) One-layer FRP shell cut in two halves (2nd step)

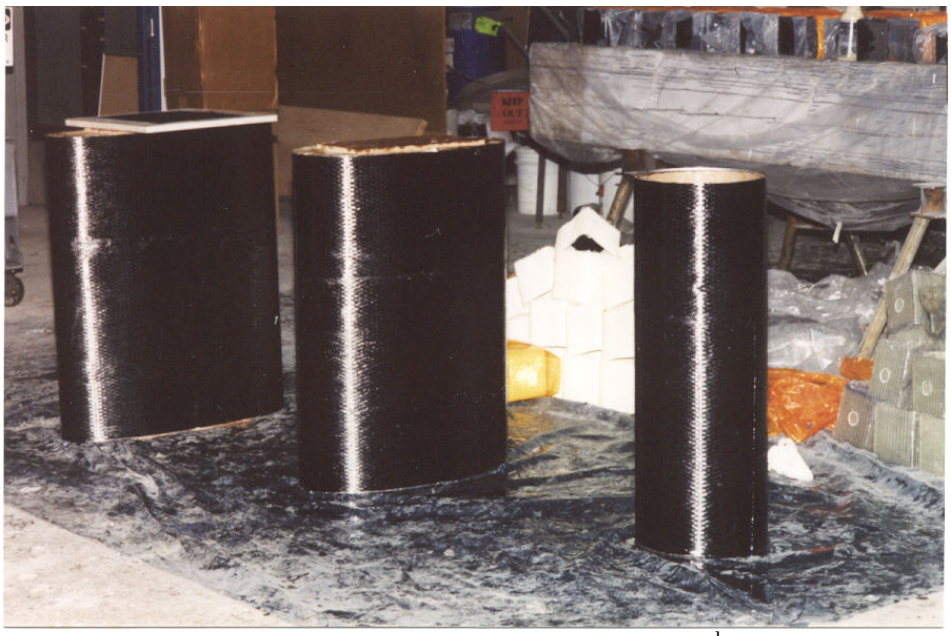

Figure 3.7(c) Stay-in-place FRP forms (3rd step)

Figure 3.7(d) Casting of expansive cement concrete (4th step)

4. TEST SETUP

4.1 Instrumentation

4.1.1 Strain gauges

The strain gauges employed in this testing program were manufactured by Measurements Group, Inc. with model designation as EA-06-125BZ-350. The resistance of these gauges at normal temperature (75°F) is 350 ohms. In order to measure the transverse strain on the FRP jacket during loading, strain gauges were placed on fibers in the hoop direction, at mid-height of the specimens. Special care was taken during the installation to avoid damage of the strain gauges. Considering the geometry of the cross sections, the layout of strain gauges was set in different ways. Figures 4.1 and 4.2 give the location of strain gauges for each geometry shape.

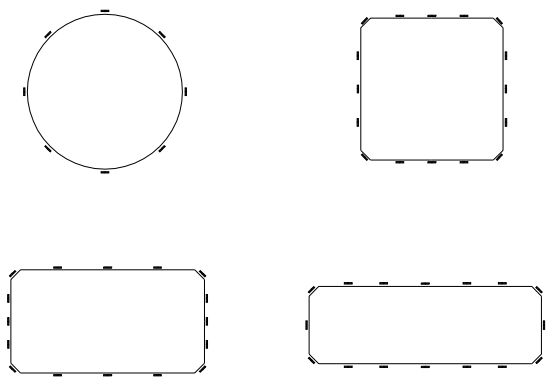

Figure 4.1 Layout of strain gauges for regular sections

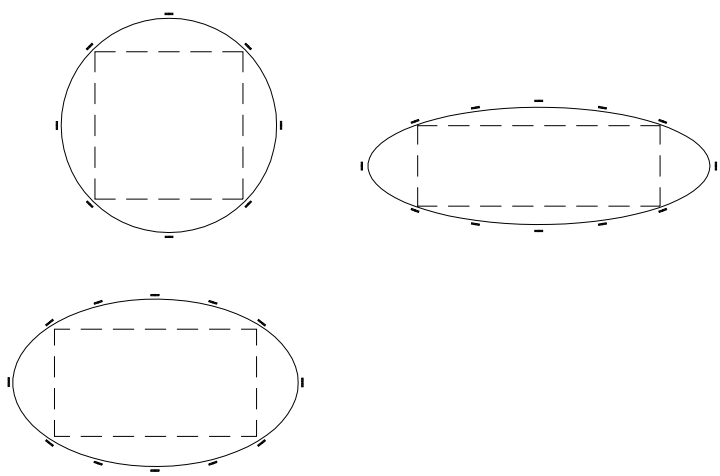

Figure 4.2 Layout of strain gauges for shape-modified sections

4.1.2 LVDT instrumentation

Linear Variable Differential Transducers (LVDTs) are used to measure average strains when the use of strain gauges is not possible or convenient. In the present tests, LVDTs were employed to measure the vertical and lateral strains; the LVDT data could be used to calculate the average axial and transverse strains over the column height and width. LVDTs were installed using aluminum angles with threaded rods at their ends; the angles were solidly clamped to the specimen for accurate readings. Figure 4.3 shows the LVDT configuration. Two types of LVDTs were used: MVL7C and MVL7, manufactured by Sensotec Company; they can measure a displacement in the range of ±0.500 in. and ±2.000 in. respectively, with high accuracy.

For the square and rectangular columns, additional LVDTs were installed on the two sides of the cross-section to measure the transverse strain in both directions, as shown in Figure 4.4.

4.2 Loading Apparatus

The specimens were tested at the University of Utah structural load frame. The actuator employed in this testing program was manufactured by Geneva Hydraulics, Inc. It can impose a compression load up to 2000 kips and is capable of a 24 in. stroke. Figure 4.5 illustrates the setup of the column compression tests. All the specimens were loaded monotonically under a displacement control mode with a constant loading rate of 0.05 in. per minute.

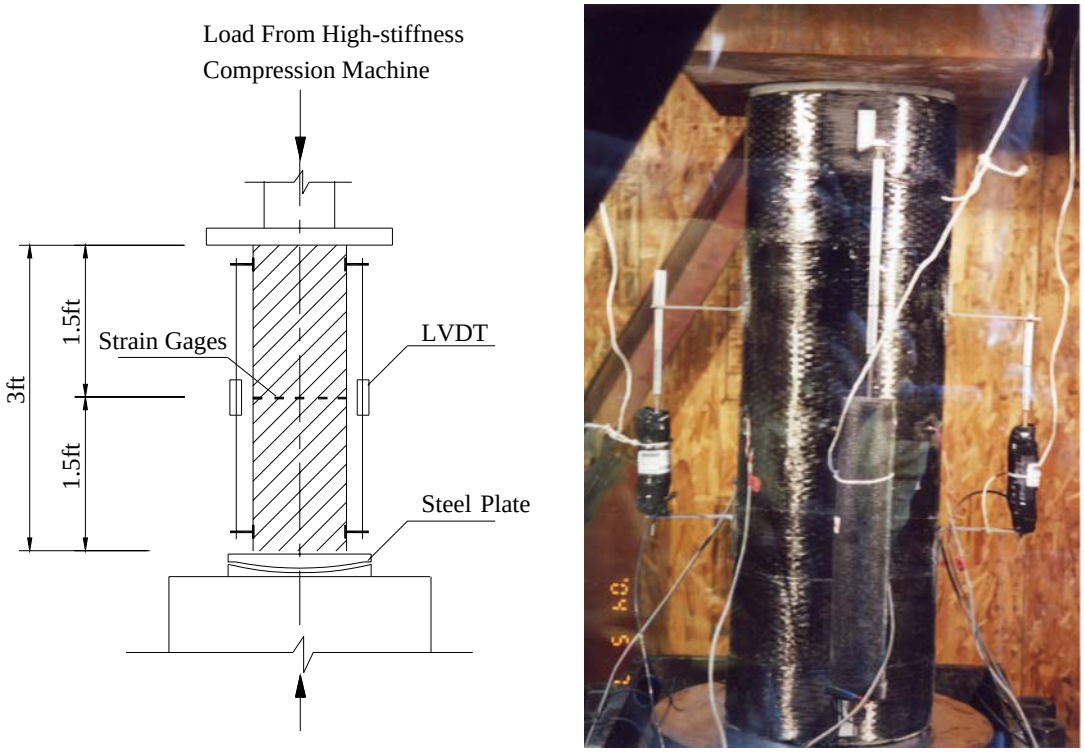

Figure 4.3 Column specimen setup

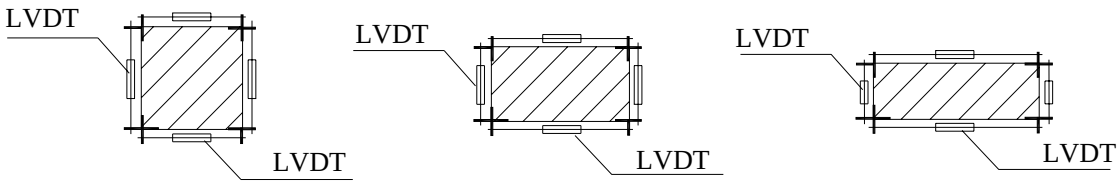

Figure 4.4 Additional LVDTs for square and rectangular columns

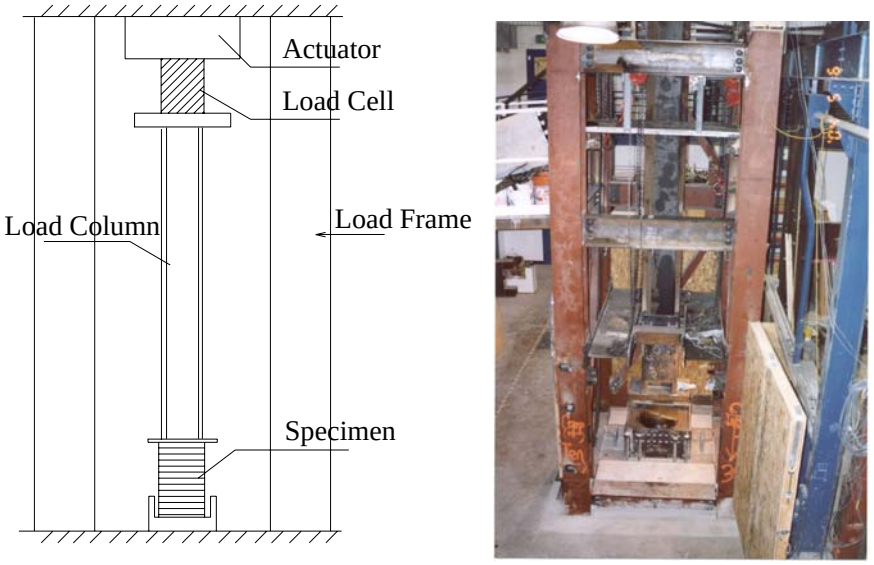

Figure 4.5 Setup of the column compression tests

4.3 Data Acquisition System

A data acquisition system was used to record the values of strains, load cell readings, actuator stroke, and LVDT deformations. The data acquisition system used in this testing program consisted of WIN5100 scanners, manufactured by th Measurements Group, with interface cards, and the *Strainsmart* software. The scanners can read electrical signals from the sensors and send this information to the computer via the interface cards. The software then converts these signals into the desired digital output. Prior to the start of testing, a configuration file had to be written in the software to assign the measured quantities to input and output channels. In addition, the calibration values of strain gauges and LVDTs were input into this configuration file. After the setup of the configuration file and immediately before testing, all the initial values were set to zero to prepare for recording. During the test, data was recorded at an interval of 0.3 seconds in the data acquisition system. Figure 4.6 shows the data acquisition and MTS system during testing.

Figure 4.6 Data acquisition and MTS system during testing

5. EXPERIMENTAL RESULTS AND DISCUSSION

5.1 General

This chapter presents experimental results for specimens described in Chapter 4. Chapter 5.2 presents the results and observations during the course of testing for circular specimens. The detailed results for square, 2:1 rectangular and 3:1 rectangular specimens along with their shape modified specimens are reported in Chapter 5.3 and 5.4. Notations reported in this chapter are summarized in Chapter 5.5. The parameters regarding stress and strain for different confinement behavior in this chapter are defined in what follows and some parameters are shown in Figure 5.1:

In Figure 5.1 (a): f_{co}' = axial strength of unconfined (baseline) concrete; ε_{co}' = axial strain corresponding to f_{co}' for unconfined (baseline) concrete.

In Figure 5.1 (b): f_{cc}' = maximum axial strength of heavily FRP-confined concrete; ε_{cc}' = axial strain corresponding to f_{cc}' for FRP-confined concrete; ε_0 = axial strain corresponding to

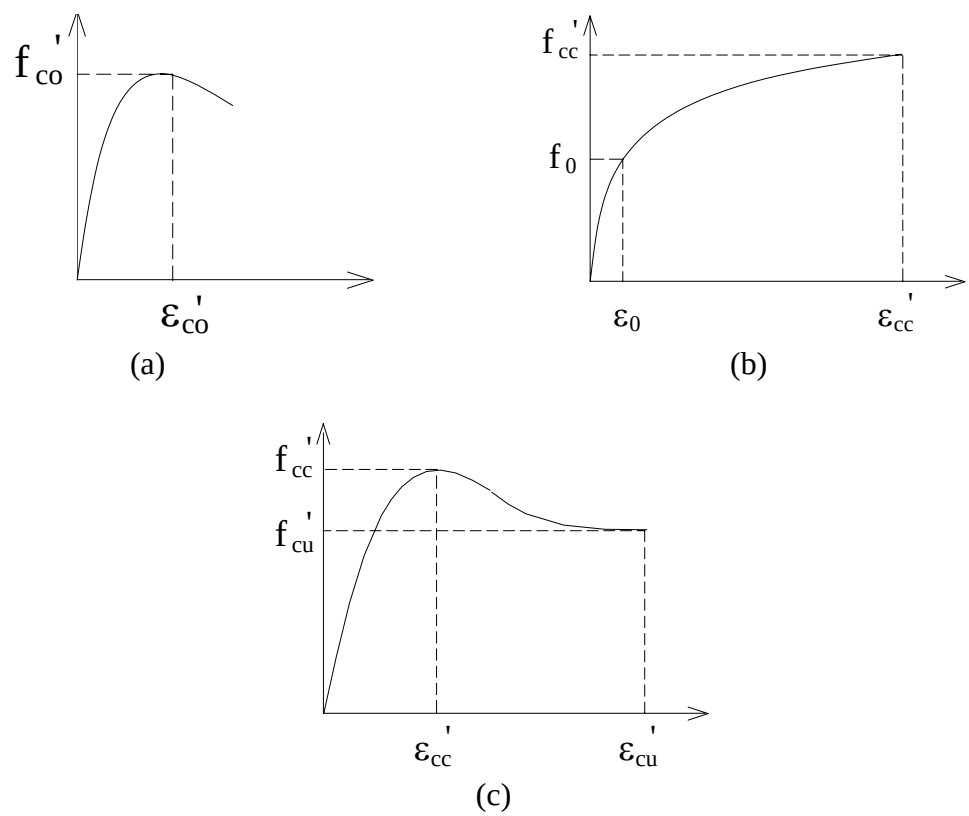

Figure 5.1 Definition of stress and strain parameters:
(a) unconfined specimen; (b) specimens with hardening behavior;
(c) specimens with softening behavior

the zero volumetric strain; f_0: axial stress corresponding to ε_0.

In Figure 5.1 (c): $f_{cu}^{'}$ = ultimate axial strength of FRP-confined concrete; this mainly applies to moderately or lightly confined specimens with post-peak softening behavior. The ultimate axial strain in specimens with post-peak softening behavior is $\varepsilon_{cu}^{'}$ and the corresponding axial strength is $f_{cu}^{'}$.

5.2 Circular Specimens

5.2.1 Specimens with regular concrete

Five circular specimens with regular concrete were tested. For the plain concrete specimen, C-0-0, very little post-peak behavior was observed after the compressive strength reached its maximal value; the specimen failed in a typical shear compression failure plane as shown in Figure 5.2, with the vertical shear cracks extending over the height of the specimen. Compared with the baseline specimen, all of the FRP strengthened specimens showed significant increases in axial strength and axial strain capacity. As seen in Table 5.1, the increase in ultimate strength ranges from 163 to 272 percent. In addition, FRP composite jackets improved the confinement of the specimens which resulted in a significant increase in axial strain capacity as presented in Table 5.1; the increase in ultimate strain ranged from 755 to 1055 percent.

Figure 5.2 Specimen C-0-0 with plain concrete before and after testing

Table 5.1 Main results of circular specimen tests with regular concrete

Specimen ID.	ρ_{FRP}	$f_{cc}'^{*}$ (psi)	f_{cc}'/f_{co}'	$\varepsilon_{cc}'^{**}$ (in./in.)	$\varepsilon_{cc}'/\varepsilon_{co}'$	ε_{ju} (in./in.)	$\varepsilon_{ju}/\varepsilon_f$	μ
C-0-0	-	2200	1.00	0.0020	1.00	-	-	0.94
C-CS-0	0.0133	3588	1.63	0.0167	8.35	0.0078	0.56	1.34
C-GS-0	0.0556	4529	2.06	0.0171	8.55	0.0100	0.71	1.42
C-C1-0	0.0133	5489	2.50	0.0151	7.55	0.0110	0.79	1.39
C-G3-0	0.0640	5982	2.72	0.0211	10.55	0.0150	0.95	1.5

* For C-0-0, f_{co}' applies.

** For C-0-0, ε_{co}' applies.

where ρ_{FRP} = FRP volumetric ratio; ε_{ju} = ultimate hoop strain on FRP jackets; μ = ductility ratio, as defined in Eq. (5.1).

The governing failure mode of the FRP composite was determined by the mechanical properties of the FRP composite material and the reinforcement scheme. Figures 5.3-5.6 show the specimens before and after testing.

Figure 5.3 Specimen C-CS-0 with 2 layers of CFRP strips before and after testing

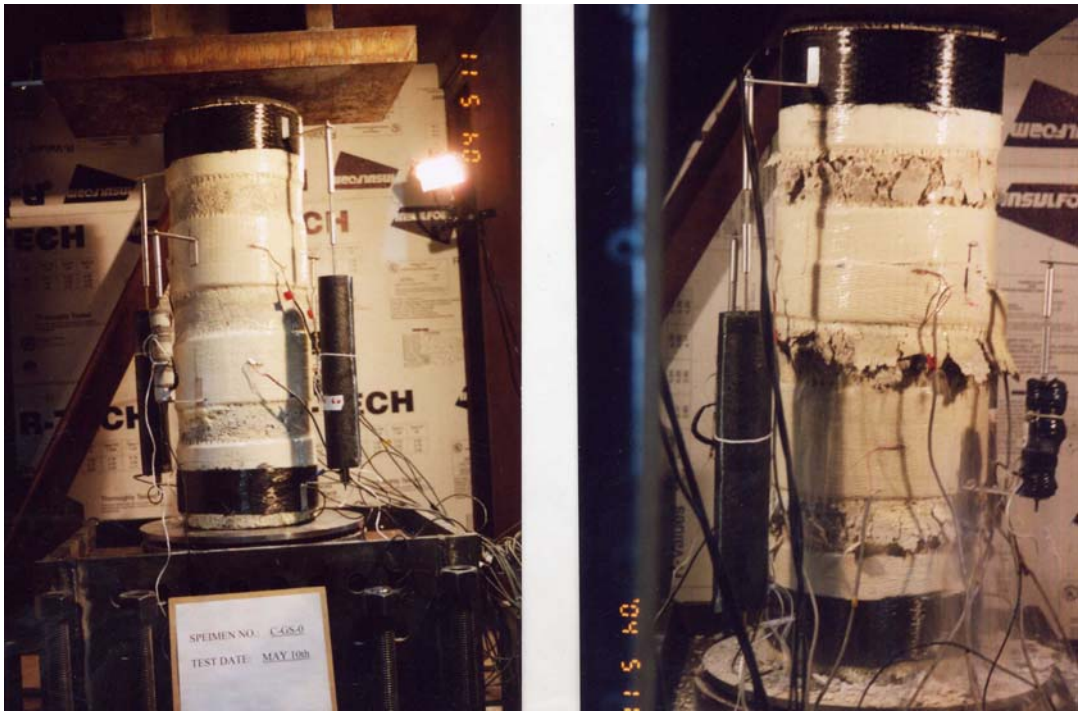

Figure 5.4 Specimen C-GS-0 with 5 layers of GFRP strips before and after testing

Figure 5.5 Specimen C-C1-0 with 1 continuous CFRP layer before and after testing

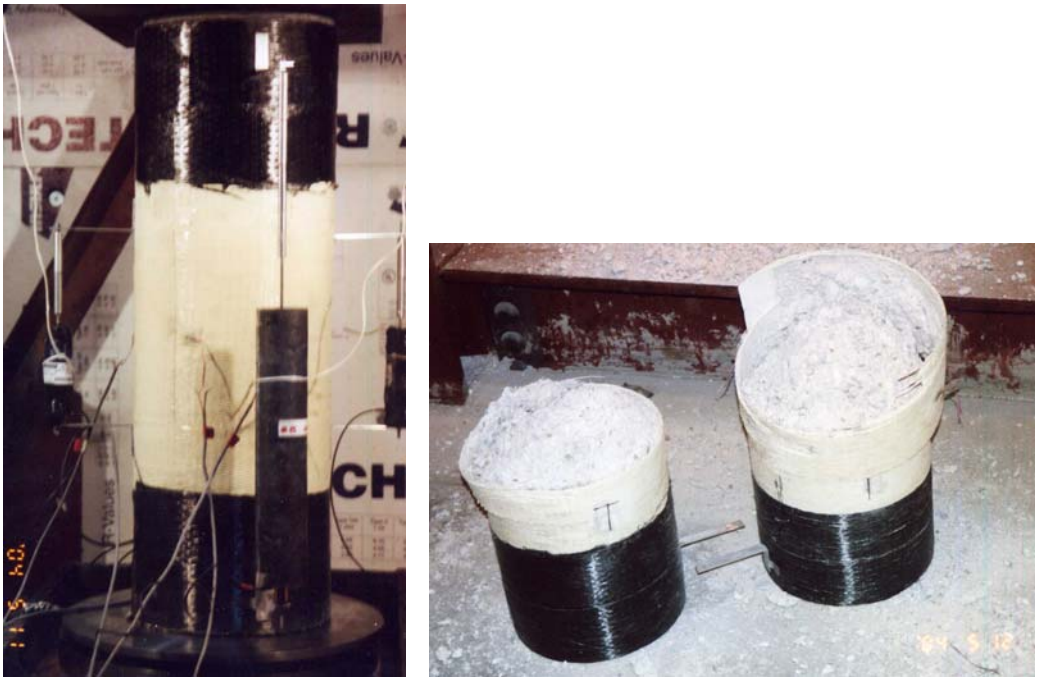

Figure 5.6 Specimen C-G3-0 with 3 continuous GFRP layers before and after testing

In this group of specimens, due to the high confinement provided by circular FRP jackets, the failure modes were consistent and occurred suddenly in an explosive manner. It was observed from the tests that the most typical failure mechanism for FRP-confined circular specimens with regular concrete was crushing of concrete, followed by the tensile failure of the FRP in the hoop direction at or near the mid-height of the specimens. Figure 5.7 shows the typical failure cone after testing. In addition, an FRP band or ring was typically formed as a result of the shearing off and separation of the fabric in the hoop direction. It is also observed from the tests that GFRP-jacketed specimens failed in a more ductile manner than CFRP-jacketed specimens. Progressive cracking sounds were heard during the tests for GFRP specimens before failure, showing a more controlled or progressive failure than that observed, for CFRP-jacketed specimens.

The stress-strain curves for the regular concrete specimens of Table 5.1 are shown in Figure 5.8. Each stress-strain curve for specimens confined with FRP composites shows an ascending branch; this is due to the increased confinement action of the elastic FRP jacket which limits the lateral dilation of concrete for circular sections.

In addition to the increased axial strength capacity, the axial strain capacity is increased as a result of the greater ability to postpone unrestrained concrete cracking, which is provided by the confining effect of the FRP composite jacket. The ductility of FRP-confined concrete specimens can be described by using the principle of energy absorption by comparing the area under the stress-strain curves. The ductility ratio, μ, is defined as the ratio of the area under the stress-strain curve to the total area bounded by the slope of constant elastic stiffness and the plastic plateau:

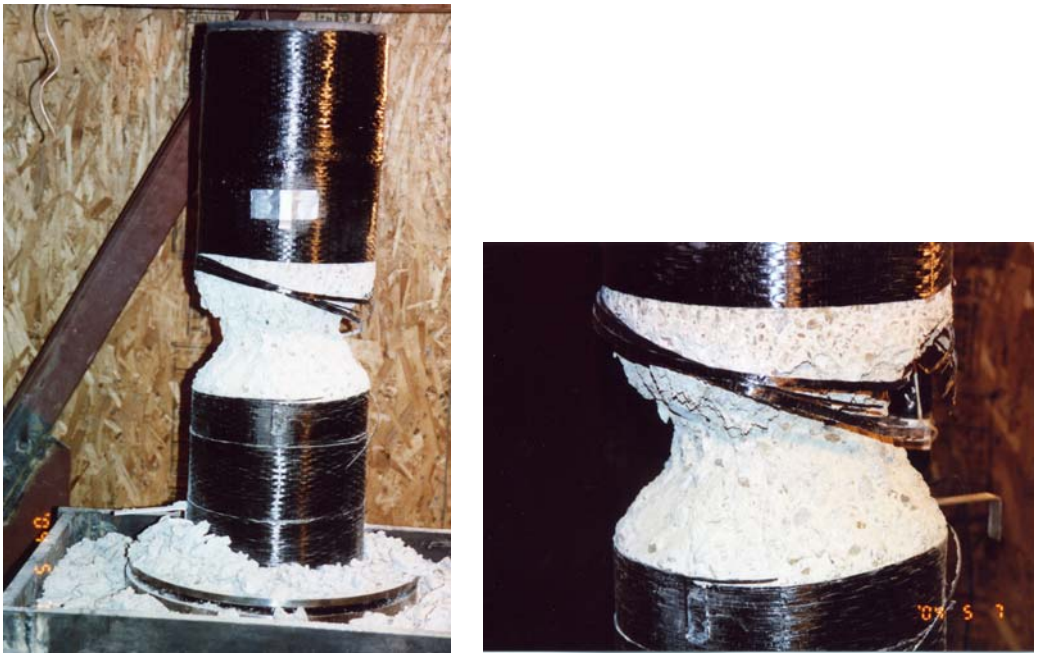

Figure 5.7 Typical failure modes of FRP-confined circular specimens

$$\mu = \frac{A_{tot}}{A_{ep}} \tag{5.1}$$

Figures 5.9 (a) and (b) show the definitions regarding the procedure for calculating the ductility ratio for different cases. The ductility ratio, μ, for specimens exhibiting softening behavior is shown in Figure 5.9 (a); A_{tot} is the cross-hatched area; A_{ep} is the total area obtained under the curve and over the curve using an elastoplastic model. When this ductility ratio is close to 1.0, the structural element shows an almost elastic-perfectly plastic behavior. For heavily FRP-confined specimens like circular jacketed specimens with many FRP composite layers, the post-peak behavior is hardening and it is difficult to identify the value of the peak stress level. Thus, the various portions of the stress-strain curve are determined as shown in Figure 5.9 (b). The longitudinal strain at failure of an unconfined specimen, $\varepsilon_{co}{}'$, is first identified. As for regular unconfined concrete, this value is set to 0.002 in./in. and usually corresponds to the strain level in the concrete when the axial stress reaches the peak compressive strength, $f_{co}{}'$. Then the value of f_{peak} is defined as the stress reached when the strain $\varepsilon_{co}{}'$ is attained; A_{tot} is the cross-hatched area, and A_{ep} is the netted area enclosed by the initial tangent and the plateau line passing through f_{peak}.

By applying the above principle, the ductility ratio for each specimen was calculated using Eq. (5.1) and was shown in Table 5.1. It is clear that the plain concrete specimen C-0-0 exhibits softening behavior, while the FRP-confined specimens in this group show hardening behavior.

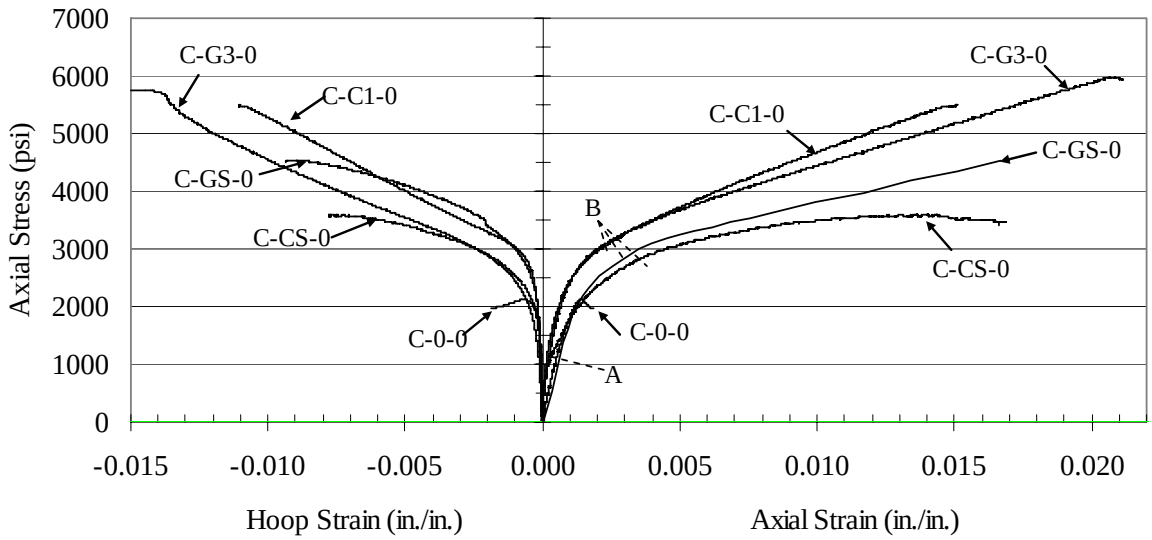

Figure 5.8 Stress-strain curves for specimens with regular concrete

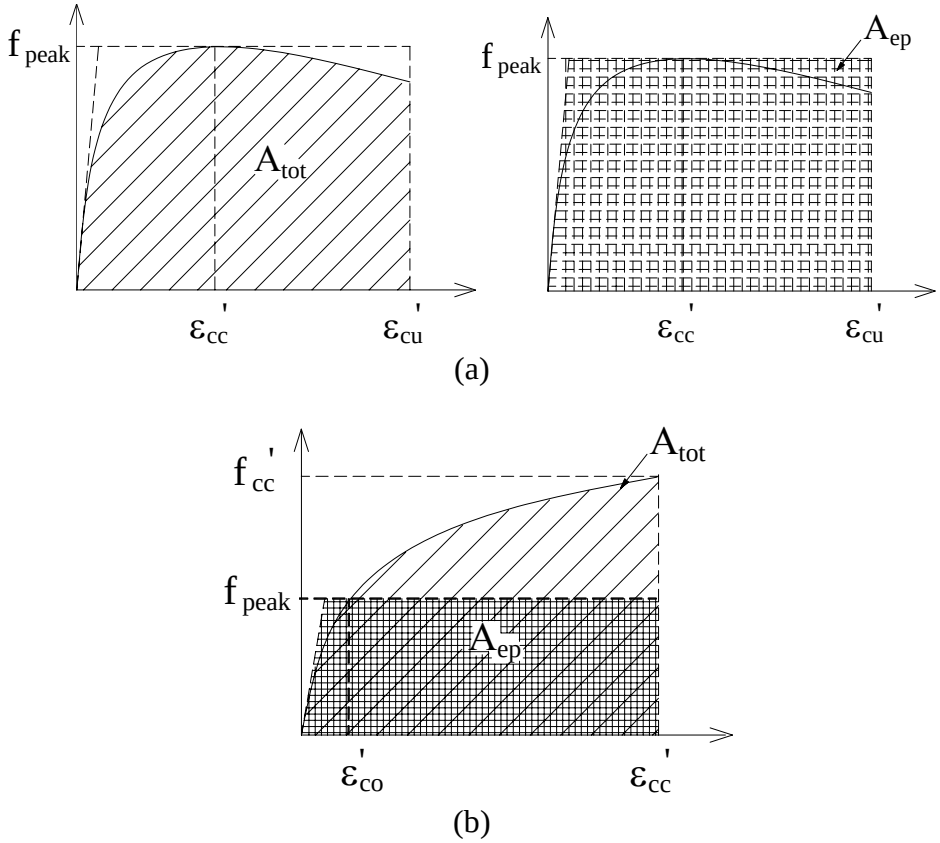

Figure 5.9 Definition of ductility ratio for FRP-confined concrete:
(a) specimens with softening behavior; (b) specimens with hardening behavior

As seen from Figure 5.8, the behavior of the FRP-confined concrete specimens with regular concrete can be divided into three phases. The first phase is from the origin to point A. Point A corresponds to the axial stress $f = 0.3 f_{co}'$, where f_{co}' is the compressive strength of the baseline specimen C-0-0. In this phase, the behavior of all specimens in Figure 5.8 is almost the same; lateral expansion is very small and the FRP stresses were very low, 16%-33% of the ultimate strength as observed from the tests. When the axial load exceeded the load corresponding to point A, the axial stress and strain started increasing quickly. Cracking noises were heard once the loading approached f_{co}', the unconfined concrete compressive strength, which marked the beginning of the FRP composite starting to contribute significantly to lateral confinement. Point B varied depending on whether the specimen was reinforced with FRP strips or continuous FRP sheets, and marked the turning point of the stress-strain curves. In the second phase, from A to B, the FRP composite participated in confinement, which resulted in the small axial strain as seen from stress-strain curves. After point B the behavior went into the third phase, in which the FRP strain increased significantly and the specimen stiffness decreased as observed form the tests; the specimens deformed largely in the axial direction and the FRP composite deformed in the radial direction. Finally, the concrete in the specimens crushed, followed by fracture of the FRP composite jacket, as shown in Figure 5.7.

These three phases represent the typical behavior of the axially loaded FRP-confined regular concrete specimens. In the beginning phase, the regular concrete has a small expansion and the FRP jacket does not participate. However, in phase AB, the concrete expands and the FRP composite jacket is put into tension; therefore, it provides partial confinement against expansion. In the third phase after B, the concrete goes into a flowing state until the FRP composite ruptures and the failure is very brittle and explosive.

In addition to stress-strain behavior, another characteristic of confined concrete is that it exhibits volumetric change when it is subjected to compressive loading. When concrete is subjected to this type of loading, it initially undergoes volumetric strain contraction; however, just prior to failure, concrete invariably exhibits a volumetric dilatancy which is caused by the propagation of microcracks in the material microstructure. Therefore, in order to get realistic analysis results, the expansive behavior of concrete, especially for the confined concrete must be considered in the nonlinear analysis since its dilatancy behavior is quite different from plain concrete. Volumetric strain, ε_V, is usually used to describe the dilatancy behavior of concrete. This parameter is related to the volume change of concrete and can be defined as:

$$\varepsilon_V = \frac{\Delta V}{V} = \varepsilon_1 + \varepsilon_2 + \varepsilon_3 \tag{5.2}$$

where ε_1, ε_2 and ε_3 are the strains in the three coordinate directions. It should be noted that for the definition of ε_V, compressive strain is negative and tensile strain is positive. Therefore, for the FRP-confined circular specimens, Eq. (5.2) can be rewritten as:

$$\varepsilon_V = \varepsilon_c + \left|2\varepsilon_j\right| \tag{5.3}$$

where ε_j is the transverse strain or hoop strain in the FRP jacket.

Concrete confined by a linear elastic confining material such as an FRP jacket, experiences a varying level of confining pressure. The different confinement level generated is a function of the volumetric strain and dilatancy rate. This dilation behavior, related to the different phases of axial behavior will be discussed in Ch.6; the experimental results for circular specimens from the tests are summarized in Figures 5.10 through 5.14.

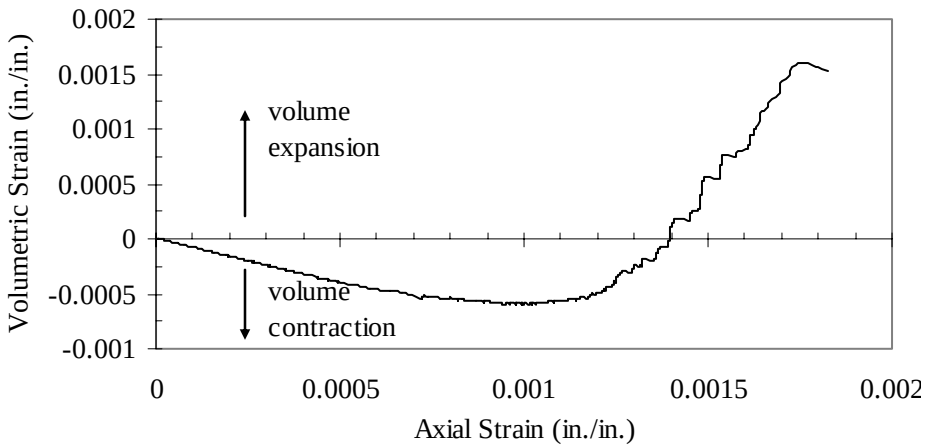

Figure 5.10 Volumetric versus axial strain for specimen C-0-0 with plain concrete

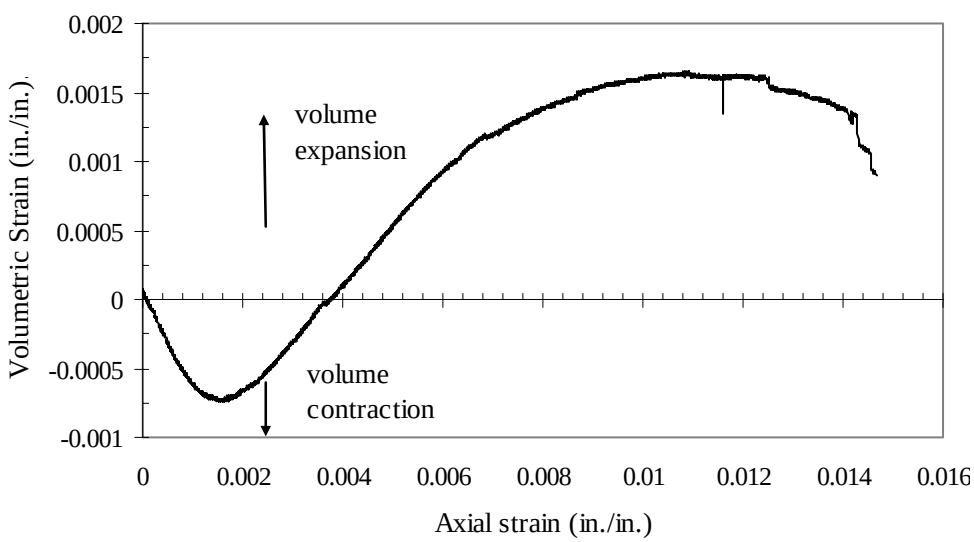

Figure 5.11 Volumetric versus axial strain for specimen C-CS-0 with 2 layers of CFRP strips

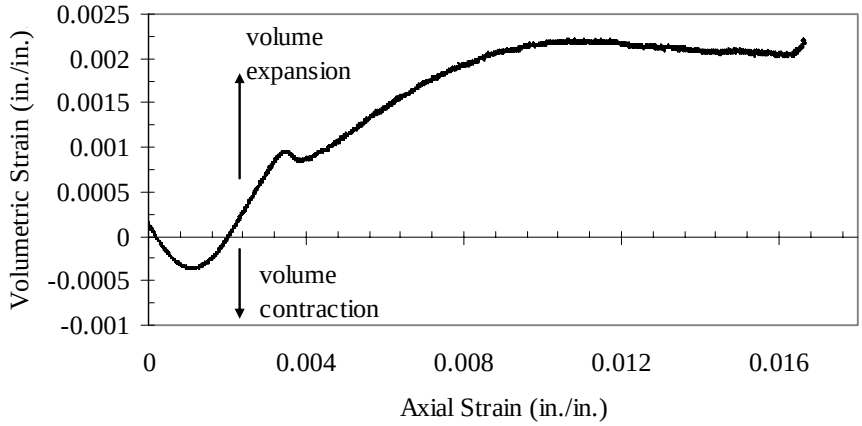

Figure 5.12 Volumetric versus axial strain for specimen C-GS-0 with 5 layers of GFRP strips

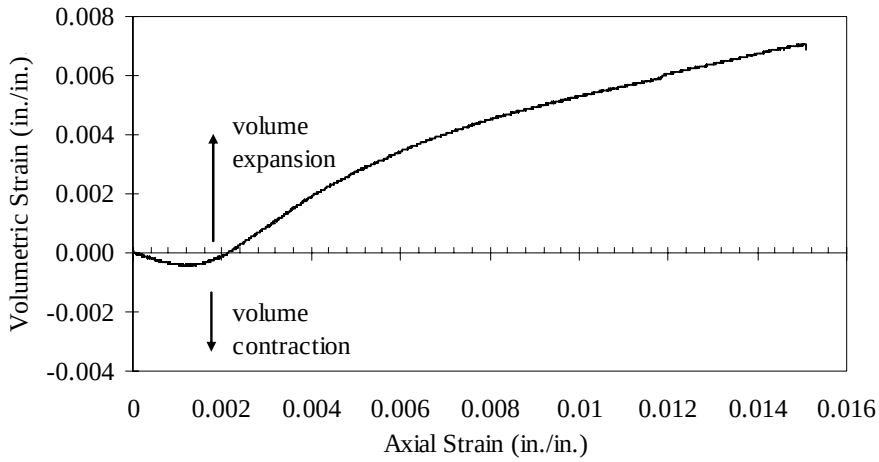

Figure 5.13 Volumetric versus axial strain for specimen C-C1-0 with 1 continuous CFRP layer

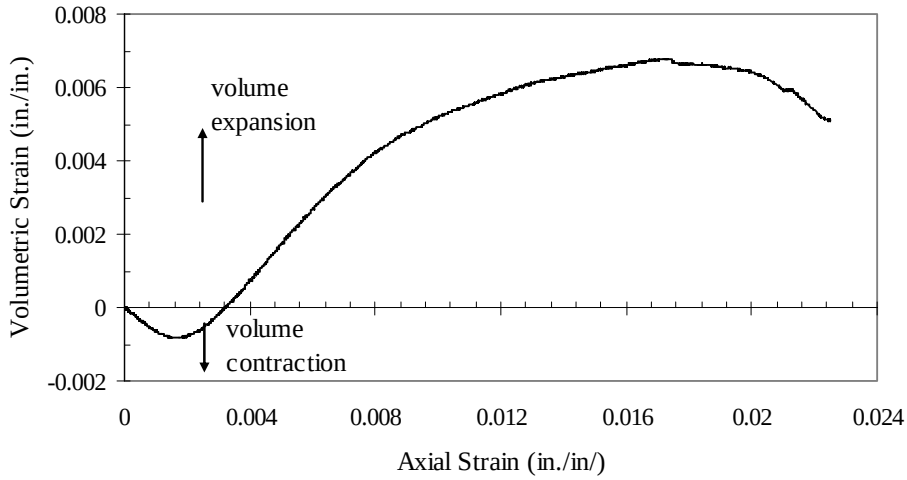

Figure 5.14 Volumetric versus axial strain for specimen C-G3-0 with 3 continuous GFRP layers

These curves show clearly the dilatancy behavior of all specimens. It can be seen that specimens start to expand when the volumetric strain, ε_V reaches zero. The axial strain at which the volumetric strain equals zero is referred to as ε_0, indicating the strain level from which concrete volume starts to dilate. This point also exactly corresponds to the turning point B on the stress-strain curves discussed above. As seen in Figures 5.8 and 5.10 for the plain concrete specimen, the value of ε_0 is lower than that for the FRP-confined specimens of Figures 5.11-5.14, and close to the ultimate strain ε_{co}'. Beyond ε_0, concrete expands in an unrestrained fashion for the plain concrete specimen until failure. However, different dilatancy behavior is observed from Figures 5.11-5.14 for FRP-confined specimens; the volumetric strain first decreases as expected since the axial strain is dominant and then reverts to zero. This is followed by volumetric expansion where hoop strains become dominant and volumetric strain increases. This expansion continues to high levels of axial strain; however, for axial strains beyond 0.01 in./in. as shown in Figures 5.11-5.14, this expansion peaks and starts to decrease and shortly thereafter the jacket ruptures. The confinement provided by the bonded FRP jacket is of the "passive" type and this confinement becomes significant only after lateral dilation starts. In addition, it is noted that ε_0 differs slightly from specimens with different jacket stiffness and the expansion is delayed as the stiffness increases. The details of zero volumetric strain, ε_0 will be discussed in Chapter 7.

5.2.2 Specimens with expansive cement concrete

Similar to the specimens with regular concrete, the experimental results of specimens with expansive cement concrete show significant enhancement in both axial stress and axial strain capacity. Compared with the unconfined concrete, the strength enhancement f'_{cc}/f'_{co} ranges from 298 to 370 percent, and the increase in axial strain varies from 1230 to 1440 percent. Table 5.2 lists the main results from the tests.

The comparison of strength enhancement ratio and ductility ratio between regular concrete specimens and expansive cement concrete specimens are listed in Figure 5.15. Note that both C-C1-0 and C-CT-E have one continuous CFRP layer, and that both C-G3-0 and C-GT-E have three continuous GFRP layers. It is seen that both strength enhancement and ductility are higher by using expansive cement concrete compared to regular concrete. The increase in compressive strength is 119 percent for CFRP and 136 percent for GFRP composites; the increase in ductility is 232 percent for CFRP and 150 percent for GFRP composites.

Table 5.2 Main results of circular specimen tests with expansive concrete

Specimen ID.	ρ_{FRP}	$f_{cc}'^{*}$ **(psi)**	$f_{cc}'/f_{co}'^{*}$	ε_{cc}' **(in./in.)**	$\varepsilon_{cc}'/\varepsilon_{co}'$	ε_{ju}^{**} **(in./in.)**	$\varepsilon_{ju}/\varepsilon_f$	μ
C-CT-E	0.0133	4470	3.43	0.0246	12.3	0.0056	0.40	3.23
C-GT-E	0.064	5548	3.70	0.0288	14.4	0.0057	0.40	2.25

* f_{co}' = 1300 psi for C-CT-E and 1500 psi for C-GT-E obtained from cylinder tests;

** Initial post-tensioning strains are not included.

Figures 5.16 and 5.17 show specimens C-CT-E and C-GT-E before and after testing.

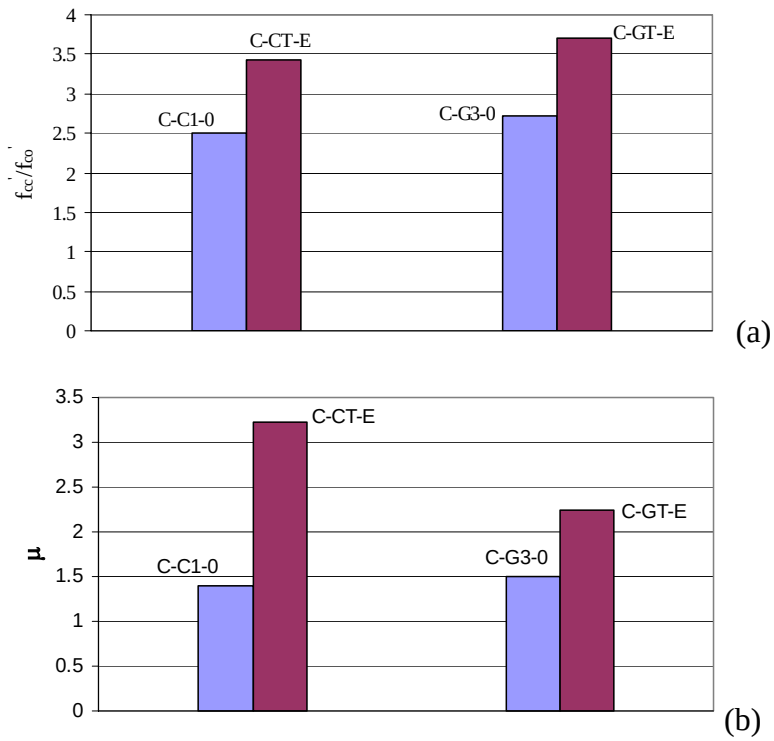

Figure 5.15 Comparisons between different types of circular specimens: (a) strength enhancement ratio; (b) ductility ratio

Figure 5.16 Specimen C-CT-E with expansive concrete and 1 CFRP layer before and after testing

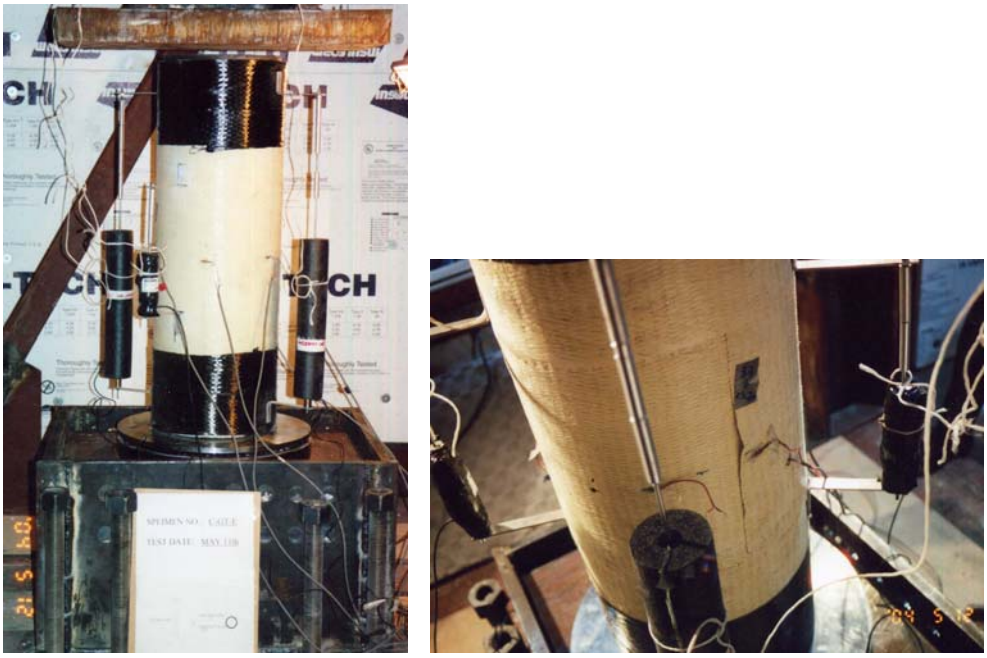

Figure 5.17 Specimen C-GT-E with expansive concrete and 3 GFRP layers before and after testing

Shear and compression failure was observed for these specimens, which is rather similar to the plain concrete specimen without any FRP jackets. This is because the FRP jackets were non-bonded and the resulting strain distribution is more uniform over the height of the jacket. Concrete failure occurred not only in the mid-height region, as the specimens with bonded jackets, but the shear cracks also propagated all the way up and down the vertical face of the specimens as well as the jackets, as shown in Figures 5.16 and 5.17. The measured ultimate axial strains at failure were lower compared to the bonded FRP jackets; however, the ductility ratios as seen in Table 5.2 were higher than those for specimens with regular concrete and bonded jackets; this shows that the ductile performance for specimens with expansive cement concrete is better than that of specimens with regular concrete.

Figure 5.18 shows the axial stress versus axial and hoop strain curves. For the left part of the curve, the initial strains for specimens C-CT-E and C-GT-E start from 0.0018 in./in. and 0.0022 in./in. respectively, indicating the post-tensioning hoop strain in the FRP jacket produced by the expansion caused by the expansive cement concrete prior to testing.

The behavior of the specimens with expansive cement concrete was different than those with regular concrete; the initial slope of the stress-strain curve is lower than that of the regular concrete specimens, which is due to the low strength of expansive cement concrete but the slope after the turning point is similar to that of regular concrete specimens.

In Figure 5.19, normalized stress-strain relations are presented for FRP-confined circular specimens for the purpose of comparing the experimental data for different types of concrete. The comparisons show that the increase in stress and strain capacity was higher for specimens

with expansive cement concrete. This behavior is in contrast to the reported phenomenon by Carey and Harris (2003) that the maximum compressive strength of regular concrete specimens with non-bonded jackets is lower than regular concrete specimens with bonded FRP jackets. The main reason for the difference is the post-tensioning effect caused by the expansive cement concrete inside the FRP jacket, which is engaged in radial confinement once concrete is axially loaded.

The dilatancy behavior is shown in plots of volumetric versus axial strain, presented in Figures 5.20 and 5.21 for specimens with expansive cement concrete. Both figures include plots in which initial hoop strains are included or excluded. In contrast to the dilatancy behavior of bonded-jacketed specimens with regular concrete, no volume expansion is observed for specimens with expansive cement concrete due to the "active" confinement action obtained by the post-tensioning effect prior to application of the axial loading. In addition, the relation between axial and volumetric strain for each specimen is approximately linear until failure.

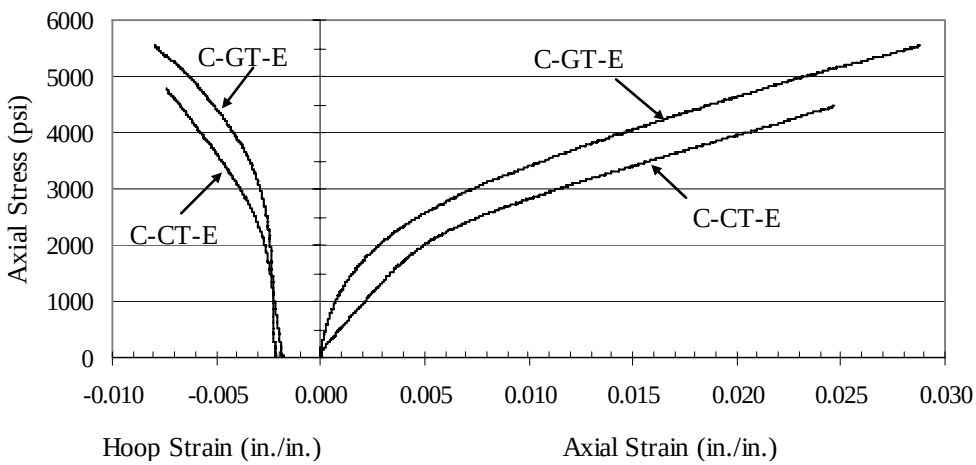

Figure 5.18 Stress-strain curves for specimens with expansive cement concrete

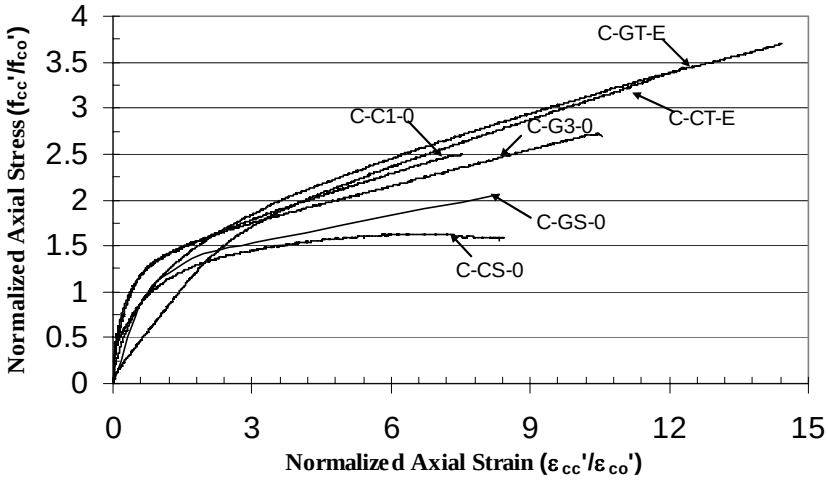

Figure 5.19 Normalized stress-strain curves for FRP-confined circular specimens

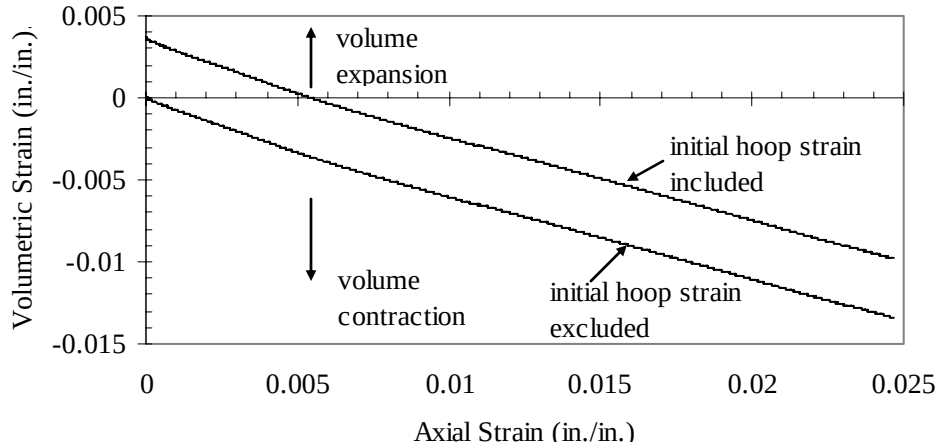

Figure 5.20 Volumetric versus axial strain curve for specimen C-CT-E

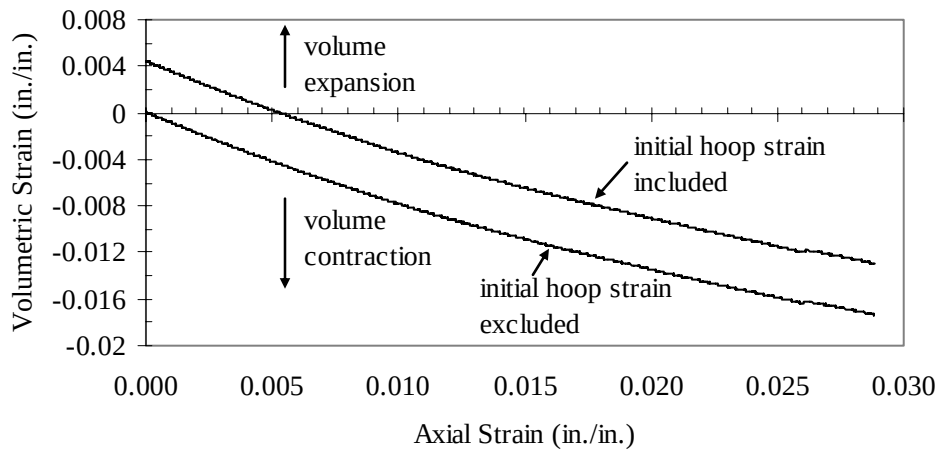

Figure 5.21 Volumetric versus axial strain curve for specimen C-GT-E

From the circular specimen tests, the following observations are made:
(1) FRP composites are very effective in increasing the load-carrying capacity and deformation ability of circular columns. Significant increases in both ultimate stress and strain are observed from the tests. The stress-strain curve can be described using a bilinear relationship. The turning point is marked by the point of zero volumetric strain, at which dilation of concrete starts. The initial slope of the stress-strain curve depends on the jacket stiffness and this value is always higher than the modulus of elasticity of unconfined concrete. This observation is in contrast to the prevailing assumption adopted by many FRP confinement models in which the initial stiffness of FRP-confined concrete is the same as that of plain concrete. The second slope in the bilinear stress-strain curve is largely dependent on the jacket stiffness because after the turning point, the FRP jacket starts to participate in confining the concrete core. Failure of the column occurs once the FRP jacket reaches its rupture strain, which is lower than the ultimate.

(2) Compared to regular concrete columns, columns with expansive cement concrete confined with FRP jackets show more deformation ability and ductility at failure. In addition, they have a

higher increase in ultimate strength. Expansive cement concrete columns confined with CFRP jackets show a higher ductility compared to similar columns confined using GFRP jackets. In both cases, active confinement is evident from post-tensioning of the jacket which is induced by the chemical prestressing effect of expansive cement concrete. The failure mode is different compared to regular concrete columns confined with FRP composites. Columns of regular cement concrete confined with FRP jackets exhibit volumetric strain contraction first, which is followed by volumetric strain expansion; at ultimate conditions the concrete cracks first and the FRP jacket then ruptures. Columns of expansive cement concrete confined with FRP jackets exhibit continuous volumetric contraction in a linear fashion; at ultimate conditions, the FRP jacket ruptures first and then vertical shear compression cracks appear in the expansive cement concrete and core concrete.

(3) For the same volumetric FRP ratio, the confinement effectiveness for specimens confined by FRP strips decreases as compared to those confined with continuous FRP jackets. Therefore, the strengthening method with FRP strips should be used with caution for the normal retrofit of bridge columns. Otherwise, the maximum spacing of FRP strips must be limited. However, strengthening with FRP strips offers the advantage of easy inspection.

(4) GFRP-jacketed columns with regular concrete show more axial strain and ductility than CFRP-jacketed columns, although they were designed to have approximately the same FRP jacket stiffness; GFRP jackets provided a slightly higher confinement than CFRP jackets. This is mainly because the GFRP composite jacket is softer than the CFRP jacket from the point of view of material properties, i.e., it has a lower modulus of elasticity. Therefore, for the retrofit of circular columns, GFRP jackets should be used to provide higher ductility and moderate strength increase. On the other hand, because of the higher modulus of CFRP jackets, this material can be used to provide concrete with higher strength increase and moderate ductility. In some cases, the combination of these two FRP composites as hybrid reinforcement should be considered.

(5) Although FRP composites could significantly improve column axial behavior, caution is required in the application of this material because of its brittle characteristics at failure. It is recommended that at least two layers of FRP composites are used in the retrofit of columns and a safety factor should also be adopted.

5.3 Square Specimens

5.3.1 Specimens without shape modification

In this group, five square specimens without shape modification were tested. The plain concrete specimens behaved similar to circular specimens, and an obvious shear compression failure was observed at failure as shown in Figure 5.22. The main experimental results of square specimens with no shape modification are listed in Table 5.3.

The observed increase in strength f_{cc}' for jacketed specimens ranged from 145 to 172 percent, which is much lower compared to specimens with circular jackets; the same is true regarding the ductility ratio. Another phenomenon observed was that the FRP strains at failure

were always lower than those of circular specimens. The relatively low jacket efficiency factor is believed to be due to corner effects that cause the jacket effectiveness to reduce, and the loss of membrane action; this behavior will be discussed further in Chapter 6.

During the test of confined specimens, bulging at the sides due to less effective confinement was observed. A sound was heard shortly before failure of FRP continuously-jacketed specimens and this is thought to be the concrete crushing inside the FRP jacket. After this sound, specimens failed quickly with the FRP jacket breaking at the cross-section's corner due to stress concentration. In specimens with FRP strips, concrete spalling was always observed during testing; failure was due to concrete crushing between the FRP strips at mid-height; an obvious post-peak behavior was seen in this group. Figures 5.23-5.26 show specimens in this group before and after testing.

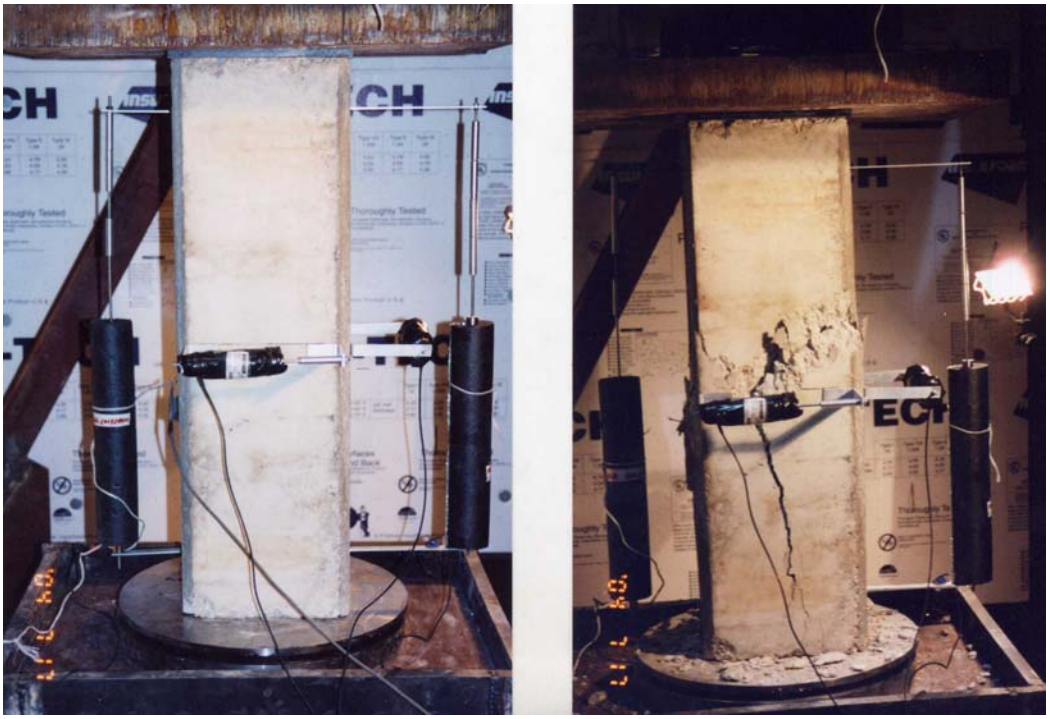

Figure 5.22 Specimen S-0-0 with plain concrete before and after testing

Table 5.3 Main results of square specimens without shape modification

Specimen ID	ρ_{FRP}	f_{cc}'(psi)*	f_{cu}'(psi)	ε_{cc}' (in./in.)**	ε_{cu}' (in./in.)	ε_{ju} (in./in.)	f_{cc}'/f_{co}'	$\varepsilon_{cu}'/\varepsilon_{co}'$	μ
S-0-0	-	2220	-	0.0020	-	-	1.00	1.00	0.94
S-C2-0	0.0255	3793	-	0.0100	-	0.0068	1.72	5.0	1.15
S-CS-0	0.0261	3394	2743	0.0045	0.033	0.0071	1.54	16.5	0.91
S-G6-0	0.1164	3200	3200	0.0031	0.020	0.0060	1.45	10.0	0.93
S-GS-0	0.1091	3582	3030	0.0042	0.028	0.0082	1.63	14.0	0.88

* For S-0-0, f_{co}' applies.

** For S-0-0, ε_{co}' applies.

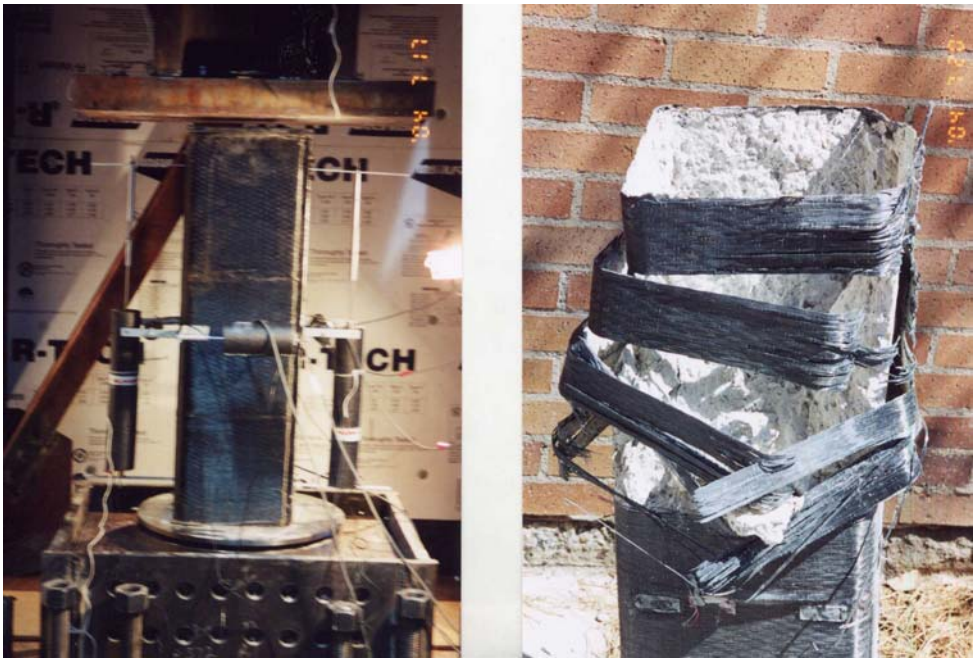

Figure 5.23 Specimen S-C2-0 with 2 CFRP layers before and after testing

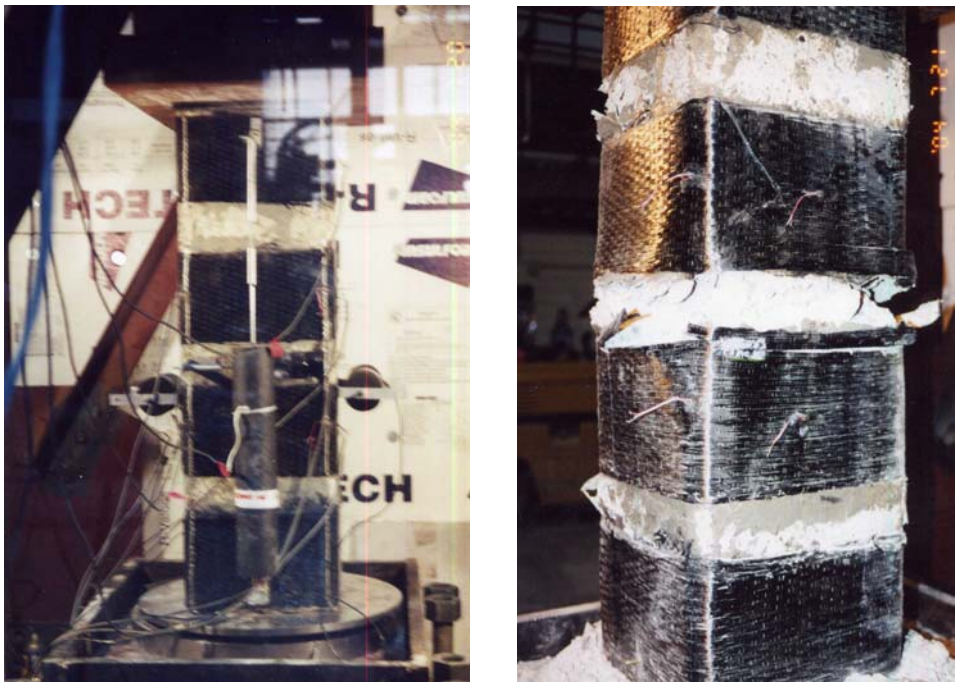

Figure 5.24 Specimen S-CS-0 with 3 layers of CFRP strips during and after testing

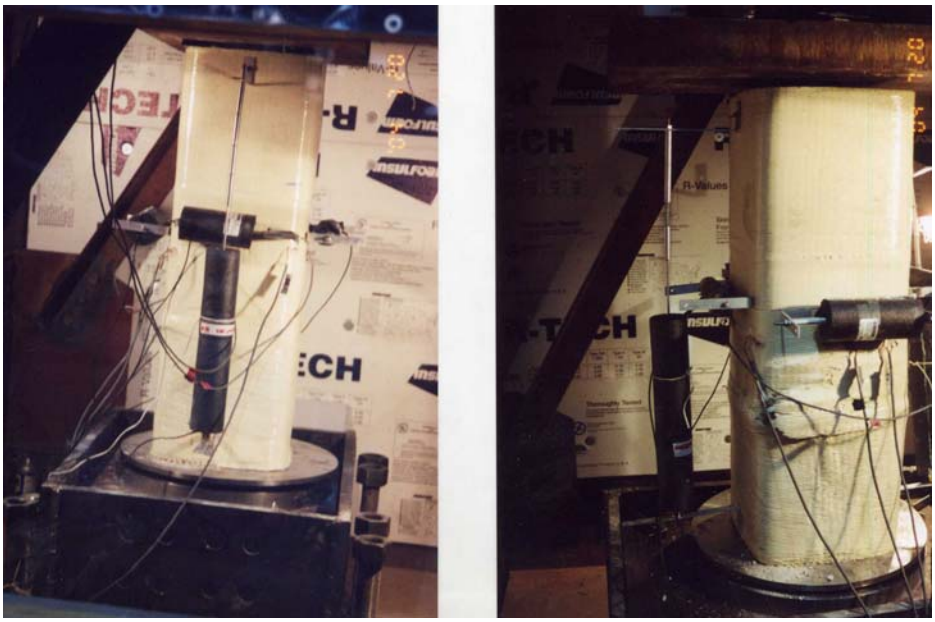

Figure 5.25 Specimen S-G6-0 with 6 GFRP layers during and after testing

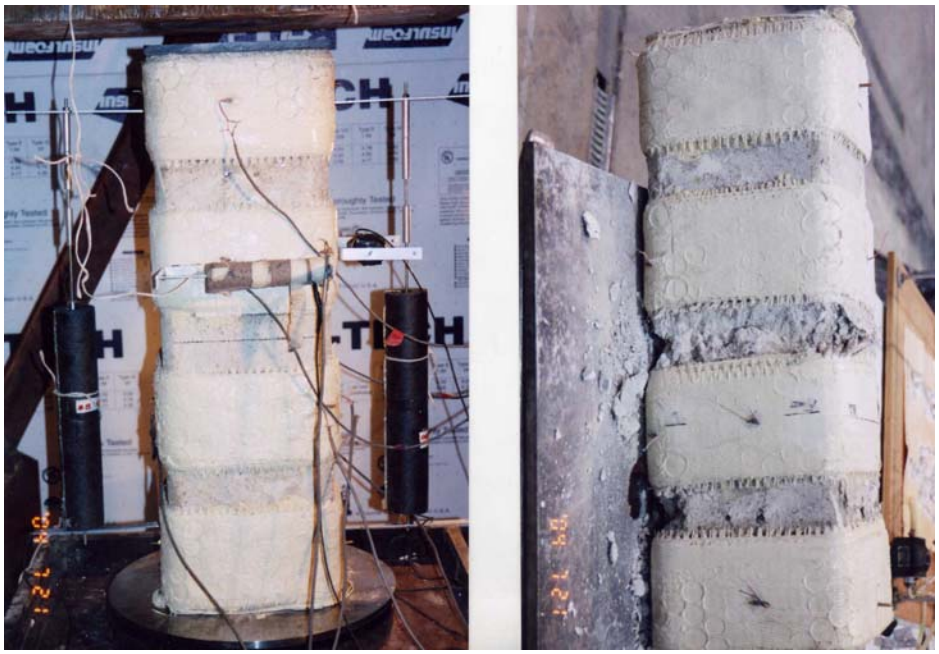

Figure 5.26 Specimen S-GS-0 with 9 layers of GFRP strips before and after testing

Stress-strain curves for FRP-confined square specimens are presented in Figures 5.27-5.30. Each curve is divided into two parts: the right part shows axial stress versus axial strain; and the left part shows axial stress versus transverse strain, fiber strain at the middle of the section side, and fiber strain at the corner. Fiber strain is the local strain measured by strain gages on the FRP jacket as shown in Figure 4.1, whereas transverse strain is an average strain measured by LVDTs for the whole side as shown in Figure 4.4.

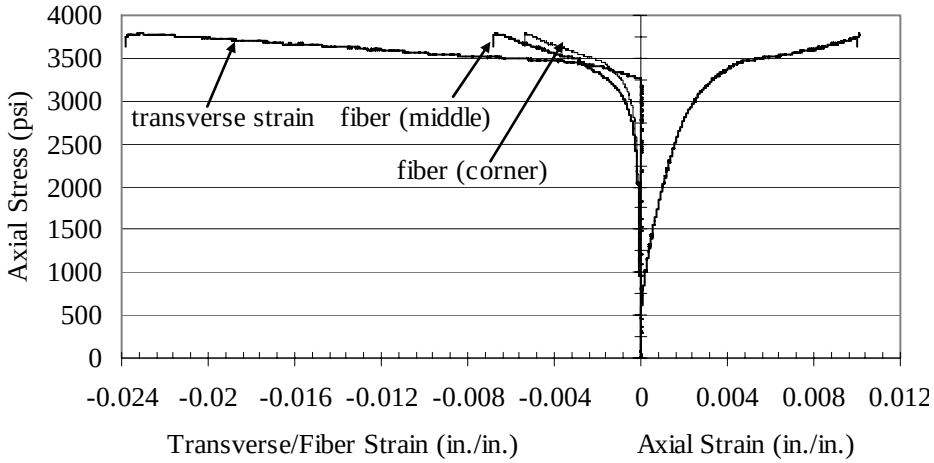

Figure 5.27 Stress-strain curves for S-C2-0 with 2 CFRP layers

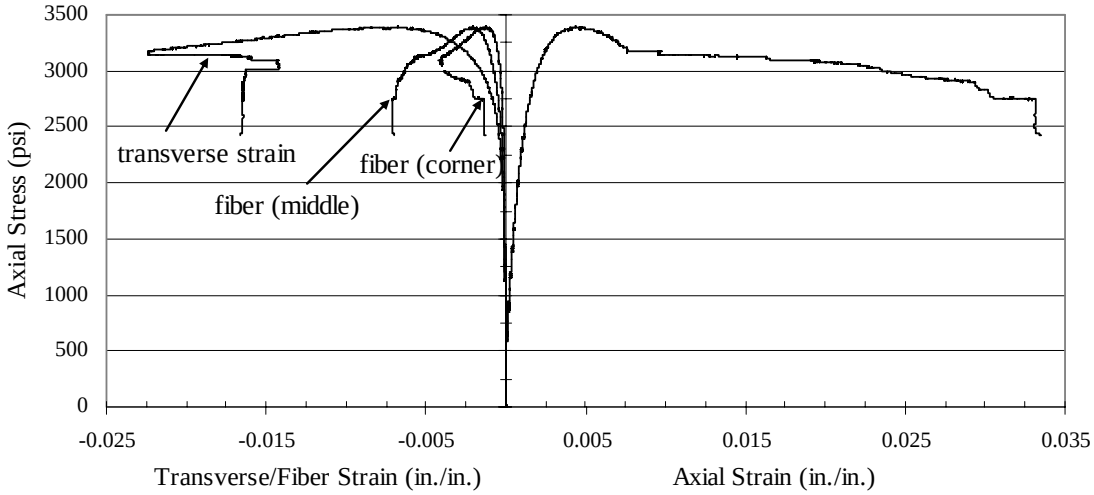

Figure 5.28 Stress-strain curves for S-CS-0 with 3 layers of CFRP strips

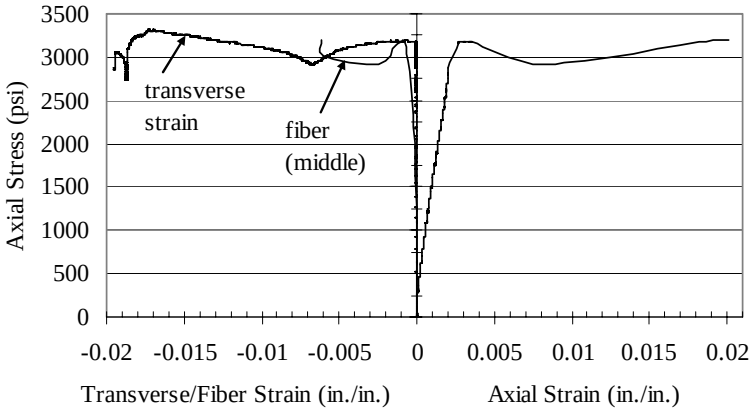

Figure 5.29 Stress-strain curves for S-G6-0 with 6 GFRP layers

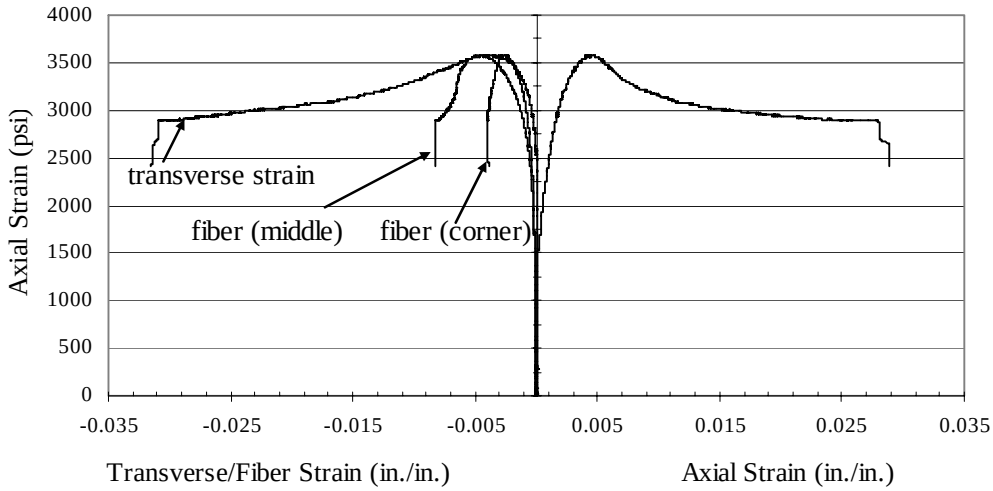

Figure 5.30 Stress-strain curves for S-GS-0 with 9 layers of GFRP strips

Unlike FRP-confined circular specimens, most square specimens demonstrated a post-peak softening behavior which can be seen from the stress-strain curves; a stress drop occurred once a peak stress was reached, after which a "plateau" was observed. Because of the different jacket confinement stiffness, these specimens illustrated different behavior patterns. It is clear that S-C2-0 shows a bilinear hardening behavior similar to circular specimens but with a reduced slope after the turning point; all of the other specimens show softening behavior with different degrees of slope depending on the confinement type. Among the specimens with softening behavior, S-CS-0 and S-GS-0 with FRP strips have steeper descending portions than S-G6-0 with 6 GFRP layers, indicating smaller confinement effectiveness.

The dilatancy behavior is studied using fiber versus axial strain, and volumetric versus axial strain relations. Figure 5.31 shows plots of fiber versus axial strain at the middle of the side and corner for FRP-confined square specimens. It is seen that fiber strains at the corner are lower than those at the middle of the side. This is because FRP confinement at the corner is more effective than at the middle of the side and concrete expansion at corners is effectively restrained.

Before the axial stress reached the peak, f_{cc}', the strain measured by the strain gauges in the fiber was consistent with the transverse strain in the concrete measured by the LVDTs, as shown in Figures 5.27-5.30. However after the peak stress, the transverse strain measured by the LVDTs increased very fast; the fiber strain increased very slowly with fiber strain at the corner remaining almost constant, as shown in Figure 5.31. It is obvious that the FRP confined concrete went into a "plastic" phase; after this point, the FRP jacket could not provide enough confinement to the concrete inside so the transverse strain in the concrete increased very quickly. This plastic behavior of the FRP confined concrete is used to explain the softening behavior of specimens with low confinement stiffness.

Figure 5.32 shows the volumetric versus axial strain relationships for square specimens.

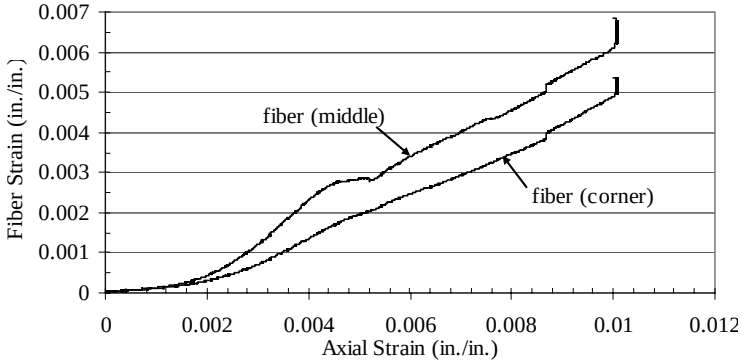

(a)

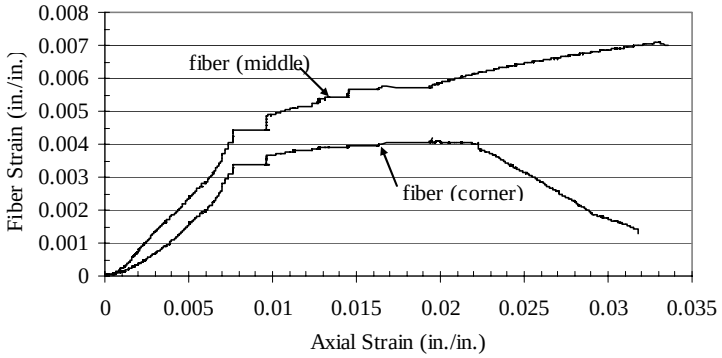

(b)

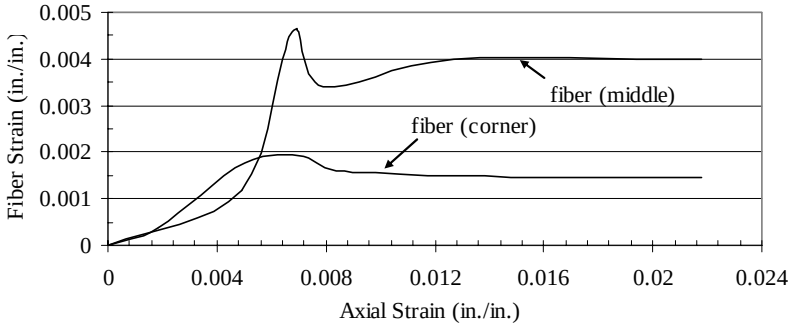

(c)

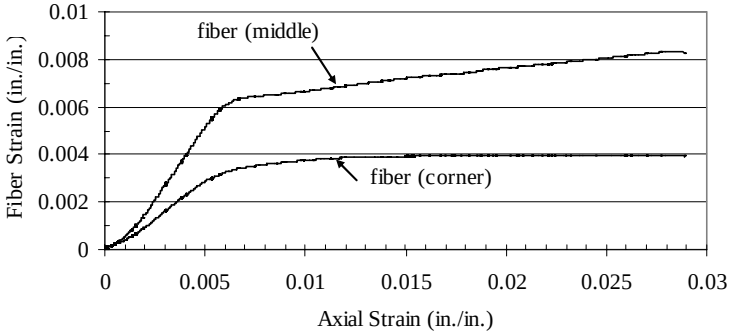

(d)

Figure 5.31 Fiber versus axial strain curves for square specimens:
(a) S-C2-0; (b) S-CS-0; (c) S-G6-0; (d) S-GS-0

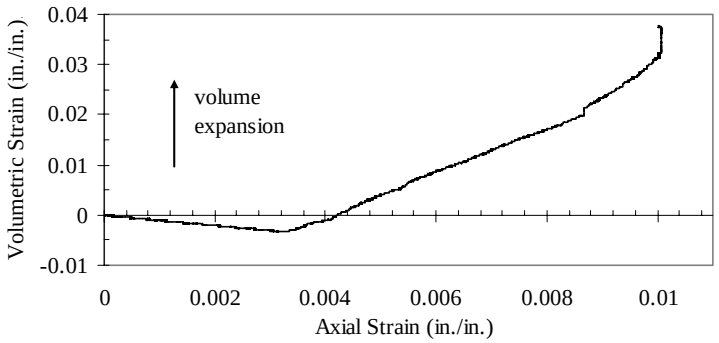

(a)

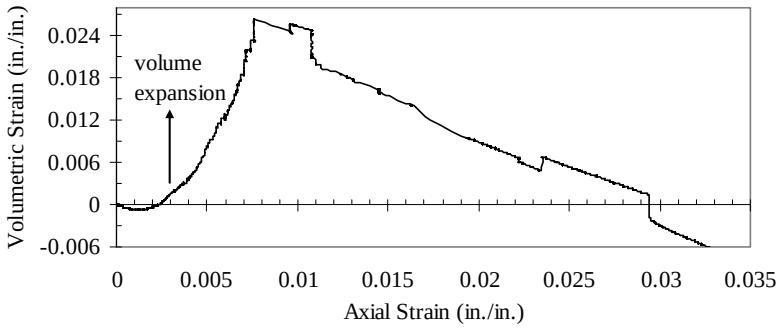

(b)

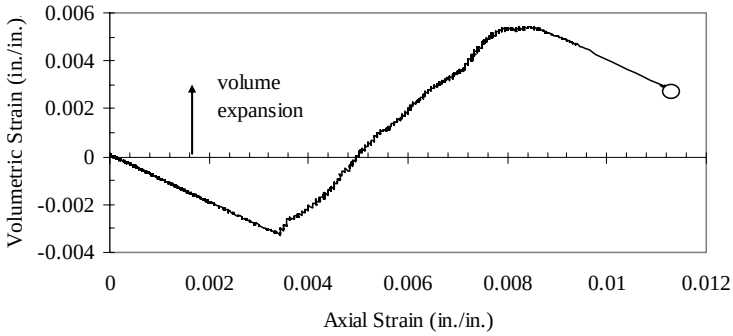

(c)

°denotes data is not available after this point

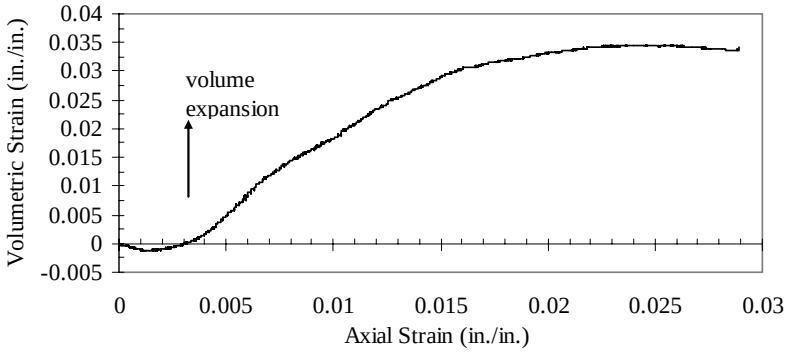

Figure 5.32 Volumetric versus axial strain curves for square specimens: (a) S-C2-0; (b) S-CS-0; (c) S-G6-0; (d) S-GS-0

Compared to the dilatancy behavior of circular specimens, these specimens show more significant volumetric expansion as expected; this indicates less confinement provided by the square FRP jacket to restrain the lateral dilation of concrete. Moreover, for those specimens S-G6-0, S-CS-0 and S-GS-0 demonstrating softening behavior, the average value of ε_0 is about 0.004 in./in. which corresponds to the peak axial stress, f_{cc}'; that is, ε_0 is equal to ε_{cc}' for specimens with softening behavior. After this point, concrete starts to expand rapidly and the FRP jacket cannot provide enough confinement, so a drop in capacity occurs.

5.3.2 Specimens with shape modification

In order to decrease corner effects and bending effects on the long sides of the section, and improve the compressive behavior of square specimens, four shape-modified specimens were built. With respect to each square, two methods were used to realize shape modification: (1) a non-shrink concrete was cast around the square column to form a circular section; after curing of the concrete, an FRP composite jacket was applied using a wet layup; (2) expansive cement concrete combined with chemical prestressing in a pre-fabricated cylindrical FRP shell was applied, transforming the square column to a circular column. For each square type, two shape-modified specimens were investigated with CFRP and two with GFRP using the different construction methods. These specimens were installed with the same thickness of FRP as the square columns without shape modification. The increase of cross-sectional area after shape modification was about 150% for both methods. Due to the different compressive strengths of regular concrete and additional concrete fill, a mean value was calculated for the unconfined concrete strength f_{co}' as:

$$f_{co}' = f_{co1}' \cdot \frac{A_o}{A} + f_{co2}' \cdot \frac{A_f}{A} \qquad (5.3)$$

where f_{co1}' = unconfined concrete strength of square specimens; f_{co2}' = unconfined strength of expansive or non-shrink cement concrete obtained from cylinder compression tests; these were 1500 psi for expansive cement concrete and 2200 psi for non-shrink cement concrete; A_o = area of square cross-section; A_f = area of expansive or non-shrink cement concrete fill; A = total area of shape-modified cross-section. By using this method, f_{co}' is calculated to be 1900 psi and 2200 psi for specimens with expansive cement concrete and non-shrink cement concrete, respectively.

As can be seen in Table 5.4, compared with specimens without shape modification all modified specimens show a significant increase in jacket efficiency, as well as strength and ductility.

The comparisons of strength enhancement ratio and ductility ratio between regular concrete specimens and expansive cement concrete specimens are listed in Figure 5.33. This figure shows that there are significant increases of both strength enhancement ratios and ductility ratios by performing shape modification on square specimens.

Table 5.4 Main results for shape-modified square specimens

Specimen ID.	ρ_{FRP}	f_{cc}' (psi)	f_{cc}'/f_{co}'*	ε_{cc}' (in./in.)	$\varepsilon_{cc}'/\varepsilon_{co}'$	ε_{ju}** (in./in.)	$\varepsilon_{ju}/\varepsilon_{FRP}$	μ
S-CT-E	0.0175	7124	3.71	0.022	10.91	0.0058	0.414	2.38
S-CT-F	0.0175	5996	2.73	0.012	6.06	0.0104	0.721	1.36
S-GT-E	0.0800	6436	3.35	0.021	10.57	0.0059	0.415	2.03
S-GT-F	0.0800	6430	2.52	0.019	9.56	0.0077	0.564	1.71

* f_{co}' = 1900 psi for S-CT-E, S-GT-E and 2200 psi for S-CT-F and S-GT-F respectively.

** Initial hoop strains due to post-tensioning effect are not included.

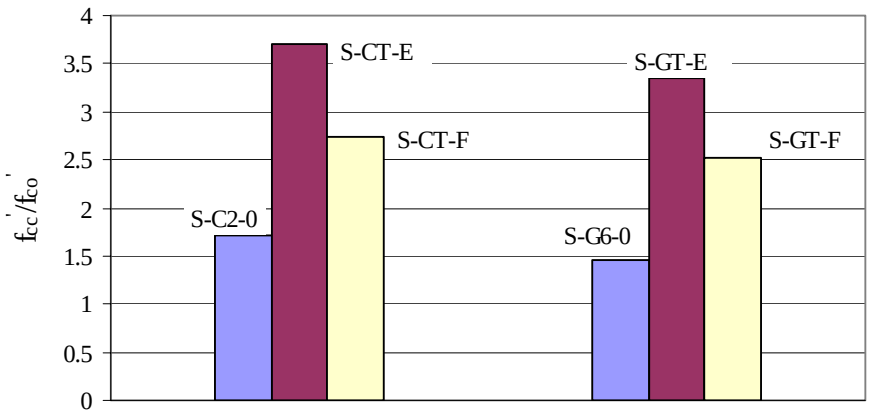

(a)

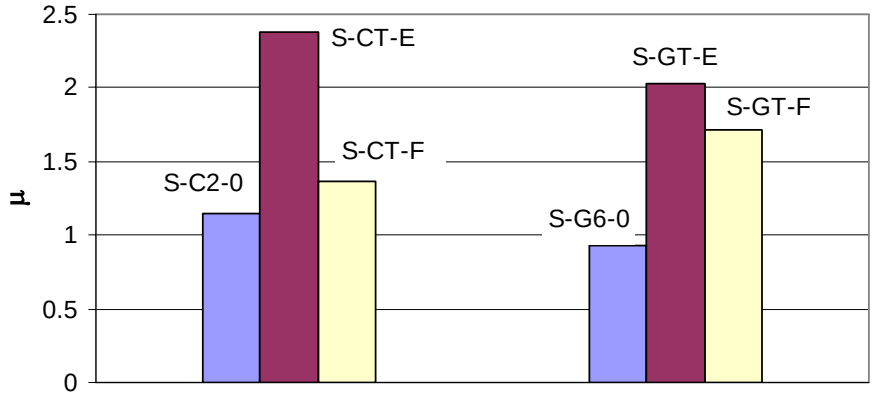

Figure 5.33 Comparisons between square and shape-modified specimens
(a) strength enhancement ratio; (b) ductility ratio.

All specimens in this group had an increasing load-displacement relation until failure. No softening behavior was observed in this group, which occurred for square specimens without shape modification. The failure of specimens was similar to circular ones with 12 in. diameter but was more catastrophic due to the larger geometric size since more energy was absorbed during the test. In particular, for CFRP-jacketed columns with expansive cement concrete,

failure is more extensive and explosive. Failure occurred very suddenly and specimens were totally destroyed. By contrast, concrete cones were clearly seen for bonded jackets with non-shrink concrete fill and the jackets broke at or near the mid-height of the specimen. Figures 5.34-5.37 show each specimen at failure.

Figure 5.34 Specimen S-CT-E with expansive cement concrete and 2 CFRP layers before and after testing

Figure 5.35 Specimen S-CT-F with non-shrink cement concrete and 2 CFRP layers before and after testing

Figure 5.36 Specimen S-GT-E with expansive cement concrete and 6 GFRP layers before and after testing

Figure 5.37 Specimen S-GT-F with non-shrink cement concrete and 6 GFRP layers after testing

To compare the effectiveness between two different methods of making shape modification, stress-strain curves are grouped together by different types of FRP as seen in Figure 5.38 and Figure 5.39. It can be seen from the stress-strain curves that the behavior of shape modified specimens with the GFRP jackets are similar, and both reached almost the same

strength, axial strain, and hoop strain. For CFRP-jacketed specimens, C-CT-E with the expansive cement concrete and two CFRP layers achieved a higher strength and an obvious increase in ductility over C-CT-F with non-shrink cement concrete and two CFRP layers.

In order to compare the shape modification effect, normalized axial stress versus normalized axial strain curves are plotted in groups for different types of FRP jacket, and comparisons of strength and ductility capacity are made as shown in Figures 5.40 and 5.41. It is seen from these figures that the stress-strain behavior is almost the same prior to reaching the turning point but deviates significantly thereafter with a much higher ultimate stress and strain for shape-modified specimens.

Figures 5.42 through 5.45 show the volumetric versus axial strain behavior for shape-modified square specimens. Similar to the dilatancy behavior of circular specimens with expansive cement concrete, S-CT-E and S-GT-E demonstrate volume contraction all the way to failure. The volumetric versus axial strain relations are almost linear as for circular specimens but with different slope. By contrast, shape-modified specimens with non-shrink concrete behaved more like circular specimens with regular concrete and bonded jacket regarding the dilatancy behavior.

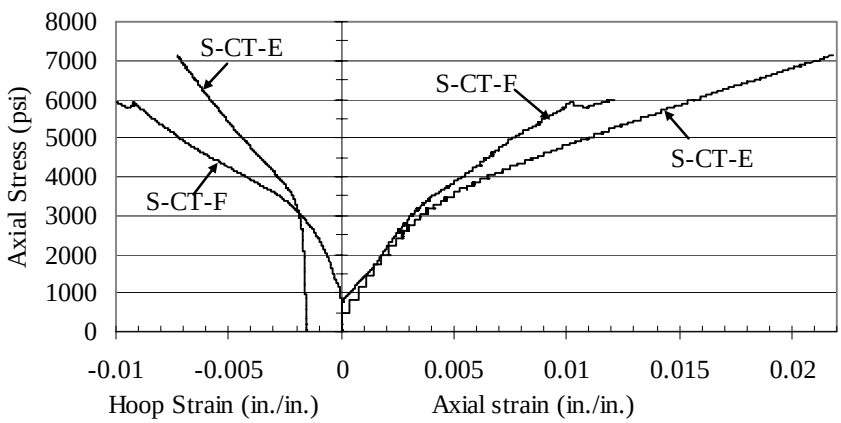

Figure 5.38 Stress-strain curves for S-CT-E & S-CT-F

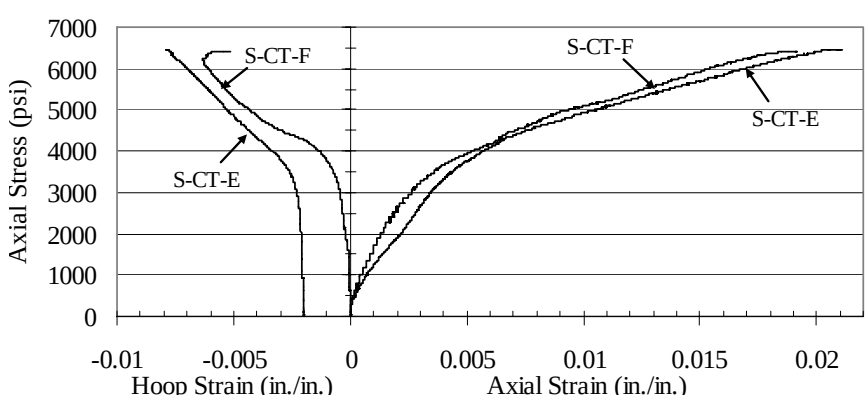

Figure 5.39 Stress-strain curves for S-GT-E & S-GT-F

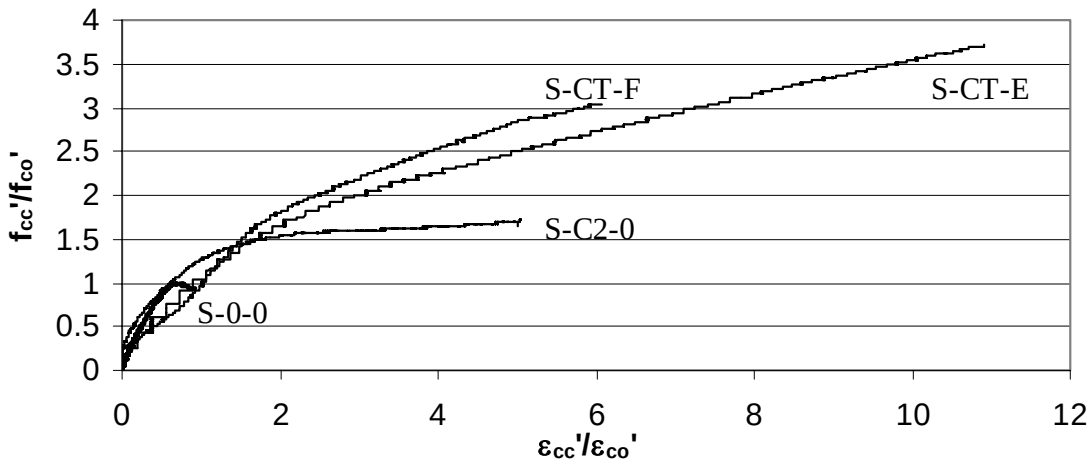

Figure 5.40 Normalized stress-strain relationships for CFRP-jacketed square specimens (S-0-0 = square specimen without FRP; S-C2-0 = square specimen with 2 CFRP layers; S-CT-E = square specimen modified with expansive cement concrete and 2 CFRP layers; S-CT-F = square specimen modified with non-shrink concrete and 2 CFRP layers)

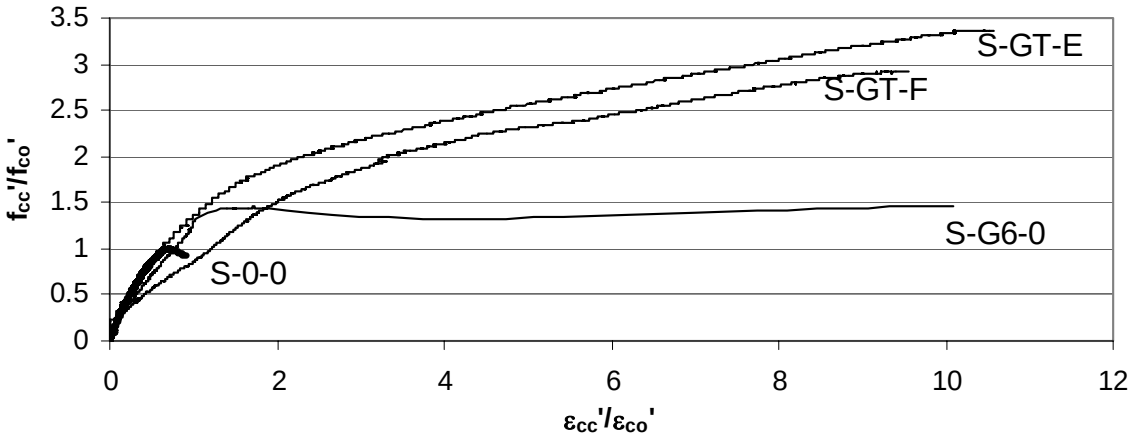

Figure 5.41 Normalized stress-strain relationships for GFRP-jacketed square specimens (S-0-0 = square specimen without FRP; S-G6-0 = square specimen with 6 GFRP layers; S-GT-E = square specimen modified with expansive cement concrete and 6 GFRP layers; S-GT-F = square specimen modified with non-shrink concrete and 6 GFRP layers)

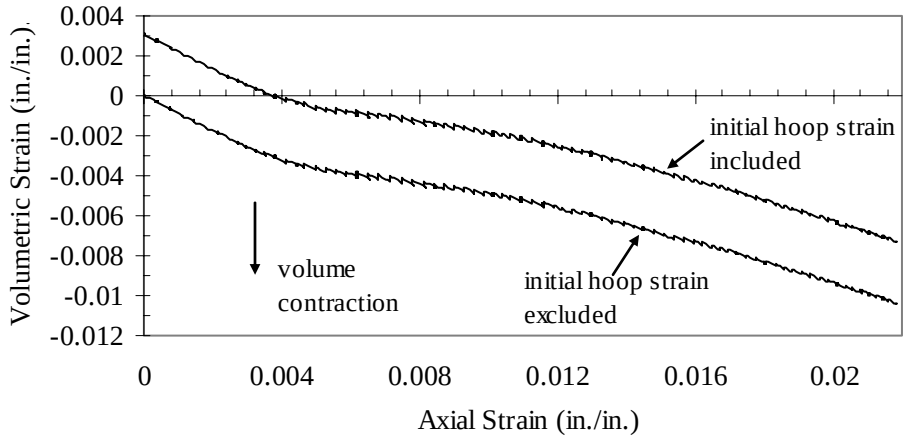

Figure 5.42 Volumetric versus axial strain curves for specimen S-CT-E

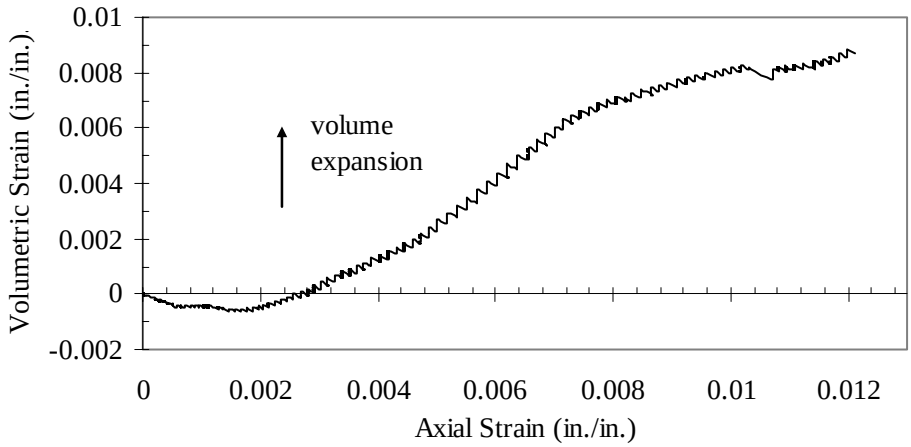

Figure 5.43 Volumetric versus axial strain curves for specimen S-CT-F

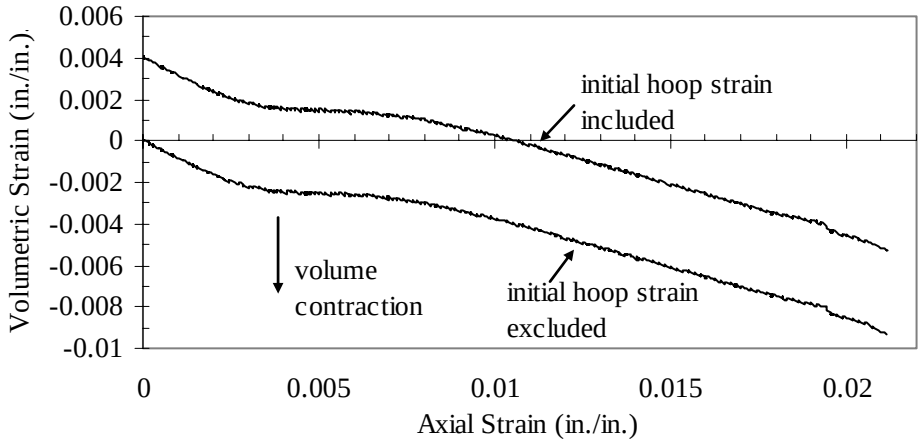

Figure 5.44 Volumetric versus axial strain curves for specimen S-GT-E

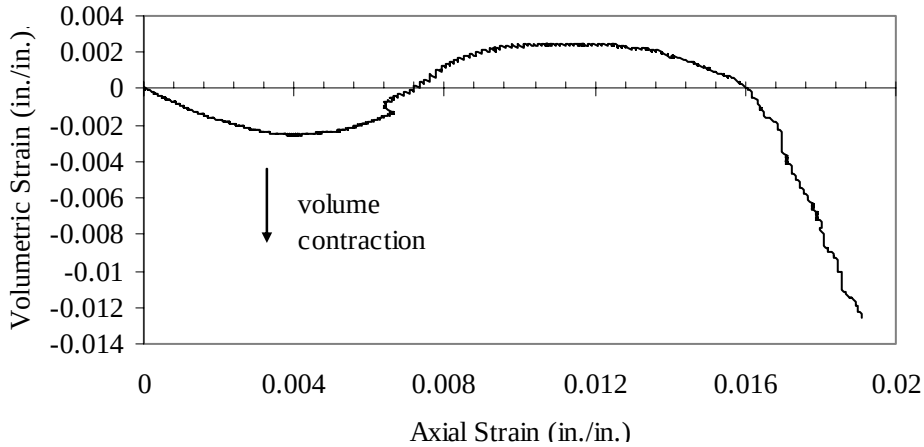

Figure 5.45 Volumetric versus axial strain curves for specimen S-GT-F

From the experimental results for square specimens, the following observations are made:
(1) Cross-section geometry significantly influences the compressive behavior of FRP jacketed columns. The effectiveness of FRP composite jackets for square columns is much less than that for circular columns. This is because of the corner effects and reduced confining pressure at the middle of the sides due to bending. For weakly confined square columns wrapped with FRP strips, obvious post-peak softening behavior occurred, indicating that confinement effects were not sufficient to restrict the expansion of concrete.

(2) The experimental results show a plastic behavior in which a higher axial strain is achieved for columns with softening, once the stress-strain curve reaches the initial peak. After this peak, the concrete expands more rapidly as the confining stress increases slightly or remains unchanged.

(3) Compared to circular columns, the efficiency of FRP jackets is reduced due to the corner effect. The observed ultimate hoop strains are less than those of circular jackets. The degree of reduction is related to the ratio of the side length to the radius of the corner.

(4) Square columns confined by FRP strips show very limited increase in axial strength. The higher axial strains observed from the tests were mainly due to the large axial deformation of the plain concrete between FRP strips. A significant softening behavior was observed for square columns with strips. Therefore, the application of FRP strips to square columns for the purpose of increasing axial stress capacity should be used with caution.

(5) Shape-modified columns show significant increases of both axial strength and ductility relative to columns with square section. These increases show that the effectiveness of circular geometry is much higher than square columns due to the membrane effect. The strength increase for specimens with expansive cement concrete is higher than that for specimens with non-shrink concrete. In addition, by using post-tensioned FRP jackets, the enhancement of ductility is more significant.

5.4 Rectangular Specimens

5.4.1 Specimens without shape modification

Two groups of rectangular specimens with aspect ratio of 2:1 (R2) and 3:1 (R3) were tested. The slenderness ratio, $\frac{L}{b}$, which is defined as the ratio of the length of specimen to the shorter size of the section was 4.5 for the R2 group and 6.0 for the R3 group. Test results for FRP jacketed specimens show an increase in both peak axial strength and axial strain. However, compared to circular specimens with the same FRP volumetric ratio, the strength enhancement is much lower. Each specimen demonstrated post-peak softening behavior and an obvious post-peak drop could be observed for the R3 group with 3:1 aspect ratio. Table 5.5 lists the main experimental results for specimens of both the R2 and R3 groups.

Table 5.5 shows that the R3 group could still achieve both strength and strain enhancements regardless of the higher aspect ratio (3:1) and slenderness ratio (6:1). The softening parameter, which is indicative of the degree of softening behavior, is defined as the ratio of ultimate axial stress f_{cu}' to the peak strength f_{cc}', $\frac{f_{cu}'}{f_{cc}'}$ as shown in Figure 5.1(c). It is noted that $\frac{f_{cu}'}{f_{cc}'}$ ranges from 75 to 90 percent for the R3 group while this value is close to 1.0 for the R2 group, which demonstrates that the R2 group can obtain more ductility than the R3 group with the same amount of FRP composite. Comparison of the ductility ratios calculated in Table 5.5 shows a better ductility for the R2 group compared to the R3 group. In general, FRP jackets can still be used to improve the compressive behavior of rectangular specimens through reasonable design. However, these increases are limited compared to circular columns, or even square specimens due to the lower effective stiffness of the FRP jacket, the corner effects, and the significant bending effects on the FRP composite at the middle of the section sides.

The failure modes of plain rectangular specimens are similar to unconfined square and circular specimens. As in the case of circular and square baseline specimens, the unjacketed rectangular plain concrete specimens exhibited axial strain at peak stress at a value of $\varepsilon_{co}' = 0.002$; very little post-peak behavior was observed during testing. Specimens failed shortly after the peak stress was reached due to a shear compression failure. Compared to unconfined circular or square specimens, these cracks were more significant.

Table 5.5 Main results for rectangular specimens without shape modification

Specimen ID	ρ_{FRP}	f_{cc}'(psi)	f_{cu}'(psi)	ε_{cc}' (in./in.)	ε_{cu}' (in./in.)	$\varepsilon_{jx,u}$ (in./in.)	$\varepsilon_{jy,u}$ (in./in.)	f_{cc}'/f_{co}'	$\varepsilon_{cu}'/\varepsilon_{co}'$	μ
R2-C2-0	0.0268	3500	3500	0.0045	0.023	0.0068	0.0089	1.59	11.5	1.14
R2-G6-0	0.1227	3180	3110	0.004	0.021	-	-	1.44	10.5	0.91
R3-C2-0	0.0311	3203	2413	0.0046	0.021	0.0062	0.0078	1.46	10.5	0.78
R3-G6-0	0.1422	3130	2820	0.0036	0.021	0.0011	0.0014	1.42	10.5	0.89

where $\varepsilon_{jx,u}$ = the ultimate fiber strain on the long side of the rectangular section; $\varepsilon_{jy,u}$ = the ultimate fiber strain on the short side of the rectangular section.

As for jacketed specimens, failure occurred suddenly. Because of the brittle behavior of the FRP composite materials, failure of the jacketed specimens occurred suddenly without warning. In almost all cases, the breakage line appeared at a corner, exactly at the end of the rounding; FRP breakage occurred in a smaller area near the mid-height of the specimens. Cracks were seen on the concrete surface but no concrete spalling was observed. This behavior is different compared to square and circular specimens, and is especially different for specimens that are heavily confined. The reason for the difference is the influence of the shape factor of rectangular sections, contributing to the weaker confinement which results in smaller energy absorption during the tests. Therefore, failure was not as sudden as that of heavily-confined specimens. Different observations for the failure modes of rectangular specimens are shown in Figures 5.46 through 5.51.

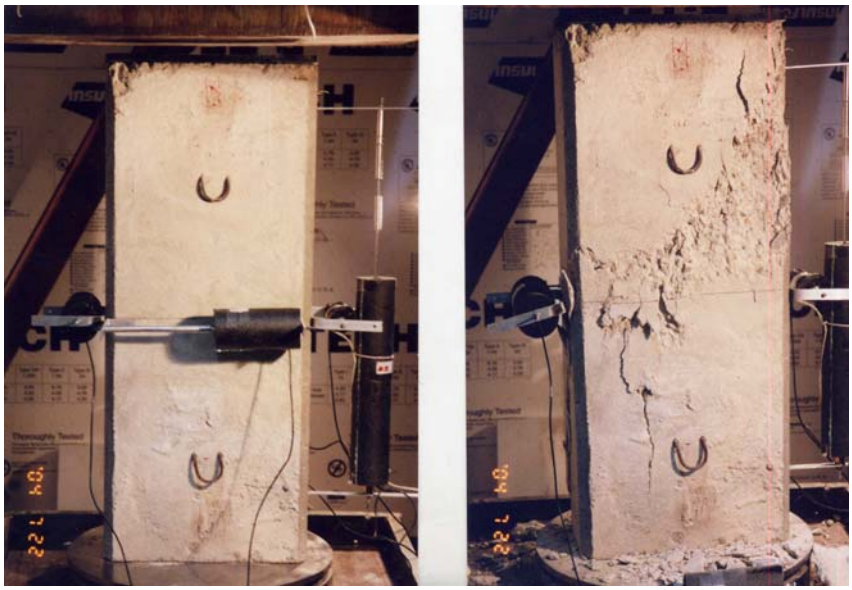

Figure 5.46 Specimen R2-0-0 with plain concrete before and after testing

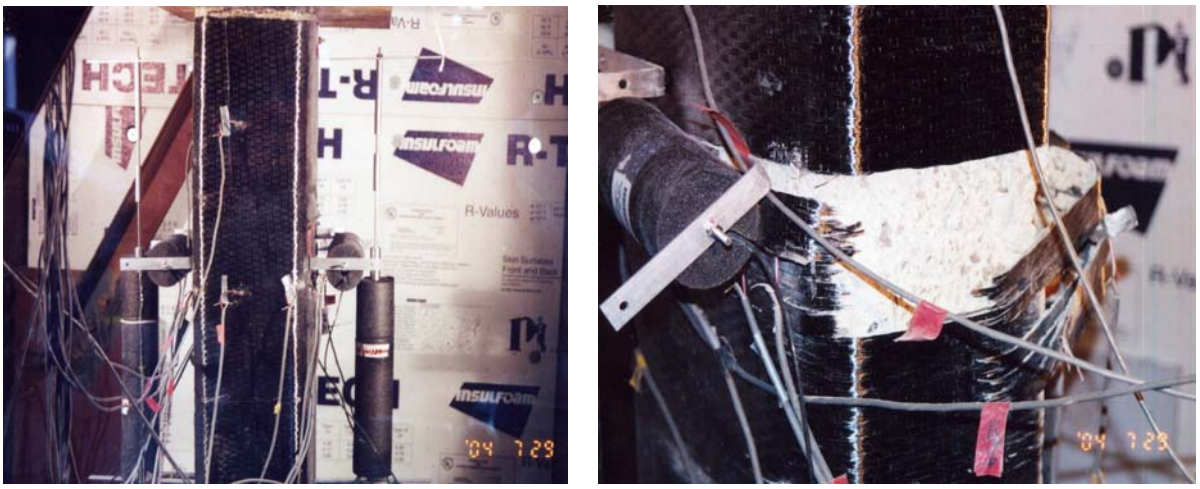

Figure 5.47 Specimen R2-C2-0 with 2 CFRP layers before and after testing

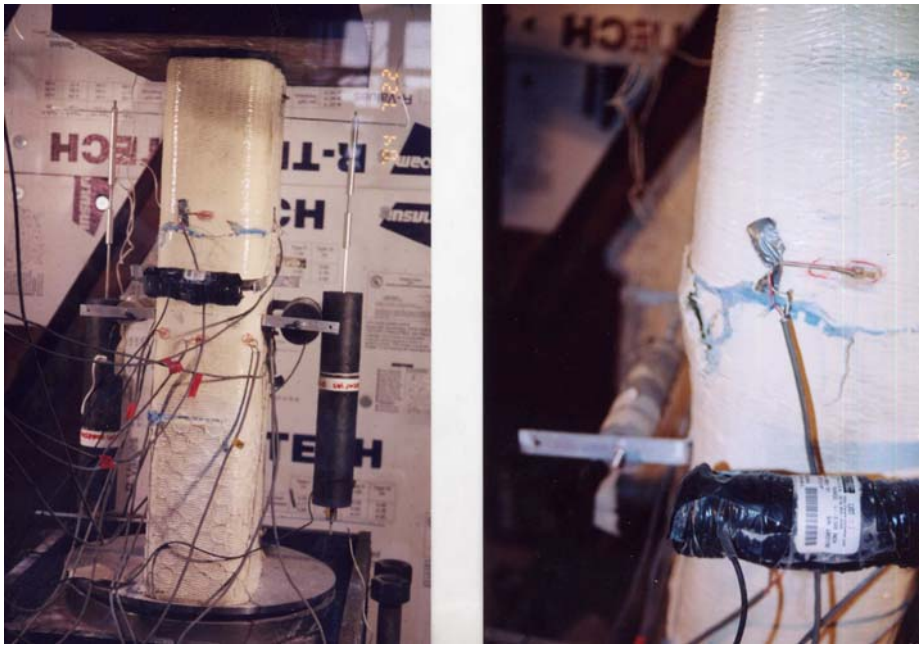

Figure 5.48 Specimen R2-G6-0 with 6 GFRP layers before and after testing

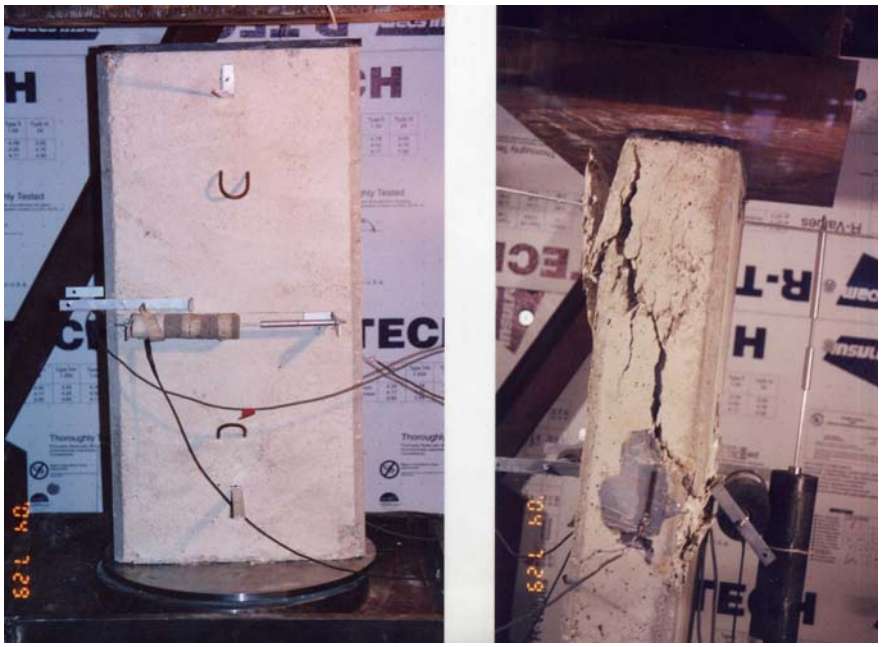

Figure 5.49 Specimen R3-0-0 with plain concrete before and after testing

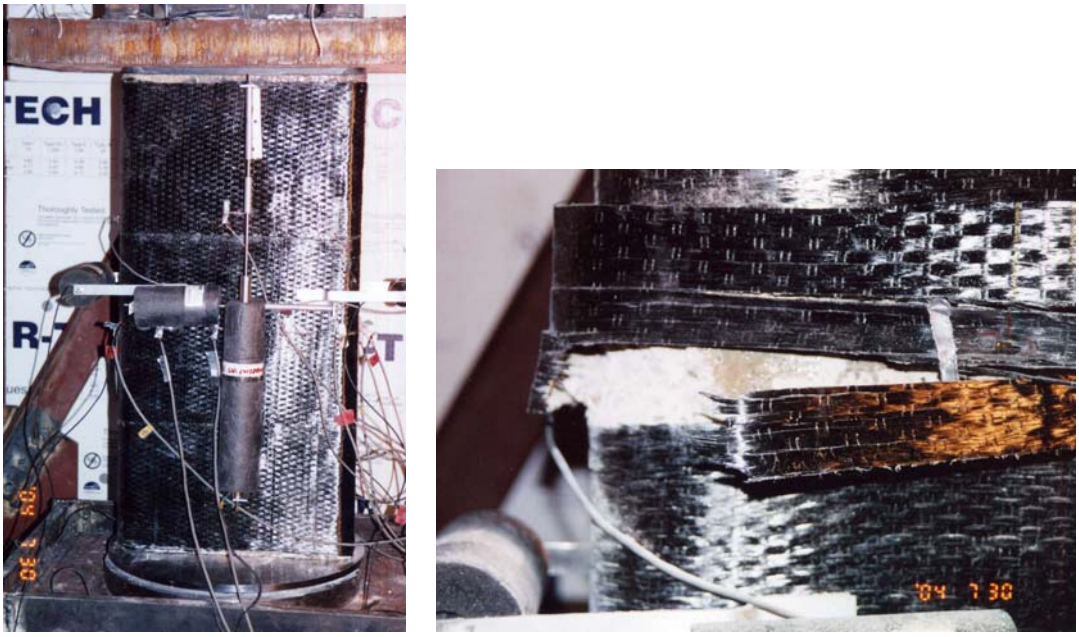

Figure 5.50 Specimen R3-C2-0 with 2 CFRP layers before and after testing

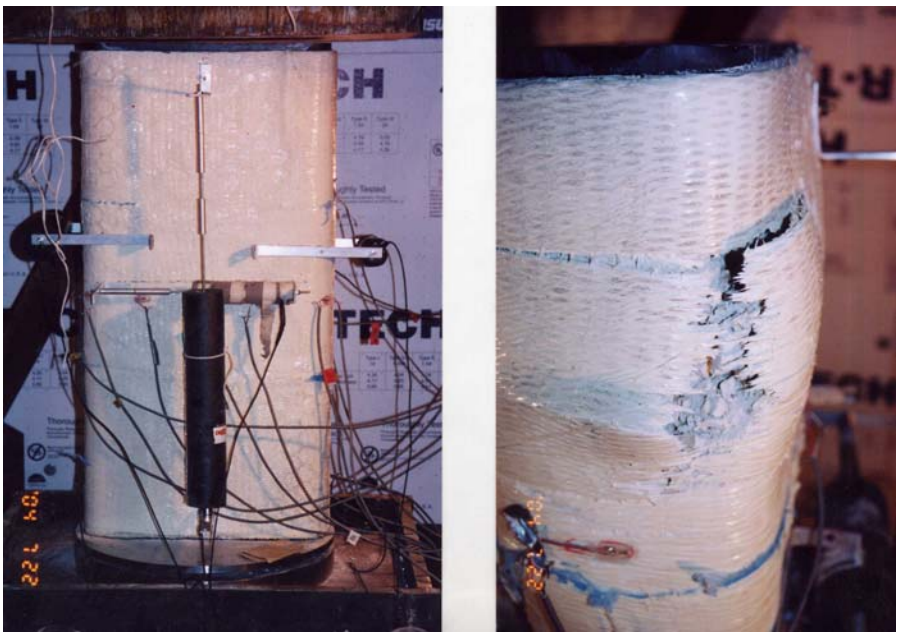

Figure 5.51 Specimen R3-G6-0 with 6 GFRP layers before and after testing

Axial stress versus axial and fiber strain curves for FRP-confined rectangular specimens are presented in Figures 5.52 through 5.55. Each curve includes two parts: the axial stress versus axial strain relation, and axial stress versus fiber strain at the middle of the short side, fiber strain at the middle of the long side, and fiber strain at the corner.

One important feature of these figures is that, for different levels of lightly-confined FRP jackets, the initial peak axial stress f_{cc}' has always been reached at the same level and for a similar axial strain of about 0.004 in./in. In all cases the post-peak drop of the curve is always followed by an increase in stiffness. In the initial ascending portion of the stress-strain curve, the FRP jacket provides an arching-effect confinement to the concrete but the level of confinement is lower due to the rectangular geometry which produces bending at the cross-section side in the FRP composite, and the corner effect which produces stress concentration in the FRP composite at the 90-degree corners. Therefore, the initial f_{cc}' is slightly improved and the corresponding axial strain ε_{cc}' is higher than ε_{co}'. When the axial stress reached its peak, concrete started to expand, but the FRP composite could not provide enough confining pressure to restrain the transverse dilation; this caused the axial capacity to decrease while the axial and transverse strain increased. After concrete expanded and the FRP jackets became fully engaged, the axial capacity was increased again and the compressive stress and axial strain increased linearly until failure.

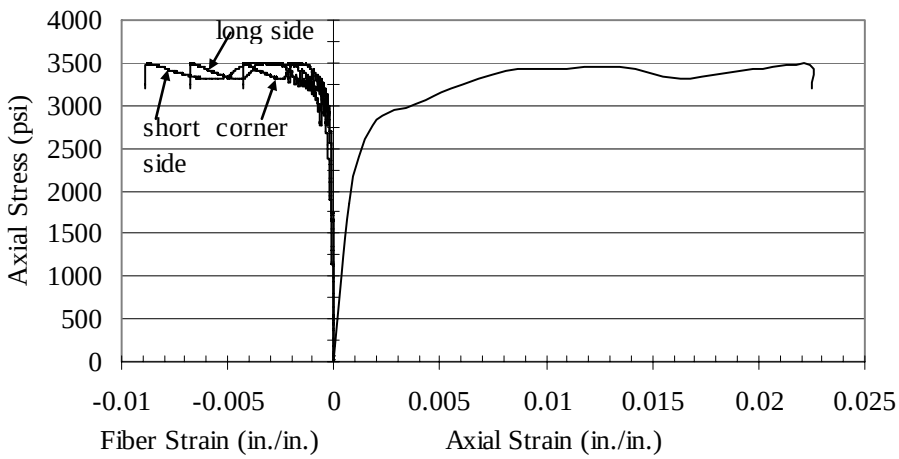

Figure 5.52 Stress-strain curves for R2-C2-0

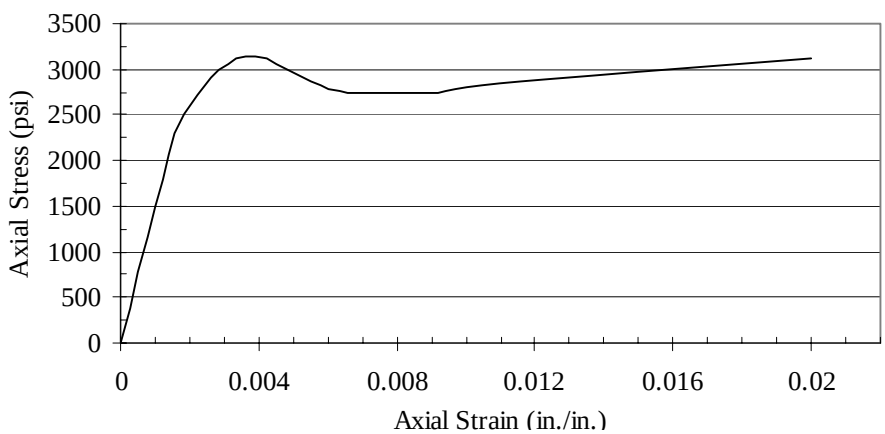

Figure 5.53 Stress-strain curves for R2-G6-0 (Due to errors during the testing of R2-G6-0 only axial strain was recorded)

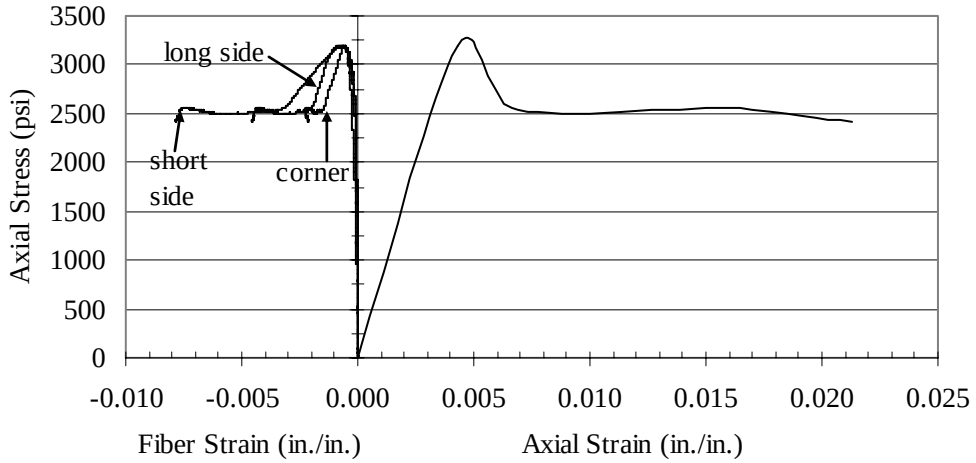

Figure 5.54 Stress-strain curves for R3-C2-0

For some weakly-confined specimens, concrete was always damaged before getting the FRP jackets effectively engaged. In this case, no ascending curve could be observed. This behavior indicates that the jacket efficiency is much lower for rectangular specimens. Another aspect observed for specimens with softening behavior is that those specimens could always reach a higher ultimate axial strain although the strength enhancement was limited. This is because the cross-section was not uniformly confined and the region near the corner was more restrained compared to other portions of the cross section; this resulted in an increase of axial stress near the corner and a decrease of axial stress (softening) in the remaining cross-section.

Transverse strains on the longer side were measured by the LVDTs showing the average strain on the side of the cross-section. Additional stress-strain curves are shown in Figures 5.56, 5.57 and 5.58 to compare transverse strains with fiber strains, as measured by strain gauges applied on the FRP composite, as was shown in Figure 4.1.

These curves clearly show that before the axial stress reached its initial peak, the fiber strains were consistent with the transverse strains; however, after the initial peak stress was reached, transverse strains increased significantly while the fiber strains changed very little. This behavior is similar to that observed from tests of lightly-confined square specimens, which indicates that the FRP jacket cannot provide enough confinement to restrain the transverse expansion of concrete once concrete starts to dilate. Also similar to square specimens, bulging was clearly evident from the larger transverse strains observed across the sides.

As for rectangular specimens, the non-uniformity of fiber strains over the cross-section perimeter is also notable. Figures 5.59, 5.60 and 5.61 show the fiber stain versus axial strain for the fiber strain on the long side, the short side and at the corner of rectangular specimens.

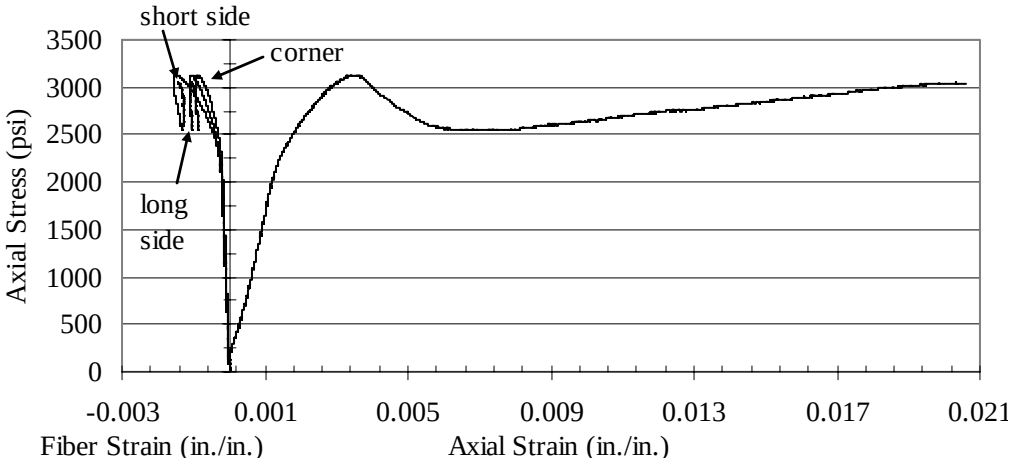

Figure 5.55 Stress-strain curves for R3-G6-0

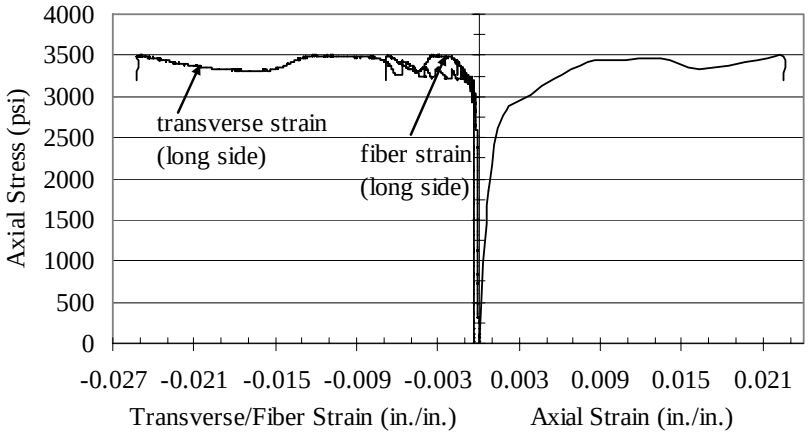

Figure 5.56 Stress-strain curves for R2-C2-0 comparing transverse and fiber strains

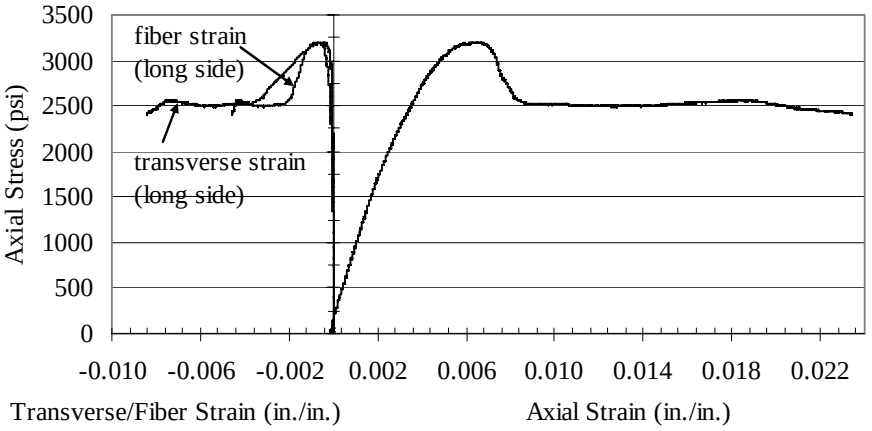

Figure 5.57 Stress-strain curves for R3-C2-0 comparing transverse and fiber strains

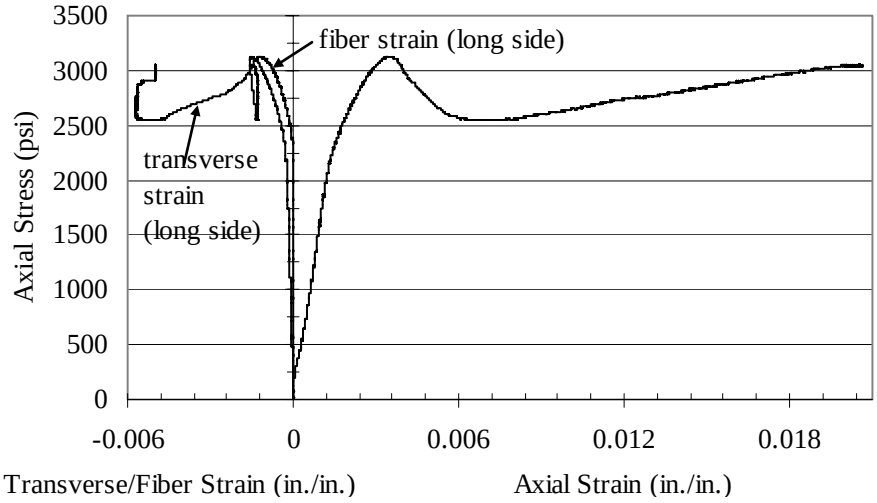

Figure 5.58 Stress-strain curves for R3-G6-0 comparing transverse and fiber strains

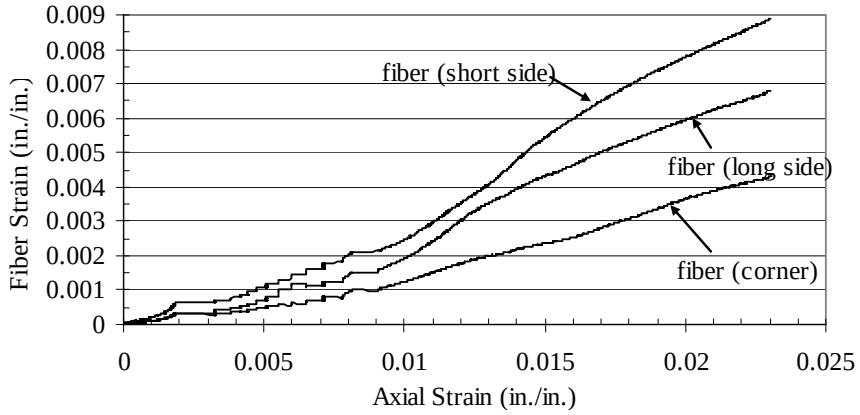

Figure 5.59 Fiber strain versus axial strain curves for R2-C2-0

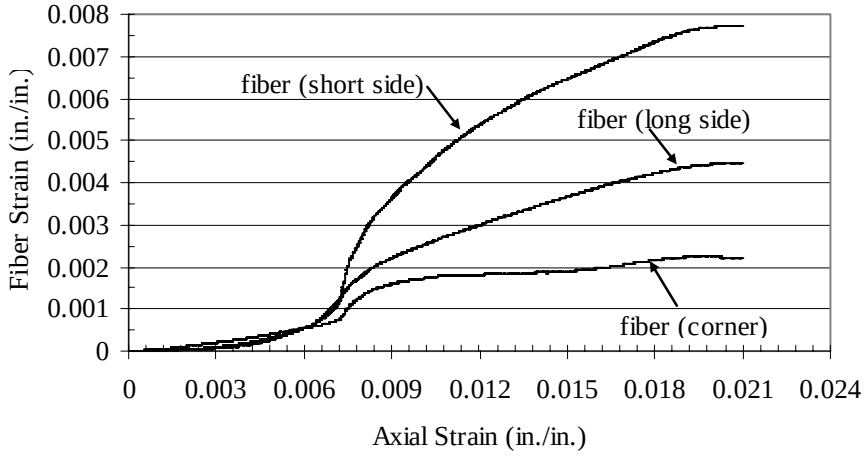

Figure 5.60 Fiber strain versus axial strain curves for R3-C2-0

It is clear from these curves that fiber strains at the middle of the short sides were always higher than at the middle of the long sides. This shows that the efficiency of the FRP composite jacket is relative to the size of the cross section and will be further discussed in Chapter 6. In addition, fiber strains at the corners were always lower than those at both the long and short sides. This observation proves that confinement provided by the FRP jacket is more effective at the corners than on the flat sides. Again, lightly-confined specimens with softening behavior exhibited plastic behavior similar to some square specimens as discussed earlier, after the initial peak stress was reached.

Figures 5.62-5.64 present volumetric versus axial strain curves for FRP-confined rectangular specimens except R2-G6-0 because no data regarding fiber strain was obtained for this specimen. Significant dilation behavior is seen in these curves and there is no sign of volume contraction beyond ε_0. The average of ε_0 was found to be 0.004 in./in. from these curves which is equal to ε_{cc}' as listed in Table 5.5 and also corresponds to the axial peak stress f_{cc}'. These observations are similar to those made for the square specimens which showed similar softening behavior.

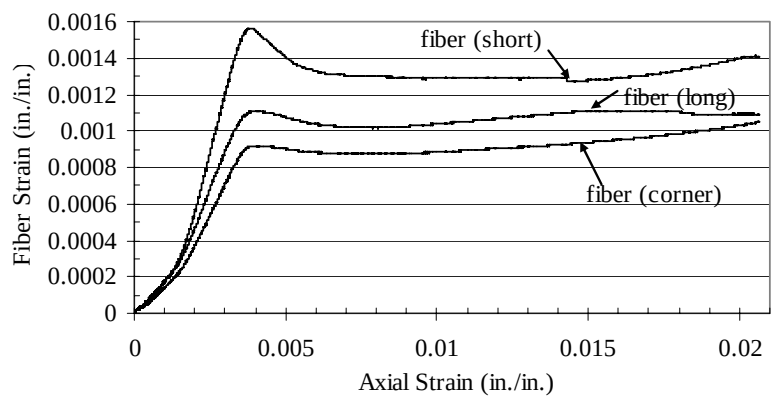

Figure 5.61 Fiber strain versus axial strain curves for R3-G6-0

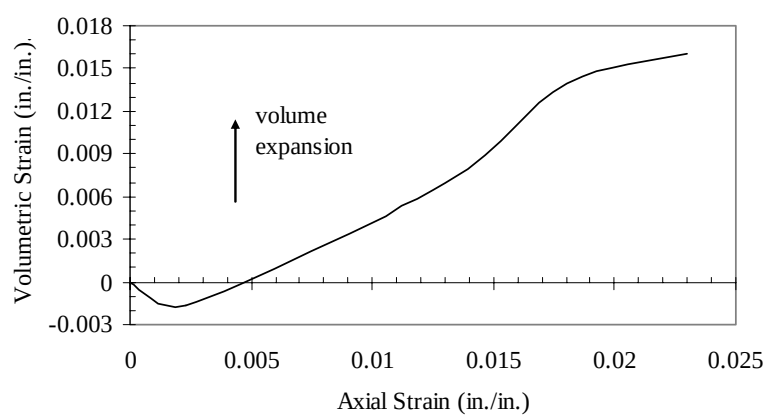

Figure 5.62 Volumetric versus axial strain curve for specimen R2-C2-0

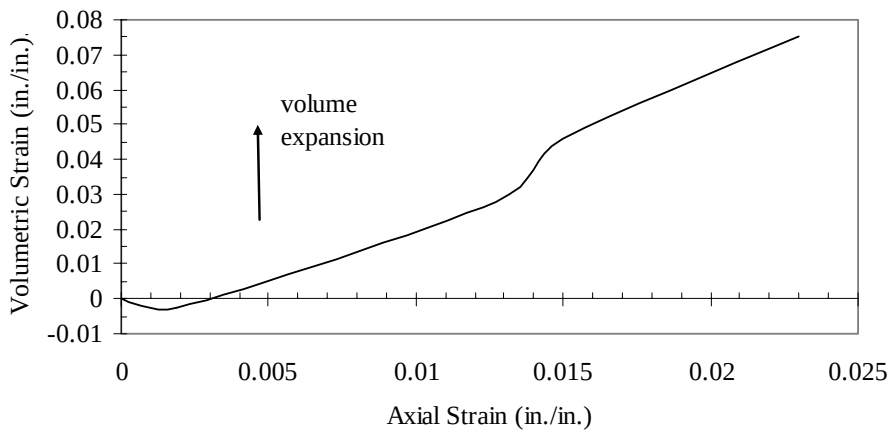

Figure 5.63 Volumetric versus axial strain curve for specimen R3-C2-0

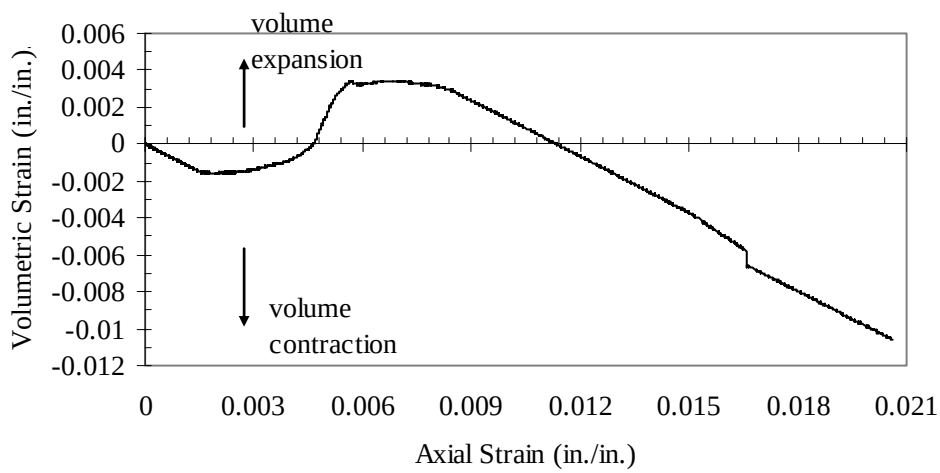

Figure 5.64 Volumetric versus axial strain curve for specimen R3-G6-0

5.4.2 Specimens with shape modification

Similar to shape-modified square specimens, eight shape-modified specimens were built by using the two different construction methods. Thus, with respect to each rectangular type, two elliptical specimens were investigated. Table 5.6 lists the properties of each specimen. Due to the differences between geometry, the mean unconfined strength f_{co}' was calculated by using Eq. (5.4) in Chapter 5.3 and the results of f_{co}' are also listed in Table 5.6.

The main test results are listed in Table 5.7 regarding ultimate axial stress, ultimate strains and ductility ratio. Compared with rectangular specimens, substantial strength and ductility gains were achieved; however, these increases were dependent on the aspect ratio B_j / D_j; that is, specimens with higher aspect ratios showed lower degrees of performance; this feature will be discussed later.

The comparisons of strength enhancement ratio and ductility ratio between regular concrete specimens and expansive cement concrete specimens for the R2 and R3 groups are listed in Figure 5.65 and Figure 5.66. It is seen from these figures that there are increases in both strength enhancement ratios and ductility ratios; however; these increases are largely dependent on the aspect ratio and the method of performing shape modification. Compared to the R2 group, both increases in strength and ductility ratio are restricted for the R3 group.

Another observation from Figures 5.65 and 5.66 is that in general, the increase in strength and ductility for shape-modified specimens with expansive cement concrete and non-bonded jackets is higher than that for specimens with non-shrink concrete and bonded FRP jackets except R2-CT-E and R3-GT-E. Compared to R2-CT-F, the increase in ductility ratio for R2-CT-E is smaller as shown in Figure 5.65(b). This is because the aspect ratio of R2-CT-F is lower than that of R2-CT-E (as shown in Table 5.6) due to construction difficulties; the rupture strain of the FRP composite is higher for R2-CT-F than the same type of specimen with a higher aspect ratio; the same explanation applies for the ductility ratio of R3-GT-E which is lower than that of R3-GT-F.

Table 5.6 Details of shape-modified rectangular specimens

Specimen ID	B_j (in.)	D_j (in.)	B_j/D_j	A (in^2)	A_f (in^2)	Increase in Cross-Sectional Area	f_{co}' (psi)
R2-CT-E	25	15 1/4	1.6:1	299	179	250%	1788
R2-CT-F	25 1/2	16 1/2	1.5:1	330	210	275%	2207
R2-GT-E	26	14 1/4	1.8:1	291	171	240%	1796
R2-GT-F	27 1/4	14	1.9:1	300	180	250%	2207
R3-CT-E	30 1/2	11	2.8:1	264	156	240%	1787
R3-CT-F	29 3/8	15	2.0:1	346	238	320%	2200
R3-GT-E	30	11 3/4	2.6:1	277	169	250%	1773
R3-GT-F	29 1/8	12 1/4	2.4:1	280	172	260%	2200

Table 5.7 Main results for shape-modified rectangular specimens

Specimen ID	ρ_{FRP}	f_{cc}'(psi)	f_{cu}'(psi)	ε_{cc}' (in./in.)	ε_{cu}' (in./in.)	$\varepsilon_{jx,u}$ (in./in.)	$\varepsilon_{jy,u}$ (in./in.)	f_{cc}'/f_{co}'	$\varepsilon_{cu}'/\varepsilon_{co}'$	μ
R2-CT-E	0.015	3975	-	0.011	-	0.0046*	0.0034*	2.22	5.50	1.69
R2-CT-F	0.014	4389	-	0.017	-	0.0079	0.0054	1.99	8.50	2.50
R2-GT-E	0.071	4094	-	0.018	-	0.0083*	0.0059*	2.32	9.00	2.72
R2-GT-F	0.071	3234	2567	0.002	0.0058	0.0061	0.0035	1.47	2.90	0.97
R3-CT-E	0.018	3717	-	0.008	-	0.0047*	0.0018*	2.08	4.30	1.45
R3-CT-F	0.015	3400	3278	0.004	0.0091	0.0062	0.0027	1.55	4.55	1.01
R3-GT-E	0.080	2682	1901	0.006	0.0210	0.0095*	0.0047*	1.51	10.50	0.93
R3-GT-F	0.073	3058	-	0.010	-	0.0041	0.0019	1.39	5.00	1.01

$\varepsilon_{jx,u}$ = ultimate fiber strain on the minor axis of the elliptical section;
$\varepsilon_{jy,u}$ = ultimate fiber strain on the major axis of the rectangular section;
* Initial post-tensioning strains are included.

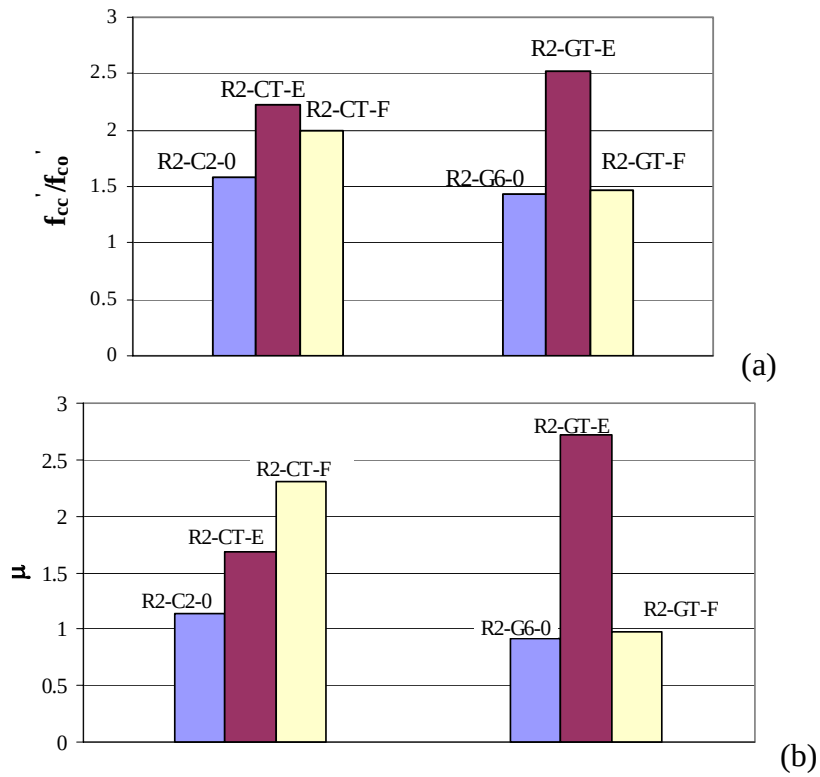

Figure 5.65 Comparisons between rectangular R2 and shape-modified specimens: (a) strength enhancement ratio; (b) ductility ratio

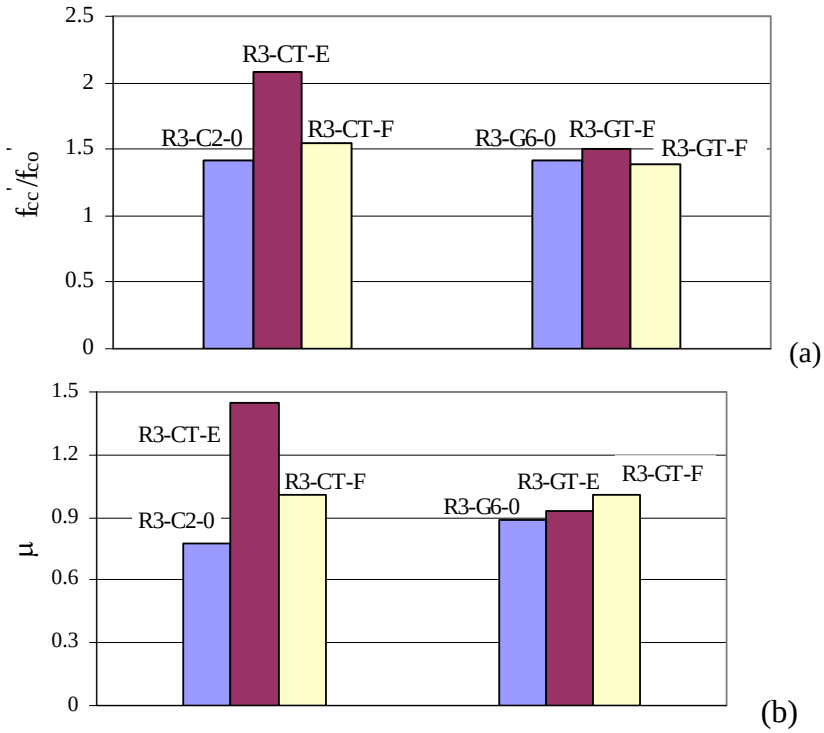

Figure 5.66 Comparisons between rectangular R3 and shape-modified specimens: (a) strength enhancement ratio; (b) ductility ratio

The observed failure modes of shape-modified rectangular specimens were different for different bond types of FRP jackets as seen in Figure 5.67 to 5.74.

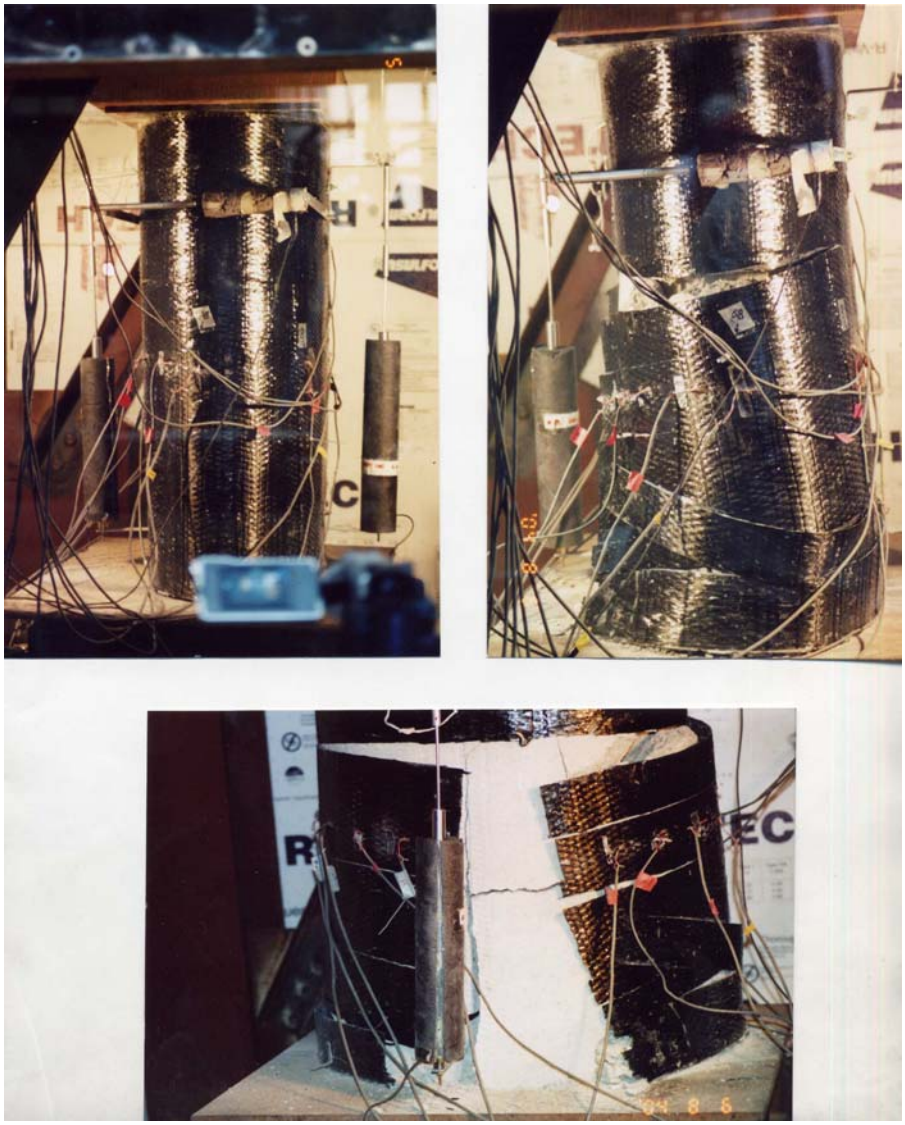

Figure 5.67 Specimen R2-CT-E with expansive cement concrete and 2 CFRP layers before and after testing

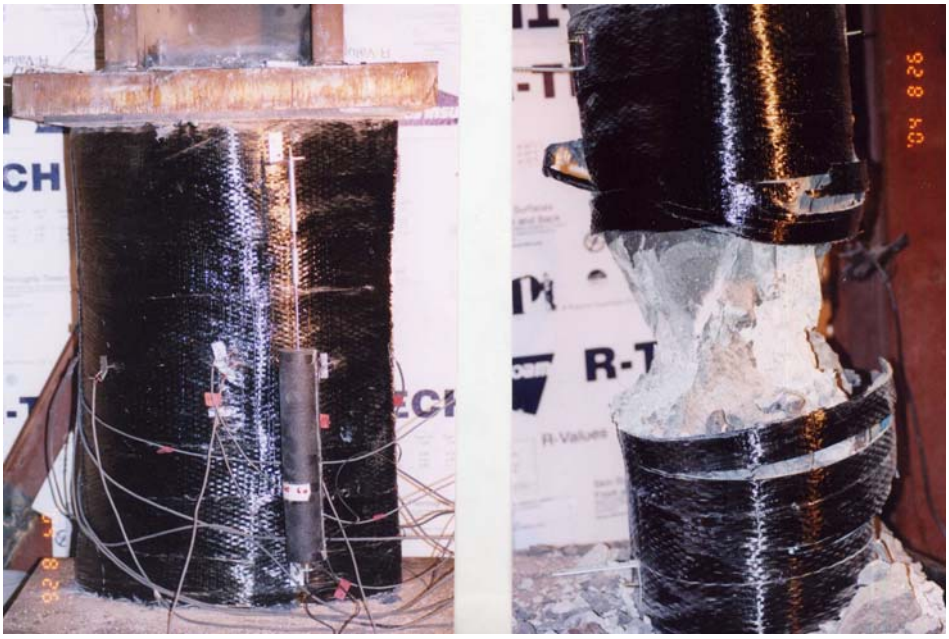

Figure 5.68 Specimen R2-CT-F with non-shrink cement concrete and 2 CFRP layers before and after testing

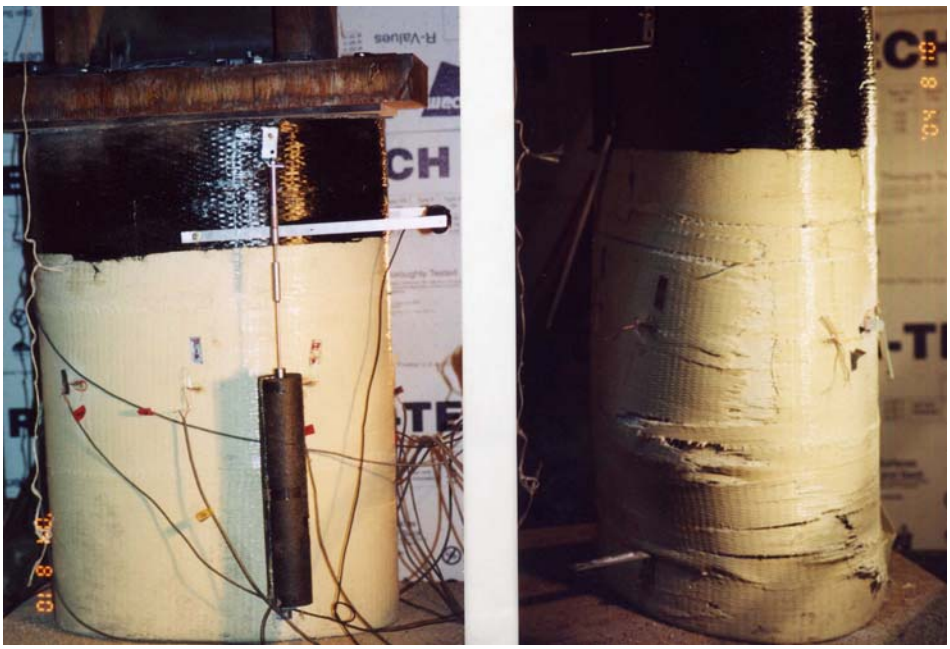

Figure 5.69 Specimen R2-GT-E with expansive cement concrete and 6 GFRP layers before and after testing

Figure 5.70 Specimen R2-GT-F with non-shrink cement concrete and 6 GFRP layers after testing

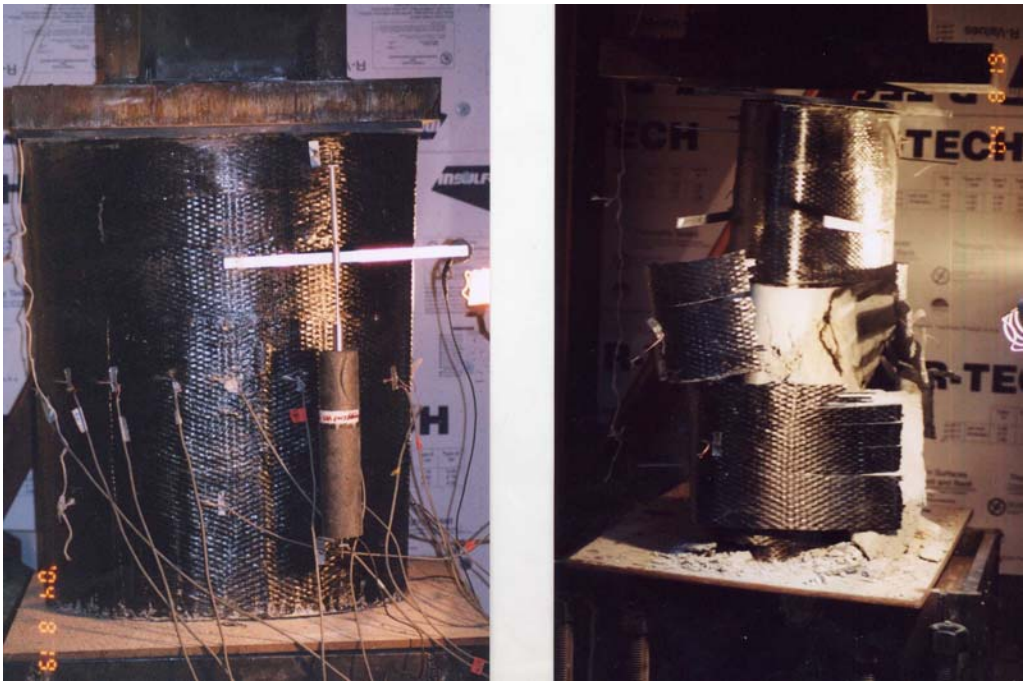

Figure 5.71 Specimen R3-CT-E with expansive cement concrete and 2 CFRP layers before and after testing

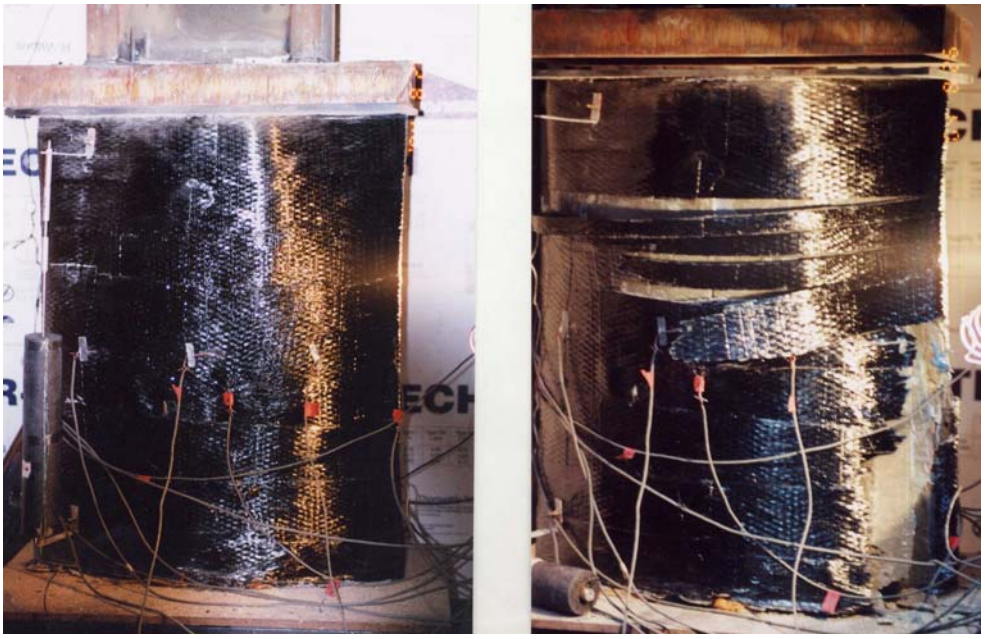

Figure 5.72 Specimen R3-CT-F with non-shrink cement concrete and 2 CFRP layers before and after testing

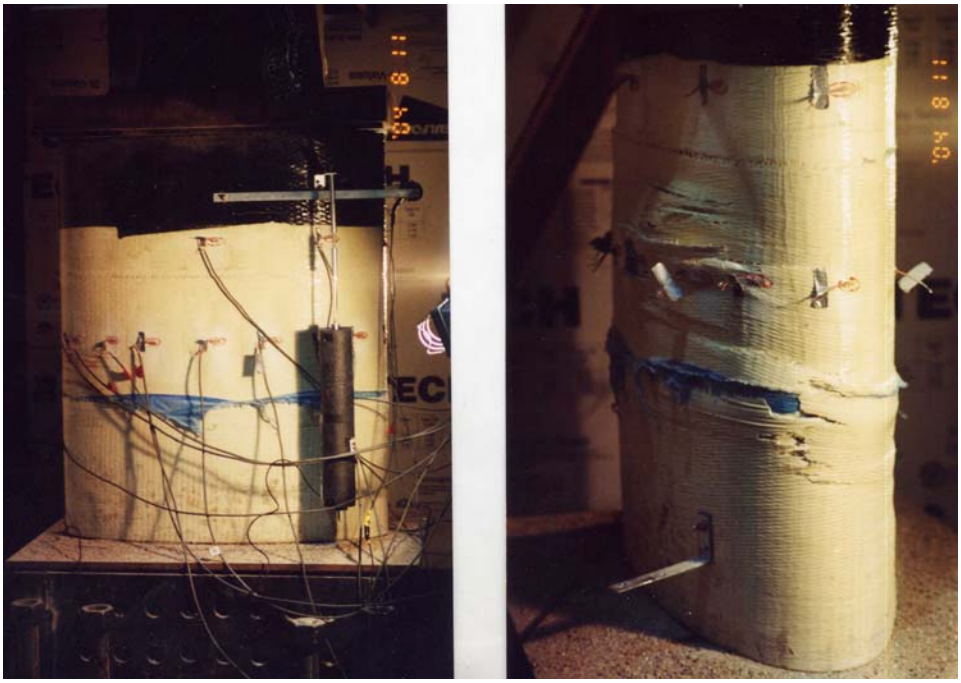

Figure 5.73 Specimen R3-GT-E with expansive cement concrete and 6 GFRP layers before and after testing

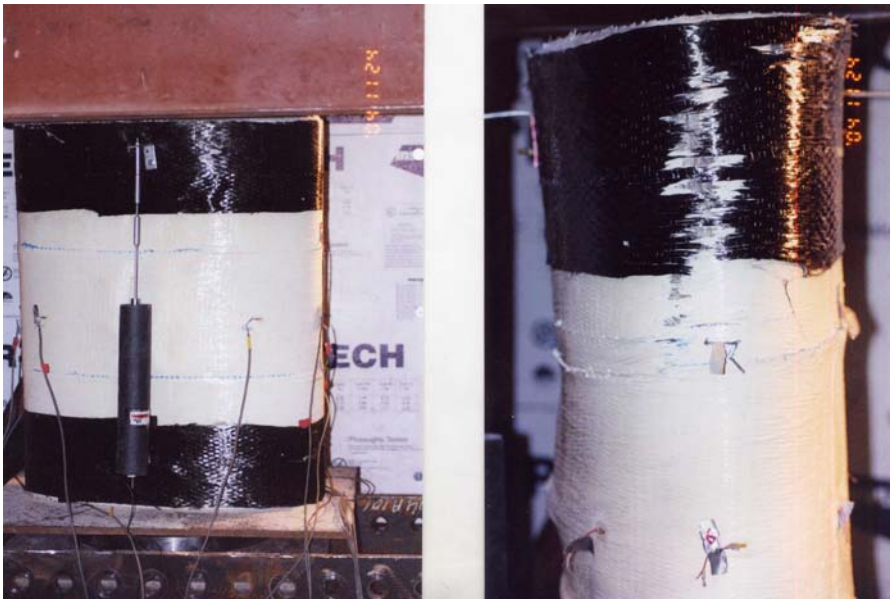

Figure 5.74 Specimen R3-GT-F with non-shrink cement concrete and 6 GFRP layers before and after testing

For bonded-jacketed specimens with non-shrink concrete, failure occurred when the concrete was crushed, and this was followed by breakage of the FRP jacket. It was clear that a concrete cone had formed at the mid-height at failure, as observed in Figure 5.68 after testing. In most cases, FRP jackets failed near the minor axis of the elliptical cross-section at mid-height of the specimen as shown in Figures 5.67, 5.71 and 5.72. As for non-bonded jacketed specimens with expansive cement concrete, the breakage line of the FRP jacket was more extensive and was not limited to the mid-height area; at failure the expansive cement concrete broke into many pieces and came off the surface of the rectangular core as shown in Figures 5.67 and 5.71. In general, the concrete in specimens with higher aspect ratio showed a lower degree of damage than in specimens with lower aspect ratio. As expected, CFRP-jacketed specimens always showed more explosive and sudden failure and higher degrees of damage compared to GFRP-jacketed specimens.

The stress-strain curves for shape-modified rectangular specimens are shown in Figures 5.75-5.82. On the left half of each curve, both the hoop strain at major vertices and minor vertices is plotted. This is the fiber strain measured by the strain gauges. In addition, for specimens with expansive cement concrete, post-tensioning strains of FRP jackets before the axial load was applied are included.

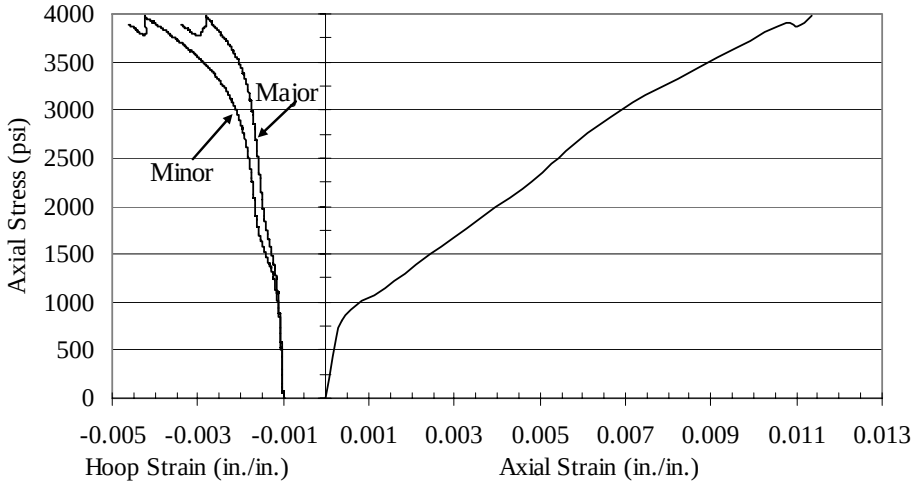

Figure 5.75 Stress-strain curves for R2-CT-E

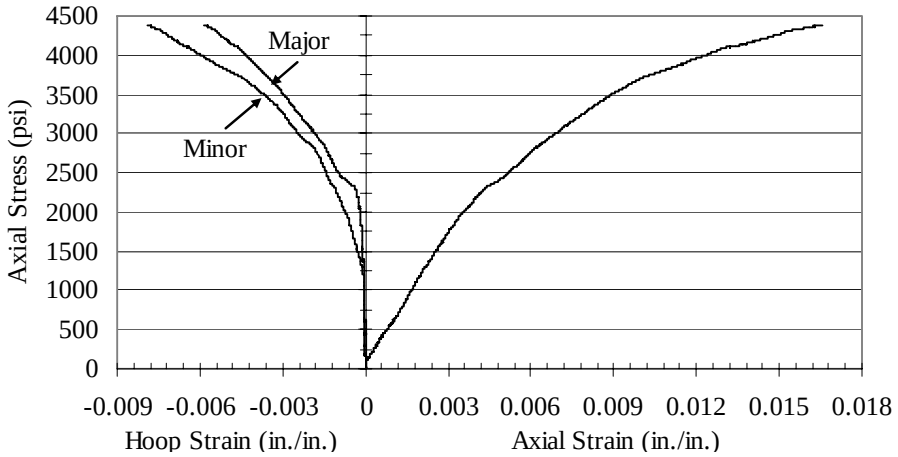

Figure 5.76 Stress-strain curves for R2-CT-F

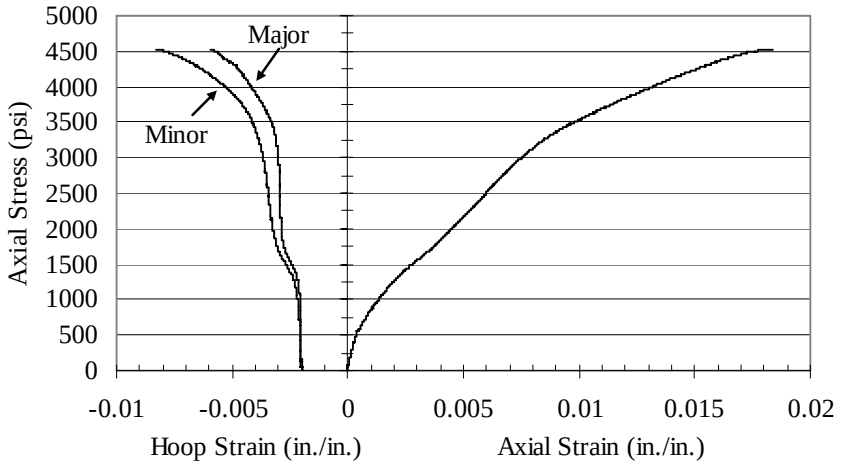

Figure 5.77 Stress-strain curves for R2-GT-E

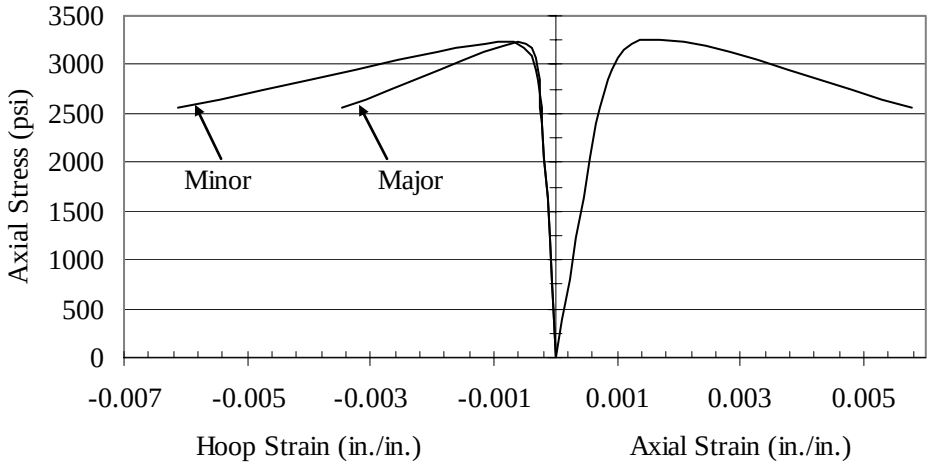

Figure 5.78 Stress-strain curves for R2-GT-F

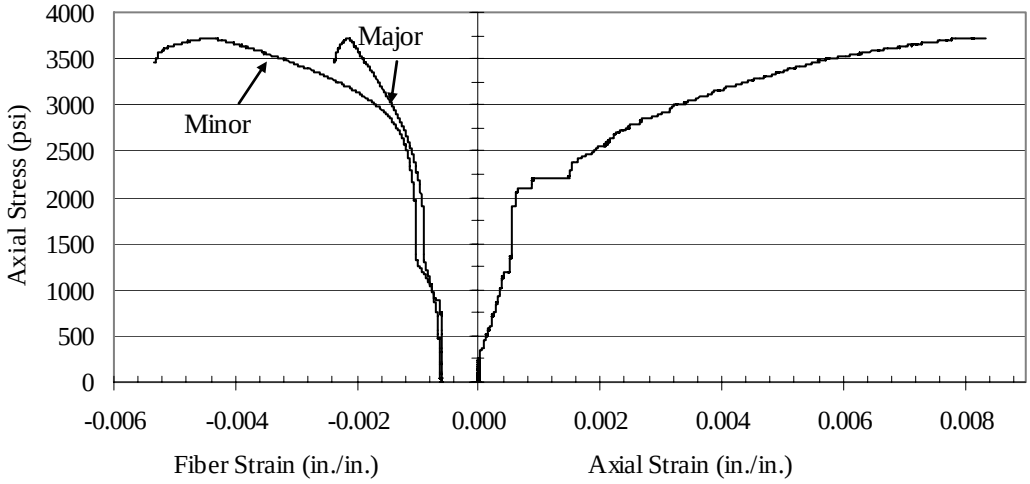

Figure 5.79 Stress-strain curves for R3-CT-E

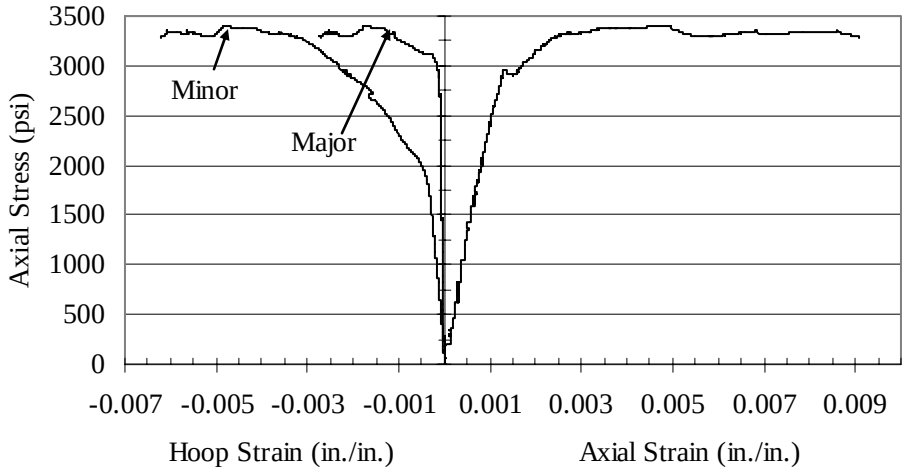

Figure 5.80 Stress-strain curves for R3-CT-F

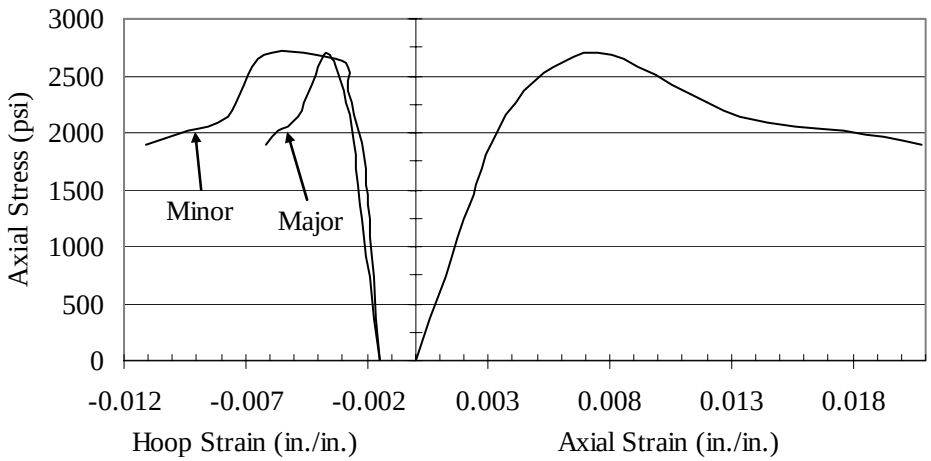

Figure 5.81 Stress-strain curves for R3-GT-E

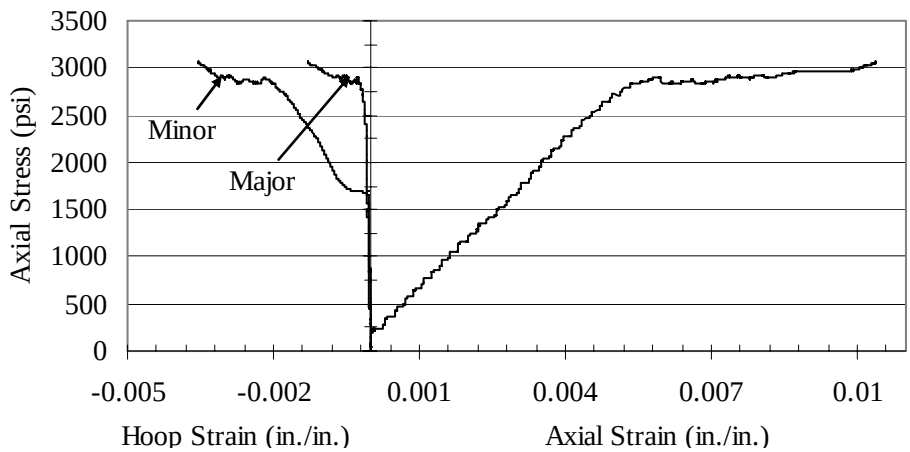

Figure 5.82 Stress-strain curves for R3-GT-F

The volumetric versus axial strain relations for shape-modified rectangular specimens are presented in Figure 5.83 through 5.89. The dilatancy behavior of specimens with expansive cement concrete demonstrated consistently an approximate linear relation between volumetric and axial strain which is similar to the results of corresponding shape-modified square specimens but with a reduced slope. This conclusion will be further discussed in Ch.6. Shape-modified rectangular specimens with non-shrink cement concrete demonstrated totally different dilatancy behavior compared to specimens with expansive cement concrete. In general, more volume expansion is expected as the aspect ratio increases.

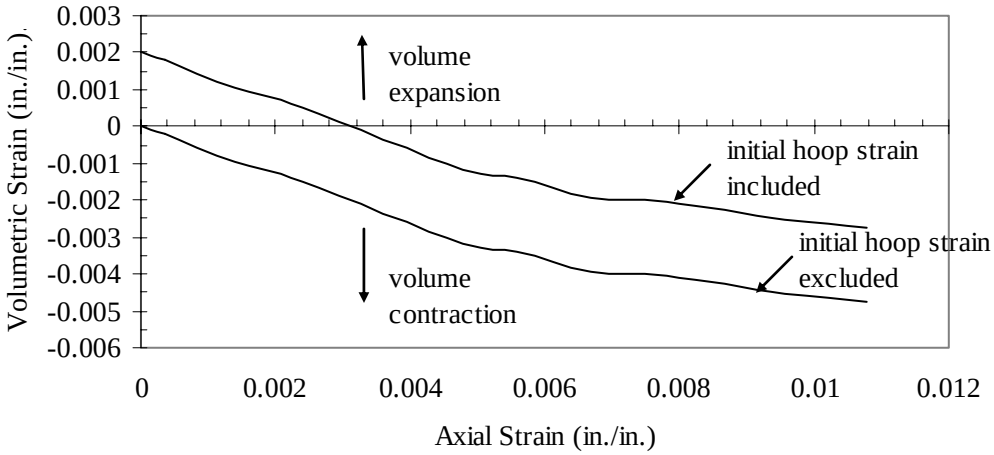

Figure 5.83 Volumetric versus axial strain curves for specimen R2-CT-E

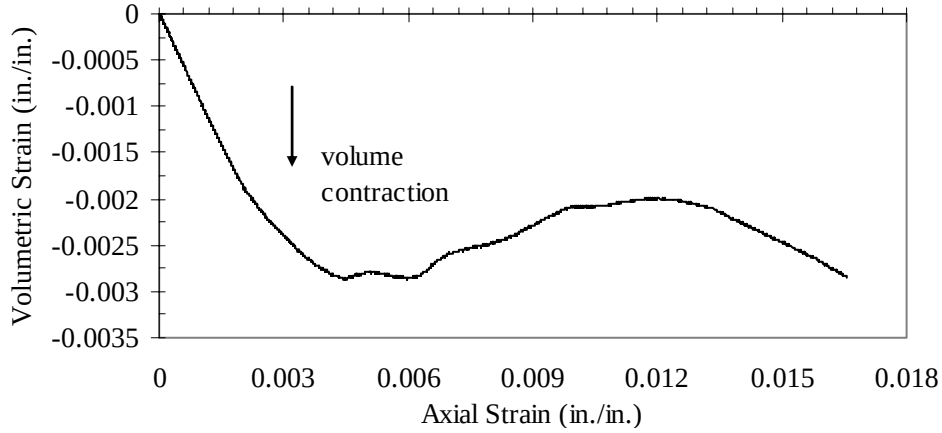

Figure 5.84 Volumetric versus axial strain curves for specimen R2-CT-F

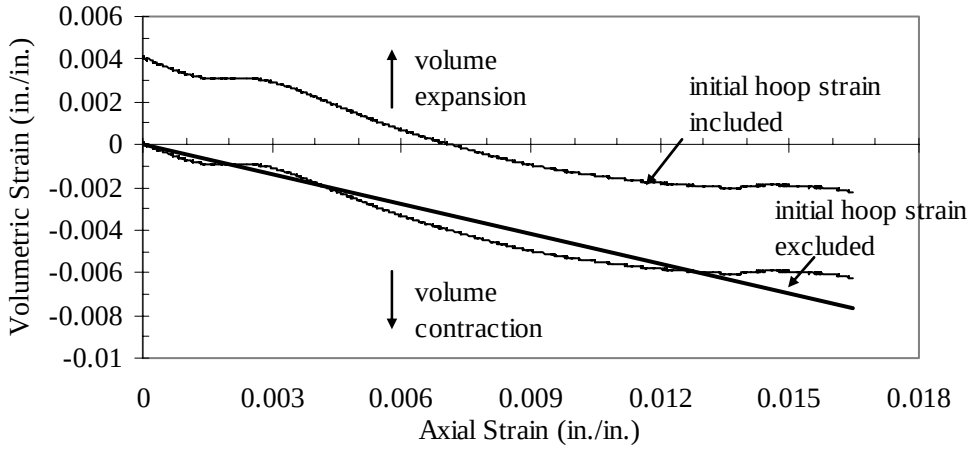

Figure 5.85 Volumetric versus axial strain curves for specimen R2-GT-E

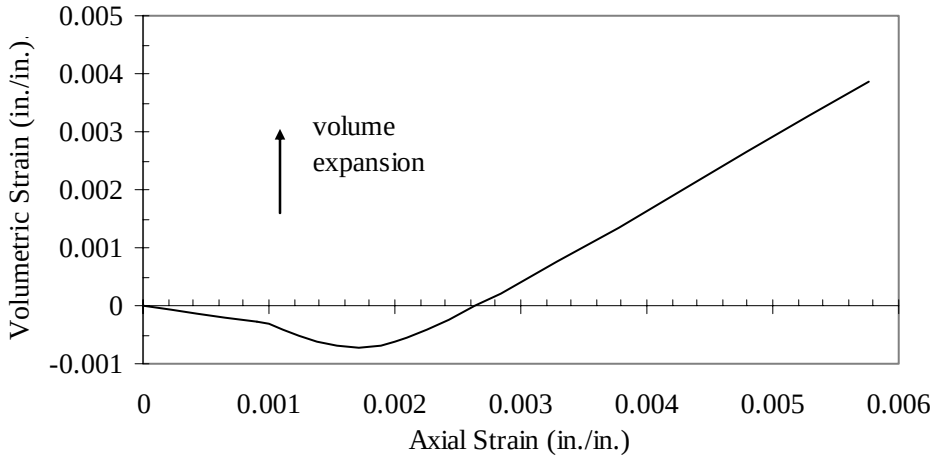

Figure 5.86 Volumetric versus axial strain curves for specimen R2-GT-F

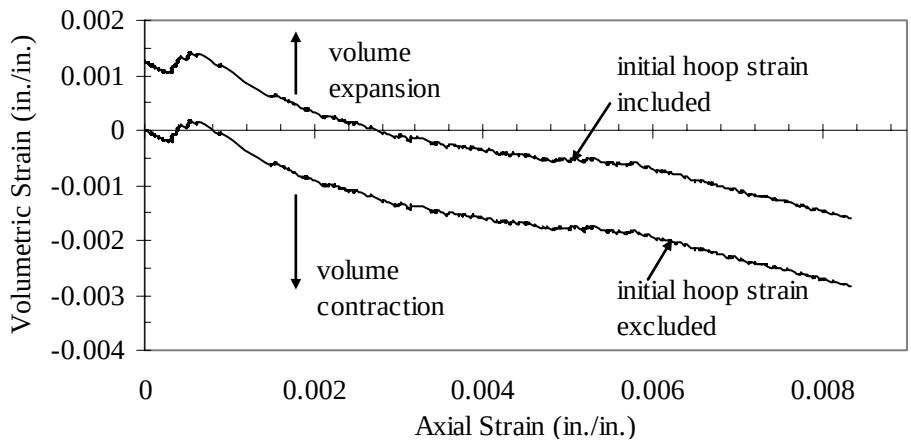

Figure 5.87 Volumetric versus axial strain curves for specimen R3-CT-E

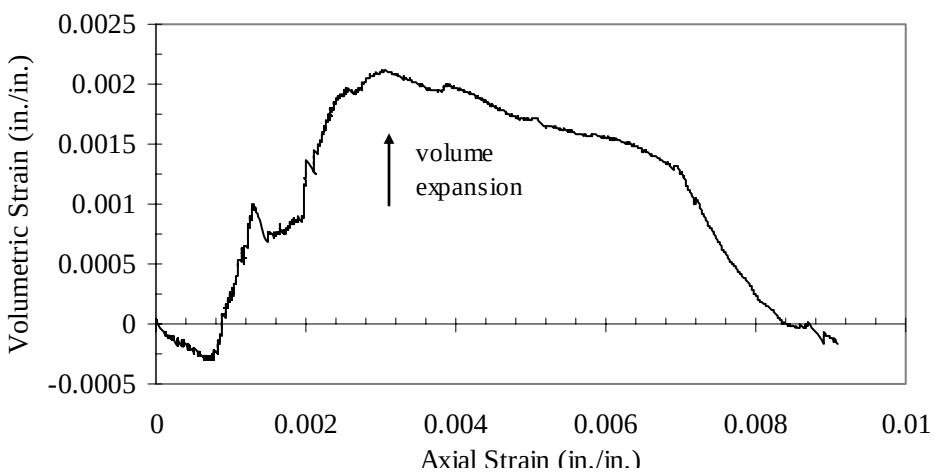

Figure 5.88 Volumetric versus axial strain curves for specimen R3-CT-F

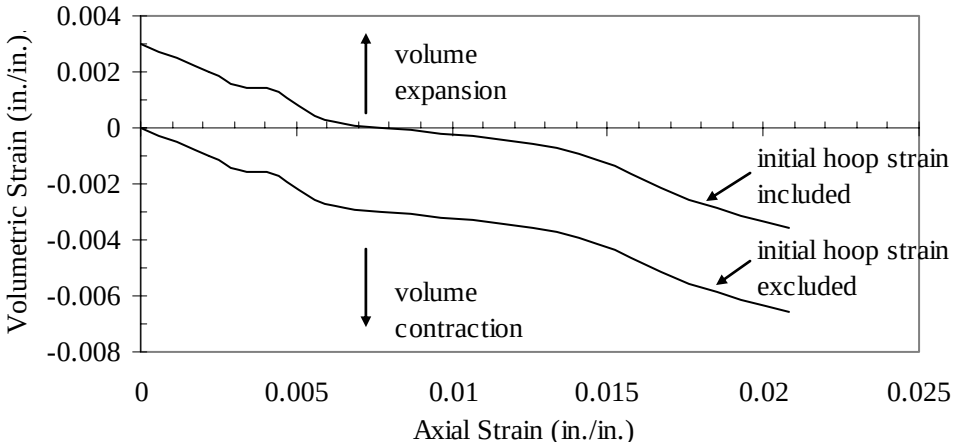

Figure 5.89 Volumetric versus axial strain curves for specimen R3-GT-E

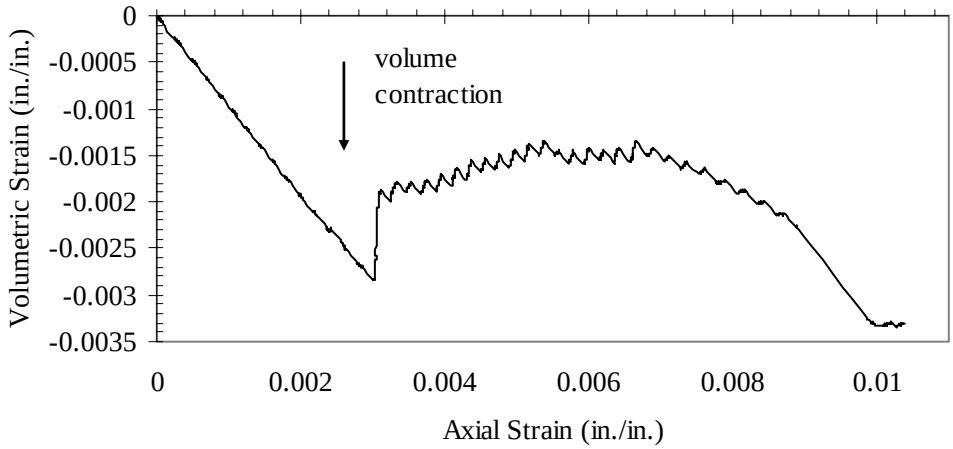

Figure 5.90 Volumetric versus axial strain curves for specimen R3-GT-F

From the experimental tests of rectangular specimens, the following observations are made:

(1) The effectiveness of FRP composite jackets for rectangular columns is much less than that for circular columns. For a 3:1 aspect ratio, the jacket effectiveness is less than that for a 2:1 aspect ratio, which is also less than that of a square column. This proves that in addition to the corner radius, the aspect ratio of the cross-section produces a significant effect on the compressive behavior of FRP confined rectangular columns. In general, the effectiveness is reduced and more significant post-peak behavior is expected as the aspect ratio increases.

(2) The experimental results show that with the same FRP volumetric ratio, rectangular columns with a different aspect ratio reach almost the same peak strength and ultimate strain. This indicates that substantial increases for both axial strength and axial strain for rectangular columns can be achieved by using FRP composites through a reasonable design, even for a higher aspect ratio. Therefore, ACI440 (2000) is rather conservative when they suggest that an aspect ratio exceeding 1.5:1 should not be confined with FRP jackets.

(3) Including circular and square columns, the slenderness effect within the range of 3:1 and 6:1 is not significant for either strength or ductility. Therefore, in the confinement design of normal size specimens, the effect of slenderness on the confinement can be neglected.

(4) Shape-modified columns show an increase in both strength and ductility relative to the original rectangular columns. However, these increases are smaller compared to the square group and depend strongly on the aspect ratio which means that the effect of shape-modification decreases as the aspect ratio increases. In addition, the R2 group benefited more from shape-modification than the R3 group, indicating that the confining FRP jacket becomes less effective as the section becomes a flatter ellipse. Therefore, to improve the increase in confinement effectiveness for rectangular columns, a lower aspect ratio after shape-modification is preferred, in the form of an oval shape.

(5) It is obvious from these tests that in most cases, for the same aspect ratio, the strength and ductility enhancement ratios of specimens with expansive cement concrete are higher than those for specimens with non-shrink concrete. This difference is due to the post-tensioning effect resulting from the initial expansion of the expansive cement concrete and the resulting effect on the FRP jacket and concrete core.

5.5 Notation

a: length of longer side of rectangular section;
b: length of shorter side of rectangular section;
B_j: length of the major axis of elliptical section;
D_j: length of the minor axis of elliptical section;
f_c: axial compressive stress of concrete;
f_{co}': axial strength of unconfined (baseline) concrete;
f_{cc}': maximum axial strength of FRP-confined concrete;
f_{cu}': ultimate axial strength of FRP-confined concrete, this is mainly applied for moderately or lightly confined specimens with post-peak softening behavior, for heavily-confined specimens, $f_{cu}' = f_{cc}'$;
ε_c: axial compressive strain of concrete;
ε_{co}': axial strain corresponding to f_{co}' for unconfined (baseline) concrete;
ε_{cc}': axial strain corresponding to f_{cc}' for FRP-confined concrete;
ε_{cu}': ultimate axial strain corresponding to f_{cu}' for FRP-confined concrete, this is mainly applied for moderately or lightly confined specimens with post-peak softening behavior, for heavily-confined specimens, $\varepsilon_{cc}' = \varepsilon_{cu}'$;
ε_j: fiber strain;
ε_{ju}: ultimate fiber strain at failure;

ε_{jx} : fiber strain on the long side of rectangular section or on the minor axis of elliptical section as shown in Figure 5.91;

ε_{jy} : fiber strain on the short side of rectangular section or on the major axis of elliptical section as shown in Figure 5.91;

$\varepsilon_{jx,u}$: ultimate strain for ε_{jx} at failure;

$\varepsilon_{jy,u}$: ultimate strain for ε_{jy} at failure;

ε_{f} : ultimate fiber strain determined form material coupon tests;

ρ_{FRP} : volumetric ratio of FRP jackets;

μ : ductility ratio.

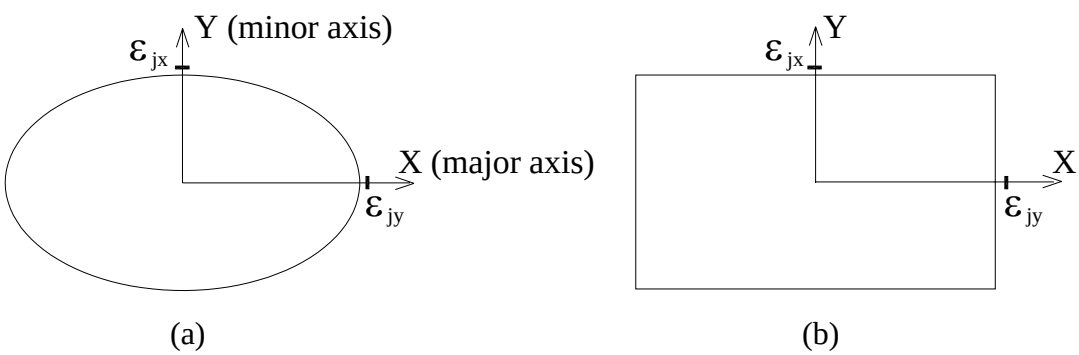

Figure 5.91 Locations of ε_{jx} and ε_{jy} for elliptical and rectangular columns: (a) elliptical columns; (b) rectangular columns

6. EVALUATION OF EXPERIMENTAL RESULTS AND DATA ANALYSIS

An extensive discussion of test results is presented in this chapter. Some important parameters and concepts are also introduced to develop a theoretical approach for FRP-confined concrete. Parameters including the volumetric ratio of FRP jacket, shape factor, confining pressure provided by the FRP jacket and jacket efficiency are presented. In this Chapter a more comprehensive view of the behavior for different types of FRP-confined columns and characteristics of confinement is investigated. Data used for regression analysis is mainly from the present study; experimental results performed by other researchers are also included.

6.1 Description of Parameters

6.1.1 Volumetric ratio of the FRP-jacket, ρ_{FRP}

The volumetric ratio of an FRP jacket ρ_{FRP} is defined as the ratio of the product of the circumference times the thickness of the jacket t_j to the area enclosed by the jacket.
For a circular column wrapped with a continuous FRP jacket, ρ_{FRP} can be expressed as:

$$\rho_{FRP} = \frac{4t_j}{D} \tag{6.1}$$

where t_j = thickness of the FRP composite jacket; and D = diameter of circular cross-section.
When the column is wrapped with a discontinuous FRP jacket made of individual strips, Eq. (6.1) can be rewritten as:

$$\rho_{FRP} = \frac{4t_j}{D(1+\frac{s}{d})} \tag{6.2}$$

where s = spacing of the FRP strips; and d = width of each FRP strip. For a rectangular column wrapped with a continuous FRP jacket, ρ_{FRP} can be expressed as:

$$\rho_{FRP} = \frac{2t_j(a+b)}{ab} \tag{6.3}$$

where a = length of the longer side of rectangular section; and b = length of the shorter side of rectangular section. In the case of a square column, $a = b$, and ρ_{FRP} can be rewritten as:

$$\rho_{FRP} = \frac{4t_j}{b} \tag{6.4}$$

For a square column wrapped by FRP strips:

$$\rho_{FRP} = \frac{4t_j}{b(1+\frac{s}{d})} \tag{6.5}$$

For an elliptical jacket, the circumference L is approximately given as:

$$L = \frac{\pi}{4}\left[3(B_j + D_j) - 2\sqrt{B_j D_j}\right] \tag{6.6}$$

where B_j = length of the major axis of elliptical section; and D_j = length of the minor axis of elliptical section. The area of the ellipse A is:

$$A = \frac{\pi B_j D_j}{4} \tag{6.7}$$

Therefore, the volumetric FRP ratio for elliptical FRP jackets can be written as:

$$\rho_{FRP} = \frac{\left[3(B_j + D_j) - 2\sqrt{B_j D_j}\right]t_j}{B_j D_j} \tag{6.8}$$

6.1.2 <u>Shape factor,</u> k_s

As observed from the experiments, the geometry of the cross-section causes a significant effect on the effectiveness of confinement provided by the FRP jacket. For square and rectangular columns, corners must be rounded to decrease stress concentration. In general, the confinement effectiveness increases as the corner radius is increased. To account for the corner effect on rectangular FRP jackets, a shape factor k_s is introduced herein to relate the effectively confined concrete area, A_c, to the total cross-sectional area, A. The effectively confined area A_c is defined by using arching-effect theory, with a second-order parabola segment extending between the rounded corners of the cross-section. Figure 6.1 shows the effectively confined area for three typical geometries: circular, rectangular and square sections.

The circular jacket provides uniform inward pressure to the concrete core and the whole section is effectively confined. That means A_c is equal to A and the shape factor, k_s is equal to 1. For a rectangular cross-section as seen in Figure 6.1, the effectively confined area A_c is the shaded area assumed to arch between points of definite confinement; confinement of the rest of the section is negligible. Therefore, the shape factor k_s can be expressed as:

$$k_s = \frac{A_c}{A} = 1 - \frac{(a-2r)^2 + (b-2r)^2}{3ab} \tag{6.9}$$

For a square cross-section, $a = b$, and the shape factor k_s can be represented by:

$$k_s = \frac{A_c}{A} = 1 - \frac{2(b/r-2)^2}{3(b/r)^2} \tag{6.10}$$

The above expressions show that the shape factor depends only on the ratio $\left(\frac{b}{r}\right)$ for square cross-sections. But for rectangular sections, not only the corner radius r but also the aspect ratio of $\left(\frac{a}{b}\right)$ is required to determine the value of k_s.

6.1.3 Longitudinal confinement effectiveness factor, k_l

In addition to the shape factor, the longitudinal confinement effectiveness factor, k_l, is introduced to account for the difference between the continuously FRP-wrapped columns and the FRP strips. As seen in Figure 6.2, the arching effect is again assumed to occur, this time vertically in the form of second order parabolas with an initial slope of 45º. Arching occurs vertically between the edges of the FRP strips.

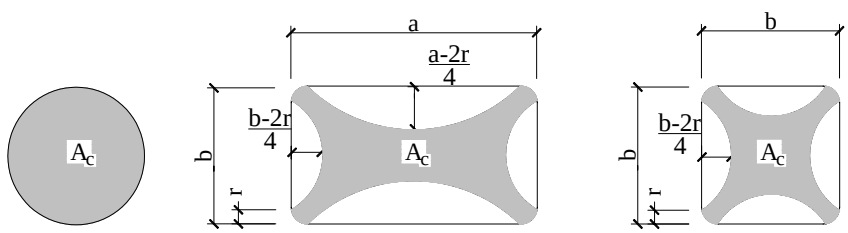

Figure 6.1 Comparison of shape factor for different geometries

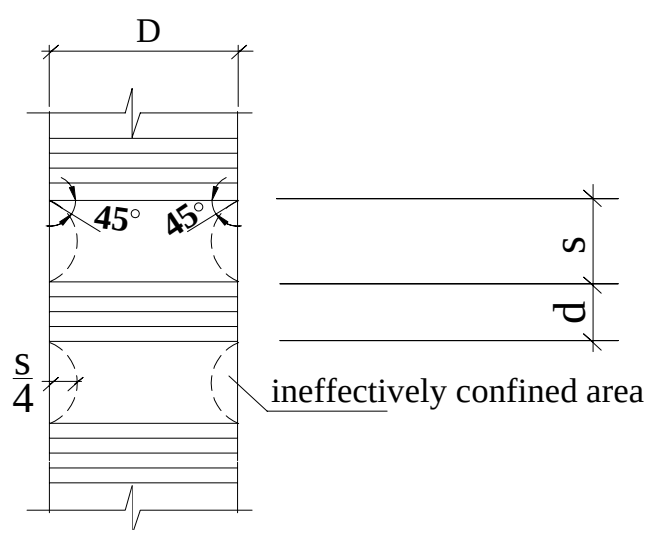

Figure 6.2 Effectively confined area by FRP strips

Figure 6.3 Experimental verification of effectively-confined area by FRP strips

This assumption can be verified from the experimental observation shown in Figure 6.3 from the shape of the concrete failure cone. The area of an effectively confined concrete core at midpoint between the edges of two FRP strips is:

$$A_e = \frac{\pi}{4} D^2 (1 - \frac{s}{2D})^2 \tag{6.11}$$

The cross-sectional area of the concrete column is:

$$A_c = \frac{\pi}{4} D^2 \tag{6.12}$$

Therefore, according to the definition, the longitudinal confinement effectiveness factor k_l for concrete columns confined with FRP strips can be expressed as:

$$k_l = \frac{A_e}{A_c} = (1 - \frac{s}{2D})^2 \tag{6.13}$$

For a square section of side b, k_l can be rewritten as:

$$k_l = (1 - \frac{s}{2b})^2 \tag{6.14}$$

If the column is wrapped with a continuous FRP jacket, k_l is equal to 1.

6.1.4 Jacket efficiency factor, k_ε

From the experimental results it was observed that the ultimate FRP jacket strains at rupture differed for various types of specimens. The reported FRP jacket strains at failure were always lower than the ultimate FRP material strain determined from tensile coupon tests. The reduced in-situ jacket efficiency results in earlier rupture of the FRP jacket and thus lowers the ultimate confining pressure that would be expected. Therefore, a jacket efficiency factor, k_ε, is proposed to account for the difference between in-situ jacket rupture strains observed in tests of FRP-confined concrete specimens and those observed in tensile coupon tests. The jacket efficiency factor k_ε is defined as the ratio of the ultimate FRP tensile hoop strain in the column tests, ε_{ju}, to the ultimate tensile strain from FRP material coupon tests, ε_f. That is:

$$k_\varepsilon = \frac{\varepsilon_{ju}}{\varepsilon_f} \tag{6.15}$$

This parameter reflects the degree of participation of the FRP jacket and the friction between concrete and FRP laminate. It is apparent that this factor is largely dependent on the bond type of the jacket and the geometry of the cross-section, especially at the corners and short sides. For bonded jacketed specimens, test results show that the rupture strains ε_{ju} of circular jackets are higher than those of other shapes with the same number of layers of the FRP composite. In addition, the strain distribution over the circumference of a circular jacket is consistent and uniform, while a large non-uniformity of strain distribution was observed in non-circular jackets.

As for square and rectangular sections, k_ε is determined by the ratio of the corner radius to the side length, $\frac{r}{L}$. The length L could be equal to the short or long side of a rectangular section. It is seen from Figure 6.4 that k_ε is proportional to the ratio of $\frac{r}{L}$ and that k_ε increases as the ratio $\frac{r}{L}$ increases. The relation between k_ε and $\frac{r}{L}$ is found to be:

$$k_\varepsilon = 0.31 + 1.42\left(\frac{r}{L}\right) \tag{6.16}$$

It is noted that experimental data performed by Rochette and Labossière (2000) is included in Figure 6.4. The dimension of the rectangular specimens they tested were 500 mm high with a cross-section of 152×203 mm. In addition to the effect of geometry, other factors such as the thickness, architecture of the jacket, and the type and quality of resin would also have an effect on the jacket efficiency. Due to many unpredicted influence factors, the experimental

results for k_ε are always scattered. From the present experimental results, summarized in Chapter 5, k_ε ranges from 75 to 85 percent for circular bonded FRP jackets (80 percent on average), 40 to 60 percent for rectangular bonded FRP jackets (50 percent on average) for an aspect ratio of 2:1 or 3:1, 40 percent for circular non-bonded FRP jackets with expansive cement concrete, and 30 percent for elliptical non-bonded FRP jackets with expansive cement concrete for an aspect ratio of 2:1 or 3:1.

For elliptical bonded FRP jackets using non-shrink concrete, the maximum hoop strain occurs at the minor axis and decreases as the ratio of the sides, $\frac{B_j}{D_j}$ increases. Therefore, the maximum jacket efficiency factor, $k_{\varepsilon,\max}$ is related to the aspect ratio $\frac{B_j}{D_j}$. Figure 6.5 shows the relation between $\frac{B_j}{D_j}$ and $k_{\varepsilon,\max}$, which can be expressed as:

$$k_{\varepsilon,\max} = 0.8\left(\frac{B_j}{D_j}\right)^{-0.87} \tag{6.17}$$

Table 6.1 lists the equations or values of k_ε for circular and square columns and $k_{\varepsilon,\max}$ for elliptical columns. In Table 6.1, $k_{\varepsilon,b}$ denotes the jacket efficiency factor for bonded FRP jackets and $k_{\varepsilon,n}$ denotes the jacket efficiency factor for non-bonded FRP jackets with expansive cement concrete.

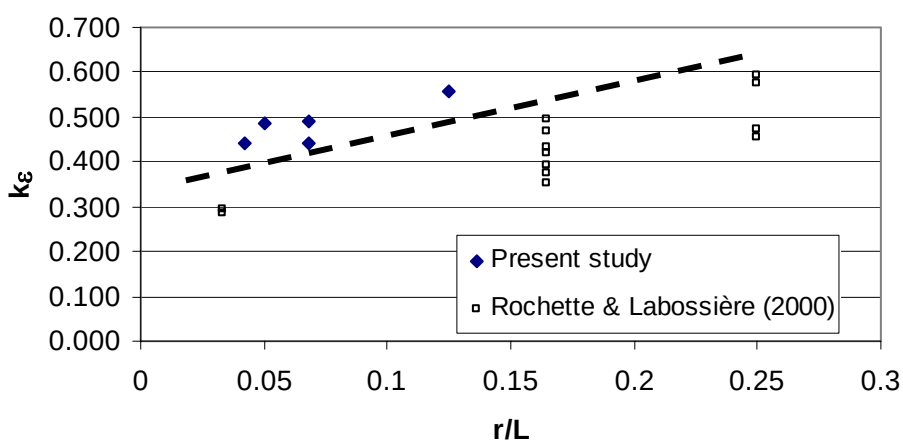

Figure 6.4 Relation between k_ε and $\frac{r}{L}$

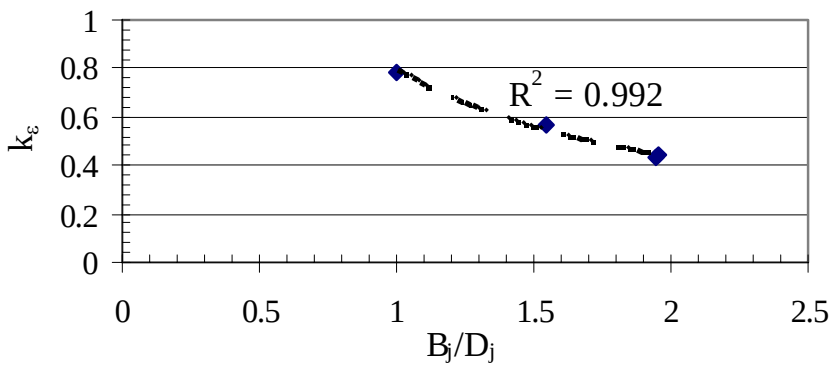

Figure 6.5 Relation between k_ε and the aspect ratio for elliptical bonded FRP jackets

Table 6.1 FRP-jacket efficiency factor, k_ε ($k_{\varepsilon,\max}$) for different types of FRP jackets and sections

Type of cross-section	CFRP jacket		GFRP jacket	
	Bonded ($k_{\varepsilon,b}$)	Non-bonded ($k_{\varepsilon,n}$)	Bonded ($k_{\varepsilon,b}$)	Non-bonded ($k_{\varepsilon,n}$)
Circular	0.8	0.4	0.95	0.4
Square	Eq. (6.16)	NA	Eq. (6.16)	NA
Rectangular	Eq. (6.16)	NA	Eq. (6.16)	NA
Elliptical*	Eq. (6.17)	0.3	Eq. (6.17)	0.6

*Due to non-uniformity of strain distribution over circumference, Table 6.1 lists only the maximum jacket efficiency factor, $k_{\varepsilon,\max}$ for the elliptical section.

6.1.5 Jacket confining pressure, f_l

The confining pressure provided by an FRP jacket can be expressed in the form:

$$f_l = \frac{1}{2} k_s k_l k_p \rho_{FRP} E_j \varepsilon_j \tag{6.18}$$

Where k_p = the contribution factor due to the post-tensioning effect. The ultimate confining pressure, f_{lu} is obtained when the FRP jacket strain ε_j reaches its ultimate or rupture strain, ε_{ju}:

$$f_{lu} = \frac{1}{2} k \rho_{FRP} E_j \varepsilon_f \tag{6.19}$$

where k is the confinement effectiveness coefficient and is computed as the product of the shape

factor k_s, the longitudinal confinement effectiveness factor, k_l, the contribution factor due to the post-tensioning effect, k_p, and the jacket efficiency factor k_ε. That is:

$$k = k_s k_l k_p k_\varepsilon \tag{6.20}$$

where factors k_s and k_l have been discussed in Ch 6.1.2 and 6.1.3; factor k_ε was discussed in Ch. 6.14; factor k_p accounts for the contribution of the post-tensioning effect caused by dilation of expansive cement concrete. The jackets already form an initial confining pressure applied to the concrete before any axial load is applied. Once the column is axially loaded, the confining pressure increases from this initial level instead of starting from zero, as is the case for the regular bonded FRP jacket. The experimental results show that non-bonded FRP jacketed specimens with expansive cement concrete can achieve a higher strength enhancement ratio compared to bonded FRP jacketed specimens, although the latter exhibited a higher jacket efficiency. Therefore, k_p is determined for a specified geometry by finding the ratio of the jacket efficiency factor for the bonded FRP jacket, $k_{\varepsilon,b}$, to the jacket efficiency factor for the non-bonded FRP jacket with expansive cement concrete, $k_{\varepsilon,n}$:

$$k_p = \frac{k_{\varepsilon,b}}{k_{\varepsilon,n}} \tag{6.21}$$

For rectangular and elliptical sections with an uneven distribution of jacket strain, ε_{ju} is calculated by computing the average of $\varepsilon_{jx,u}$ and $\varepsilon_{jy,u}$; $\varepsilon_{jx,u}$ is the ultimate strain at the long side of the rectangular section or the minor axis of the elliptical section, and $\varepsilon_{jy,u}$ is the ultimate strain at the short side of the rectangular section or the major axis of the elliptical section, as shown in Figure 5.91:

$$\varepsilon_{ju} = \frac{\varepsilon_{jx,u} + \varepsilon_{jy,u}}{2} \tag{6.22}$$

The effective confinement ratio, $\frac{f_{lu}}{f_{co}'}$ is thereby introduced as indicative of the maximum confining pressure provided by the FRP jacket relative to the unconfined concrete strength, where f_{co}' = unconfined concrete strength. The level of $\frac{f_{lu}}{f_{co}'}$ is directly related to the ultimate or peak strength because this ratio includes the effect of shape factor, longitudinal confinement effectiveness factor, jacket efficiency and other factors which would influence the confinement stiffness. The relation between $\frac{f_{cc}'}{f_{co}'}$ and $\frac{f_{lu}}{f_{co}'}$ will be discussed further in Chapter 7.

6.1.6 Effective confining stiffness for circular columns with bonded FRP jackets, C_j

The effective confining stiffness for circular columns with bonded FRP jackets, C_j can be defined as the ratio of the increments of confinement stress Δf_l and hoop strain, $\Delta\varepsilon_j$, as follows:

$$C_j = \frac{\Delta f_l}{\Delta\varepsilon_j} \tag{6.23}$$

Therefore, the confining stress can be rewritten as:

$$f_l = C_j \varepsilon_j \tag{6.24}$$

Also C_j is expressed from Eq. (6.18) for circular columns with bonded FRP jackets as:

$$C_j = \frac{1}{2} k_l k_s \rho_{FRP} E_j \tag{6.25}$$

The normalized effective confining stiffness, C_e, is defined as the ratio of the unconfined concrete strength, f_{co}', to the effective confining stiffness, C_j:

$$C_e = \frac{f_{co}'}{C_j} \tag{6.26}$$

It is seen from this definition that C_e is an indication of the confining stiffness of the FRP jacket relative to the unconfined concrete strength.

6.2 Evaluation of Experimental Results

6.2.1 Evaluation of circular columns with bonded FRP jackets

6.2.1.1 Compressive behavior

The typical axial stress versus axial strain, axial stress versus hoop strain, hoop strain versus axial strain, and volumetric strain versus axial strain relationships for circular concrete columns confined with bonded FRP jackets are shown in Figure 6.6.

It is seen from Figure 6.6 (a) that the stress-strain relationship for circular columns shows an increasing branch, which is due to the increasing confinement action of the elastic FRP jacket that limits lateral dilation of the concrete. This confinement behavior can be better explained in Figure 6.6 (c) from the volumetric strain vs. axial strain relationship. As seen from Figure 6.6,

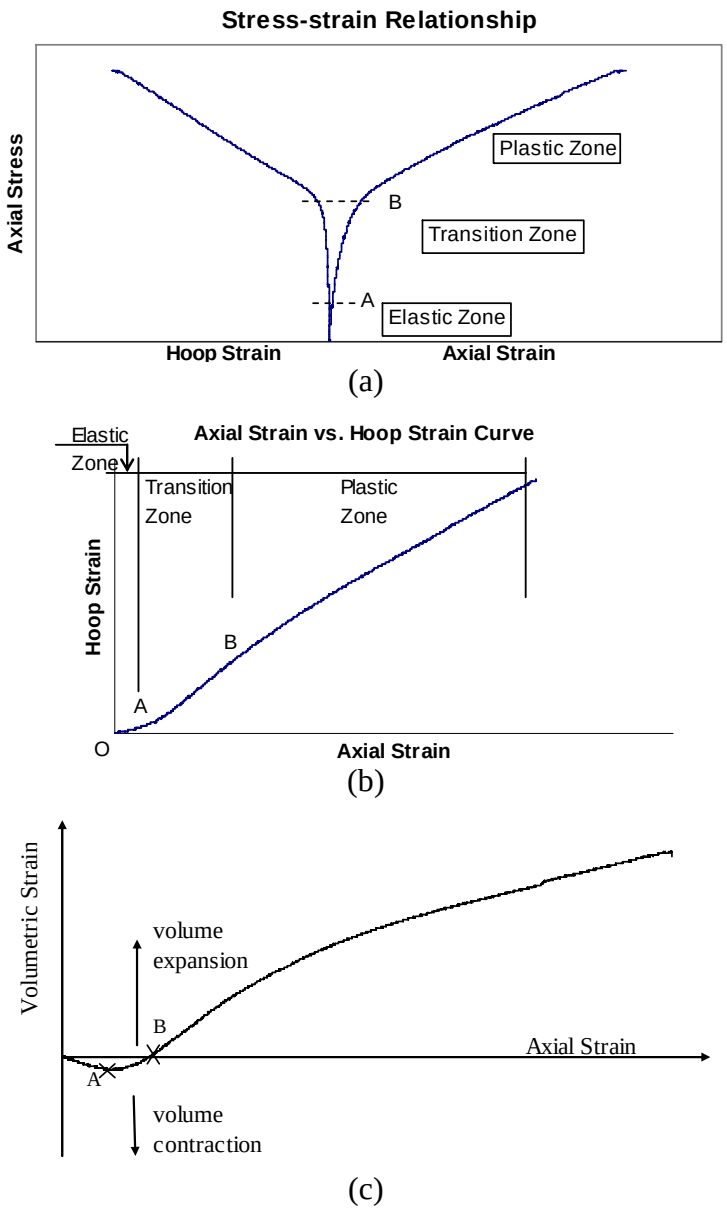

Figure 6.6 Typical compressive behavior for circular columns with bonded FRP jackets: (a) axial stress vs. axial and hoop strain; (b) hoop vs. axial strain; (c) volumetric vs. axial strain

the compressive behavior of the FRP-confined concrete can be divided into three phases. The 1st phase, which is defined as the contraction phase in the elastic zone, starts from the origin and ends at point A , which corresponds to the axial stress $f = 0.3 f_{co}^{'}$. In this initial phase, concrete behaves linearly elastic and its volumetric strain is reduced; i.e., there is more axial contraction than hoop expansion. The initial slope of the axial strain and hoop strain relationships are consistent with the following theoretical equation based on the generalized Hooke's law, with C_j being sufficiently smaller than E_0 :

$$\varepsilon_j = \frac{\upsilon_c}{1+(C_j / E_0)(1-\upsilon_c - 2\upsilon_c^{\ 2})}\varepsilon_c \tag{6.27}$$

where υ_c = elastic Poisson's ratio, which is approximately equal to 0.2 for normal concrete. (Note that ε_j is in tension while ε_c is in compression).

The 2nd phase is from point A to point B and is defined as the transition zone, which marks the reduction of volume contraction. In this phase, the FRP composite participates in confinement and point B is the turning point on the stress-strain curve after which the volumetric strain starts to expand. As seen in Figure 6.6, point B corresponds to ε_0, the axial strain at zero volumetric strain. Pantazoupolou and Mills (1995) suggested the following theoretical expression for the hoop strain vs. axial strain relation in the region from point A to point B:

$$\varepsilon_j = \upsilon_c \varepsilon_c + \frac{1}{2}(1-2\upsilon_c)\varepsilon_0 \left(\frac{\langle \varepsilon_{\lim} - \varepsilon_c \rangle}{\varepsilon_{\lim} - \varepsilon_0} \right)^2 \tag{6.28}$$

where $\varepsilon_{\lim}$ is the axial strain at which cracking occurs in the lateral direction; for unconfined concrete $\varepsilon_{\lim} \approx -0.001$ in./in. The experimental results show that for FRP-confined circular columns in this category, ε_0 ranges from 0.002 in./in. to 0.004 in./in. The calculation of ε_0 will be discussed in Chapter 7. The McAuley bracket $\langle x \rangle$ means that the quadratic term is only considered when $\varepsilon_c > \varepsilon_{\lim}$; when $\varepsilon_c < \varepsilon_{\lim}$, Eq. (6.27) can be used.

In the 3rd phase, after point B, which is defined as the expansion phase or expansion zone, concrete dilates and a passive pressure provided by the FRP jackets opposes such dilation, and improves the compressive behavior until the FRP jacket brakes. As concrete degrades, the ratio between hoop and axial strain also increases, indicating the acceleration of lateral dilation of the concrete. The hoop vs. axial strain curve in Figure 6.6 (b) appears to eventually converge to a straight line, which can be expressed as:

$$\varepsilon_j = \varepsilon_{\text{int}} + \nu_c^{'} \varepsilon_c \tag{6.29}$$

where ε_{int} is the value of the intercept of a straight line on the axis of hoop strain; from the experimental results shown in Figure 6.7, ε_i is found to be:

$$\varepsilon_{ini} = -0.0005 \text{ in./in.} \tag{6.30}$$

$\nu_c^{'}$ is a plastic Poisson's ratio similar to the definition of Poisson's ratio in the elastic zone. Moreover, $\nu_c^{'}$ is the slope of the straight line in the plastic zone as shown in Figure 6.7.

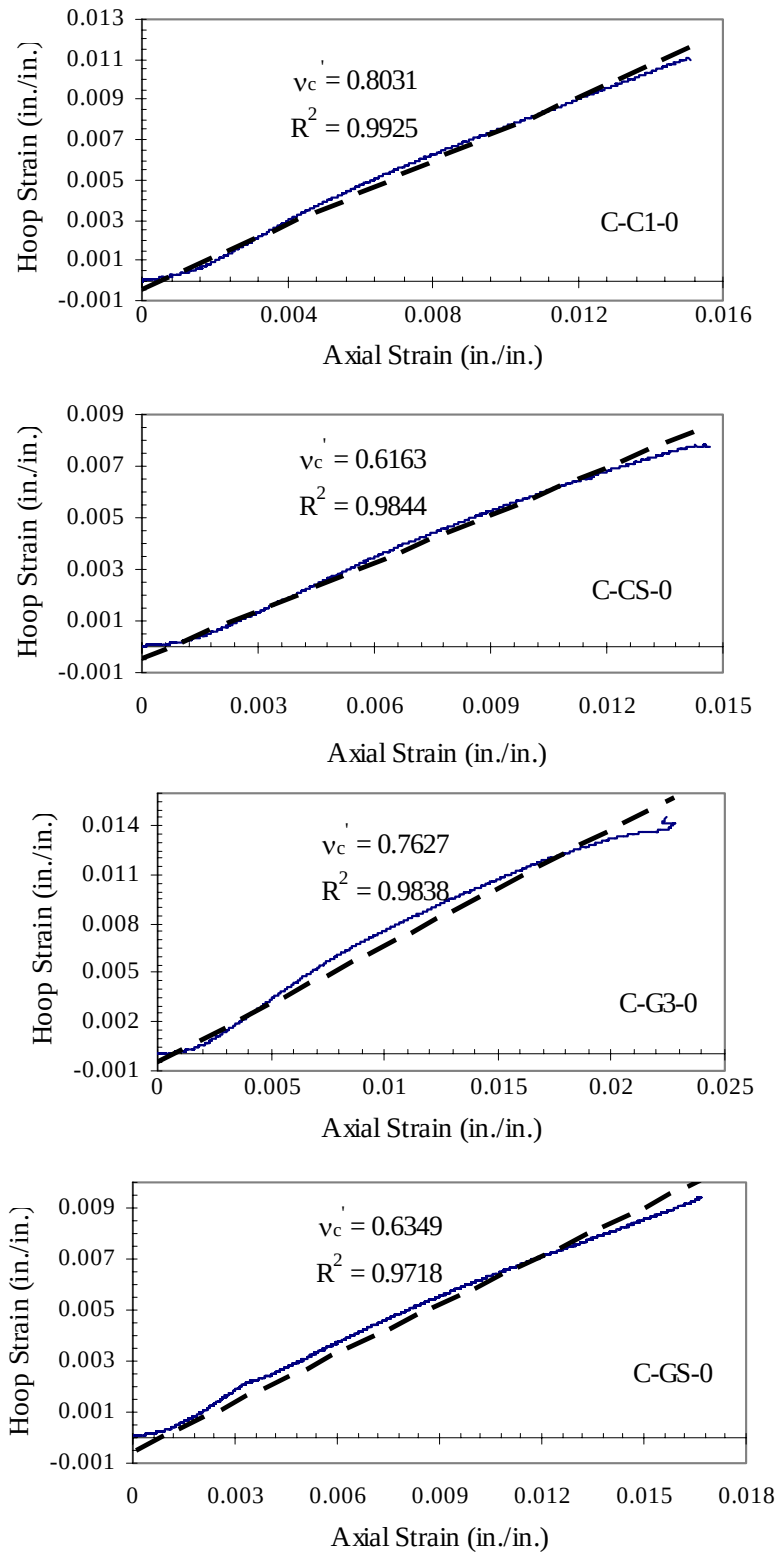

Figure 6.7 Hoop strain vs. axial strain at plastic zone (3rd phase) for circular columns with bonded FRP jackets

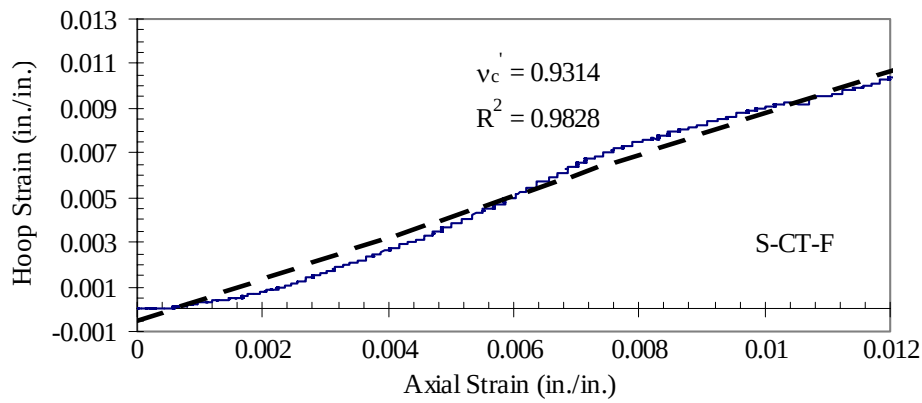

(Figure 6.7 continued)

The plastic Poisson's ratio, $\nu_c^{'}$ is believed to be a function of the normalized effective confining stiffness, C_e, because the FRP jacket takes on an important role in the 3rd phase. Figure 6.8 shows the relation between $\nu_c^{'}$ and C_e. In Figure 6.8, five data points were obtained from the present experimental study for circular specimens confined by bonded FRP jackets; one other point was found from the results of large-scale circular column tests with bonded CFRP jackets performed by Carey and Harries (2003). For each case, C_e was calculated using Eq. (6.26). The best-fit curve to the relationship is found to be:

$$\nu_c^{'} = 0.12 C_e^{-0.5} \tag{6.31}$$

Therefore, the expression of the compressive behavior in the 3rd phase can be written as:

$$\varepsilon_j = -0.0005 + 0.12 C_e^{-0.5} \varepsilon_c \tag{6.32}$$

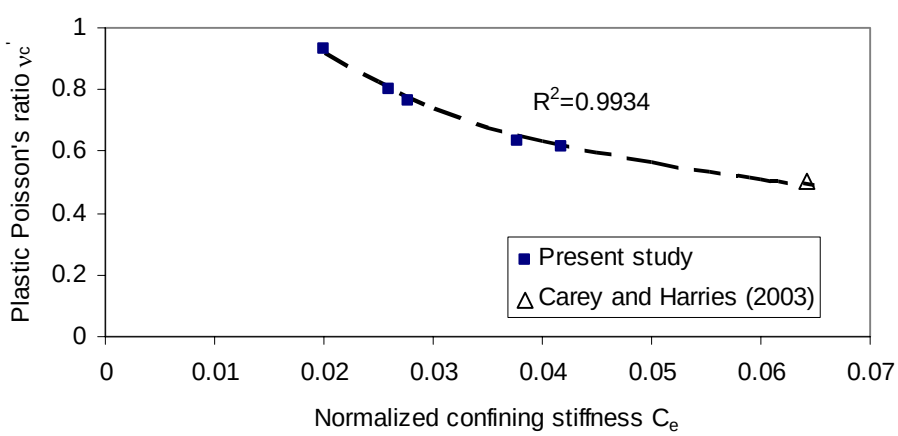

Figure 6.8 The relationship between $\nu_c^{'}$ and C_e

6.2.1.2 Degradation of the elastic modulus

It is proposed that the degradation of the elastic stiffness is a manifestation and direct consequence of development and propagation of cracks in the concrete. It has been shown by consideration of the radial strain measurements, that cracking induces lateral expansion, referred to as area strain, ε_a which is considered to be an indication of the level of lateral expansion caused by axial compression. For FRP-confined concrete, ε_a is referred to as the jacket area strain which is defined as the sum of fiber strain in the x and y directions:

$$\varepsilon_a = \varepsilon_{jx} + \varepsilon_{jy} \tag{6.33}$$

For circular columns, because $\varepsilon_{jx} = \varepsilon_{jy} = \varepsilon_j$, the jacket area strain ε_a can be expressed as:

$$\varepsilon_a = 2\varepsilon_j \tag{6.34}$$

Therefore, the degree of damage in a uniaxially loaded column is best represented by the amount of expansion, due to microcracking, suffered by the area supporting the axial load. Furthermore, the development of cracking (damage) reduces the area supporting the load which in turn causes degradation of the elastic modulus. Due to this cause-effect relationship, a mathematical expression was sought to describe the degradation of elastic modulus in terms of ε_a consistent with experimental evidence. The expression proposed by Pantazopoulou and Mills (1995) is:

$$\frac{E_c}{E_0} = \frac{1}{1+\beta\varepsilon_a} \tag{6.35}$$

where E_0 = initial elastic modulus, and β = normalizing constant which is associated with the jacket stiffness. It is seen that the left hand side of the above equation represents the degradation of stiffness and the right hand portion is a function of the jacket area strain, ε_a. This means that the degradation of concrete stiffness can be represented by the degree of expansion of ε_a through a constant β, which is determined by the stiffness of the FRP jacket.

Figure 6.9 shows the different values of β which were obtained throughout the loading history for circular column tests with bonded FRP jackets carried out in this study. It can be seen that β increases as the jacket effective confinement ratio, $\frac{f_{lu}}{f_{co}'}$ decreases, indicating that a higher degree of damage would occur to the column with the lower jacket confinement at the same loading level.

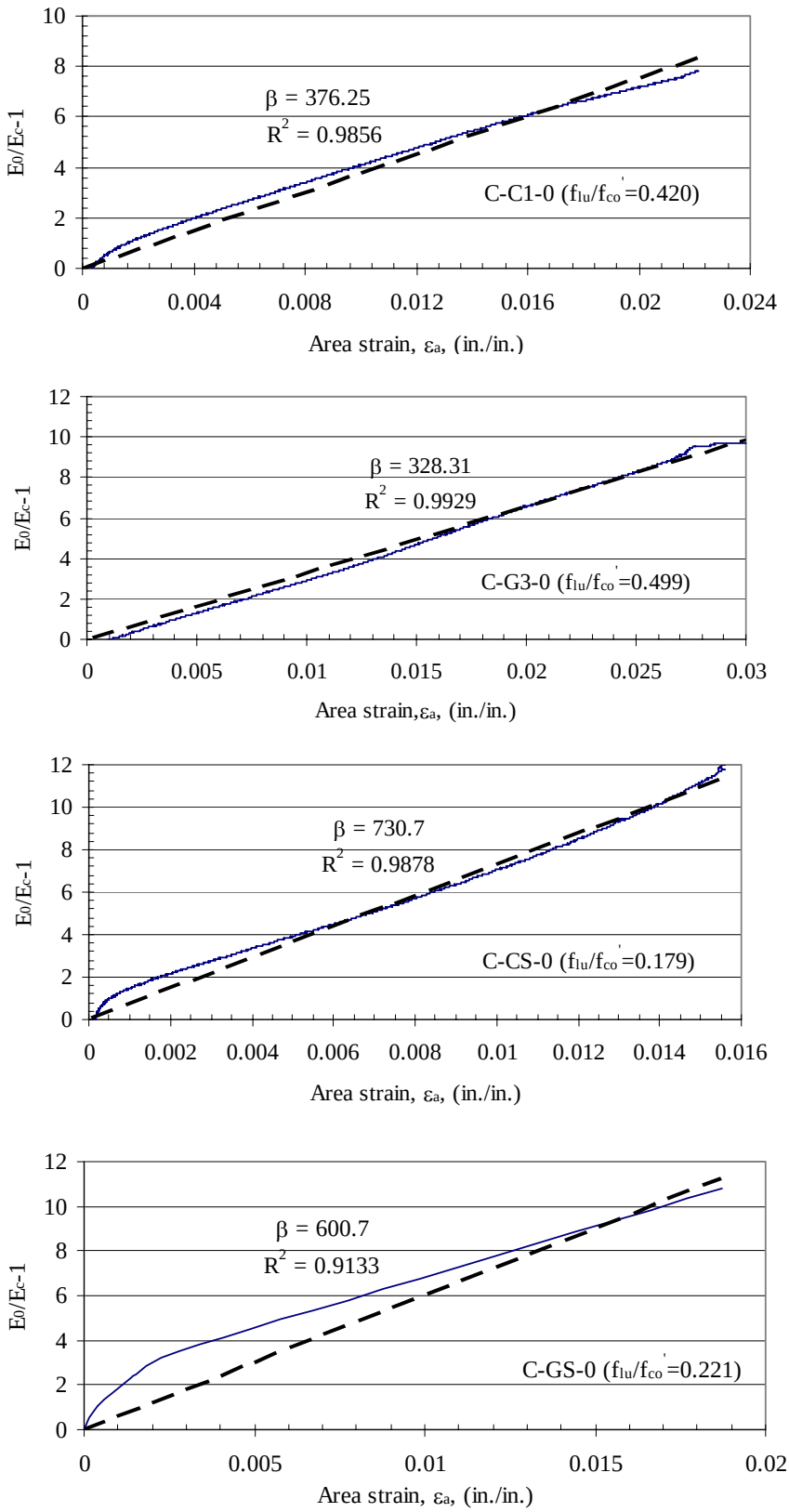

Figure 6.9 Values of β for circular columns with bonded FRP jackets

6.2.2 Evaluation of square and rectangular columns with bonded FRP jackets

6.2.2.1 Compressive behavior

Because of the shape factor effect, most square and rectangular specimens in the present study show softening behavior, in which the axial stress capacity decreases when the axial stress reaches the initial peak. It is observed that the ultimate strength f_{cu}' is always lower than the peak or maximum strength f_{cc}' as seen in Figure 5.1 (c). This means that the ratio of $\frac{f_{cu}'}{f_{cc}'}$ is smaller than 1.0 for specimens with softening behavior. This is believed to be dependent on the effective confinement ratio, $\frac{f_{lu}}{f_{co}'}$, as defined in Ch 6.1.5.

Figure 6.10 presents the results for specimens with softening behavior in the present study. The values of $\frac{f_{lu}}{f_{co}'}$ were calculated using Eq. (6.19). The relation between $\frac{f_{cu}'}{f_{cc}'}$ and $\frac{f_{lu}}{f_{co}'}$ can be found as:

$$\frac{f_{cu}'}{f_{cc}'} = 0.0768 \ln\left(\frac{f_{lu}}{f_{co}'}\right) + 1.122 \qquad (6.36)$$

It is seen from Eq. (6.36) that $\frac{f_{cu}'}{f_{cc}'}$ increases as $\frac{f_{lu}}{f_{co}'}$ increases. The upper limit of $\frac{f_{cu}'}{f_{cc}'}$ is 1.0 which corresponds to the case with hardening behavior. Therefore, taking $\frac{f_{cu}'}{f_{cc}'}$ to be 1.0 and solving this equation gives the threshold value of $\frac{f_{lu}}{f_{co}'}$:

$$\left\langle \frac{f_{lu}}{f_{co}'} \right\rangle_{threshold} = 0.2 \qquad (6.37)$$

This means that the column would exhibit a strain softening behavior if the effective confinement ratio, $\frac{f_{lu}}{f_{co}'}$, is smaller than $\left\langle \frac{f_{lu}}{f_{co}'} \right\rangle_{threshold}$, which is found to be 0.2. Otherwise, when $\frac{f_{lu}}{f_{co}'}$ is larger than 0.2, the column would exhibit a strain hardening behavior.

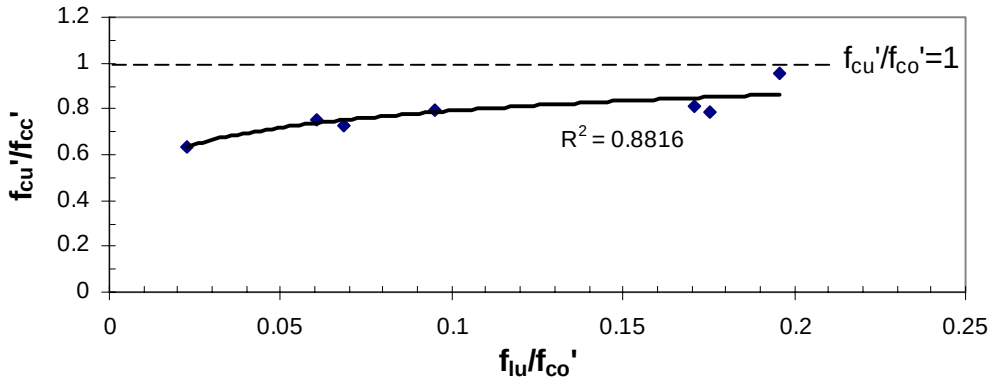

Figure 6.10 Relation between $\frac{f_{cu}'}{f_{cc}'}$ and $\frac{f_{lu}}{f_{co}'}$ for specimens with softening behavior

Figure 6.11 shows the plots of $\frac{f_{cc}'}{f_{co}'}$ versus $\frac{f_{lu}}{f_{co}'}$. Included are thirty-three data points from the present study for four circular, four square, two rectangular and five shape-modified rectangular columns, tests; performed by Rochette and Labossiere (2000) for 12 square and 4 rectangular columns; and tests performed by Pessiki et al. (2001) for 4 square columns. For each case, the value of $\frac{f_{lu}}{f_{co}'}$ was calculated using Eq. (6.19). Figure 6.12 shows a group of stress-strain curves chosen from the present study with different values of $\frac{f_{lu}}{f_{co}'}$. The results shown in Figure 6.11 are further verified by Figure 6.12, which shows that 0.2 is a threshold value for $\frac{f_{lu}}{f_{co}'}$ that can distinguish between the different types of behavior of FRP-confined columns; columns with $\frac{f_{lu}}{f_{co}'}$ smaller than 0.2 show softening behavior and those with $\frac{f_{lu}}{f_{co}'}$ larger than 0.2 show hardening behavior. From Figure 6.11, the relation between $\frac{f_{cc}'}{f_{co}'}$ and $\frac{f_{lu}}{f_{co}'}$ could be expressed as in Eq. (6.38) and this equation can be used for an approximate prediction of the maximum strength f_{cc}' based on the effective confinement ratio $\frac{f_{lu}}{f_{co}'}$, for all FRP-confined columns tested in this study.

$$\frac{f_{cc}'}{f_{co}'} = 0.8 + 4\frac{f_{lu}}{f_{co}'} \qquad (6.38)$$

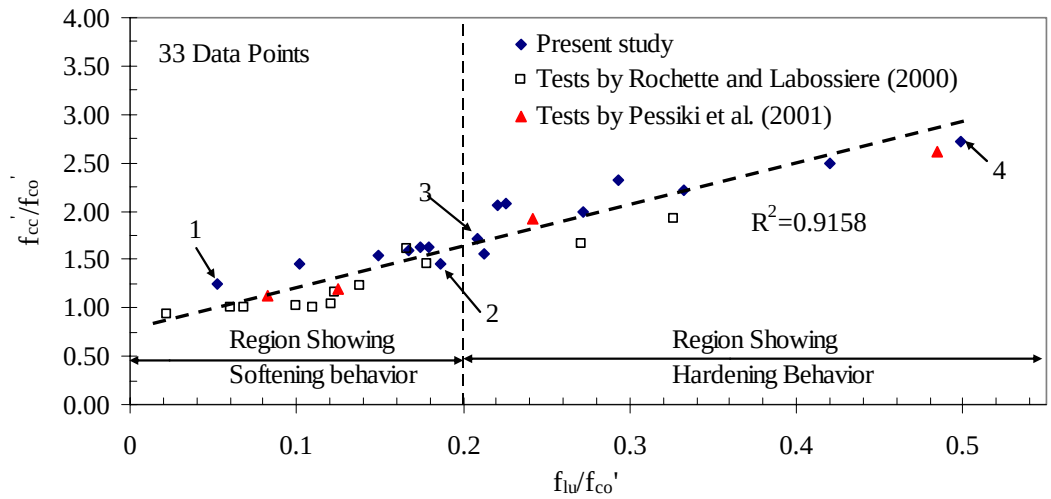

Figure 6.11 Strength enhancement ratio $\frac{f_{cc}'}{f_{co}'}$ vs. effective confinement ratio $\frac{f_{lu}}{f_{co}'}$

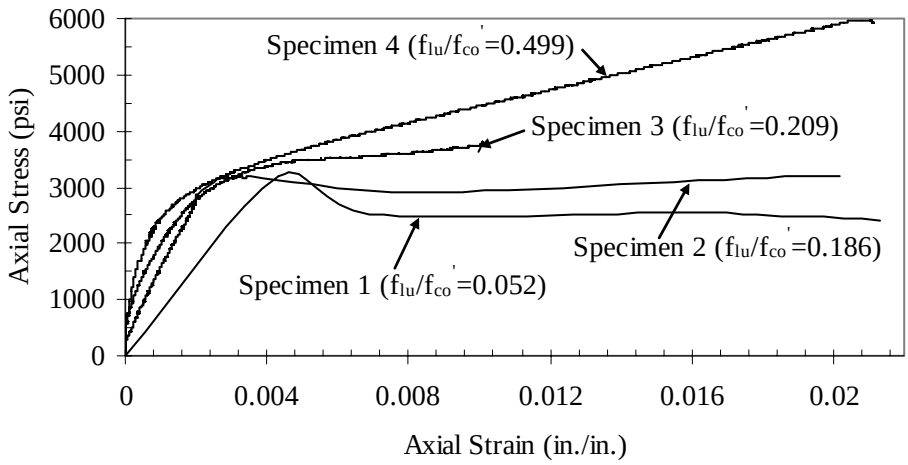

Figure 6.12 Verification of hardening and softening behavior (Eq. (6.37))
(specimen 1 = R3-C2-0; specimen 2 = S-G6-0; specimen 3 = S-C2-0; specimen 4 = C-G3-0)

6.2.2.2 <u>Degradation of the elastic modulus</u>

As discussed in Ch. 6.2.1.2, another important characteristic of uniaxially loaded FRP-confined columns is the degradation behavior of the elastic modulus. For FRP-confined rectangular columns, the jacket area strain ε_a is computed by adding the average fiber strain at the long side and that at the short side as expressed in Eq. (6.33). Similar to circular columns, for square columns ε_a can be expressed using Eq. (6.34); the values of β obtained from the loading history for square and rectangular columns with bonded FRP jackets are shown in Figure 6.13.

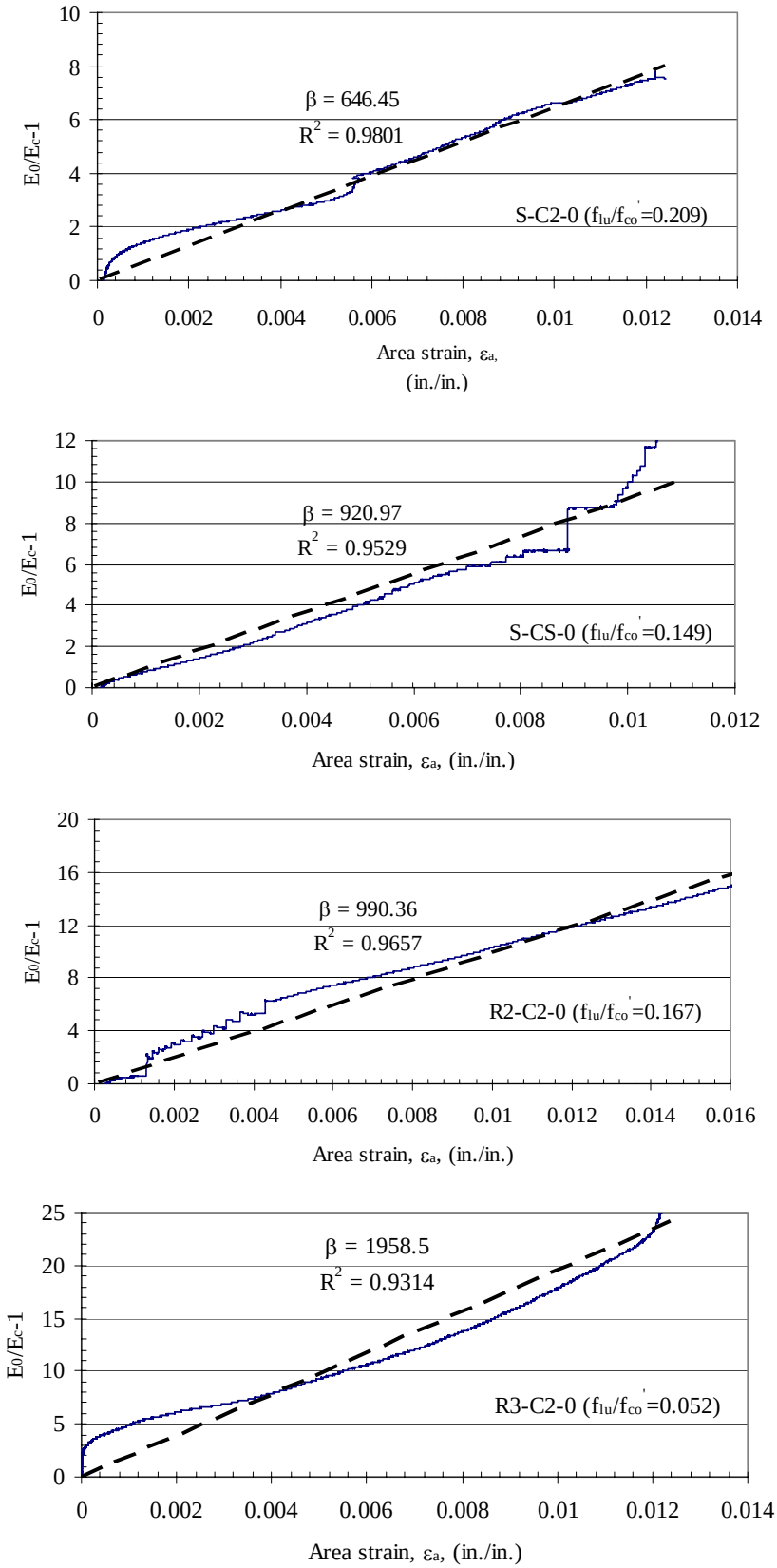

Figure 6.13 Values of β for square/rectangular columns with bonded FRP jackets

Similar to circular columns, the value of β increases as the jacket confining stiffness decreases. A combined plot, including data points from circular columns, is shown in Figure 6.14 for the relationship between β and the effective confinement ratio, $\frac{f_{lu}}{f_{co}'}$. The best-fit trend line for the relation between f_{lu} / f_{co}' and β can be expressed as:

$$\beta = 190\left(\frac{f_{lu}}{f_{co}'}\right)^{-0.8} \tag{6.39}$$

6.2.3 <u>Evaluation of shape-modified columns confined by non-bonded FRP jackets with expansive cement concrete</u>

As discussed in Chapter 5, the post-tensioning effect due to the expansive cement concrete changes the FRP confinement action from passive to active, in which the volumetric contraction is dominant throughout the history of axial loading. The FRP jacket deforms more uniformly throughout the height of the column in this case. The volumetric behavior of columns with expansive cement concrete and non-bonded FRP jackets shows that an approximately linear relationship between volumetric strain, ε_V and axial strain ε_c exists. This relationship can be expressed in the following form:

$$\varepsilon_V = -\alpha\varepsilon_c \tag{6.40}$$

where α corresponds to the slope of the volumetric strain vs. axial strain curve and varies for different effective confinement ratios, f_{lu} / f_{co}'. Figure 6.15 shows the values of α obtained from regression analysis of the volumetric strain vs. axial strain relationships for columns with expansive cement concrete and non-bonded FRP jackets.

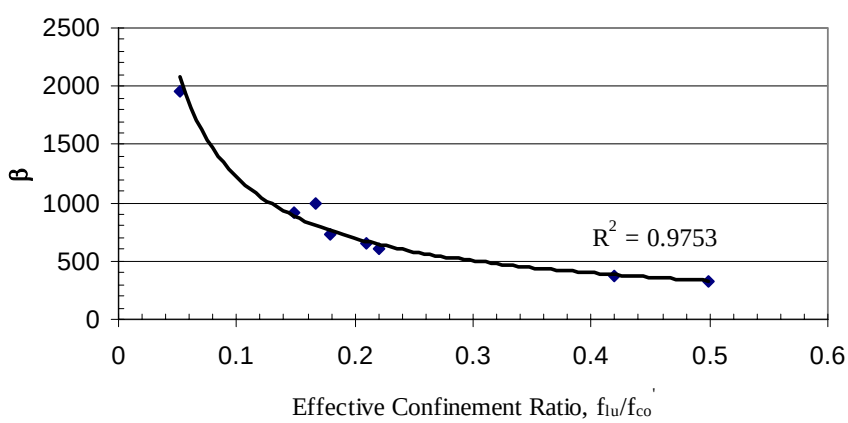

Figure 6.14 Relationship between β and f_{lu} / f_{co}' using circular, square and rectangular columns

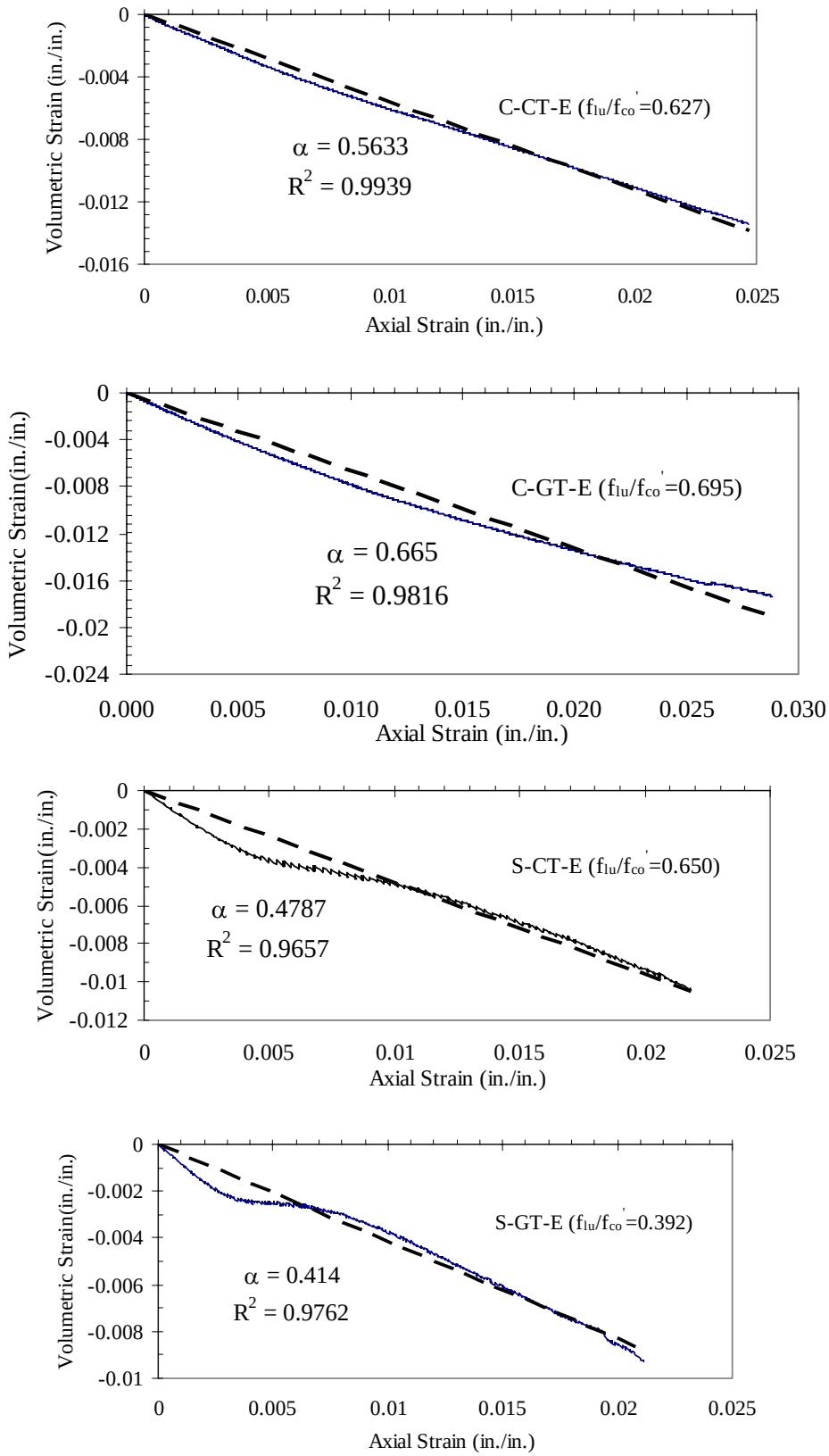

Figure 6.15 Values of α for columns with expansive concrete and non-bonded FRP jackets

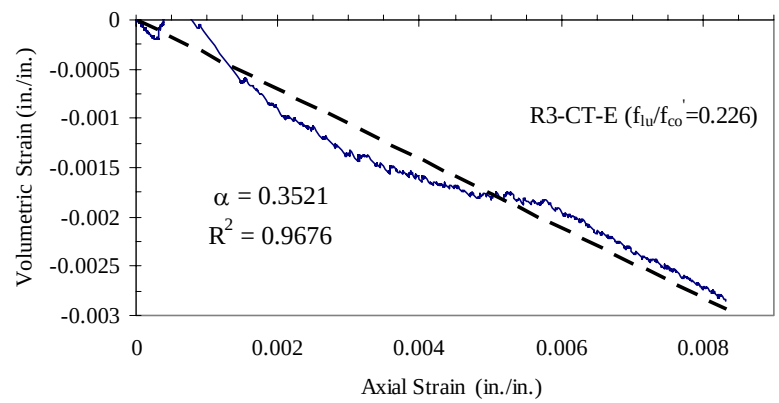

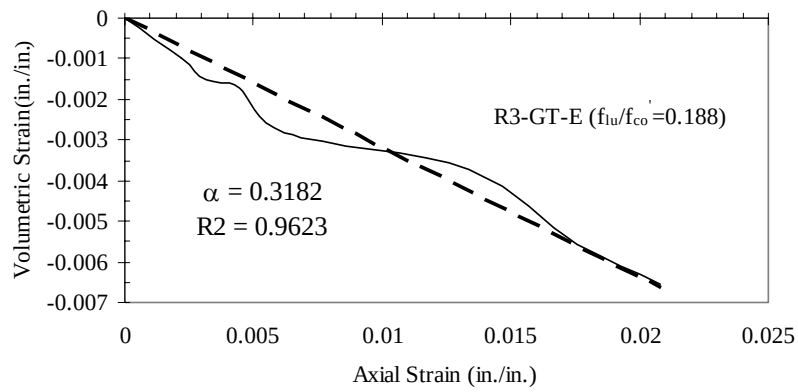

(Figure 6.15 continued)

For each column with expansive cement concrete and non-bonded FRP jacket, the effective confinement ratio, $\frac{f_{lu}}{f_{co}'}$ was calculated. The plot of α versus $\frac{f_{lu}}{f_{co}'}$ is shown in Figure 6.16. The relationship is approximately linear and can be expressed as:

$$\alpha = 0.26 + 0.428\left(\frac{f_{lu}}{f_{co}'}\right) \tag{6.41}$$

An apparent phenomenon observed for FRP-confined elliptical columns with both bonded and non-bonded jackets was that the hoop strains at the major axis, ε_{jy} were almost consistently smaller than those at the minor axis, ε_{jx}. This is the opposite condition for bonded FRP jackets observed in rectangular sections, in which ε_{jy} is bigger than ε_{jx}. This means that the concrete at the corner around the minor axis is effectively confined compared to the region near the major axis for elliptical columns. Therefore, bulging was always significant in the minor axis outwards; flexural bending increases the hoop strain at the minor axis and decreases the hoop strain at the major axis. It is also noted that the ratio of the hoop strain at the minor axis, ε_{jx} to the hoop strain at the major axis, ε_{jy} is almost constant for each elliptical column

throughout the loading history. In addition, the ratio of $\frac{\varepsilon_{jx}}{\varepsilon_{jy}}$ is related to the aspect ratio of $\frac{B_j}{D_j}$; $\frac{\varepsilon_{jx}}{\varepsilon_{jy}}$ increases as $\frac{B_j}{D_j}$ increases, which means that a higher aspect ratio would cause more uneven distribution of hoop strains over the section circumference. The lower limit of $\frac{\varepsilon_{jx}}{\varepsilon_{jy}}$ is equal to 1.0, which corresponds to the case of a circular column. Figure 6.17 shows the relationship between $\frac{\varepsilon_{jx}}{\varepsilon_{jy}}$ and $\frac{B_j}{D_j}$. For elliptical specimens tested in this study, this relationship is found as:

$$\frac{\varepsilon_{jx}}{\varepsilon_{jy}} = \left(\frac{B_j}{D_j}\right)^{0.65} \quad ; \quad 1.0 \le \frac{B_j}{D_j} \le 2.8 \qquad (6.42)$$

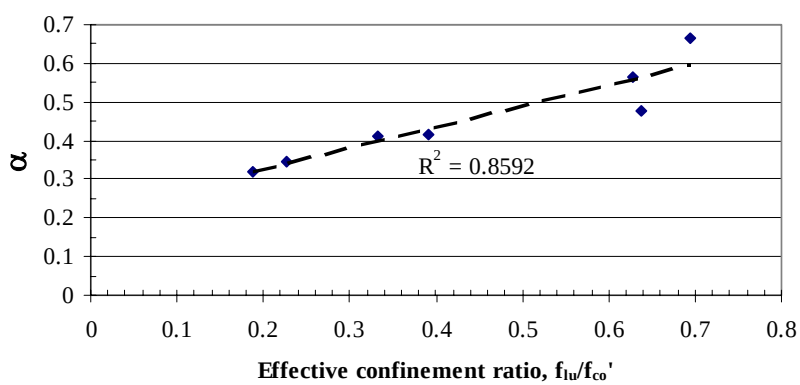

Figure 6.16 The relationship between f_{lu} / f_{co}' and α

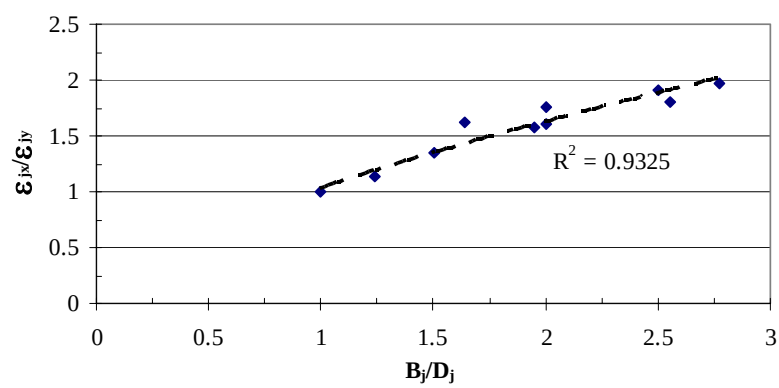

Figure 6.17 The relationship between $\frac{\varepsilon_{jx}}{\varepsilon_{jy}}$ and $\frac{B_j}{D_j}$ for elliptical columns

7. DESIGN RECOMMENDATIONS AND DESIGN-ORIENTED FRP-CONFINED CONCRETE MODELS

The most important application of FRP composite jackets for concrete columns is to increase the load-carrying capacity and the ultimate deformation capacity. In this Chapter, a simple compressive strength model is proposed for each type of FRP-confined concrete columns based on the experimental results of the present study. The parameters needed for design were presented in Chapter 6. Detailed design procedures are also described, and a simplified approach for developing the stress-strain relationship is proposed.

7.1 Design Recommendations for FRP-Confined Concrete Columns

7.1.1 Circular concrete columns confined with bonded FRP jackets

For circular columns, the ultimate axial strain of FRP-confined concrete columns, ε_{cu} can be obtained from Eq. (6.32) as:

$$\varepsilon_{cc}' = 8.33(\varepsilon_{ju} + 0.0005)C_e^{1/2} \tag{7.1}$$

where C_e = the normalized effective confining stiffness and defined in Eq. (6.26); ε_{ju} is the ultimate hoop strain achieved in the FRP –jacket and is expressed as:

$$\varepsilon_{ju} = k_\varepsilon \varepsilon_f \tag{7.2}$$

However, for engineering design purposes, the value of k_ε should be reduced for construction and environmental considerations. A reduction factor, ϕ was proposed to account for the design FRP material properties. Pantelides et al. (2004) suggested ϕ to be 0.75 for a CFRP composite ambient temperature curing system and 0.80 for a high temperature curing system. Therefore, Eq. (7.2) can be rewritten as:

$$\varepsilon_{ju} = \phi k_\varepsilon \varepsilon_f \tag{7.3}$$

For circular columns with bonded FRP jackets, k_ε is taken as 0.8 as shown in Table 6.1.

A theoretical analysis based on the plasticity approach using the modified five-parameter concrete model which proposed by William-Warnke (1973) shows that the strength enhancement ratio of FRP-confined concrete, $\frac{f_{cc}'}{f_{co}'}$ is related to the effective confinement ratio $\frac{f_{lu}}{f_{co}'}$ and can be calculated from:

$$\frac{f_{cc}^{'}}{f_{co}^{'}} = 4.721\sqrt{1+4.193\frac{f_{lu}}{f_{co}^{'}}} - 2\frac{f_{lu}}{f_{co}^{'}} - 4.322; \quad \left(\frac{f_{lu}}{f_{co}^{'}} > 0.08\right) \tag{7.4}$$

where $\frac{f_{lu}}{f_{co}^{'}}$ is obtained from Eq. (6.19) and should be higher than 0.08. For the case in which $\frac{f_{lu}}{f_{co}^{'}}$ is smaller than 0.08, $f_{cc}^{'}$ is equal to 1.0, which means no strength gain will be obtained for the weakly-confined column. That is:

$$\frac{f_{cc}^{'}}{f_{co}^{'}} = 1 \quad \left(\frac{f_{lu}}{f_{co}^{'}} \le 0.08\right) \tag{7.5}$$

Alternatively, based on the theory of degradation of the elastic modulus with jacket area strain, the ultimate strength of FRP-confined circular columns, $f_{cc}^{'}$ can be obtained from Eq. (6.35) and expressed as:

$$f_{cc}^{'} = \frac{E_0 \varepsilon_{cc}^{'}}{1+2\beta\varepsilon_{ju}} \tag{7.6}$$

where β is obtained from Eq. (6.39); E_0 is the initial elastic modulus of FRP-confined concrete and is expressed as:

$$E_0 = 68400\sqrt{f_{co}^{'}} \tag{7.7}$$

As seen in Figure 5.1 (b), two parameters, f_0 and ε_0, the axial stress and strain of the turning point on the stress-strain curve for circular concrete columns with bonded FRP jackets need to be considered. By applying the definition of volumetric strain ε_V, ε_0 is obtained from Eq. (6.32) as:

$$\varepsilon_0 = \frac{0.001}{0.24C_e^{-0.5} - 1} \tag{7.8}$$

The corresponding axial stress, f_0 can be calculated in terms of Eq. (6.35) and can be expressed as:

$$f_0 = \frac{E_0 \varepsilon_0}{1+\beta\varepsilon_0} \tag{7.9}$$

Figure 7.1 shows the flowchart of the design procedure for circular columns with bonded FRP jackets. This procedure could be performed either by a computer program or spreadsheet. Tables 7.1 and 7.2 summarize the design results for circular columns confined by bonded FRP jackets for the present study. It is seen that the calculated results agree with the tests in a satisfactory manner. It is noted that for f_{cc}', predictions by Eq. (7.4) show better agreement with the test results compared to using Eq. (7.6).

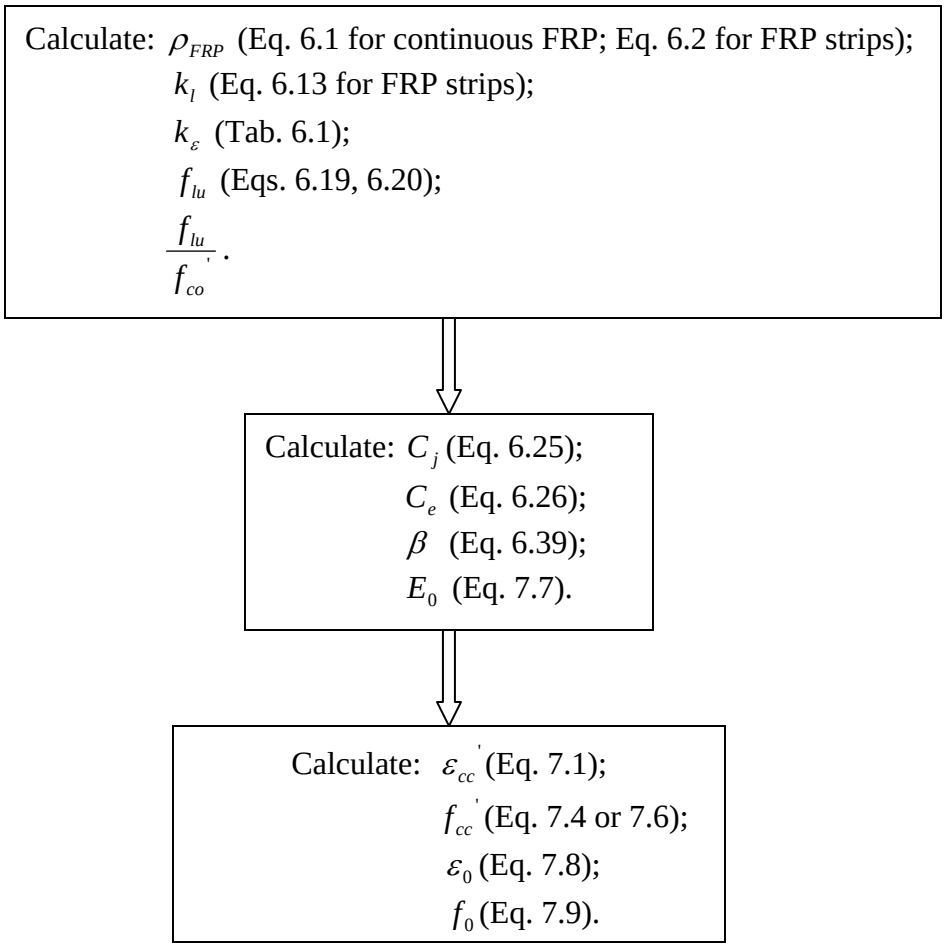

Figure 7.1 Design procedure for circular columns confined by bonded FRP jackets

Table 7.1 Calculated results of circular columns with bonded FRP jackets (1)

Speci. ID	t_j (in.)	s (in.)	d (in.)	ρ_{FRP} Eq. (6.1,2)	ε_{ju} (in./in.) Tab. (6.1)	k_s	k_l Eq. (6.13)	C_e Eq. (6.26)	$f_{lu}/f_{co}'^{*}$ Eq. (6.19)	f_{cc}'/f_{co}' Eq. (7.4)	f_{cc}'/f_{co}' Exp.	Diff. $(f_{cc}'/f_{co}')^{**}$
C-CS-0	0.070	4.67	5.25	0.012	0.0078	1.0	0.649	0.044	0.179	1.57	1.63	4%
C-GS-0	0.267	3.67	6.00	0.055	0.0100	1.0	0.718	0.045	0.221	1.79	2.06	13%
C-C1-0	0.040	-	-	0.013	0.0110	1.0	1.000	0.026	0.420	2.68	2.50	7%
C-G3-0	0.192	-	-	0.064	0.0140	1.0	1.000	0.028	0.499	2.98	2.72	9%
S-CT-F	0.070	-	-	0.018	0.0100	1.0	1.000	0.020	0.501	2.99	2.73	9%
S-GT-F	0.320	-	-	0.080	0.0100	1.0	1.000	0.022	0.445	2.78	2.52	9%

* f_{co}' = 2200 psi for specimens in Table 7.1

** Comparison between Eq. (7.4) and experimental results

Table 7.2 Calculated results of circular columns with bonded FRP jackets (2)

Speci. ID	β Eq. (6.39)	f_{cc}' (psi) Eq. (7.6)	Diff. (f_{cc}'/f_{co}') Eq. (7.6) with Exp.	ε_{cc}' (in./in.) Eq. (7.1)	$\varepsilon_{cc}'/\varepsilon_{co}'$ Eq. (7.1)	$\varepsilon_{cc}'/\varepsilon_{co}'$ Exp.	Diff. $(\varepsilon_{cc}'/\varepsilon_{co}')$ Eq. (7.1) with Exp.
C-CS-0	713	3820	10%	0.0144	7.22	8.35	14%
C-GS-0	603	4574	14%	0.0186	9.31	8.55	9%
C-C1-0	360	5572	6%	0.0155	7.75	7.55	3%
C-G3-0	314	6231	5%	0.0202	10.12	10.55	4%
S-CT-F	313	5462	19%	0.0124	6.18	6.06	2%
S-GT-F	344	5465	12%	0.0181	9.05	9.56	5%

7.1.2 Square and rectangular concrete columns confined with bonded FRP jackets

Because of the reduced effectiveness of the FRP jacket, lightly-confined square or rectangular columns always show softening behavior in which the ultimate values f_{cu}' and ε_{cu}' need to be considered in addition to f_{cc}' and ε_{cc}'. Therefore, for the design of square or rectangular columns, the effective confinement ratio, $\frac{f_{lu}}{f_{co}'}$ should be first calculated and compared to $\left\langle \frac{f_{lu}}{f_{co}'} \right\rangle_{threshold}$ which was presented in Eq. (6.37). For square columns, the jacket efficiency factor, k_{ε} can be determined by Eq. (6.16) and is equal to:

$$k_{\varepsilon} = \left[0.31 + 1.42(\frac{r}{b}) \right] \tag{7.10}$$

where b = side length of the square section and r = corner radius; for rectangular columns, due to the non-uniformity of distribution of hoop strain over the circumference, the average ε_{ju} is computed using Eq. (6.22) and the average k_{ε} over the circumference can be expressed in the form:

$$k_{\varepsilon} = \left[0.31 + 0.71(\frac{r}{a} + \frac{r}{b}) \right] \tag{7.11}$$

where a = length of long side of rectangular column; b = length of short side of rectangular column.

The design procedures are different between columns with hardening and softening behavior as described below:

For square and rectangular columns with softening behavior, since the confinement provided by the FRP jacket increases very little after the axial stress reaches its peak, the maximum strength, f_{cc}' can still be calculated by using Eq. (7.4) or (7.5) although f_{cc}' does not correspond to the ultimate strain of the FRP jacket, ε_{ju}. The axial strain which corresponds to f_{cc}', ε_{cc}' is found to be 0.004 in./in. on average for square and rectangular FRP-confined concrete columns tested in this study. As defined in Chapter 5.3, the softening factor, $\frac{f_{cu}'}{f_{cc}'}$ is determined by the effective confinement ratio, $\frac{f_{lu}}{f_{co}'}$. Therefore, the ultimate axial stress of the square and rectangular columns with softening behavior, f_{cu}' can be calculated by using Eq. (6.36). The

ultimate axial strain, ε_{cu}' is defined as the axial strain which corresponds to f_{cu}' and the ultimate hoop strain in the FRP jacket, ε_{ju}. Therefore, the secant modulus E_{cu} at ε_{cu}' can be calculated from:

$$E_{cu} = \frac{f_{cu}'}{\varepsilon_{cu}'} \tag{7.12}$$

From the definitions of ε_a and k_ε as shown in Eq. (6.15), (6.22) and (6.33), the jacket area strain, ε_a at ε_{cu}' can be expressed as:

$$\varepsilon_a = 2k_\varepsilon \varepsilon_f \tag{7.13}$$

Substituting Eqs. (7.12) and (7.13) in Eq. (6.35) gives:

$$\frac{f_{cu}'}{\varepsilon_{cu}'} = \frac{E_0}{1 + 2\beta k_\varepsilon \varepsilon_f} \tag{7.14}$$

It is noted that in Eq. (7.14), k_ε is obtained by using Eq. (7.10) for square columns and Eq. (7.11) for rectangular columns. Rewritting Eq. (7.14) gives the expression for ε_{cu}':

$$\varepsilon_{cu}' = \frac{f_{cu}'(1 + 2\beta k_\varepsilon \varepsilon_f)}{E_0} \tag{7.15}$$

For square and rectangular columns with hardening behavior, similar to FRP-confined circular columns, f_{cc}' can be calculated using the plasticity approach of Eq. (7.4); ε_{cc}' can be calculated using a similar form to Eq. (7.15) as:

$$\varepsilon_{cc}' = \frac{f_{cc}'(1 + \beta k_\varepsilon \varepsilon_f)}{E_0} \tag{7.16}$$

The axial stress at the turning point in the stress-strain curve, f_0 can be calculated from Eq. (7.9), and ε_0 is found to be 0.004 in./in. from the present study and Lam and Teng's tests (2003) for square and rectangular concrete columns with hardening behavior.

Figure 7.2 shows the flowchart of the design procedure for square and rectangular concrete columns confined with bonded FRP jackets. Tables 7.3-7.6 list the calculated results for square and rectangular columns for the present study and comparisons are made between the calculated and test results. In general, both square and rectangular FRP-confined concrete columns with an aspect ratio of 2:1 are predicted with satisfactory accuracy. It is also seen that

the predicted peak axial stress f_{cc}' for R3-C2-0 and R3-G6-0 have significant discrepancies compared to the test results. This is because the shape factor, k_s calculated from Eq. (6.9) is underestimated. This also means that Eq. (6.9) may not be applicable for the case of FRP-confined columns with aspect ratio equal to or higher than 3.

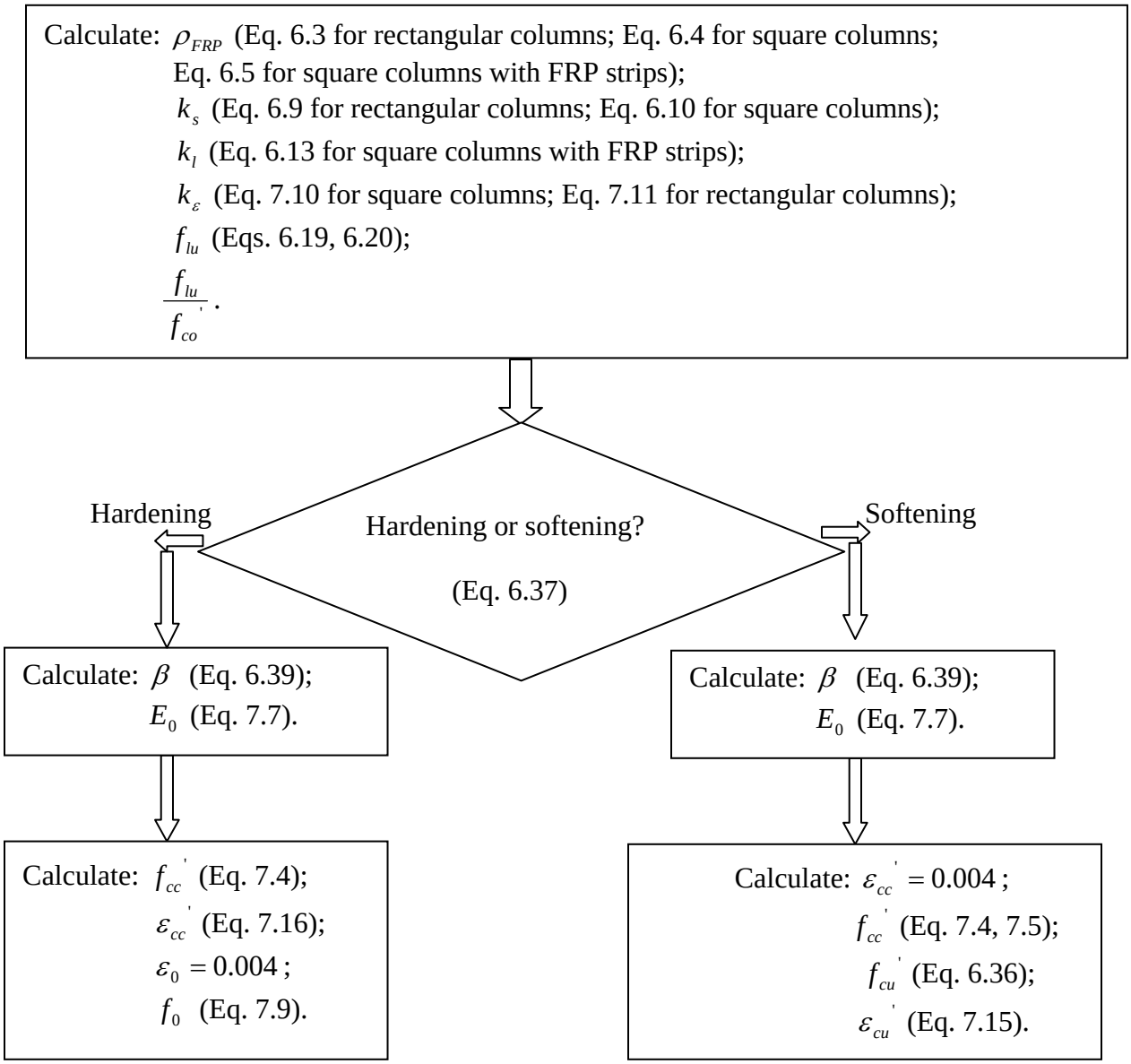

Figure 7.2 Design procedure for square and rectangular columns confined by bonded FRP jackets

Table 7.3 Calculated results of square columns with bonded FRP jackets (1)

Speci. ID	t_j (in.)	s (in.)	d (in.)	ρ_{FRP} Eq. (6.4)	k_ε Eq. (7.10)	k_s Eq. (6.10)	k_l Eq. (6.13)	f_{lu}/f_{co}' Eq. (6.19)	$f_{cc}'/f_{co}'^{*}$ Eq. (7.4)	f_{cc}'/f_{co}' Exp.	Diff. (f_{cc}'/f_{co}')
S-C2-0	0.070	-	-	0.0255	0.407	0.503	1.000	0.209	1.73	1.72	0%
S-CS-0	0.115	3.67	6.00	0.0261	0.407	0.503	0.694	0.149	1.40	1.54	9%
S-G6-0	0.320	-	-	0.1164	0.407	0.503	1.000	0.186	1.60	1.45	11%
S-GS-0	0.480	3.67	6.00	0.1091	0.586	0.503	0.694	0.174	1.54	1.63	6%

* f_{co}' = 2200 psi for specimens in Table 7.3.

Table 7.4 Calculated results of square columns with bonded FRP jackets (2)

Speci. ID	Behavior** Eq. (6.37)	β Eq. (6.39)	f_{cu}' (psi) Eq. (6.36)	f_{cu}' (psi) Exp.	Diff. (f_{cu}')	ε_{cu}' (in./in.) Eq. (7.15, 7.16)	$\varepsilon_{cu}'/\varepsilon_{co}'$ Eq. (7.15, 7.16)	$\varepsilon_{cu}'/\varepsilon_{co}'$ Exp.	Diff. ($\varepsilon_{cu}'/\varepsilon_{co}'$) Eq. (7.15, 7.16) with Exp.
S-C2-0	Hardening	665	-*	-*	-*	0.010*	5.07*	5.0	1%
S-CS-0	Softening	872	2994	2743	9%	0.026	13.40	16.5	18%
S-G6-0	Softening	730	3499	3200	9%	0.019	9.50	10.0	5%
S-GS-0	Softening	769	3343	3030	10%	0.026	13.00	14.0	7%

* For S-C2-0, ε_{cc}' applies instead of ε_{cu}' and f_{cu}' doesn't apply due to hardening behavior as defined in Figure 5.1 (b).

** f_{lu}/f_{co}' was calculated in Table 7.3.

Table 7.5 Calculated results of rectangular columns with bonded FRP jackets (1)

Speci. ID	t_j (in.)	a (in.)	b (in.)	ρ_{FRP} Eq. (6.3)	k_ε Eq. (7.11)	k_s Eq.(6.9)	k_l Eq. (6.13)	$f_{lu}/f_{co}'^{*}$ Eq. (6.19)	f_{cc}'/f_{co}' Eq. (7.4,5)	f_{cc}'/f_{co}' Exp.	Diff. (f_{cc}'/f_{co}')
R2-C2-0	0.070	15	8	0.0268	0.412	0.376	1.000	0.167	1.50	1.59	6%
R2-G6-0	0.320	15	8	0.1227	0.412	0.376	1.000	0.148	1.39	1.44	3%
R3-C2-0	0.070	18	6	0.0311	0.428	0.097	1.000	0.052	1.00	1.45	31%
R3-G6-0	0.320	18	6	0.1422	0.428	0.097	1.000	0.046	1.00	1.20	17%

* f_{co}' = 2200 psi for specimens in Table 7.3.

Table 7.6 Calculated results of rectangular columns with bonded FRP jackets (2)

Speci. ID	Behavior* Eq. (6.37)	β Eq. (6.39)	f_{cu}' (psi) Eq.(6.36)	f_{cu}' (psi) Exp.	Diff. (f_{cu}')	ε_{cu}' (in./in.) Eq. (7.15)	$\varepsilon_{cu}'/\varepsilon_{co}'$ Eq. (7.15, 7.16)	$\varepsilon_{cu}'/\varepsilon_{co}'$ Exp.	Diff. ($\varepsilon_{cu}'/\varepsilon_{co}'$) Eq. (7.15, 7.16) with Exp.
R2-C2-0	Softening	810	3244	3500	7%	0.020	10.00	11.5	13%
R2-G6-0	Softening	891	2989	3110	4%	0.020	10.00	10.5	5%
R3-C2-0	Softening	2087	1968	2413	18%	0.023	11.74	10.5	12%
R3-G6-0	Softening	2296	1948	2820	31%	0.021	10.40	10.5	1%

* f_{lu}/f_{co}' was calculated in Table 7.5.

7.1.3 Elliptical concrete columns confined with bonded FRP jackets

Similar to FRP-confined rectangular columns, ε_{ju} for elliptical columns confined by bonded FRP jackets is computed by taking the average of $\varepsilon_{jx,u}$ and $\varepsilon_{jy,u}$ using Eq. (6.22). Therefore, the average k_ε over the circumference can be calculated by using Eqs. (6.15), (6.17), (6.22) and (6.42) as expressed in the form below:

$$k_\varepsilon = 0.4\left(\frac{B_j}{D_j}\right)^{-0.87}\left(1+\left(\frac{B_j}{D_j}\right)^{-0.65}\right) \tag{7.17}$$

For elliptical columns confined by bonded FRP jackets, the design procedure is similar to that for square and rectangular columns confined by bonded FRP jackets. The flowchart for the design of elliptical columns confined by bonded FRP jackets is shown in Figure 7.3. Tables 7.7 and 7.8 list the calculated results for elliptical columns with bonded FRP jackets for the present study and comparisons are made between the calculated and test results.

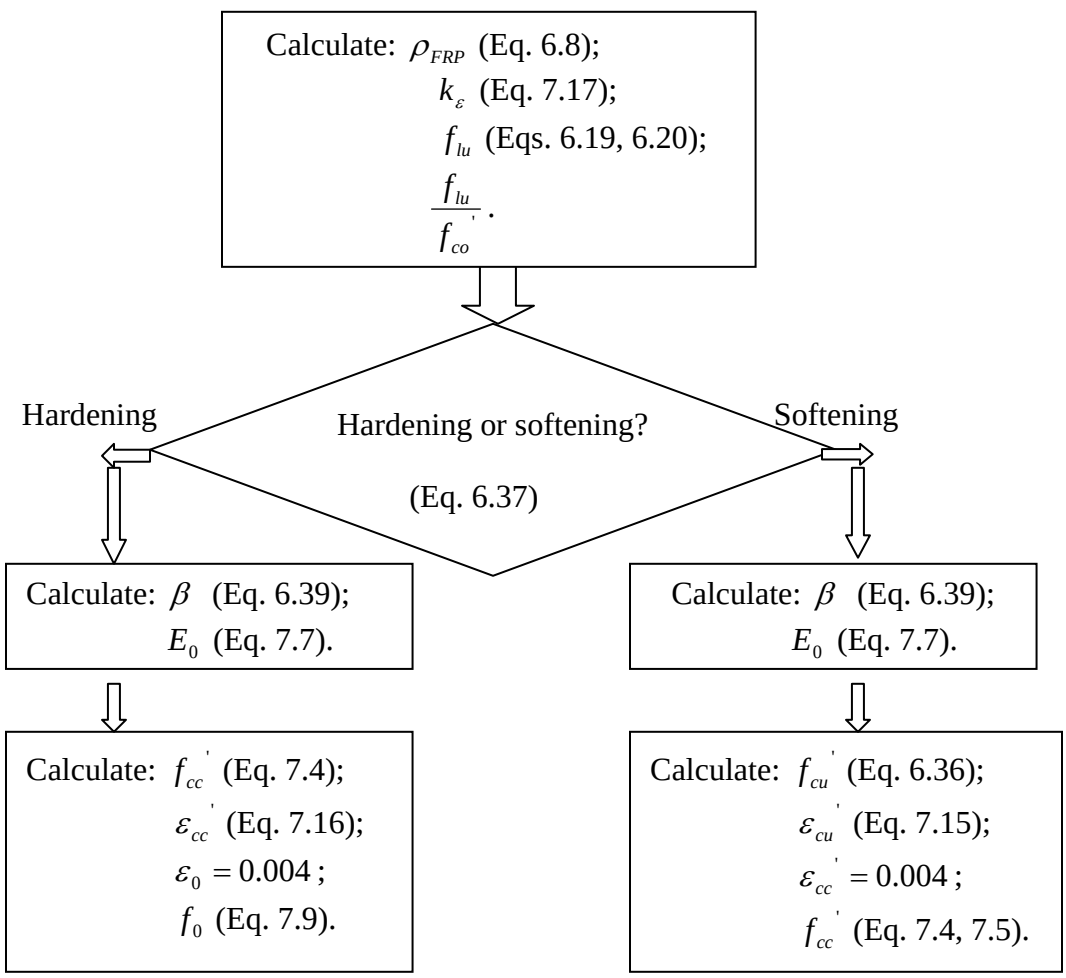

Figure 7.3 Design procedure for elliptical columns confined by bonded FRP jackets

Table 7.7 Calculated results of elliptical columns with bonded FRP jackets (1)

Speci. ID	t_j (in.)	ρ_{FRP} Eq. (6.8)	k_s	k_l Eq. (6.13)	k_ε Eq. (7.17)	f_{lu}/f_{co}' Eq. (6.19)	$f_{cc}'/f_{co}'^{*}$ Eq. (7.4)	f_{cc}'/f_{co}' Exp.	Diff. (f_{cc}'/f_{co}')
R2-CT-F	0.070	0.0141	1.0	1.0	0.480	0.272	2.04	1.99	3%
R2-GT-F	0.320	0.0710	1.0	1.0	0.370	0.205	1.19	1.47	19%
R3-CT-F	0.070	0.0145	1.0	1.0	0.367	0.213	1.75	1.55	13%
R3-GT-F	0.320	0.0730	1.0	1.0	0.295	0.168	1.51	1.39	8%

* The values of f_{co}' were listed in Table 5.6.

Table 7.8 Calculated results of elliptical columns with bonded FRP jackets (2)

Speci. ID	β Eq. (6.39)	ε_{cc}' (in./in.) Eq. (7.16)	$\varepsilon_{cc}'/\varepsilon_{co}'$ Eq. (7.16)	$\varepsilon_{cc}'/\varepsilon_{co}'$ Exp.	Diff. ($\varepsilon_{cc}'/\varepsilon_{co}'$) Eq. (7.16) with Exp.
R2-CT-F	544	0.012	6.99	8.50	18%
R2-GT-F	686	0.007	3.31	2.90	12%
R3-CT-F	664	0.009	4.69	4.55	3%
R3-GT-F	804	0.008	3.95	5.00	19%

* For R2-GT-F, ε_{cu}' applies instead of ε_{cc}' due to softening behavior as defined in Figure 5.1 (c).

7.1.4 Circular and elliptical columns with non-bonded FRP jackets and expansive cement concrete

As discussed in Chapter 6.2.3, the volumetric versus axial strain relationship is approximately linear and the slope α is determined by the effective confinement stiffness, $\frac{f_{lu}}{f_{co}'}$, as shown in Eq. (6.41). By applying the definitions of the volumetric strain, ε_V and the area strain, ε_a respectively, the ultimate axial strain, ε_{cc}' for circular and elliptical columns with non-bonded FRP jackets and expansive cement concrete can be derived from Eq. (6.41) and expressed as:

$$\varepsilon_{cc}' = \frac{2k_\varepsilon \varepsilon_f}{1-\alpha} \tag{7.18}$$

where k_ε is obtained from Table 6.1 for circular columns; due to the non-uniformity of the strain distribution over the circumference, the average jacket efficiency factor, k_ε for elliptical columns with non-bonded FRP jackets and expansive cement concrete should be taken as the average of the jacket hoop strains at the major and minor axis which are $\varepsilon_{jy,u}$ and $\varepsilon_{jy,u}$ respectively; k_ε can be expressed by using Eqs. (6.15), (6.22), (6.42) as:

$$k_\varepsilon = \frac{k_{\varepsilon,\max}}{2}\left(1+\left(\frac{B_j}{D_j}\right)^{-0.65}\right) \tag{7.19}$$

where $k_{\varepsilon,\max}$ is obtained from Table (6.1).

The axial strain, ε_0, at which the volumetric strain including the initial hoop strain due to the post-tensioning effect reaches zero, can be calculated by the following method as described in Figure 7.4. Figure 7.4 presents the volumetric versus axial strain relationship in which the initial hoop strain $\varepsilon_{j,ini}$ due to the post-tensioning effect is included. The intercept of the approximately straight line on the axis of volumetric strain is $2\varepsilon_{j,ini}$. Thus, ε_0 is found to be:

$$\varepsilon_0 = \frac{2\varepsilon_{j,ini}}{\alpha} \tag{7.20}$$

where $\varepsilon_{j,ini}$ is obtained from Eqs. (3.1) and (3.2). The corresponding axial stress, f_0 can be obtained from Eq. 7.9, accounting for degradation of the elastic modulus, based on the concrete model of Eq. (6.35) proposed by Pantazopoulou and Mills (1995). Similar to the design procedure for columns with bonded FRP jackets, the ultimate axial stress, f_{cc}' can be obtained by using Eq. (7.4). For columns with softening behavior, the design procedure can follow that of columns confined by bonded FRP jackets with softening behavior. The differences are the jacket

efficiency factor, k_ε and the contribution factor due to the post-tensioning effect, k_p, which needs to be included while calculating the effective confinement ratio, $\frac{f_{lu}}{f_{co}'}$, as shown in Eqs.(6.19) and (6.20).

Figure 7.5 shows the flowchart of the design procedure for circular and elliptical concrete columns confined with non-bonded FRP jackets and expansive cement concrete. Tables 7.9-7.12 list the calculated results for circular and elliptical columns with non-bonded FRP jackets and expansive cement concrete for the present study; comparisons are made between the calculated and test results. It is seen from Tables 7.9-7.12 that the calculated results of circular columns show better agreement with the tests compared to the elliptical columns and circular columns with full expansive cement concrete show better agreement than shape modified square columns with partial expansive cement concrete. The reason is that the actual geometries of the shape modified columns are not exactly the elliptical shape expected due to construction difficulties; this caused differences between the theoretical calculations and the actual tests for some parameters.

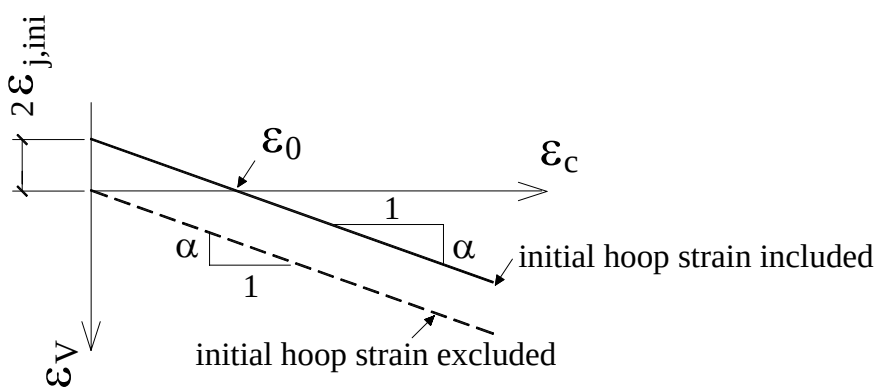

Figure 7.4 Calculation of ε_0 for columns with non-bonded jackets and expansive cement concrete

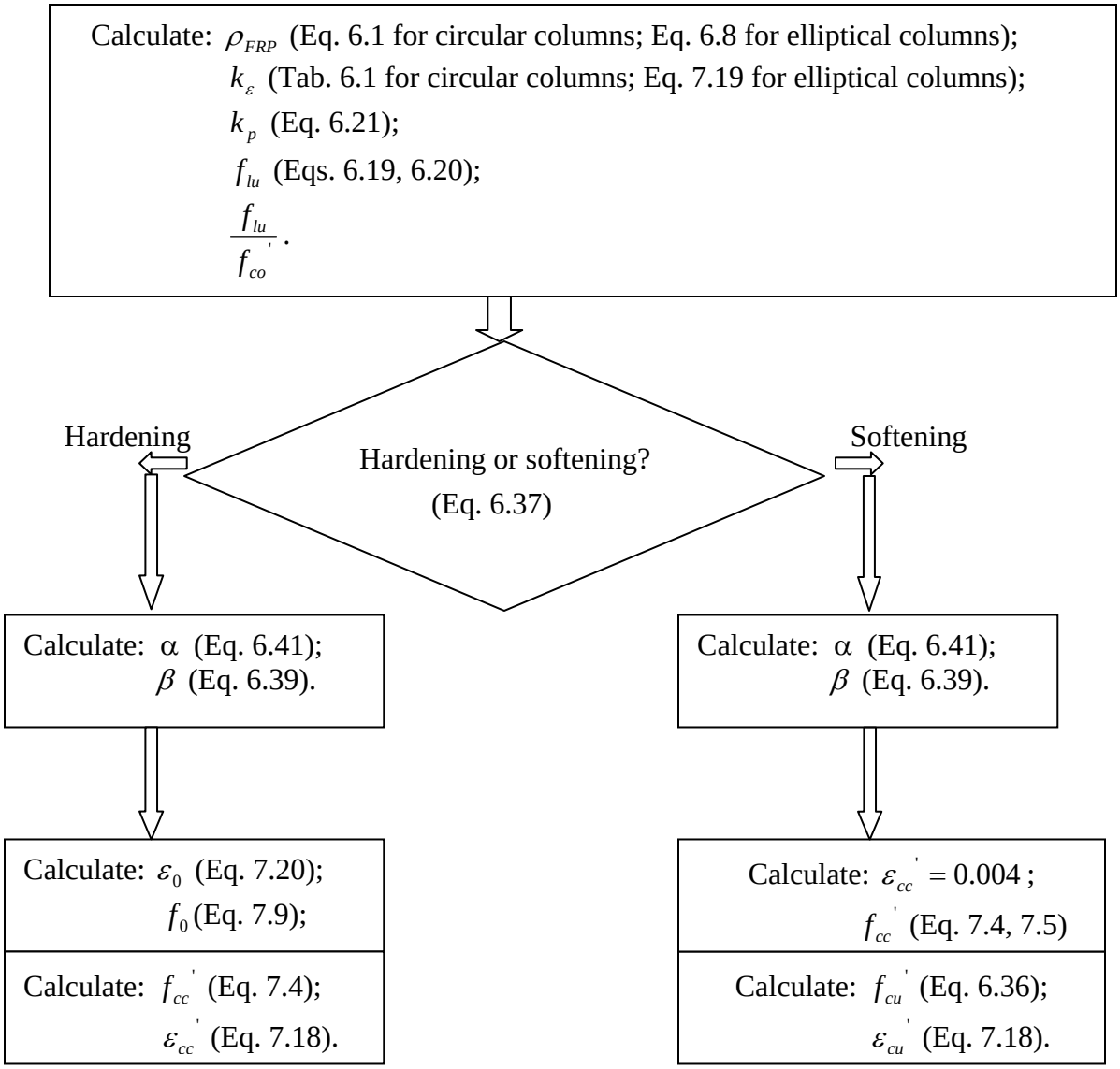

Figure 7.5 Design procedure for columns with non- bonded FRP jackets and expansive cement concrete

Table 7.9 Calculated results of circular columns with non-bonded FRP jackets and expansive cement concrete (1)

Speci. ID	t_j (in.)	ρ_{FRP} Eq. (6.1)	k_p Eq. (6.21)	k_s	k_l Eq. (6.13)	k_ε Tab. (6.1)	$f_{lu}/f_{co}'^{*}$ Eq. (6.19)	f_{cc}'/f_{co}' Eq. (7.4)	f_{cc}'/f_{co}' Exp.	Diff. (f_{cc}'/f_{co}')
C-CT-E	0.040	0.013	2.000	1.0	1.0	0.400	0.627	3.42	3.43	0%
C-GT-E	0.192	0.064	2.375	1.0	1.0	0.400	0.695	3.63	3.70	2%
S-CT-E	0.070	0.018	2.000	1.0	1.0	0.400	0.650	3.49	3.71	6%
S-GT-E	0.320	0.080	1.356	1.0	1.0	0.400	0.392	2.57	2.72	6%

* f_{co}' = 1300 psi and 1500 psi for C-CT-E and C-GT-E respectively, and f_{co}' = 1900 psi for S-CT-E and S-GT-E.

Table 7.10 Calculated results of circular columns with non-bonded FRP jackets and expansive cement concrete (2)

Speci. ID	α Eq. (6.41)	ε_{cc}' (in./in.) Eq. (7.18)	$\varepsilon_{cc}'/\varepsilon_{co}'$ Eq. (7.18)	$\varepsilon_{cc}'/\varepsilon_{co}'$ Exp.	Diff. Eq. (7.18) with Exp.
C-CT-E	0.549	0.025	12.40	12.30	1%
C-GT-E	0.580	0.027	13.33	14.40	7%
S-CT-E	0.499	0.022	11.18	10.91	2%
S-GT-E	0.440	0.020	10.00	10.57	5%

Table 7.11 Calculated results of elliptical columns with non-bonded FRP jackets and expansive cement concrete (1)

Speci. ID	t_j (in.)	ρ_{FRP} Eq. (6.8)	k_p Eq. (6.21)	k_s	k_l Eq. (6.13)	k_ε Eq. (7.19)	$f_{lu}/f_{co}'^{*}$ Eq. (6.19)	f_{cc}'/f_{co}' Eq. (7.4)	f_{cc}'/f_{co}' Exp.	Diff. Eq. (7.4) with Exp.
R2-CT-E	0.070	0.015	1.735	1.0	1.0	0.259	0.332	2.32	2.22	4%
R2-GT-E	0.320	0.071	1.580	1.0	1.0	0.398	0.293	2.14	2.32	8%
R3-CT-E	0.070	0.018	1.099	1.0	1.0	0.227	0.226	1.81	2.08	13%
R3-GT-E	0.320	0.080	1.180	1.0	1.0	0.386	0.188	1.61	1.51	6%

* The values of f_{co}' were listed in Table 5.6.

Table 7.12 Calculated results of elliptical columns with non-bonded FRP jackets and expansive cement concrete (2)

Speci. ID	α Eq. (6.41)	ε_{cc}'(in./in.) Eq. (7.18)	$\varepsilon_{cc}'/\varepsilon_{co}'$ Eq. (7.18)	$\varepsilon_{cc}'/\varepsilon_{co}'$ Exp.	Diff. Eq. (7.18) with Exp.
R2-CT-E	0.413	0.012	6.17	5.50	12%
R2-GT-E	0.395	0.018	9.22	9.00	2%
R3-CT-E	0.364	0.010	4.90	4.30	11%
R3-GT-E	0.346	0.017	8.27	10.57	22%

7.2 Design-Oriented Model for FRP-Confined Columns

The proposed model for FRP-confined columns is based on a bilinear four-parameter relationship suggested by Richard and Abbott (1975) as:

$$f_c = \frac{(E_0 - E_p)\varepsilon_c}{\left[1 + \left(\frac{(E_0 - E_p)\varepsilon_c}{f_i}\right)^n\right]^{\frac{1}{n}}} + E_p \varepsilon_c \tag{7.21}$$

where ε_c and f_c : axial strain and stress of FRP-confined concrete; E_0 and E_p : first and second slopes on the stress-strain curve; f_i : reference plastic stress at the intercept of the second slope with the stress axis; n : a curve shape parameter which mainly controls the curvature in the transition zone. Figure 7.6 shows the definition of these parameters:

These four parameters need to be determined for developing the confinement model. The first slope of the stress-strain curve, E_0 is given by Eq. 7.7. The reference plastic stress, f_i and the second slope, E_p can be calculated as described in Figure 7.7. As shown in Figure 7.7(a), for the FRP-confined columns with hardening behavior, E_p can be expressed as:

$$E_p = \frac{f_{cc}' - f_0}{\varepsilon_{cc}' - \varepsilon_0} \tag{7.22}$$

f_i can be calculated by:

$$f_i = f_{cc}' - E_p \varepsilon_{cc}' \tag{7.23}$$

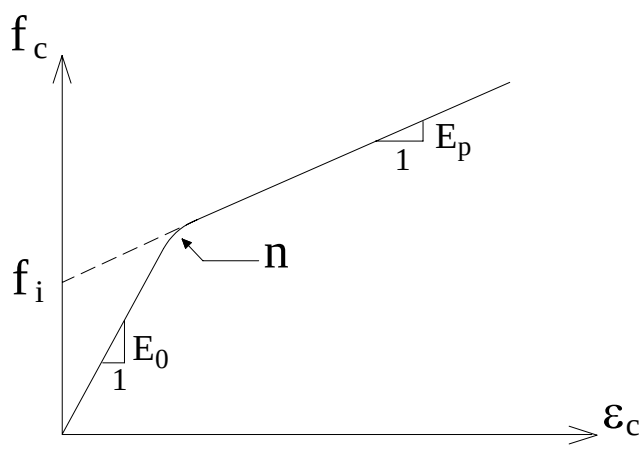

Figure 7.6 Parameters of four-parameter confinement model

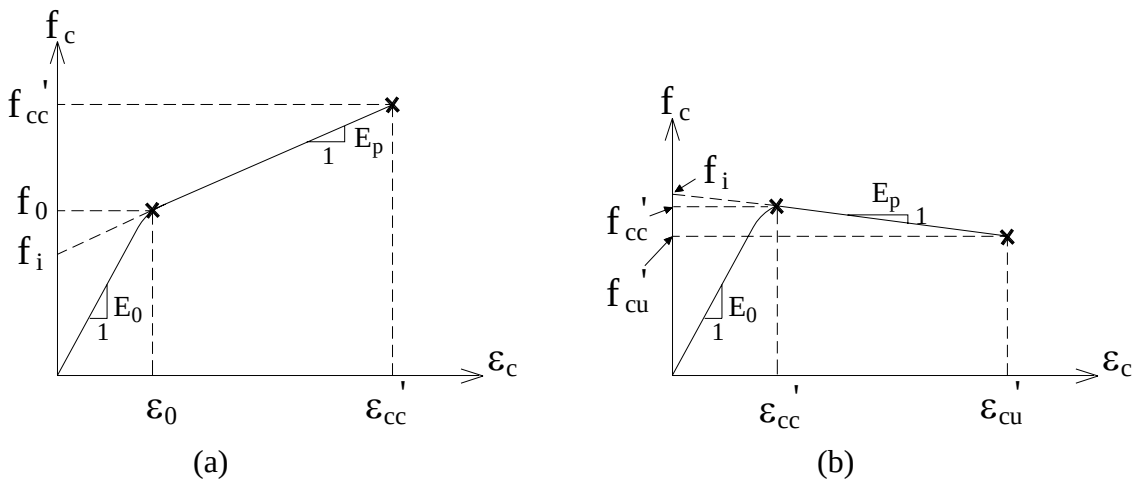

Figure 7.7 Calculation of f_i and E_p:
(a) columns with hardening behavior; (b) columns with softening behavior

For columns with softening behavior as shown in Figure 7.7 (b), Eq. (7.22) can be rewritten as:

$$E_p = \frac{f_{cc}' - f_{cu}'}{\varepsilon_{cu}' - \varepsilon_{cc}'} \tag{7.24}$$

It should be noted that in this case E_p is a negative value. f_i is found to be:

$$f_i = f_{cu}' - E_p \varepsilon_{cu}' \tag{7.25}$$

Parameter n is defined as a curve shape parameter which mainly controls the curvature in the transition zone and is therefore related to the secant modulus E_{c0} of the line passing through the origin and the turning point. For columns with hardening behavior, E_{c0} can be expressed as:

$$E_{c0} = \frac{f_0}{\varepsilon_0} \tag{7.26}$$

and for columns with softening behavior, E_{c0} can be expressed as:

$$E_{c0} = \frac{f_{cc}'}{\varepsilon_{cc}'} \tag{7.27}$$

The shape parameter, n is then found to be:

$$n = 1 + \frac{1}{\frac{E_0}{E_{c0}} - 1} \tag{7.28}$$

Alternatively, n can be obtained by the following method. Figure 7.8 shows the normalized axial stress, $\frac{f_{cc}'}{f_{co}'}$, versus the normalized axial strain, $\frac{\varepsilon_{cc}'}{\varepsilon_{co}'}$ for the part of stress-strain curve prior to the turning point for different values of n, ranging from 1 to 25. It is seen that values between 1 and 3 would be the best choice for fitting the stress-strain curve of the FRP-confined concrete. Therefore, for design convenience, n is usually set to 2.

It is seen from Eq. (7.21) that the stress-strain relationship can be found when the four parameters: E_0, E_p, f_i, and n are known. Equation (7.21) can be calculated by using a computer program or spreadsheet in which the axial strain, ε_c is divided into many increments in the range from 0 to ε_{cc}' for columns with hardening behavior, or in the range from 0 to ε_{cu}' for columns with softening behavior.

As a design example for columns with hardening behavior, the procedure used to develop the stress-strain model for circular column, C-C1-0 is described:

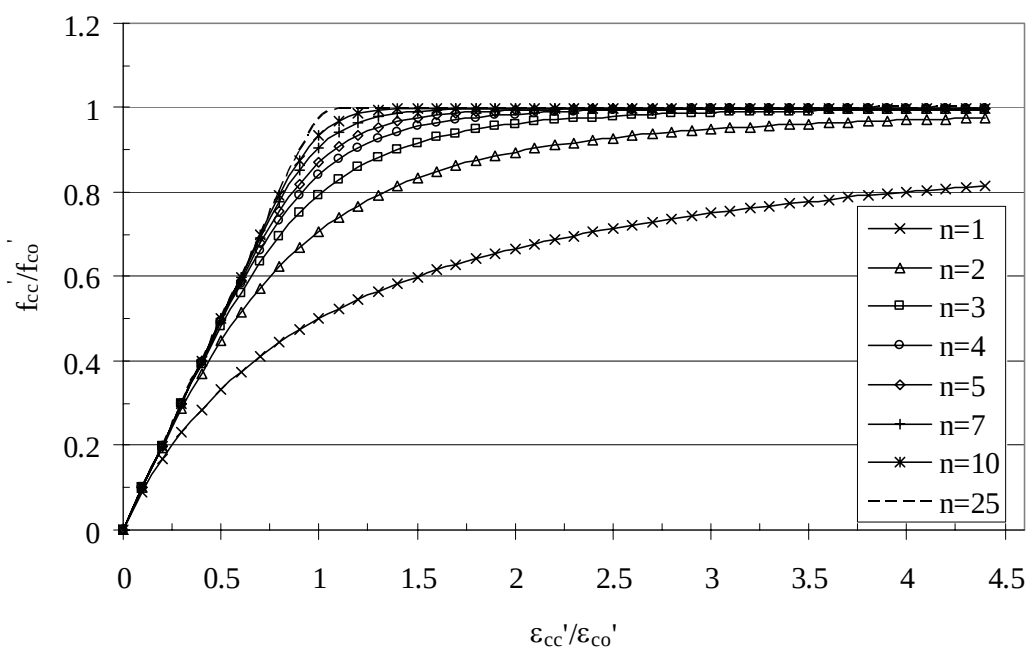

Figure 7.8 Normalized stress-strain relationships with different values of n

The ultimate axial strain and stress, ε_{cc}' and f_{cc}' are calculated to be 0.0155 in./in. and 5896 psi, respectively from Tables 7.1 and 7.2 for f_{cc}' = 2200 psi and ε_{cc}' = 0.002 in./in; ε_0 and f_0 are calculated to be 0.002 in./in. and 3640 psi respectively from Eqs. (7.8) and (7.9) respectively. By using Eq. (7.22), E_p is found to be 172214 psi and from Eq. (7.23) f_i is found to be 3295 psi; n is calculated to be 2.3 from Eq. (7.28). Therefore, substituting the corresponding terms in Eq. (7.21), the stress-strain relationship of C-C1-0 can be expressed as:

$$f_c = \frac{3036030}{\left[1+\left(\frac{3036030\varepsilon_c}{3295}\right)^{2.3}\right]^{\frac{1}{2.3}}} + 172214\varepsilon_c \qquad (7.29)$$

By using a spreadsheet, the stress-strain relation curve is developed and comparison is made between the design-oriented model and the experimental results for C-C1-0 as shown in Figure 7.9. Moreover, by using the same procedure, the design-oriented model for square column, S-C2-0 is developed as shown in Figure 7.10.

As another design example for columns with softening behavior, a simplified procedure for developing a stress-strain model for rectangular column, R2-C2-0 is described below:

Tables 7.5 and 7.6 show that the peak axial stress, f_{cc}' and the ultimate axial stress, f_{cu}' are calculated as 3300 psi and 3244 psi, respectively; the ultimate strain, ε_{cu}' is calculated to be 0.020 in./in. and the axial strain corresponding to f_{cc}' is set to 0.004 in./in. The value of E_p is obtained from Eq. (7.24) as -3500 psi and from Eq. (7.25) f_i is found as 3314 psi. Parameter n is calculated from Eq. (7.28) as 1.3. Thus, the stress-strain relationship of R2-C2-0 obtained from Eq. (7.21) can be expressed as:

$$f_c = \frac{3211744}{\left[1+\left(\frac{3211744\varepsilon_c}{3314}\right)^{1.3}\right]^{\frac{1}{1.3}}} - 3500\varepsilon_c \qquad (7.30)$$

Figure 7.11 shows the stress-strain curve for R2-C2-0 obtained from the design-oriented model and comparison is made with the experimental results.

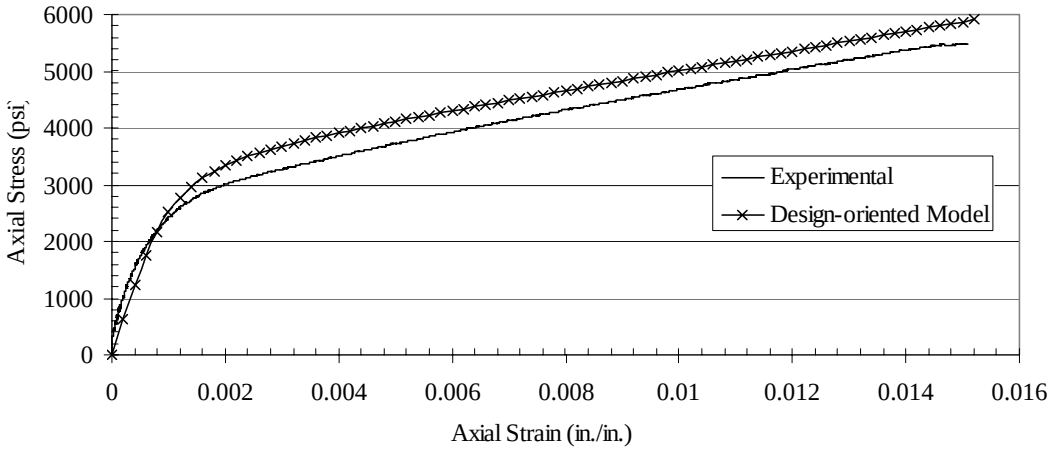

Figure 7.9 Comparison between the design-oriented model and experimental results for C-C1-0

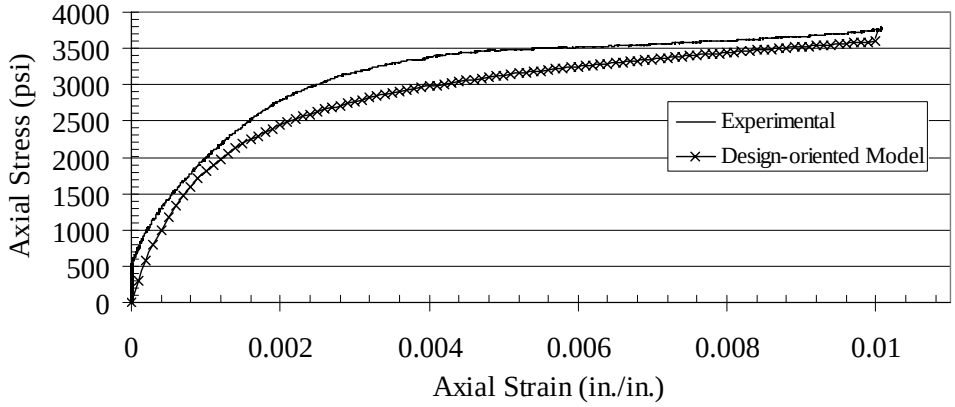

Figure 7.10 Comparison between the design-oriented model and experimental results for S-C2-0

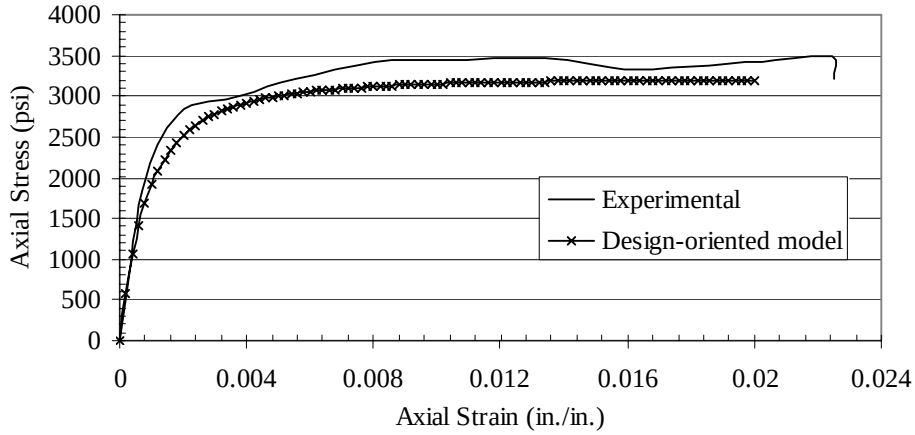

Figure 7.11 Comparison between the design-oriented model and experimental results for R2-C2-0

It is seen for Figure 7.1 for circular columns, Figure 7.2 for square and rectangular columns and Figure 7.3 for elliptical concrete columns confined with bonded FRP jackets, that the confined concrete strength capacity depends on the confining pressure as expressed in Eqs. (6.18), (6.19) and (6.20). These equations account for the different levels of effectiveness of the FRP jacket: these include the geometric shape of the cross-section, whether or not a continuous FRP jacket or FRP strips are used, and the jacket efficiency factor which depends on the corner radius and aspect ratio of the cross-section. The ultimate strain capacity of a concrete column confined by the bonded FRP jacket is predicted from the relationship of the secant modulus with the jacket area strain.

For concrete columns confined with non-bonded FRP jackets and expansive cement concrete, the strain characteristics are defined by the linear relationship between the volumetric and axial strain; the slope of this linear relationship is determined by the jacket confining pressure in which the post-tensioning effect is included. In all cases, the confined concrete strength is predicted by concrete plasticity theory.

To construct a model for FRP-confined concrete column, the stress and strain parameters: f_0, ε_{cu}, $f_{cc}^{'}$, and $\varepsilon_{cc}^{'}$ for columns with hardening behavior or $f_{cc}^{'}$, $\varepsilon_{cc}^{'}$, $f_{cu}^{'}$, and $\varepsilon_{cu}^{'}$ for columns with softening behavior need to be calculated. Then four parameters E_0, E_p, f_i, and n can be found to develop the stress-stain model based on the polynomial concrete model as shown in Eq. (7.21).

8. FINITE ELEMENT ANALYSIS

The finite element method is a numerical method for solving problems of engineering and mathematical physics. This method has a number of advantages that have made it popular in structural engineering to solve problems involving complicated geometries and structures composed of several different materials. To provide an alternative analytical approach for FRP-confined concrete columns, a nonlinear finite analysis is conducted by using the finite element software package-ANSYS 6.0 (ANSYS 2000).

8.1 Plasticity Approach

Concrete is a nonlinear plastic material. The classic elastic linear theory cannot describe the physical properties of concrete. ANSYS provides several options for using different plasticity approaches including a bilinear isotropic hardening, a multi-linear isotropic hardening, a multi-linear kinematic hardening, and the Drucker-Prager model. For the present comparison, a two-parameter model, the Drucker-Prager plasticity model is used. This model assumes an elasto-plastic material response with an associative or nonassociative flow rule. Some parameters that describe the Drucker-Prager (DP) model are given below; more details of the model can be found in the work of Chen and Han (1982). The yield function of the DP model is a linear relationship between the hydrostatic and deviatoric components of the stress tensor as expressed in Eq. (8.1):

$$\rho = c + 3\sin\phi \cdot \sigma_a \tag{8.1}$$

where ρ = deviatoric stress component; σ_a = hydrostatic stress component; c = cohesion value of concrete; ϕ = angle of internal friction of concrete.

It can be seen that the yield surface of the DP model is a circular cone as shown in Figure 8.1; σ_a and ρ correspond to the X and Y axis respectively; c corresponds to the intercept with the ρ axis; $\tan\phi$ is the slope of the straight line.

For the concrete, the state of triaxial stresses is represented as a function of the individual component, $f(\{\sigma\})$, which can be interpreted as an equivalent stress σ_e; where $\{\sigma\}$ is the stress vector. In the DP model, σ_e can be expressed as:

$$\sigma_e = 3\beta\sigma_a + \left[\frac{1}{2}\{\rho\}^T[M]\{\rho\}\right]^{\frac{1}{2}} \tag{8.2}$$

where $\{M\}$ is a special diagonal matrix and β is a material constant which is a function of the angle of internal friction ϕ, and given by:

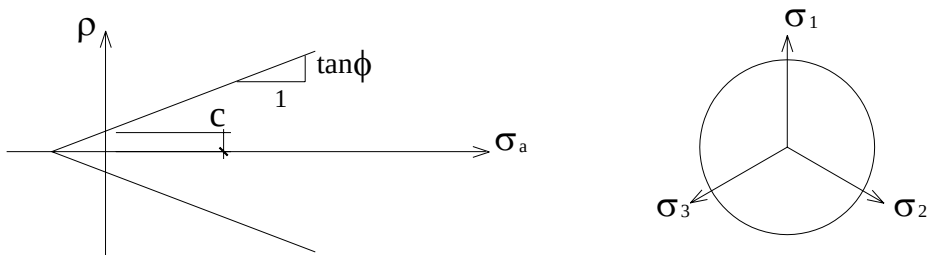

Figure 8.1 Yield surface of Drucker-Prager model and its cross-section

$$\beta = \frac{2\sin\phi}{\sqrt{3}(3-\sin\phi)} \tag{8.3}$$

The yield parameter of the plastic concrete is defined as:

$$\sigma_y = \frac{6c\cos\phi}{\sqrt{3}(3-\sin\phi)} \tag{8.4}$$

In the present FE study, the values of ϕ and c proposed by Rochette and Labosière (1996) are used in the form of Eqs. (8.5) and (8.6), respectively as:

$$\phi = \sin^{-1}\frac{3}{1+0.00159 f_{co}'} \tag{8.5}$$

$$c = \left(f_{co}' - 1256\right)\frac{3-\sin\phi}{6\cos\phi} \tag{8.6}$$

where f_{co}' = compressive strength of unconfined concrete; for shape-modified columns with bonded FRP jackets, the mean compressive strength of the cross-section is used. In addition, Rochette and Labossière (1996) suggested that a non-associative flow rule could be used in the FE analysis of FRP-confined concrete based on the DP plasticity model; plastic straining occurring normal to the yield surface is neglected.

8.2 FE Modeling

The first task in any finite element analysis is to set up the model. Four types of models were developed according to the geometric characteristics of the specimens. SOLID65, which is an eight-node brick element with 3 DOFs at each node, was used to model concrete. This element is capable of cracking in tension and crushing in compression so that the post-cracking effect of concrete is included for assembling the total stiffness matrix after cracking occurs. SHELL41 is a four-noded element having membrane (in-plane) stiffness with negligible out-of-plane stiffness that is well-suited to model FRP composite materials. For FRP materials, only

the tensile stress is considered. The material properties c and ϕ for concrete were obtained from the DP plasticity approach using Eqs. (8.5) and (8.6). The initial elastic modulus was calculated by using Eq. (7.7). The FRP composite was considered as an orthotropic linear material with different elastic moduli in different directions. In order to limit the effect of the FRP jacket to confinement only, its elastic modulus in the directions except the fiber direction was set close to zero. Considering the symmetry of each column, only one-quarter of the column section along its longitudinal axis was modeled; symmetrical boundary conditions were applied at the symmetrical borders along the X and Y axes and all nodes on each plane of symmetry were fixed only in the direction normal to that plane, but were free to move within that plane. Figures 8.2 through 8.13 show the meshed FE models for the circular, square, rectangular and elliptical columns with bonded FRP jackets.

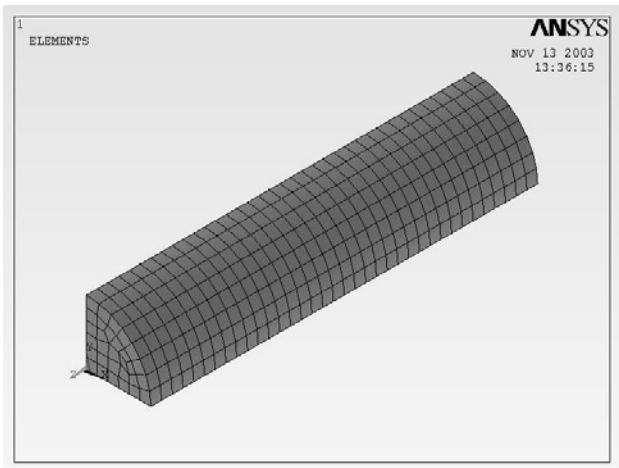

Figure 8.2 Typical elevation of circular model with the FRP jacket (total 2137 nodes; 1080 concrete elements)

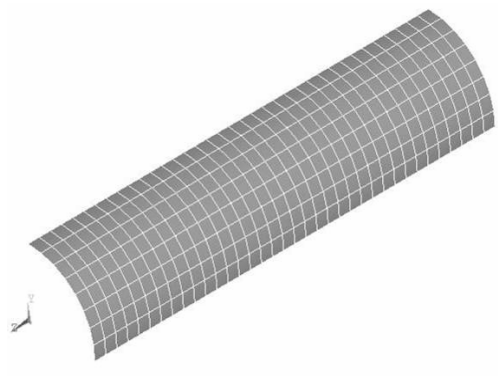

Figure 8.3 Typical elevation of the circular FRP jacket (total 288 shell elements)

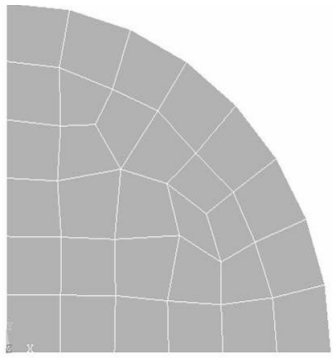

Figure 8.4 Typical cross-section of circular model

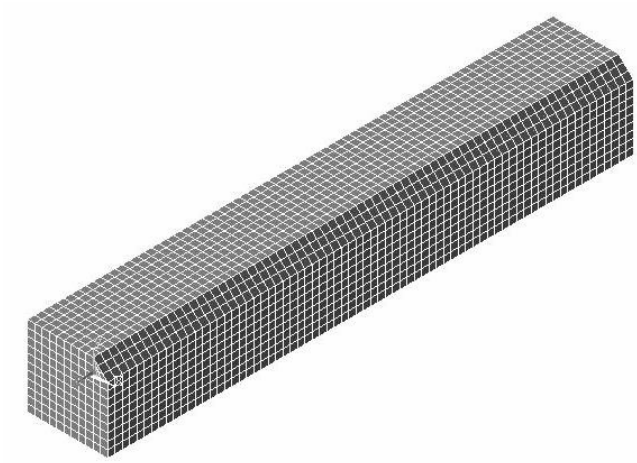

Figure 8.5 Typical elevation of square model with the FRP jacket (total 6860 nodes; 4356 concrete elements)

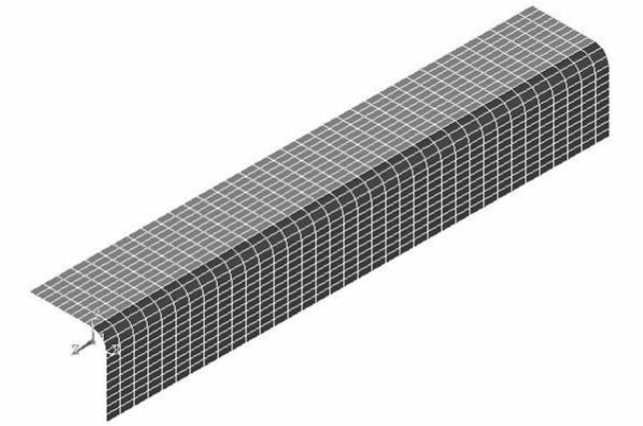

Figure 8.6 Typical elevation of the square FRP jacket (total 756 shell elements)

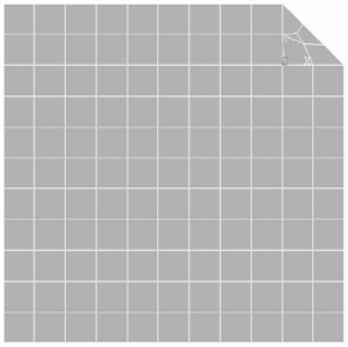

Figure 8.7 Typical cross-section of square model

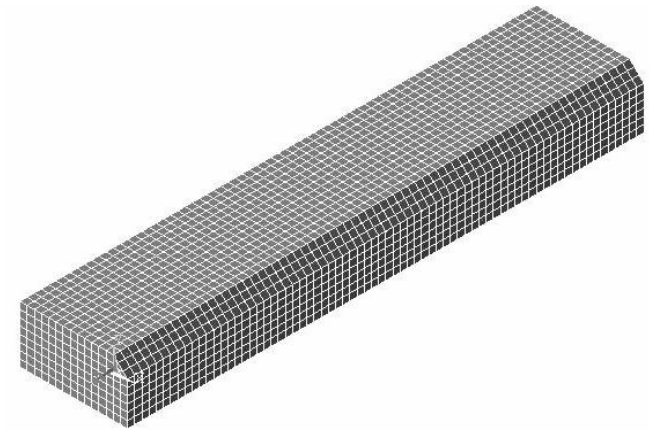

Figure 8.8 Typical elevation of rectangular model with the FRP jacket (total 13701 nodes; 8640 concrete elements)

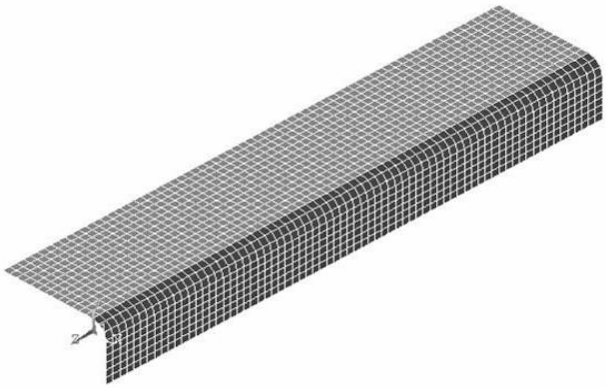

Figure 8.9 Typical elevation view of the rectangular FRP jacket (total 756 shell elements)

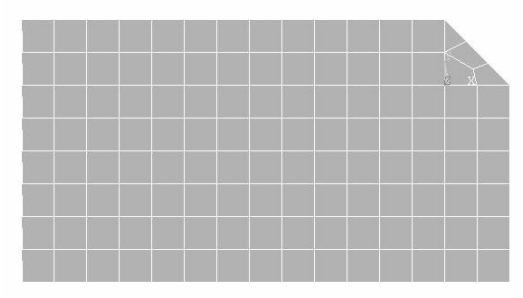

Figure 8.10 Typical cross-section of rectangular model

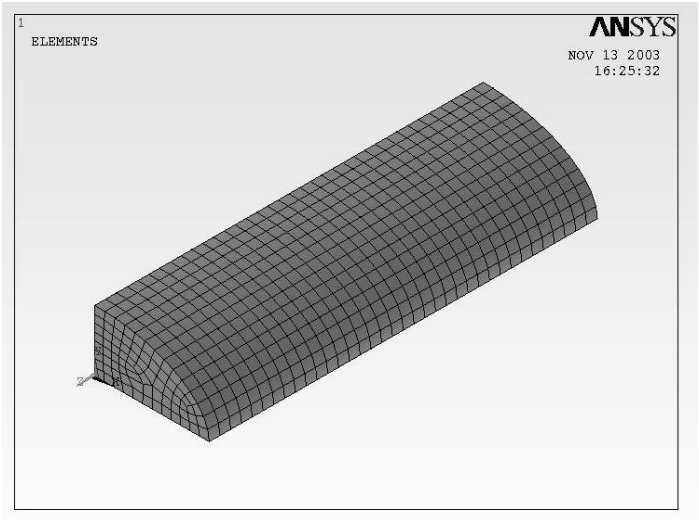

Figure 8.11 Typical elevation of elliptical model with the FRP jacket (total 4018 nodes; 2268 concrete elements)

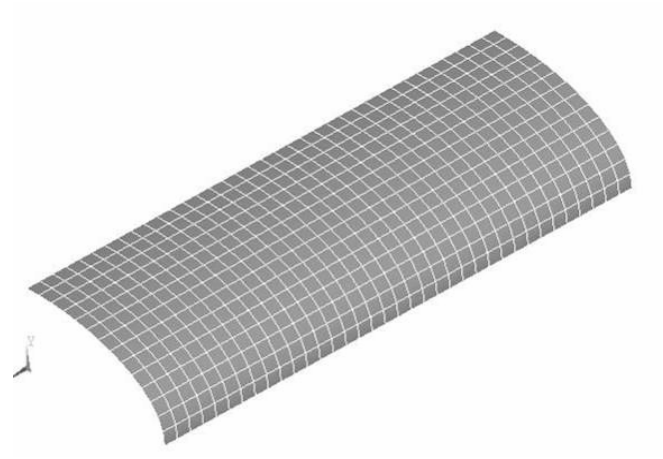

Figure 8.12 Typical elevation of the elliptical FRP jacket (total 504 shell elements)

For the shape-modified columns with expansive cement concrete, tetrahedral concrete elements were used to model the expansive cement grout as shown in Figures 8.14 and 8.15. In this case, the original square or rectangular column concrete was modeled by hexahedral concrete elements.

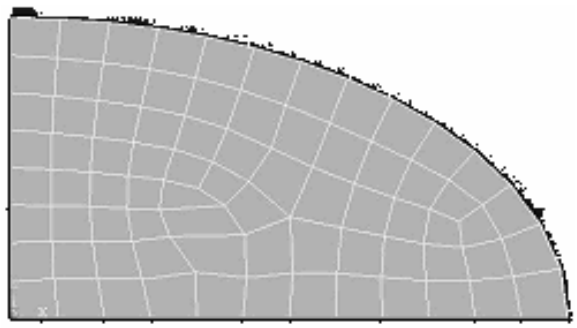

Figure 8.13 Typical cross-section of elliptical model

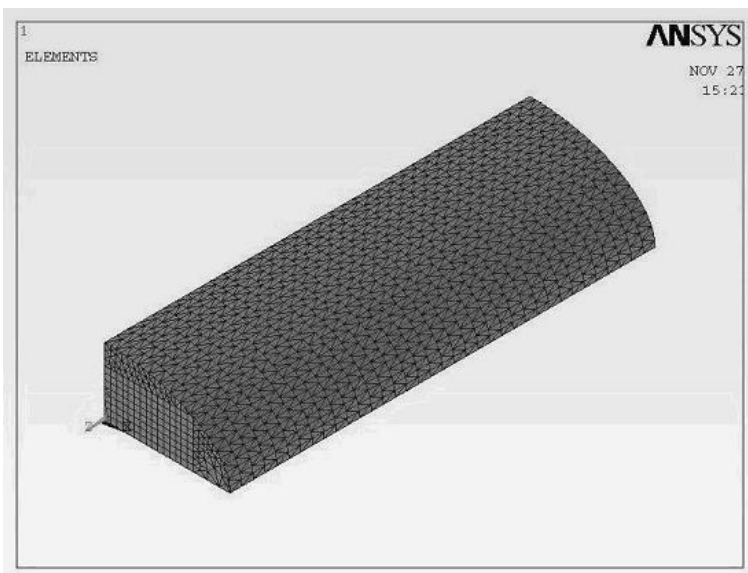

Figure 8.14 Typical elevation of elliptical model with the FRP jacket and expansive cement concrete (total 4018 nodes; 2268 concrete elements)

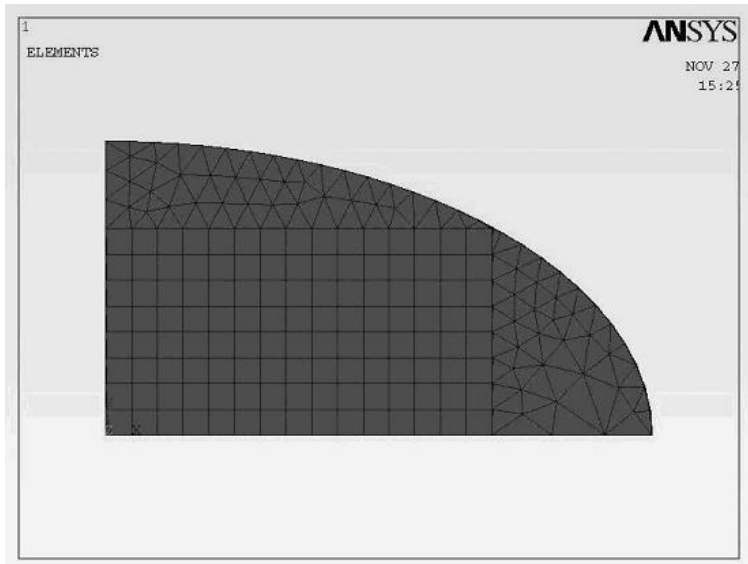

Figure 8.15 Typical cross-section of elliptical model with the FRP jacket and expansive cement concrete

In all cases, the bottom of the columns was fixed so that no degree freedom was allowed there to simulate the boundary condition for the uniaxially loaded columns. In addition, to model the "post-tensioning" effect of the expansive cement concrete on the FRP jackets, an equivalent thermal gradient was applied on the FRP composite jacket to obtain the post-tensioning effect and the initial hoop strain, prior to the application of the axial loading. For each model, a nonlinear analysis was conducted considering both material and geometric nonlinear behavior. The loading process was divided into many incremental steps, in which an incremental axial displacement was applied to the top surface of each column and all nodes on the top face were tied together so that a uniform compressive displacement could be exerted. Every increment would be iterated until convergence was met with respect to the criteria of force and displacement. The calculations were terminated when the hoop strain of the FRP jacket reached its ultimate limit, ε_{ju}, as defined in Chapter 6.1.

To optimize the calculation, each load step was divided into 20 substeps to expedite the process of convergence. Two examples with input files are listed in the Appendix to illustrate the procedures for constructing the FE models: column C-C1-0 for a concrete column confined by a bonded FRP jacket, and column S-CT-E for a concrete column confined by a non-bonded FRP jackets with expansive cement concrete.

8.3 Results and Discussion of FE Analysis

The output of ANSYS results consists of the nodal displacement, element stress, element strain and other information. Figures 8.16 through 8.23 illustrate typical results regarding the deformed shape for one loading step. The hidden lines represent the undeformed (original) edges of the column while the solid lines represent the deformed shape of the column.

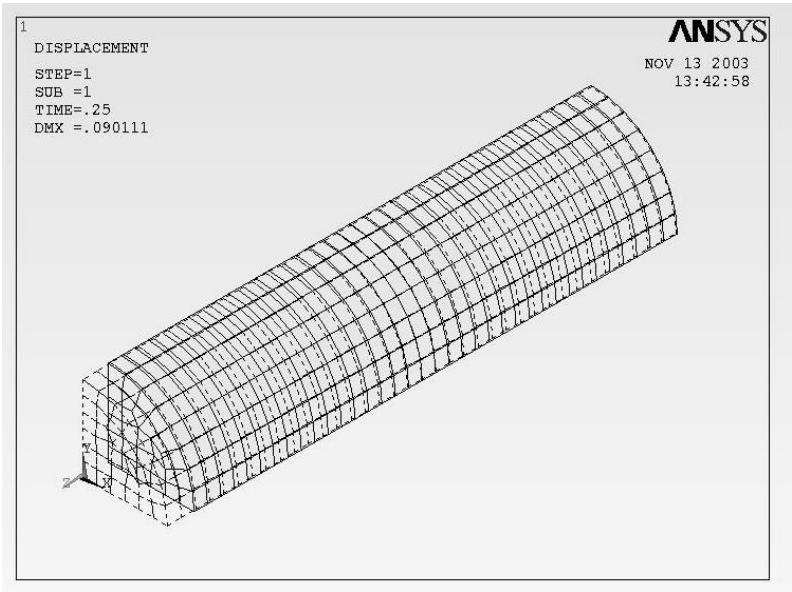

Figure 8.16 Deformed shape of circular model after axial loading

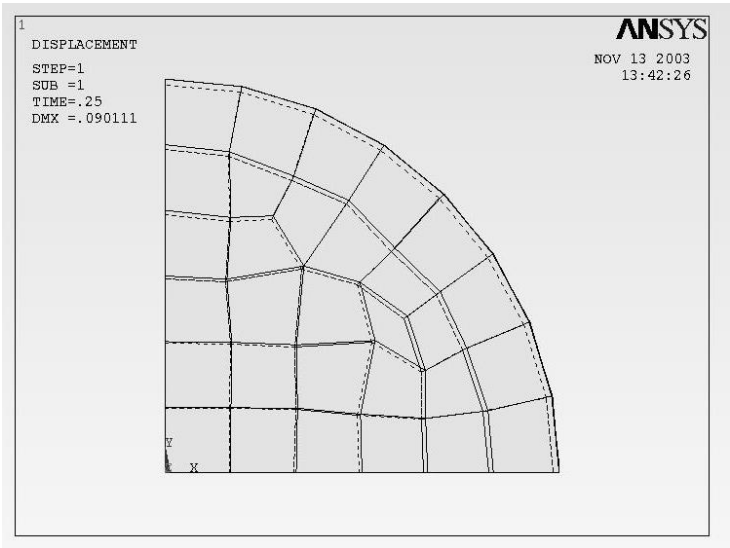

Figure 8.17 Deformed shape of cross section of circular model

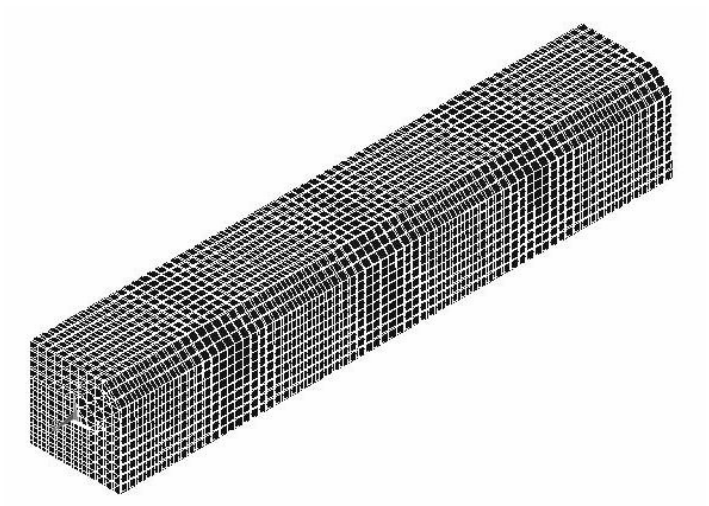

Figure 8.18 Deformed shape of square model after axial loading

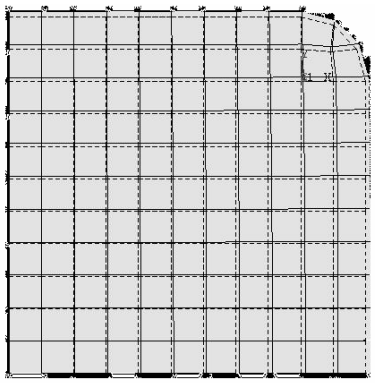

Figure 8.19 Deformed shape of cross section of square model

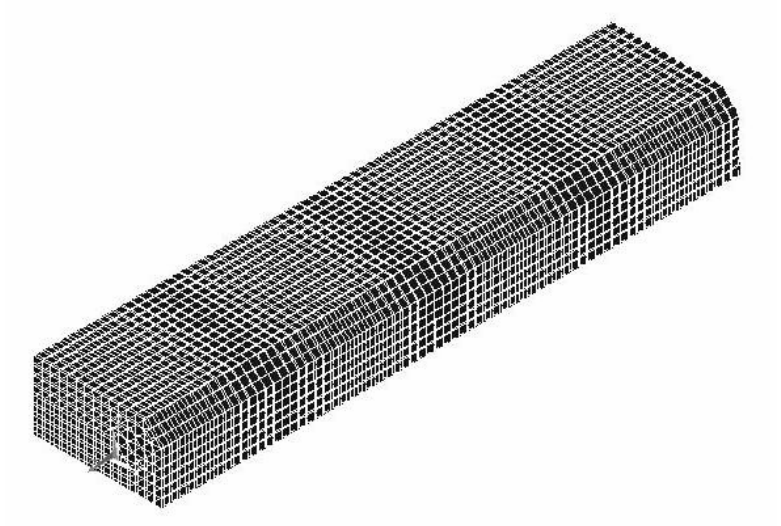

Figure 8.20 Deformed shape of rectangular model after axial loading

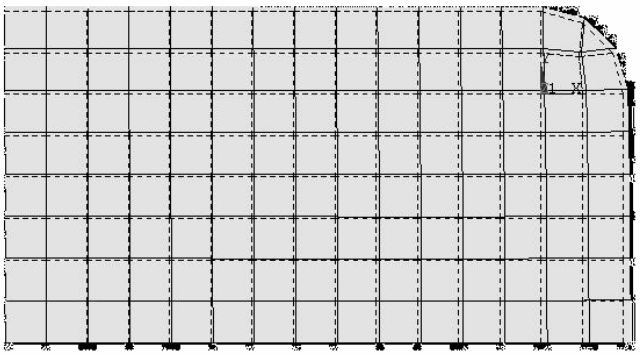

Figure 8.21 Deformed shape of cross section of rectangular model

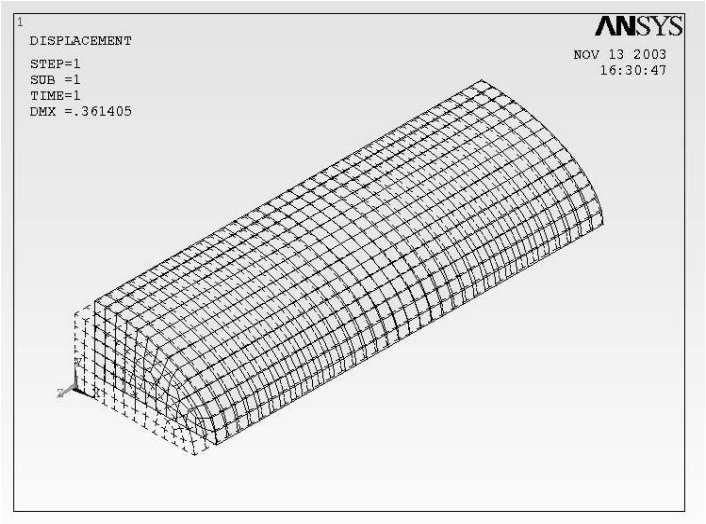

Figure 8.22 Deformed shape of elliptical model after axial loading

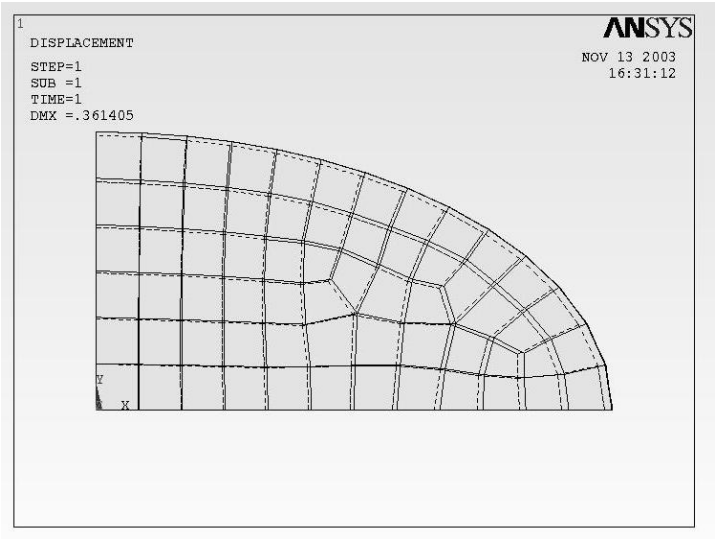

Figure 8.23 Deformed shape of cross section of elliptical model

For the axial stress in each step, a mean value was calculated by taking the average of the longitudinal 6 elements along the central line of the model. The data from time-history FE analysis was transported into a spreadsheet to develop the stress-strain response for each case.

The predicted axial stress versus axial strain relation curves for different types of columns wrapped with CFRP jackets are presented in Figures 8.24 through 8.28. The selected specimens are C-C1-0 (12” diameter circular column wrapped with 1 layer of bonded CFRP); S-C2-0 (11”×11” square column wrapped with 2 layers of bonded CFRP); R3-C2-0 (6”×18” rectangular column wrapped with 2 layers of bonded CFRP); S-CT-E (shape modified 11”×11” square column with expansive cement concrete and wrapped with 2 layers of non-bonded CFRP); and R3-CT-E (shape modified 6”×18” rectangular column with expansive cement concrete and wrapped with 2 layers of non-bonded CFRP). The experimental stress-strain relation curves are also plotted to compare to the predicted FE results. It is seen that the FE results agree well with the test results in general. The discrepancies are mainly due to the simplicity of the DP model which may not accurately reflect the actual behavior of concrete plasticity. In addition, the bond between concrete and FRP composite is not perfect as assumed in the FE model, and the FRP composite develops stress concentrations, that can not be simulated by the FE model.

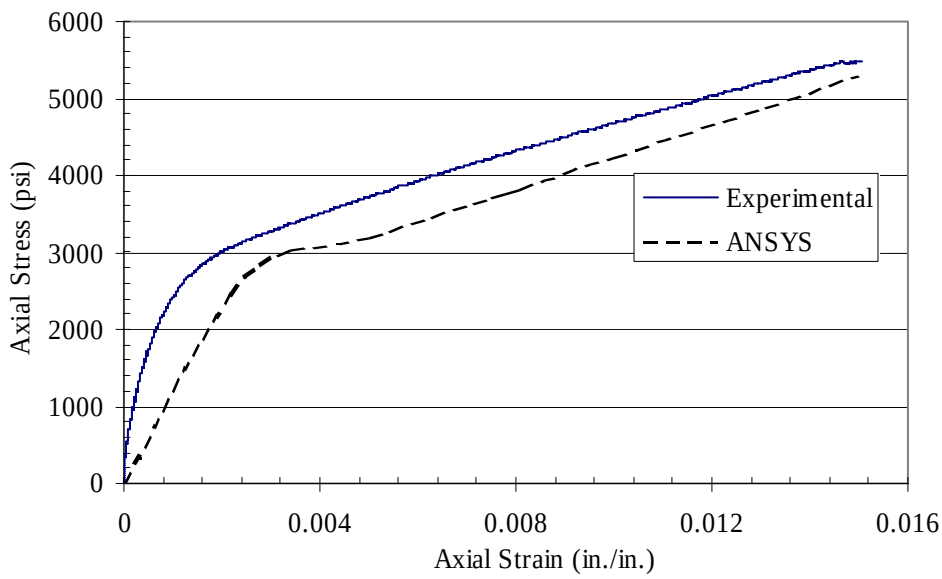

Figure 8.24 Comparison of FE model with experimental results for C-C1-0

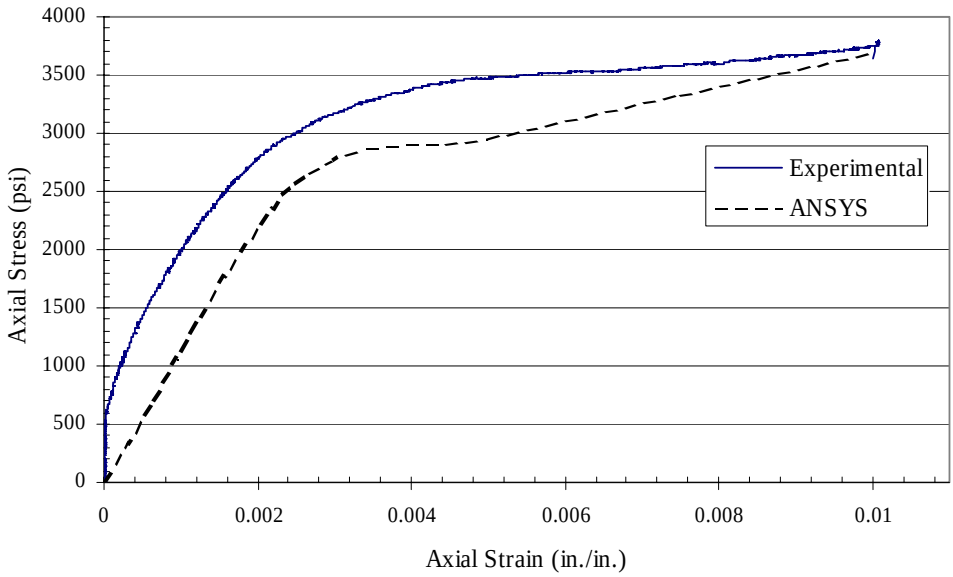

Figure 8.25 Comparison of FE model with experimental results for S-C2-0

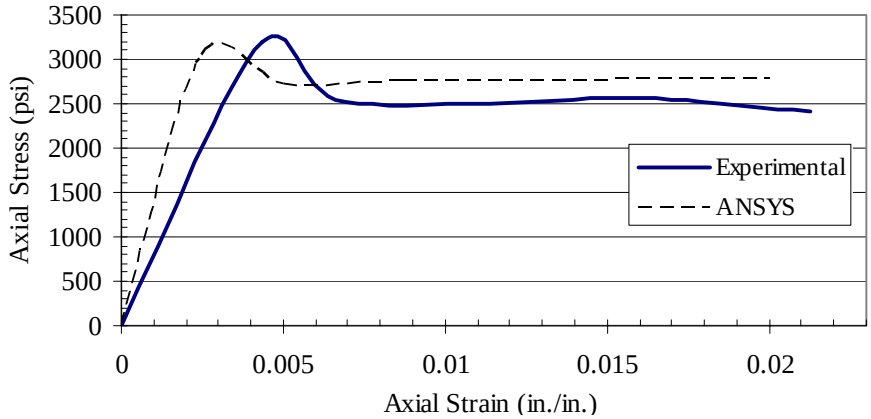

Figure 8.26 Comparison of FE model with experimental results for R3-C2-0

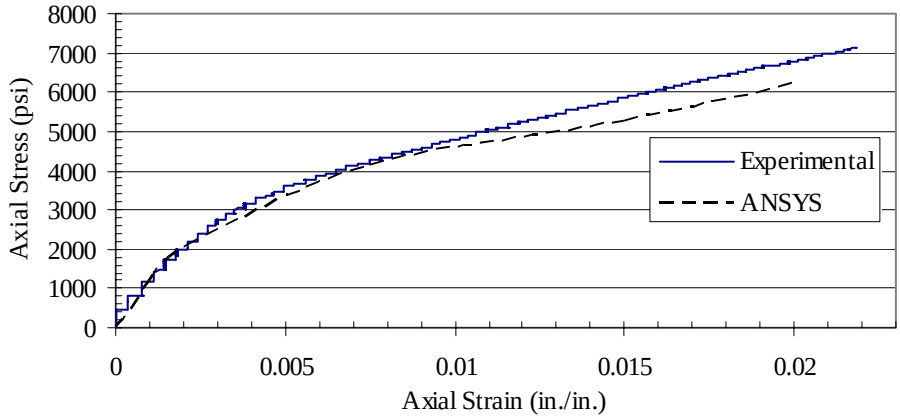

Figure 8.27 Comparison of FE model with experimental results for S-CT-E

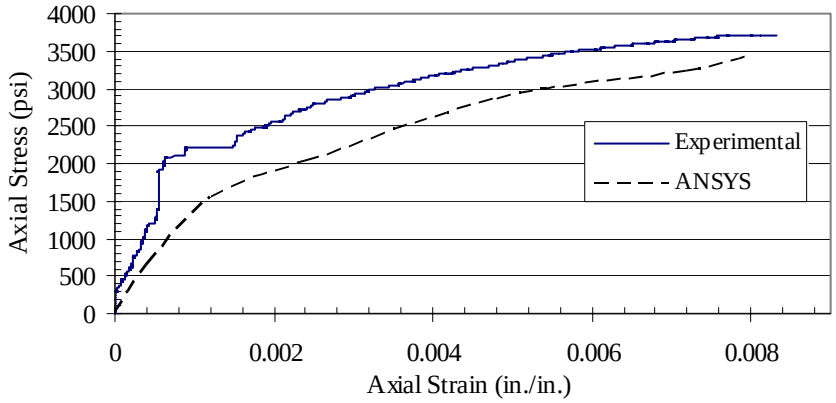

Figure 8.28 Comparison of FE model with experimental results for R3-CT-E

9. PARAMETRIC STUDY

This section discusses the shape effect of the geometry for performing shape modification through an example as describe below. In this example, the possible geometries for shape modification are presented; the stress-strain models are developed; their corresponding results are summarized and compared. This example also illustrates that a parametric study should be necessarily performed to find the optimal method for applying shape modification based on the comprehensive consideration of strengthening effect, cost, and construction difficulties.

The original rectangular concrete column selected is R3-0-0 in the present experimental study, which is 36” high with a cross-section of 18”x6”. Option (1) for strengthening R3-0-0 is to apply 2 layers of CFRP wet lay-up without shape modification. Options (2) through (6) are to perform shape modification with different geometries and aspect ratios. All these shape-modified columns are made by using non-bonded FRP jackets and expansive cement concrete. These strengthening options are listed as below:

- Option (1): 2 layers of CFRP wet lay-up without shape modification (R3-C2-0);
- Option (2): 2 layers of non-bonded CFRP jacket and an elliptical section of $B_j \times D_j = 30.5'' \times 11''$ after shape modification (R3-CT-E);
- Option (3): 2 layers of non-bonded CFRP jacket and an elliptical section of $B_j \times D_j = 24'' \times 12''$ after shape modification;
- Option (4): 2 layers of non-bonded CFRP jacket and an elliptical section of $B_j \times D_j = 22'' \times 16''$ after shape modification;
- Option (5): 2 layers of non-bonded CFRP jacket and a circular section with a diameter of 20” after shape modification;
- Option (6): 1 layer of non-bonded CFRP jacket and a circular section with a diameter of 20” after shape modification;

The details of the strengthening schemes are shown in Figure 9.1.

The compressive strength for unconfined rectangular concrete and expansive cement concrete are assumed as 2200 psi and 1500 psi respectively, as mentioned in Chapter 5. The mean unconfined strength, $f_{co}^{'}$ for the shape-modified cross-section is calculated by Eq. (5.3). Based on the design procedures discussed in Chapter 7, other parameters such as ρ_{FRP}, k_{ε}, k_p, $\frac{f_{lu}}{f_{co}^{'}}$, and α were calculated and results are listed in Table 9.1. It is seen that all columns with shape modification would behave in a hardening manner since the effective confinement ratio, $\frac{f_{lu}}{f_{co}^{'}}$ are larger than 0.2. Axial stress versus axial strain relationships for all options are developed by the analytical approach and grouped together as shown in Figure 9.2. As seen in Figure 9.2, option 1, the column confined by the bonded FRP jacket without shape modification, shows a softening behavior with very little increase in the axial strength; all shape-modified columns show an improvement of the compressive behavior with different levels: Option 5, which has a circular cross-section after shape modification, shows the highest increase in both

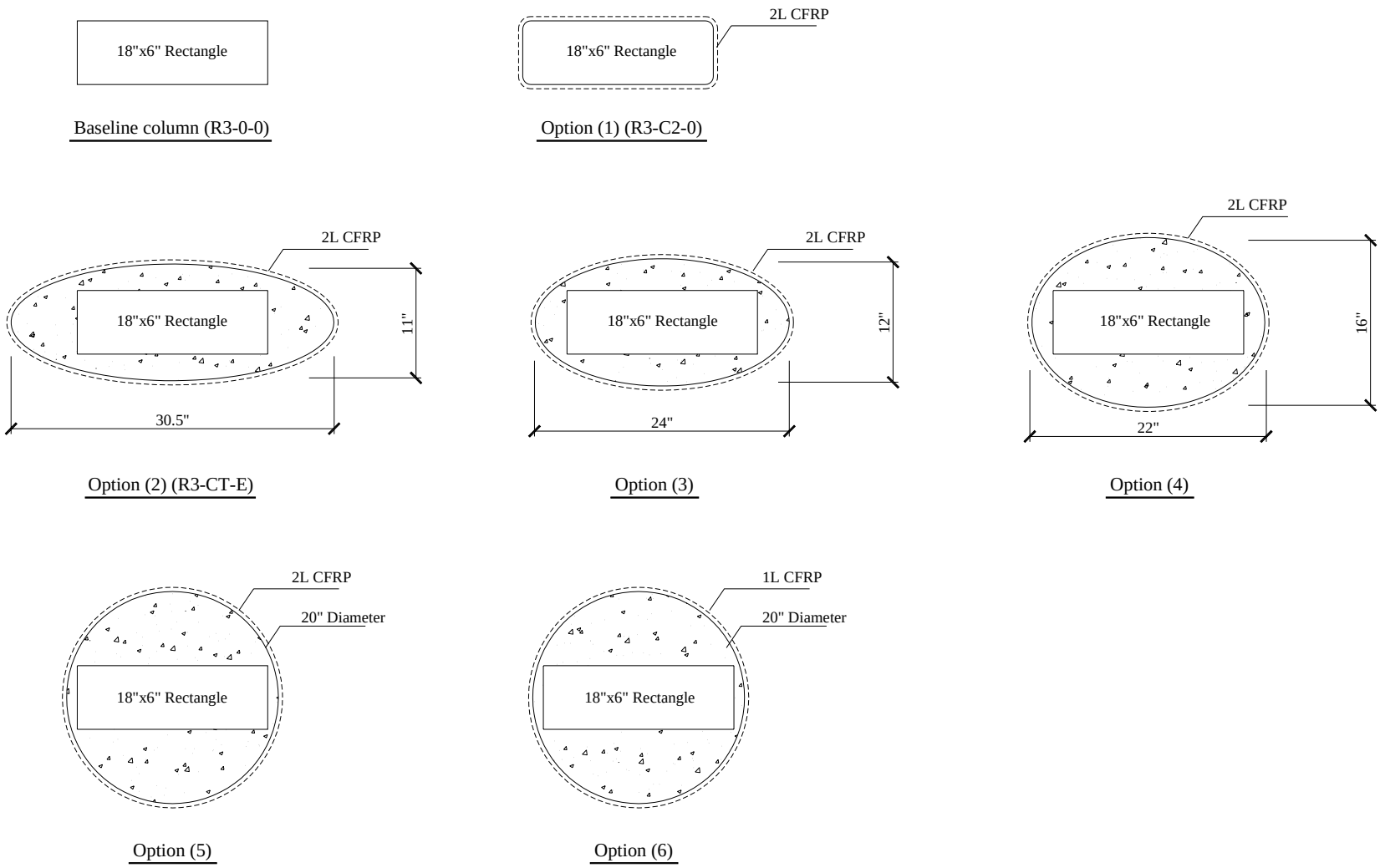

Figure 9.1 Strengthening options 1-6

axial strength and ultimate axial strain, and option 2 with a largest aspect ratio shows the lowest increase. However, the disadvantage of options 5 is that it requires more expansive grout to achieve shape modification which would consequently result in the increase in cost.

Table 9.2 lists the results of volume, area of FRP jacket, axial strength f_{cc}', ultimate axial strain ε_{cc}' or ε_{cu}', and the ductility ratio μ. All these factors need to be considered for determining the optimal geometry for shape modification. In order to compare the effect for all cases, Table 9.3 shows the increase of items for options 2-7 compared to option 1 without shape modification. Note that the minus sign means a decrease instead of an increase.

It is known that the increase of the column cross-section and the FRP jacket area will be related to the issue of cost and construction period, and the effect of shape modification can be evaluated by the increase of f_{cc}', ε_{cc}', and μ. Therefore, several options are available from the construction and cost point of view, and if a high increase of capacity is required and the volume increase is not a big concern, option 5 should be considered.

Table 9.1 Dimensions and calculated parameters for options 1-6

Option	t_j (in.)	B_j (in.)	D_j (in.)	ρ_{FRP}	f_{co}' (psi)	k_ε	k_p	f_{lu}/f_{co}'	α
(1)	0.070	18.0	6	0.031	2200	0.43	-	0.052	-
(2)	0.070	30.5	11	0.018	1900	0.23	1.1	0.212	0.351
(3)	0.070	24.0	12	0.018	1900	0.25	1.5	0.299	0.388
(4)	0.070	22.0	16	0.015	1800	0.27	2.0	0.388	0.426
(5)	0.070	20.0	20	0.014	1800	0.40	2.0	0.520	0.483
(6)	0.035	20.0	20	0.007	1800	0.40	2.0	0.260	0.371

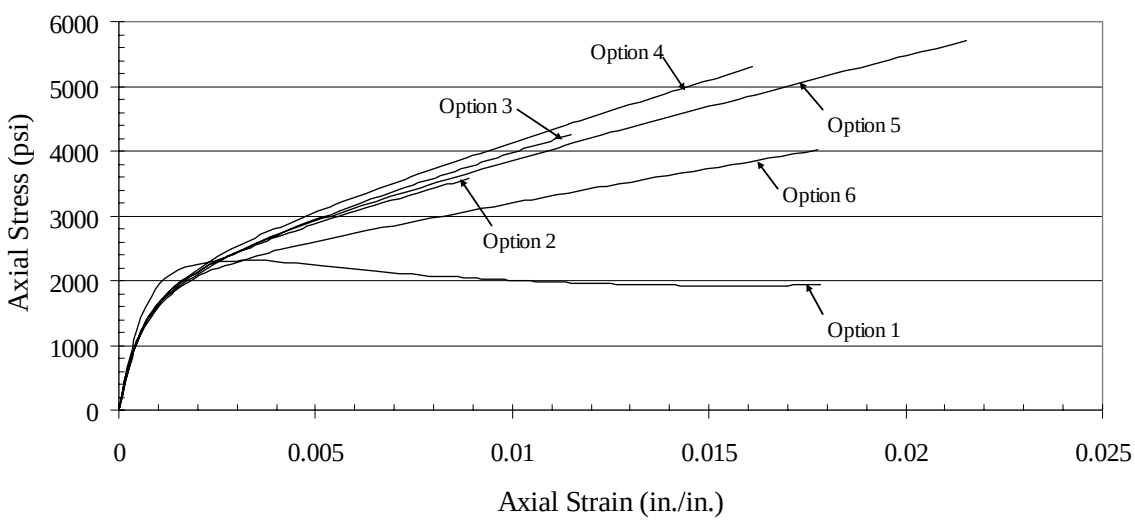

Figure 9.2 Axial stress-axial strain relationships for options 1-6

Table 9.2 Result summary for options 1-6

Option	Original cross-sectional area (ft^2)	Added cross-sectional area of expansive concrete (ft^2)	Area of FRP jacket (ft^2)	f_{cc}' (psi)	ε_{cc}' (ε_{cu}') (in./in.)	μ
(1)	0.75	0.00	24	2307	0.0181	0.78
(2)	0.75	1.08	35	3581	0.0089	1.45
(3)	0.75	0.82	29	4258	0.0115	1.51
(4)	0.75	1.17	30	5297	0.0161	1.65
(5)	0.75	1.43	31	5703	0.0215	1.76
(6)	0.75	1.43	31	4013	0.0178	1.35

Table 9.3 Comparisons of options 2-6 with option 1

Option	Ratio of area change*	Increase of the total area of FRP jacket	Increase of f_{cc}'	Increase of ε_{cc}'	Increase of μ
(2)	144%	44%	55%	-51%	86%
(3)	109%	21%	85%	-36%	94%
(4)	156%	25%	130%	-11%	112%
(5)	191%	31%	147%	19%	126%
(6)	191%	-33%	74%	-2%	73%

* The ratio of area change means the ratio of the added cross-sectional area of expansive cement concrete to the original cross-sectional area.

10. CONCLUSIONS AND RECOMMENDATIONS

The present study investigated FRP strengthening for improving the axial capacity of concrete columns for different types of confinement, geometry and FRP composite materials. An extensive study was carried out regarding the shape modification for the purpose of significantly increasing the effect of FRP composite confinement of concrete for square and rectangular columns. Thirty full-scale concrete columns were tested in uniaxial compression until failure. Design procedures were developed and compared to the experimental results. Finally, finite element models and design-oriented models were proposed for the FRP-confined concrete columns. From the results of this study, conclusions and recommendations for future research and implementation are made.

10.1 Conclusions

(1) Circular columns

Both CFRP and CFRP confinement are very effective for circular concrete columns by significantly increasing the axial strength, ultimate axial strain and ductility. With the same FRP jacket stiffness, $E_j t_j$, GFRP-confined columns can obtain approximately the same or slightly higher increase in axial strength, ultimate axial strain, and ductility compared to CFRP-confined columns. In addition, GFRP-confined columns show more ductile behavior than CFRP-confined columns at failure. Therefore, GFRP should be used to provide higher ductility and moderate strength for circular columns due to the lower modulus of the GFRP material. On the other hand, because of the higher modulus of CFRP, this material can be used to provide circular concrete columns with higher strength increase and moderate ductility. Extra caution may need to be paid for CFRP strengthening for material brittleness. In some cases, the combination of these two FRP composites as a hybrid reinforcement could be considered.

Because of the ease of inspection, FRP strips may be applied to strengthen circular concrete columns in some cases. However, the confinement effectiveness is reduced as compared to those confined by continuous FRP jackets with the same FRP volumetric ratio. Thus, FRP strips should be used with extra caution for increasing axial stress capacity; the maximum spacing of FRP strips must be limited.

The proposed design methods for circular concrete columns agree well with the test results. For engineering practice, a reduction factor, ϕ for the jacket efficiency factor k_ε should be used to account for the influences of construction, environment and column size. In addition, an upper limit should be set on the ultimate confining stress, f_{lu}. Based on the present study, this value is suggested as $0.8 f_{cc}'$.

(2) Square and rectangular columns

The confinement effectiveness for square columns is much less than that for circular columns due to the presence of corners and long sides; the efficiency is reduced as the corner radii are decreased. Because of concrete softening for moderate or low FRP lateral confinement,

FRP confined square concrete columns can still obtain a significant increase in ultimate axial strain, but a moderate gain in strength enhancement and a limited increase in ductility.

The confinement effectiveness is reduced further for square concrete columns confined with FRP strips compared to the continuously-confined square columns with the same FRP volumetric ratio. Since the FRP strips cannot provide enough confinement to the concrete due to the corner effect and the weak link of plain concrete between FRP strips, the square concrete columns with FRP strips cannot increase the axial strength to a satisfactory level. Therefore, such a strengthening method is not recommended unless testing demonstrates its effectiveness.

Shape modification has proven to be a very effective method to significantly increase the compressive behavior for square columns either by using bonded FRP jackets or non-bonded FRP jackets with expansive cement concrete. The increased cross-sectional area is proposed to be 60% which is the minimum area inscribing the square section. The conclusions regarding shape modification will be presented in the next section.

The compressive behavior of FRP-confined rectangular columns is similar to that of square columns but displays a more significant softening. Compared to square concrete columns, the confinement effectiveness for FRP-confined rectangular columns is reduced because the shape effect is more significant and the effectiveness decreases as the aspect ratio, $\frac{a}{b}$ increases. The effect of shape modification for rectangular columns varies and is strongly dependent on the geometry after the shape modification; this was verified by the parametric study presented in Chapter 9, and the conclusions will be given in the next section.

It is noted that with approximately the same FRP jacket stiffness, $E_j t_j$, CFRP jackets can provide higher axial strength and more ductility than GFRP jackets while GFRP-confined columns show more axial strain capacity than CFRP-confined columns. This behavior is different from that for circular columns which indicates that GFRP is more sensitive to the shape effect; CFRP is more suitable for strengthening of square and rectangular columns for the purpose of increasing the axial capacity and ductility. Again, because of the brittleness of CFRP at failure, this material should be used with extra caution. For some cases, in which a significant axial strain capacity is required, the use of GFRP should be considered but probably with a larger number of layers, or the combination of both FRP composites as in a hybrid FRP composite.

In general, the proposed design methods for square and rectangular columns showed a good agreement with experimental results performed by the present study, and studies carried out by Rochette and Labossière (2000) and Pessiki et al. (2001). However, the predicted axial strength by the theoretical model for rectangular columns with an aspect ratio of 3:1 is much lower than observed in the present experimental study; this indicates that the proposed shape factor, k_s, as presented in Chapter 6, is underestimated and may not apply to rectangular columns with an aspect ratio higher than 2:1. In addition, similar to circular columns, a reduction factor, ϕ for the jacket efficiency factor k_ε should be used for design purposes.

(3) Shape modification

Two methods of performing shape modification were investigated in the present study. In general, the strengthening effect of using non-bonded FRP jackets combined with expansive cement concrete is better than that of using non-shrink concrete combined with wet FRP lay-up; this is due to the post-tensioning effect from the expansive cement concrete. Compared to the original square or rectangular columns with the same number of layers of FRP composite, higher increase in strength, ultimate axial strain, and ductility were obtained for shape-modified columns with the non-bonded FRP jacket and expansive cement concrete than those with the bonded FRP jacket and non-shrink concrete. In addition, from the practical point of view, the non-bonded FRP jacket can be used as a stay-in-place form which would save construction time and the additional expense of formwork. Therefore, non-bonded FRP jackets combined with expansive cement concrete are recommended for performing shape modification.

The effect of shape modification varies with the aspect ratio. It is obvious that the most optimal shape is the circular cross-section. However, for some rectangular columns, especially for those with a large aspect ratio, this geometry change may require a large amount of grout to realize. A parametric study regarding the effects of shape modification with different geometries and aspect ratios was performed and is shown in Chapter 9. For strengthening of rectangular concrete columns by shape modification, influence factors such as volume increase, increase in surface area, strength, ductility, and ultimate axial strain, need to be considered together and compared to each other to find an optimal solution.

Similar to the FRP-confined square and rectangular columns, CFRP-confined shape-modified columns generally show more increase in strength and ductility compared to GFRP-confined shape-modified columns with approximately the same jacket stiffness. By contrast, GFRP-confined columns always show more ultimate axial strain than CFRP-confined columns. It is also noted that for some elliptical sections with an aspect ratio close to a circular cross-section, the ductility increase for GFRP-confined columns is higher than that for CFRP-confined specimens. Therefore, CFRP composites are recommended as the material of choice for the general case of shape modification. For the cases in which the purpose is to increase the ductility of elliptical columns with an aspect ratio smaller than 2:1, GFRP composites should be used.

The proposed design methods show a satisfactory agreement with experimental results for most shape-modified square and rectangular columns. However, some predicted results for shape-modified rectangular columns do not agree with the test results in a satisfactory manner. This is mainly due to construction difficulties which caused the actual cross-section to finally form in a constructed shape, different from the exact elliptical shape.

In the shape modification methods selected, the cross-section must be modified for the full height of the column. Depending on the desired increase in strength and ductility, a gradual change of the number of FRP layers can be implemented.

10.2 Recommendations for Future Research

At the conclusion of the present study, the following are identified to be issues for future research:

(1) Verification of assumptions

Some parameters in the present study are based on certain assumptions. For example, the shape factor, k_e is proposed based on the arching effect assumption with an arch height about one-fourth of the side length; the contribution factor, k_p is suggested to be the ratio of the jacket efficiency factor of the bonded FRP jacket to that of the non-bonded FRP jacket. Although these have proven to be in good agreement with the experimental results of the present study, further investigations should be made regarding the above assumptions.

(2) Verification of expressions

Most data used for the regression analysis in this research were based on the experimental findings from the full-scale concrete column tests carried out in the experimental study. Because of the limited quantity of specimens tested, the recommended expressions may not be accurate enough to reflect the actual behavior of a large population of specimens and therefore need to be further verified.

(3) Mechanism of expansive cement concrete

The present study has developed the concept of using non-bonded FRP jackets combined with expansive cement concrete; this induces post-tensioning of the FRP jacket and in turn improves jacket efficiency and compressive behavior of concrete under axial loading. This method has proven to be effective and verified by both an experimental and an analytical approach. However, in order to use this technique more effectively, more research should be done on the material properties of expansive cement, especially regarding the working mechanism of such special cement for large columns of substantial height. In addition, the extent of hoop strain caused by the expansion and the volume effect on the hoop expansion should also be investigated.

(4) Distinction between hardening and softening behavior

FRP-confined concrete specimens show either hardening or softening behavior. The present study suggests that the different behavior depends on the value of the effective confinement ratio, $\frac{f_{lu}}{f_{co}'}$; a threshold value to distinguish between the two different behaviors was proposed based on the experimental results. Further work, including theoretical and experimental research is required to verify or adjust the suggested value.

(5) Practical application

A demonstration project involving shape modification of actual-size columns could be performed to answer several issues regarding the practical implementation of this method. Measurement of hoop strain during the curing period of the expansive cement concrete should be carried out.

10.3 Recommendations for Implementation

The results of this study have shown that the best shape for a column section, that is a candidate for retrofit with FRP composites, is a circular cross-section. Glass FRP is preferred to carbon FRP for the same jacket stiffness, $E_j t_j$, for improving ultimate compressive strength, ultimate compressive strain and ductility. However, the durability issues related to glass FRP, namely alkali reaction, must be considered depending on the geographic location of the bridge. Confinement effectiveness is less for square columns compared to circular columns, due to the presence of corners and long flat sides. Carbon FRP jackets are preferred to glass FRP jackets of the same jacket stiffness, $E_j t_j$, for improving ultimate compressive strength and ductility; however, glass FRP jackets show higher ultimate compressive strain capacity. FRP-confined rectangular columns behave similar to square columns, however they exhibit more softening. As the aspect ratio is increased, the confinement effectiveness decreases.

FRP composite strips are preferred in some cases because of the ease of inspection of the retrofitted column. However, the confinement effectiveness is less compared to columns confined with continuous FRP jackets with the same volumetric ratio of FRP composite to concrete. In addition, the maximum spacing of the strips should be limited, depending on the column size and cross-section. Based on the results of this study, FRP composite strips are not recommended for strengthening square or rectangular columns because they cannot increase the compressive capacity to a satisfactory level; however, they can improve the ductility. In general, FRP strips could be used only for strengthening circular columns, and are not recommended for square or rectangular cross-sections.

Shape modification of square and rectangular columns to a circular or oval shape is a viable method for improving ultimate compressive strength, compressive strain and ductility. Shape modification using expansive cement concrete and a non-bonded FRP jacket is the preferred method. Carbon FRP composite jackets combined with expansive cement concrete show a larger increase in compressive strength and ductility compared to glass FRP; however, glass FRP shows higher ultimate compressive strain capacity. The issue of relative cost is an important one. One advantage of shape modification using an FRP composite shell with expansive cement concrete is that the jacket is also the stay-in-place form; thus, the cost of formwork is eliminated. In addition, chemical prestressing is superior to regular shape modification using a wet lay-up for increasing the ultimate compressive strength, compressive strain and ductility. However, the optimal solution must be obtained using a comparison which includes: 1) the volume increase, 2) the increase in surface area, 3) retrofitting the whole column height, and (4) material costs. At present, the price of expansive cement is two to three times the price of Portland cement; however, this is a small cost compared to the total cost of the retrofit.

Circular columns should be wrapped with FRP composites using a wet lay-up; for certain conditions glass or carbon FRP composites are equally advantageous for implementation. FRP

strips should be considered for circular columns only. For square and rectangular columns, shape modification to a circular or oval shape is a viable option and should be considered; compared to the original square or rectangular columns with the same number of FRP composite layers, a higher increase in ultimate compressive strength, ultimate compressive strain, and ductility can be achieved.

The present study has focused on the axial strength capacity and ductility increase of columns. The strength of columns subjected to lateral loads is beyond the scope of this study. The lateral capacity of columns retrofitted with FRP composites has been studied by Pantelides et al. (2001), through in-situ lateral load tests of reinforced concrete bridge bents. Based on the results of this study, the following recommendations for practical application are offered:

(1) For strengthening existing square or rectangular columns to improve their axial strength capacity to carry gravity loads, a wet-layup procedure of the column in the as-is condition is sufficient. This study has shown that the axial strength of square columns can be increased by a factor ranging from 1.5 to 1.7 times the original axial load capacity; however, no significant improvement of the ductility can be expected in this case. For strengthening existing square or rectangular columns to resist seismic forces, it is preferable to transform the square and rectangular cross-sections to circular, and elliptical or oval, respectively. The preferred implementation makes use of FRP composite prefabricated shells and expansive cement concrete. In this study, the axial load capacity of square columns, which were modified to circular using FRP shells and expansive cement concrete, was increased by a factor ranging from 3.4 to 3.7 times the original axial load capacity; the ductility was increased by a factor ranging from 2.0 to 2.4 times the original column ductility.

(2) This study has found that the use of FRP composite straps or hoops is beneficial for columns with a circular cross-section but not for columns with a square or rectangular cross-section.

(3) In the case of using FRP composite prefabricated shells, it is advantageous to use expansive cement concrete rather than non-shrink grout to achieve the shape modification. Square columns, which were modified to circular using FRP composite prefabricated shells and expansive cement concrete, showed an increase in axial strength capacity by a factor ranging from 3.4 to 3.7 times the original axial load capacity, and a ductility increase ranging from 2.0 to 2.4 times the original column ductility. Square columns, which were modified to circular using FRP composite prefabricated shells and non-shrink grout, showed an increase in axial strength capacity by a factor ranging from 2.5 to 2.7 times the original axial load capacity, and a ductility increase ranging from 1.4 to 1.7 times the original column ductility.

(4) Design guidelines for the FRP composite retrofit of circular columns are provided in Figure 7.1 of this report; guidelines for the FRP composite retrofit of square and rectangular columns are provided in Figure 7.2; guidelines for the FRP composite retrofit of elliptical columns are provided in Figure 7.3; and guidelines for the retrofit of columns with FRP composite prefabricated shells and either non-shrink grout or expansive cement concrete are provided in Figure 7.5 of this report.

11. REFERENCES

ACI 440 (2002). "ACI Committee 440. Guide for the Design and Construction of Externally Bonded FRP System for Strengthening Concrete Structures. (ACI440.2R-02)." *American Concrete Institute*, Detroit, Mich.

ANSYS User's Manual (2000): *Procedures*, Vol. I, Swanson Analysis Systems, Inc.

Benuska, K. L., Bertero, V. V., and Polivka M. (1971). "Self-Stressed Concrete for Precast Building Units." *PCI Journal*, March-April 1971, 72-84.

Carey, S. A., and Harries, K. A. (2003). "The Effect of Shape, Gap and Scale on the Behavior and Modeling of Variably Confined Concrete." *Research Report ST03-05*, Department of Civil and Environmental Engineering, University of South Carolina, December 2003.

Chen, W. F., and Han, D. J. (1982). "Plasticity for Structural Engineering." Springer-Verlag, New York: 1982.

Fardis, M. N. and Khalili, H. (1981). "Concrete Encased in Fiberglass Reinforced Plastic." *ACI Journal*, 78(6), 440-446.

Gergely, I., Pantelides, C. P., Nuismer, R. J., and Reaveley, L. D. (1998). "Bridge Pier Retrofit Using Fiber-Reinforced Plastic Composites." *Journal of Composites for Construction*, ASCE, 2(4), 165- 174.

Karbhari, V. M., and Gao, Y. (1997). "Composite Jacketed Concrete under Uniaxial Compression-Verification of Simple Design Equations." *Journal of Materials for Civil Engineering*, ASCE, 9(4), 185-193.

Klein, A., Karby, T., and Polivka, M. (1961). "Properties of An Expansive Cement for Chemical Prestressing." *ACI Journal, Proceedings*, Vol. 58, No. 1, July 1961, 59-82.

Lam L., and Teng J. G. (2003). "Design-oriented Stress-Strain Model for FRP-confined Concrete in Rectangular Columns." *Journal of Reinforced Plastics and Composites*, Vol.22, No. 13/2003. 1149-86.

Mander J. B., Priestley J. N., and Park R. (1988). "Theoretical Stress-Strain Model for Confined Concrete." *Journal of Structural Engineering*, ASCE.114(8),1804-902.

Mirmiran, A., and Shahawy, M. (1997). "Behavior of Concrete Columns Confined by Fiber Composites." *Journal of Structural Engineering*, ASCE, 123(5), 583-590.

Mirmiran, A., Shahawy, M., Samaan, M., and El Echary, H. (1998). "Effect of Column Parameters on FRP-Confined Concrete." *Journal of Materials for Civil Engineering*, ASCE, 2(4), 175- 185.

Miyauchi, K., Nishibayashi, S., and Inoue, S. (1997). "Estimation of Strengthening Effects with Carbon Fiber Sheet for Concrete Column." *Non-Metallic (FRP) Reinforcement for Concrete Structures*. *Proceedings, 3rd International Symposium*, Sapporo, Japan, Vol. 1, 217-224.

Moran D. A., and Pantelides, C. P. (2002a). "Variable Strain Ductility for FRP-Confined Concrete." *Journal of Composites for Construction*, ASCE, 6(4). 224-232.

Moran D. A., and Pantelides, C. P. (2002b). "Stress-Strain Model for FRP-Confined Concrete." *Journal of Composites for Construction*, ASCE, 6(4). 233-240.

Pantazopoulou, S. J., and Mills, R. H. (1995). "Microstructural Aspects of the Mechanical Response of Plain Concrete." *ACI Materials Journal*, 92, 605-616.

Pantelides, C.P., Gergely, J., and Reaveley, L.D. (2001). "In-situ Verification of Rehabilitation and Repair of Reinforced Concrete Bridge Bents under Simulated Seismic Loads." *Earthquake Spectra*, Earthquake Engineering Research Institute, 17(3), 507-530.

Pantelides, C.P., Cercone, L., and Policelli, F. (2004). "Development of a Specification for Bridge Seismic Retrofit with CFRP Composites." *Journal of Composites for Construction*, ASCE, 8(1), 88-96.

Pessiki, S., Harries, K. A., Kestner, J. T., Sause, R., and Ricles, J. M. (2001). "Axial Behavior of Reinforced Concrete Columns Confined with FRP Jackets." *Journal of Composites for Construction*, ASCE, 2001, 5(4), 237-245.

Richard, R. M., and Abbott, B. J. (1975). "Versatile Elastic-Plastic Stress-Strain Formula." *Journal of Engineering Mechanics*, 101(4), 511-515.

Rochette, P., and Labossière, P. (1996). "A Plasticity Approach for Concrete Columns Confined with Composite Materials." *Journal of Composites for Construction*, ASCE, 2000, 4(3), 129-136.

Rochette, P., and Labossière, P. (2000). "Axial Testing of Rectangular Column Models Confined with Composites." *Advanced Composite Materials in Bridges and Structures*, M.M. El-Bardy, (Ed.), Canadian Society for Civil Engineering, 359-366.

Samaan M., Mirmiran A., and Shahawy M. (1999). "Model of Concrete Confined by Fiber Composites." *Journal of Composites for Construction*, ASCE, 124(9),1025-1031.

Spoelstra, M.R., and Monti, G. (1999). "FRP Confined Concrete Model." *Journal of Composites for Construction*, ASCE, 3(3), 146-150.

Stanton, J. F., Owen, L. M., and MacRae, G. A. (1998). "Stress-strain Properties of Confined Concrete." *Proceeding, 6th U.S. National Conference on Earthquake Engineering*, EERI, May 31-June 4, Oakland, CA.

William, K. J., and Warnke, E. P. (1975). "Constitutive Model for the Triaxial Behavior of Concrete." *Proceedings, International Association for Bridge and Structural Engineering*, Vol. 19, 1-30.

Xiao, Y., Wu, H. (2000). "Compressive Behavior of Concrete Confined by Carbon Fiber Composite Jackets." *Journal of Materials for Civil Engineering*, 12(2), 139-146.

APPENDIX

(1). ANSYS Input File for C-C1-0

```
/BATCH
! /COM,ANSYS RELEASE  6.0    UP20010919       11:13:50    08/08/2004
/input,menust,tmp,  ,,,,,,,,,,,,,,,1
! /GRA,POWER
! /GST,ON
! /PLO,INFO,3
! /COL,PBAK,ON,1,BLUE
! /GRO,CURL,ON
!*
/NOPR
/PMETH,OFF,0
KEYW,PR_SET,1
KEYW,PR_STRUC,1
KEYW,PR_THERM,0
KEYW,PR_FLUID,0
KEYW,PR_ELMAG,0
KEYW,MAGNOD,0
KEYW,MAGEDG,0
KEYW,MAGHFE,0
KEYW,MAGELC,0
KEYW,PR_MULTI,0
KEYW,PR_CFD,0
/GO
!*
! /COM,
! /COM,Preferences for GUI filtering have been set to display:
! /COM,  Structural
!*
/PREP7
!*
ET,1,SOLID65
!*
KEYOPT,1,1,0
KEYOPT,1,5,0
KEYOPT,1,6,0
KEYOPT,1,7,1
!*
ET,2,SHELL41
!*
KEYOPT,2,1,2
KEYOPT,2,2,0
KEYOPT,2,4,0
KEYOPT,2,5,0
KEYOPT,2,6,0
!*
!*
R,1, , , , , , ,
RMORE, , , , , , ,
!*
R,2,.08,.08,.08,.08, , ,
RMORE, ,
```

```
!*
!*
MPTEMP,,,,,,,,
MPTEMP,1,0
MPDATA,EX,1,,2673537
MPDATA,PRXY,1,,0.2
TB,DP,1,,,0
TBMODIF,1,1,490
TBMODIF,1,2,41.7
TBMODIF,1,3,
TB,CONC,1,1,9,
TBTEMP,0
TBDATA,,,,220,,,
TBDATA,,,,,,,
MPTEMP,,,,,,,,
MPTEMP,1,0
MPDATA,EX,2,,1.26e07
MPDATA,EY,2,,6.9e05
MPDATA,EZ,2,,6.9e05
MPDATA,PRXY,2,,
MPDATA,PRYZ,2,,
MPDATA,PRXZ,2,,
MPDATA,GXY,2,,4.2e05
MPDATA,GYZ,2,,3.35e05
MPDATA,GXZ,2,,3.35e05
K,1,0,0,,
K,2,6,0,,
K,3,0,6,,
LSTR,      1,      2
LSTR,      1,      3
!*
LARC,3,2,1,6,
FLST,2,3,4
FITEM,2,2
FITEM,2,3
FITEM,2,1
AL,P51X
! /VIEW, 1 ,1,1,1
! /ANG, 1
! /REP,FAST
!*
VOFFST,1,36, ,
CM,_Y,AREA
ASEL, , , ,      4
CM,_Y1,AREA
CMSEL,S,_Y
!*
CMSEL,S,_Y1
AATT,      2,      2,   2,      0,
CMSEL,S,_Y
CMDELE,_Y
CMDELE,_Y1
!*
CM,_Y,VOLU
VSEL, , , ,      1
CM,_Y1,VOLU
```

```
CMSEL,S,_Y
!*
CMSEL,S,_Y1
VATT,      1,      1,   1,      0
CMSEL,S,_Y
CMDELE,_Y
CMDELE,_Y1
!*
FLST,5,3,4,ORDE,2
FITEM,5,7
FITEM,5,-9
CM,_Y,LINE
LSEL, , , ,P51X
CM,_Y1,LINE
CMSEL,,_Y
!*
LESIZE,_Y1, , ,36, , , , ,0
!*
FLST,5,4,4,ORDE,4
FITEM,5,1
FITEM,5,-2
FITEM,5,4
FITEM,5,6
CM,_Y,LINE
LSEL, , , ,P51X
CM,_Y1,LINE
CMSEL,,_Y
!*
LESIZE,_Y1, , ,6, , , , ,0
!*
FLST,5,2,4,ORDE,2
FITEM,5,3
FITEM,5,5
CM,_Y,LINE
LSEL, , , ,P51X
CM,_Y1,LINE
CMSEL,,_Y
!*
LESIZE,_Y1, , ,8, , , , ,0
!*
CM,_Y,AREA
ASEL, , , ,      4
CM,_Y1,AREA
CHKMSH,'AREA'
CMSEL,S,_Y
!*
MSHKEY,1
AMESH,_Y1
MSHKEY,0
!*
CMDELE,_Y
CMDELE,_Y1
CMDELE,_Y2
!*
CM,_Y,VOLU
VSEL, , , ,      1
```

```
CM,_Y1,VOLU
CHKMSH,'VOLU'
CMSEL,S,_Y
!*
VSWEEP,_Y1
!*
CMDELE,_Y
CMDELE,_Y1
CMDELE,_Y2
!*
! LPLOT
FINISH
/SOLU
FLST,2,2,5,ORDE,2
FITEM,2,3
FITEM,2,5
DA,P51X,SYMM
FLST,2,1,5,ORDE,1
FITEM,2,2
!*
/GO
DA,P51X,UX,0
FLST,2,1,5,ORDE,1
FITEM,2,2
!*
/GO
DA,P51X,UY,0
FLST,2,1,5,ORDE,1
FITEM,2,2
!*
/GO
DA,P51X,UZ,0
FLST,2,1,5,ORDE,1
FITEM,2,1
!*
/GO
DA,P51X,UX,0
FLST,2,1,5,ORDE,1
FITEM,2,1
!*
/GO
DA,P51X,UY,0
FLST,2,1,5,ORDE,1
FITEM,2,1
!*
/GO
DA,P51X,UZ,-0.72
NSUBST,10,0,0
OUTRES,ALL,1
AUTOTS,0
RESCONTRL,DEFINE,ALL,1,1
! SAVE, file,db,
! /STATUS,SOLU
SOLVE
! LGWRITE,",",",COMMENT
! LGWRITE,'circularcolumn','lgw',",COMMENT
```

(2). ANSYS Input File for S-CT-E

```
/BATCH
! /COM,ANSYS RELEASE  6.0    UP20010919       13:28:46    12/21/2004
/input,menust,tmp,  ,,,,,,,,,,,,,,,1
! /GRA,POWER
! /GST,ON
! /PLO,INFO,3
! /COL,PBAK,ON,1,BLUE
! /GRO,CURL,ON
!*
/NOPR
/PMETH,OFF,0
KEYW,PR_SET,1
KEYW,PR_STRUC,1
KEYW,PR_THERM,0
KEYW,PR_FLUID,0
KEYW,PR_ELMAG,0
KEYW,MAGNOD,0
KEYW,MAGEDG,0
KEYW,MAGHFE,0
KEYW,MAGELC,0
KEYW,PR_MULTI,0
KEYW,PR_CFD,0
/GO
!*
! /COM,
! /COM,Preferences for GUI filtering have been set to display:
! /COM,  Structural
!*
/PREP7
!*
ET,1,SOLID65
!*
ET,2,SHELL41
!*
KEYOPT,1,1,0
KEYOPT,1,5,0
KEYOPT,1,6,0
KEYOPT,1,7,1
!*
KEYOPT,2,1,2
KEYOPT,2,2,0
KEYOPT,2,4,0
KEYOPT,2,5,0
KEYOPT,2,6,0
!*
!*
R,1, , , , , , ,
RMORE, , , , , , ,
!*
R,2,0.08,0.08,0.08,0.08, , ,
RMORE, ,
!*
!*
```

```
MPTEMP,,,,,,,,
MPTEMP,1,0
MPDATA,EX,1,,2.5e06
MPDATA,PRXY,1,,0.2
TB,DP,1,,,0
TBMODIF,1,1,454
TBMODIF,1,2,35
TBMODIF,1,3,
MPTEMP,,,,,,,,
MPTEMP,1,0
MPDATA,EX,2,,1.65e06
MPDATA,PRXY,2,,0.2
TB,DP,2,,,0
TBMODIF,1,1,300
TBMODIF,1,2,35
TBMODIF,1,3,
MPTEMP,,,,,,,,
MPTEMP,1,0
MPDATA,EX,3,,1.26e07
MPDATA,EY,3,,6.9e05
MPDATA,EZ,3,,6.9e05
MPDATA,PRXY,3,,
MPDATA,PRYZ,3,,
MPDATA,PRXZ,3,,
MPDATA,GXY,3,,4.2e05
MPDATA,GYZ,3,,3.35e05
MPDATA,GXZ,3,,3.35e05
MPTEMP,,,,,,,,
MPTEMP,1,0
UIMP,3,REFT,,,
MPDATA,ALPX,3,,-6.3e-08
MPDATA,ALPY,3,,2.88e-05
MPDATA,ALPZ,3,,2.88e-05
K,1,0,0,,
K,2,5.5,0,,
K,3,5.5,5.5,,
K,4,0,5.5,,
K,5,6,0,,
K,6,0,8,,
K,7,8,0,,
KDELE,      5
LSTR,       1,      2
LSTR,       2,      3
LSTR,       3,      4
LSTR,       4,      1
!*
LARC,6,7,1,8,
LSTR,       4,      6
LSTR,       2,      7
FLST,2,4,4
FITEM,2,4
FITEM,2,3
FITEM,2,2
FITEM,2,1
AL,P51X
FLST,2,5,4
```

```
FITEM,2,6
FITEM,2,3
FITEM,2,2
FITEM,2,7
FITEM,2,5
AL,P51X
!*
VOFFST,1,36, ,
! /VIEW, 1 ,1,1,1
! /ANG, 1
! /REP,FAST
! LPLOT
!*
VOFFST,2,36, ,
VDELE,      2
FLST,2,2,5,ORDE,2
FITEM,2,8
FITEM,2,10
ADELE,P51X
! APLOT
FLST,2,4,5,ORDE,3
FITEM,2,9
FITEM,2,11
FITEM,2,-13
ADELE,P51X
! LPLOT
FLST,2,10,4,ORDE,2
FITEM,2,16
FITEM,2,-25
LDELE,P51X
! LPLOT
!*
VOFFST,2,-36, ,
! VPLOT
CM,_Y,VOLU
VSEL, , , ,      1
CM,_Y1,VOLU
CMSEL,S,_Y
!*
CMSEL,S,_Y1
VATT,      1,      1,   1,      0
CMSEL,S,_Y
CMDELE,_Y
CMDELE,_Y1
!*
! /VIEW, 1 ,,,1
! /ANG, 1
! /REP,FAST
CM,_Y,VOLU
VSEL, , , ,      2
CM,_Y1,VOLU
CMSEL,S,_Y
!*
CMSEL,S,_Y1
VATT,      2,      1,   1,      0
CMSEL,S,_Y
```

```
CMDELE,_Y
CMDELE,_Y1
!*
! /VIEW, 1 ,1,1,1
! /ANG, 1
! /REP,FAST
CM,_Y,AREA
ASEL, , , ,      10
CM,_Y1,AREA
CMSEL,S,_Y
!*
CMSEL,S,_Y1
AATT,       3,       2,   2,       0,
CMSEL,S,_Y
CMDELE,_Y
CMDELE,_Y1
!*
FLST,5,4,4,ORDE,4
FITEM,5,13
FITEM,5,-14
FITEM,5,22
FITEM,5,-23
CM,_Y,LINE
LSEL, , , ,P51X
CM,_Y1,LINE
CMSEL,,_Y
!*
LESIZE,_Y1, , ,36, , , , ,0
!*
FLST,5,4,4,ORDE,2
FITEM,5,8
FITEM,5,-11
CM,_Y,LINE
LSEL, , , ,P51X
CM,_Y1,LINE
CMSEL,,_Y
!*
LESIZE,_Y1, , ,11, , , , ,0
!*
FLST,5,2,4,ORDE,2
FITEM,5,16
FITEM,5,18
CM,_Y,LINE
LSEL, , , ,P51X
CM,_Y1,LINE
CMSEL,,_Y
!*
LESIZE,_Y1, , ,5, , , , ,0
!*
! /VIEW, 1 ,,,1
! /ANG, 1
! /REP,FAST
FLST,5,1,4,ORDE,1
FITEM,5,5
CM,_Y,LINE
LSEL, , , ,P51X
```

```
CM,_Y1,LINE
CMSEL,,_Y
!*
LESIZE,_Y1, , ,22, , , , ,0
!*
! /VIEW, 1 ,1,1,1
! /ANG, 1
! /REP,FAST
CM,_Y,AREA
ASEL, , , ,      10
CM,_Y1,AREA
CHKMSH,'AREA'
CMSEL,S,_Y
!*
MSHKEY,1
AMESH,_Y1
MSHKEY,0
!*
CMDELE,_Y
CMDELE,_Y1
CMDELE,_Y2
!*
FLST,5,2,6,ORDE,2
FITEM,5,1
FITEM,5,-2
CM,_Y,VOLU
VSEL, , , ,P51X
CM,_Y1,VOLU
CHKMSH,'VOLU'
CMSEL,S,_Y
!*
VSWEEP,_Y1
!*
CMDELE,_Y
CMDELE,_Y1
CMDELE,_Y2
!*
! LPLOT
FINISH
/SOLU
FLST,2,4,5,ORDE,4
FITEM,2,4
FITEM,2,-5
FITEM,2,9
FITEM,2,11
DA,P51X,SYMM
FLST,2,2,5,ORDE,2
FITEM,2,1
FITEM,2,-2
!*
/GO
DA,P51X,UZ,0
FLST,2,2,5,ORDE,2
FITEM,2,3
FITEM,2,8
!*
```

```
/GO
DA,P51X,UZ,-1.08
FLST,2,1,5,ORDE,1
FITEM,2,10
!*
BFA,P51X,TEMP,-25000
NSUBST,8,0,0
OUTRES,ALL,1
AUTOTS,1
RESCONTRL,DEFINE,ALL,1,1
! SAVE, file,db,
! LGWRITE,",",",COMMENT
```